

University of Alberta

Scalable, Modular, Integrated Genetic Analysis Systems

by

Allison Christel Elizabeth Bidulock

A thesis submitted to the Faculty of Graduate Studies and Research
in partial fulfillment of the requirements for the degree of

Master of Science

in

Micro-Electro-Mechanical Systems (MEMs) and Nanosystems

Department of Electrical and Computer Engineering

©Allison Christel Elizabeth Bidulock

Fall 2011

Edmonton, Alberta

Permission is hereby granted to the University of Alberta Libraries to reproduce single copies of this thesis and to lend or sell such copies for private, scholarly or scientific research purposes only. Where the thesis is converted to, or otherwise made available in digital form, the University of Alberta will advise potential users of the thesis of these terms.

The author reserves all other publication and other rights in association with the copyright in the thesis and, except as herein before provided, neither the thesis nor any substantial portion thereof may be printed or otherwise reproduced in any material form whatsoever without the author's prior written permission.

EXAMINING COMMITTEE

Christopher J. Backhouse, Electrical and Computer Engineering

James M. McMullin, Electrical and Computer Engineering

Michael Brett, Electrical and Computer Engineering

Suzanne M. Kresta, Chemical and Materials Engineering

*To my loving grandmother,
for your unending confidence in me.*

*To my inspiring father,
for always encouraging me to grow further.*

And to persevering myself:

You did it.

ABSTRACT

This thesis addresses the need for inexpensive microfluidic platforms by contributing to the collaborative development of a modularised, integrated system capable of molecular diagnostics using bead-based sample preparation, polymerase chain reaction and capillary electrophoresis analysis techniques. Although the entire system is briefly presented here, the primary focus of this project had three central goals: contribution to the system architecture through the sole development of in-house, modular software and firmware-software interface protocol; verification of the system's capabilities through extensive testing and strict characterisation of its performance; and, the identification of challenges associated with the characterised system and discussion of possible or implemented solutions. With a total component cost of less than \$1000, this system has optical sensitivity comparable to traditional electrophoretic analysis methods, the ability to amplify from a few molecules, and represents a significant advancement for the use of lab-on-a-chip technologies in point of care applications.

ACKNOWLEDGEMENTS

I am deeply grateful to my supervisor, Dr. Christopher Backhouse, for the opportunity to work at the Applied Miniaturisation Laboratory (AML) in the fields of microfluidics and lab-on-a-chip. I would further like to thank both of my supervisors, Dr. Backhouse and Dr. James McMullin, for their guidance and wisdom over the course of this thesis project. Our group meetings always brought me a further understanding and confidence in my work.

I owe very much to Dr. Mohammad Behnam, with whom I worked closely during the course of my program. His team leadership, thought-provoking questions and detailed explanations increased my knowledge on many subjects, and allowed me to achieve more than I thought able; he was my mentor, my colleague and my friend. I am also very grateful to Dr. Govind Kaigala, who provided me with much of the knowledge I needed to begin my project and always made himself available for questions and encouragement. His guidance and support was invaluable, and extended long after he graduated from the AML.

Support, advice and friendship also came from many other staff and students at the AML and Molecular Diagnostics Group (MDG), including: Abraham Jang, who fabricated all of the chips in this thesis; Christopher Barga, who drew all the mechanical designs; Robert Johnstone, Nilufar Poshtiban, Shane Groendahl and Jose Martinez-Quijada, who contributed much to the system described in this thesis; Ayo Olanrewaju, whose project ran parallel to mine and provided me with an understanding friend; John Crabtree and Alex Stickel, who often helped direct me to the questions I needed to ask; Jana Lauzon, my best non-engineer critic; and Jana, Dammika Manage, Alexey Atrazhev, Brian Taylor, and Dr. Linda Pilarski, who provided much support with the molecular biology and protocol development used in this thesis.

Last but not least, I would like to thank my parents, who reminded me (when I needed it most) that their support and encouragement is unending, for any and every endeavour I so desire to seek. I am also very appreciative of the family and friends who saw me through this degree from start to finish, and made up my own personal cheering squad.

TABLE OF CONTENTS

INTRODUCTION.....	1
1.1 Project Description.....	1
1.1.1 Motivation.....	1
1.1.2 Lab-on-a-Chip Vision.....	2
1.2 Molecular Diagnostics.....	3
1.2.1 Introduction.....	3
1.2.2 Sample Preparation.....	4
1.2.3 Amplification.....	5
1.2.4 Detection.....	7
1.2.5 Conclusion.....	12
1.3 Lab-on-a-Chip Systems.....	12
1.3.1 Microfluidic Chips for PCR-CE.....	13
1.3.2 Lab-on-a-Chip Systems for PCR-CE.....	16
1.4 Scope of Thesis.....	17
MODULAR AND SCALABLE SYSTEM.....	23
2.1 Introduction.....	23
2.2 Hardware.....	27
2.3 Firmware.....	29
2.4 Command-Line Interface Protocol.....	33
2.4.1 Hardware and Firmware Structure.....	33
2.4.2 Commands and Messages.....	35
2.5 Software.....	44
2.5.1 Software Modules.....	44
2.5.2 Software Output Files.....	52
2.6 Concluding Remarks.....	60
MICROCHIP CAPILLARY ELECTROPHORESIS.....	63
3.1 Introduction.....	63
3.2 System.....	66
3.2.1 Optical Design.....	67
3.2.2 Anomalous Intensity Spikes.....	70
3.2.3 Signal Processing.....	72
3.2.4 Detection Factors.....	79
3.3 Protocol.....	87
3.3.1 On-chip Procedure.....	87
3.3.2 Sample Stacking.....	88
3.3.3 Mobilities and Resolution.....	91
3.3.4 Run-to-Run Variability.....	93

3.3.5	Buffering Capacity.....	93
3.4	System Performance.....	94
3.4.1	Limit of detection.....	94
3.4.2	Sensitivity.....	97
3.4.3	Load-to-Load Variability.....	98
3.5	Concluding remarks.....	98

MICROCHIP POLYMERASE CHAIN REACTION AND INTEGRATED PCR-CE 101

4.1	Introduction.....	101
4.2	System Integration.....	105
4.2.1	Thermal Controller.....	106
4.2.2	Anomalous Temperature Spikes.....	109
4.2.3	Microfluidic Chip.....	111
4.2.4	On-Chip Procedure.....	113
4.3	System Performance.....	116
4.3.1	System Level PCR-CE Results.....	116
4.3.2	Variability.....	119
4.3.3	Relative Yield.....	124
4.4	System Analysis.....	125
4.4.1	System Hardware: Measuring the Heater Resistance.....	126
4.4.2	Chip Calibration: Heater Resistance & Temperature.....	127
4.4.3	System Firmware: Determining Heater Temperature.....	129
4.4.4	System Calibration: Heater & Chamber Temperature.....	130
4.4.5	Troubleshooting: Heater Resistance & Temperature.....	133
4.4.6	Troubleshooting: Heater & Chamber Temperature.....	142
4.4.7	On-Chip PCR Results Revisited.....	147
4.5	Concluding remarks.....	149

INTEGRATED SAMPLE PREPARATION-PCR-CE..... 153

5.1	Introduction.....	153
5.1.1	Sample Preparation Techniques.....	154
5.1.2	SP Integrations with PCR and CE.....	155
5.1.3	Bead-based Nucleic Acid Extraction.....	156
5.2	System Integration.....	158
5.2.1	Instrument.....	158
5.2.2	Microfluidic chip.....	159
5.2.3	On-chip Procedure.....	160
5.3	System Performance.....	163
5.3.1	System Level SP-PCR-CE Results.....	163
5.3.2	Variability.....	165
5.3.3	Relative Yield.....	166

5.4	Concluding Remarks.....	166
CONCLUSIONS		168
6.1	Summary of Work	168
6.2	Future Work.....	169
BIBLIOGRAPHY		172
APPENDICES		183
A.	Command-Line Interface Protocol.....	183
A.1	Firmware Operation.....	187
A.2	Process Commands Summary	189
A.3	Process Commands in Detail	191
A.4	Firmware Messages	200
B.	Software User Guide	202
B.1	Installing the GUI	202
B.2	Starting the GUI	202
B.3	User Interface.....	203
B.4	Notebook Buttons.....	205
B.5	Other Components	210
C.	Limit of Detection Protocol	212
D.	TTK PCRCE4 On-Chip PCR & CE Protocol.....	214
D.1	General Considerations.....	214
D.2	System Requirements	217
D.3	On-Chip PCR Procedure.....	218
D.4	On-Chip CE Procedure.....	228
E.	AML TTK SP-PCR-CE Protocol for PCR-CE-4 Chips.....	234
E.1	General Considerations.....	234
E.2	On-chip SP-PCR Procedure	237
E.3	On-Chip CE Procedure.....	243
E.4	PCR Conditions	246
E.5	CE Reagents.....	247
E.6	Unrepresentative Data.....	248

LIST OF TABLES

Table 2.1-A: Delegation of the required operation tasks for the genetic analysis system between the microcontroller and the graphical user interface	25
Table 2.4-A: Example of the data flow across the firmware-software interface	33
Table 2.4-B: System information & testing CLI commands.....	36
Table 2.4-C: External EEPROM CLI commands	37
Table 2.4-D: High voltage supply & optical detection unit CLI commands	37
Table 2.4-E: Thermal regulation & temperature monitoring unit CLI commands.....	39
Table 2.4-F: Pneumatic pump & valve unit CLI commands.....	42
Table 2.4-G: Firmware system status messages specified by the CLI protocol	43
Table 3.2-A: Data from the electropherogram seen in Figure 3.2-D. The photodiode signal is automatically converted from an ADC value to a voltage signal via the software (Chapter 2).....	71
Table 3.3-A: Variability and average intensity increase for different magnitudes of sample buffer concentration to determine the optimal concentration for desired sample stacking.	90
Table 4.2-A: Data from the electropherogram seen in Figure 4.2-B. Time is recorded in the log file in seconds but was converted into minutes here for easier interpretation with Figure 4.2-C.....	110
Table 4.2-B: Conversion table for peaks on the custom-built instrument to the expected peaks on the commercial system as determined from the LOD results (which were run with a PMT gain of 0.7).	115
Table 4.3-A: Average PCR relative yields and average variability for groups of on-chip PCR runs ran using v0.3.4 of the firmware, using the same calibration protocols, single-labelled reverse primer, and 10^7 BKV template; grouped by minor variations in temperatures (2°C) and flush-out buffer.	121

Table 4.3-B: Comparison of the variabilities from the mean PCR relative yield (effectively the PCR variability) and the mean product peak intensity (effectively the PCR-CE variability).....	123
Table 4.4-A: Example calibration coefficient data given to the user for a resistive element.....	129
Table 4.4-B: Colour of thermal liquid crystals (TLC) at specific temperatures.....	130
Table 4.4-C: Calibrated room temperature resistances vs. measured dmm resistances and their error limits. If the limits overlap, the measured heater resistance was within error and the initial calibration was unchanged. Only chips that experienced shifted resistances are shown.....	137
Table 4.4-D: Calibration data before/after ambient-temperature resistance changes were observed.....	139
Table 4.4-E: Calculated TCR and the error in the TCR for chips experiencing changes in ambient-temperature resistance.....	139
TABLE 4.4-F: Thermal conductivities of PCR chamber contents ¹⁰⁵	143
Table 5.2-A: Sample preparation CLI commands.....	159

LIST OF FIGURES

Figure 1.2-A: The general sample-to-answer molecular diagnostic process	4
Figure 2.1-A: Diagram of our developed lab-on-a-chip toolkit set-up as a PCR-(LIF)CE instrument. The inset figure is an image of the actual instrument, with dimensions of 30x20x11 cm for the electronics box, the top box containing the microfluidic chip. © The Royal Society of Chemistry ⁴³ , 2010.....	24
Figure 2.1-B: Diagram of the three separated functionalities of the instrument components and their interface protocols that allow for independent upgrades of the hardware, firmware and software.....	26
Figure 2.2-A: Diagram of the modular architecture of our developed instruments' design. It is based on multiple single-function electronic boards with common power and communication buses, allowing future boards to be added and/or current boards removed as the system design and application evolves. © The Royal Society of Chemistry ⁴³ , 2010.	28
Figure 2.3-A: Operation flow chart of the firmware states as described above. The Esc character is the abort character.	32
Figure 2.4-A: Simplified process flow of the firmware pertaining to the firmware-software interface.....	34
Figure 2.5-A: Class hierarchy of the software	45
Figure 2.5-B: Simplified process flow of the software pertaining to the firmware-software interface.....	48
Figure 3.2-A: A diagram of the system modules necessary for CE, adapted from ⁴³	66
Figure 3.2-C: A diagram of the non-confocal set-up in the custom-built instrument ³⁹ . The laser is focused onto the separation channel over the GRIN lens/interference filter wherein the photodiode collects the light intensity (not drawn to scale). © The Royal Society of Chemistry ⁴³ , 2010.	67
Figure 3.2-D: Ray diagram with the lengths and distances of the optical components (to scale).	69

Figure 3.2-E: Example of isolated, anomalous intensity spikes in the electropherogram due to power cables to other modules passing over the optical detection unit. The bottom part of the figure is the processed signal (see Section 3.2.4), leading to these isolated points appearing to be peaks.71

Figure 3.2-G: Magnitude (left) and impulse response (right) of the software filter.....74

Figure 3.2-H: A diagram of the signal processing flow from the raw data (top left), after the low-pass filtering (top right), and post median subtraction with two different widths: 1500 points (15 seconds, bottom left) and 400 points (4 seconds, bottom right).....75

Figure 3.2-I: Demonstration of how smaller median subtraction lengths lead to unreal artifacts when peaks are close together; 1500 points was used on the left and 400 points on the right.76

Figure 3.2-J: Comparison of the two described signal processing methods for an AlfExpress DNA ladder sample; LPF and median subtraction (1500s) on the left, S.Choi’s method on the right.....77

Figure 3.2-K: An example output jpeg image of the stand alone signal processing executable as developed by S. Choi. The original data file was collected from the custom instrument set-up as described in this thesis and written by the software, as seen in Figure 3.2-J.78

Figure 3.2-L: Diagram illustrating the laser beam’s position in relation to the grin lens and the chip holder, and which directions are defined as x, Y, and Z.....79

Figure 3.2-M: Images of raw data collected after the laser was electrically insulated from the holder but also unexpectedly thermally insulated the laser. Erratic changes in intensity give the dramatic oscillations and mode-hopping behaviour seen here.....82

Figure 3.2-N: An image of the first 25 minutes of a new laser being characterised by the software. The first five minutes are very noisy, but after about 15 minutes of warm-up, the signal stabilises.84

Figure 3.2-O: An image After 100 minutes of the same laser in the previous figure being characterised by the software. Small bursts of noise can be seen in the 110, 115 and 125min traces.85

Figure 3.2-P: Images taken by A. Jang demonstrating the increased roughness on the diced surfaces of the glass plates. On the left, the top plate shows the 1/3 rough and 2/3 smooth surface as described; on the right, the entire diced face is considerably rougher than the cleaner surface on the left.	86
Figure 3.4-A: Limit of detection electropherograms for 0.749 ng/ μ L, 0.498 ng/ μ L, and 0.249 ng/ μ L of end-labelled BKV reverse-primer DNA. © The Royal Society of Chemistry ⁴³ , 2010.	96
Figure 4.2-A: A diagram of the system modules necessary for PCR and PCR-CE, adapted from ⁴³	105
Figure 4.2-B: Diagram of the thermal controller states for PCR. Pre-denaturation and post-extension, if included, have the same states as denaturation and extension, respectively.	107
Figure 4.2-D: Design of the integrated PCR-CE chip, emphasising the PCR section of the microdevice containing the PCR chamber, valves, fluidic channel and wells, and the heater ring of heating/sensing element (labelled parts are not drawn to scale).	111
Figure 4.3-A: Three consecutive microchip-based PCR-CE results. For each run, the primer peak is on the left and the product on the right, representing the presence of BK Virus in the sample.	118
Figure 4.3-B: On the left: an example of a chip loaded multiple times with PCR mix (larger volume of mix in contact with the same surface area). On the right: a chip loaded once with PCR mix. Both on-chip products were analysed on the conventional CE system (same mix used for both experiments).	125
Figure 4.4-A: Wheatstone bridge circuit diagram.....	126
Figure 4.4-C: Images of the calibration data entered into the GUI for the verification of the heater calibration, and examples of the calibration data agreeing with the DMM resistance and not.	140
Figure 4.4-D: experimental predictive functions determined from two different systems by S.Groendahl, with a given heatsink temperature of 23°C for comparison purposes.	146

Figure 4.4-E: A comparison of the system’s experimental predictive function before heat sink temperature was included and after, with set points of 21°C and 26°C.148

Figure 5.1-A: Illustration of the principle of the chargeswitch beads.....157

Figure 5.2-A: Design of the integrated SP-PCR-CE chip, emphasising the SP section of the microdevice. The permanent magnet moves beneath the microfluidic chip along pre-defined paths set by the SP module, manipulating the magnetic beads within this section of the chip (not drawn to scale).160

Figure 5.3-A: This electropherogram demonstrates the successful result of the integrated SP-PCR-CE instrument. Four consecutive runs are shown here to demonstrate repeatability with two negative controls to rule out contamination.164

LIST OF SYMBOLS AND ABBREVIATIONS

μ CE	Microchip CE
μ TK	Microfluidic Toolkit
ADC	Analog-to-Digital Converter
BKV	BK virus
BLAST	Basic Local Alignment Search Tool
bp	base-pairs
CCD	Charge-Coupled Device
CE	Capillary Electrophoresis
CLI	Command-Line Interface
DAC	Digital-to-Analog Converter
DNA	Deoxyribonucleic Acid
EOF	Electro-osmotic Flow
FEM	Finite Element Method
FIR	Finite Impulse Response
FWHM	Full Width at Half the Maximum
GUI	Graphical User Interface
IR	Infrared
LIF	Laser Induced Fluorescence
LOC	Lab-on-a-Chip
LOD	Limit of Detection
LPA	Linear Polyacrylamide
MCA	Melt-Curve Analysis
MCU	Microcontroller Unit
MEMs	Micro-Electro-Mechanical Systems
OS	Operating System
PCB	Printed Circuit Board
PCR	Polymerase Chain Reaction
PI	Proportional Integral
PID	Proportional Integral Derivative
PMT	Photomultiplier Tube

POC	Point-of-Care
RMD	Relative Mean Deviation
RNA	Ribonucleic Acid
SNR	Signal-to-Noise Ratio
SP	Sample Preparation
SPI	Serial Peripheral Interface
TAS	Total Analysis System
TLC	Thermochromic Liquid Crystals
USB	Universal Serial Bus

Introduction

CHAPTER 1

1.1 PROJECT DESCRIPTION

1.1.1 Motivation

Genetic analysis techniques are crucial tools in the medical field used to diagnose diseases, quantify treatment progress with specific medications, and confirm recovery. Countless nucleic acid-based detection technologies have been developed for an amazing range of applications, such as detecting and identifying different strains of malaria, establishing an individual's susceptibility to drug resistance or adverse drug effects, and diagnosing cancer. Unfortunately, the majority of genetic testing is expensive and complex, so these technologies are restricted to advanced hospitals and extensive clinical laboratories in developed countries, with limited to no availability in remote locations and the developing world.

Factors contributing to the cost and complexity of genetic analysis techniques are numerous, and our lab believes the key causes to be as follows:

- The required equipment and supporting infrastructure is expensive; even in a modest diagnostic laboratory, this could be on the order of millions of dollars.
- Much of the required instrumentation is specialized for one specific operation, requiring a single sample to be run through multiple pieces of equipment to complete one standard molecular diagnostic test.
- Extensively trained operators are needed to operate equipment and transfer samples from one machine to another, while ensuring samples and reagents are not contaminated; this not only contributes to the cost of each clinical assay, but also potentially introduces inter-run and inter-operator variability.
- Presently, most processing equipment requires large sample volumes to be taken from the patient and large volumes of costly reagents must be used to

process this sample; this macroscopic analysis contributes to the cost of the test as some of the processing reagents are extremely expensive.

- Due the large costs associated with each test, samples are often gathered from various collection points and processed in one batch. This, in addition to long processing times associated with the specific test, can result in clinical assays taking days and possible lead to sample degradation.

Healthcare for people in both developed countries, remote locations and the developing world could be greatly improved if genetic analysis techniques could be used in medical clinics and point-of-care (POC) settings. The miniaturisation and integration of conventional laboratory equipment onto inexpensive, portable and automated instruments could overcome the aforementioned factors and revolutionise healthcare.

1.1.2 Lab-on-a-Chip Vision

Interchangeably termed lab-on-a-chip (LOC) or micro total analysis systems (μ TAS), this field is aimed at developing micro-scale devices that perform entire analytical processes on a single system. The vision and motivation behind μ TAS is attributed to a publication by Manz *et al.*¹ in 1990, although a few innovative miniaturised analysis systems were reported before this². Manz's paper¹ describes a device that can translate chemical information into electronic information and is a miniaturised version of a conventional total analysis system (TAS) composed of multiple laboratory instruments. While conventional laboratory systems are reliable, they are also bulky and expensive. By replicating the functions of large analytical instruments on small units, reagent and sample consumption are reduced and analysis times are decreased, improving efficiency and thus expense³. Since 1990, a large amount of research has been focused on the development of this field due to its potential to provide point-of-care diagnostics and its implications for drug discovery^{3,4,5,6,7,8,9,10}.

Rapid advancement of LOC devices in the last two decades stems from the application of standard micro-photolithographic techniques developed by the microelectronics

industry to silicon, glass or polymer substrates to create microfluidic-based micro-electro-mechanical systems (MEMs). These microfluidic chips are capable of transporting and manipulating volumes ranging from nL to μL through etched micro-diameter channels. Reducing the dimensions of the flow channels improves limitations associated with analyzing samples with small volumes (increasing the volume leads to a less concentrated sample) and yields better resolution. Moreover, microfluidic chips allow the possibility for integration of various functionalities normally spread across multiple laboratory systems into a single device, improving efficiency and enabling automation of the integrated functions^{4,5}.

Commercial LOC instruments are currently available from many companies employing a variety of diagnostic techniques. However, these systems are quite large and confined to a laboratory bench, like the instruments they were initially meant to replace. For example, the Applied Biosystems 3500 Genetic Analyzer¹¹ has dimensions of 61x61x72cm, weighs 82kg and only performs one step of the genetic analysis process. Similarly, the Agilent 7100 Capillary Electrophoresis System¹² has dimensions of 35x59x51cm and a weight 35kg. While research must still be done to effectively transport conventional assays onto microfluidic devices, a major challenge is miniaturisation of the LOC platform for portability outside of the laboratory and further reduction in testing costs.

1.2 MOLECULAR DIAGNOSTICS

1.2.1 Introduction

The molecular diagnostic process is a relatively complex one, involving many intermediate steps between the sample collection and its detection, and many different types of samples and target information.

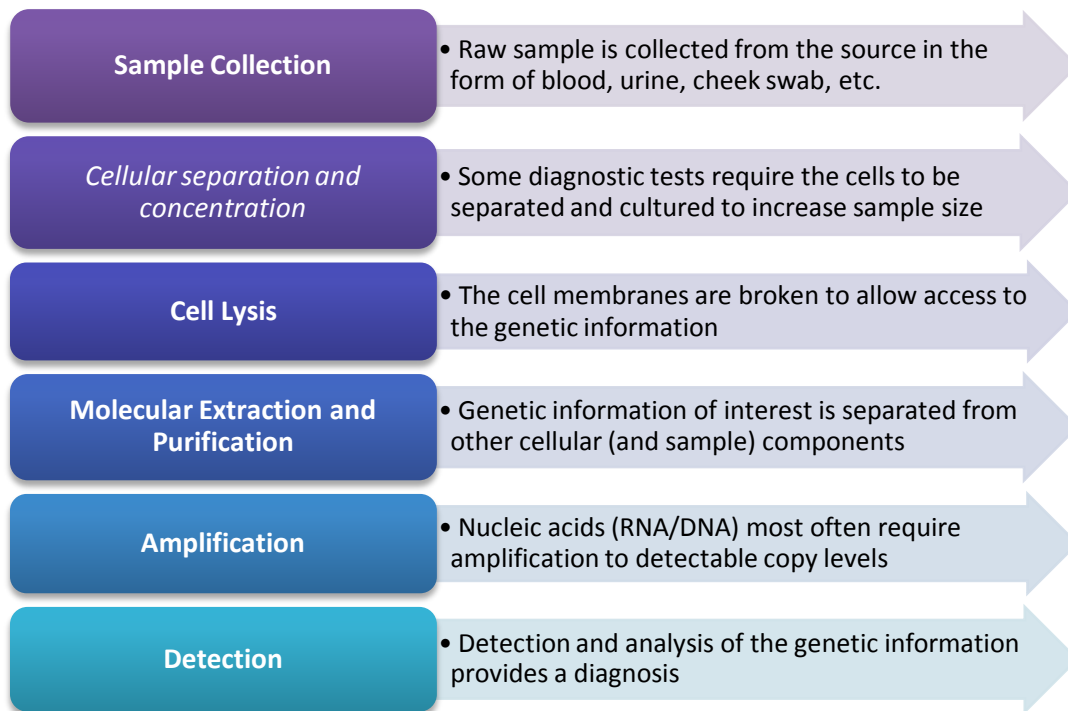


FIGURE 1.2-A: THE GENERAL SAMPLE-TO-ANSWER MOLECULAR DIAGNOSTIC PROCESS

1.2.2 Sample Preparation

In this thesis, sample preparation (SP) will be defined as including all steps from collection of the sample to the molecular extraction and purification. Many different specimen types exist, such as whole blood, serum, saliva, spinal fluid, urine, stool, and biopsied tissues. As one might expect, each of these specimen types must undergo a different sample preparation process to extract the necessary target information. In some cases, this requires the cell to be separated from other collected materials and/or concentrated to increase the amount of target sample such as DNA or RNA. Buccal (cheek cell) swabs are one of the easiest specimens for genetic analysis as they are moderately pure, allowing them to be lysed directly.

CELL LYSIS

Once the cells are separated and/or concentrated, the cell membrane must be broken or disrupted to release the nucleic acids contained within. This process is termed cell lysis. Procedures vary depending on the type of the cell and the steps to follow in the diagnostic process, and these include methods such as the addition of lysing reagents or enzymatic steps¹³.

MOLECULAR EXTRACTION AND PURIFICATION

Once lysis is complete, a variety of extraction and/or purification methods can then be used. Chaotropic reagents are typically used to purify DNA and RNA as nucleic acids bind to silica in the presence of these reagents, and are released when they are removed¹⁴. In this manner, the other cellular components can be washed away, leaving the silica-bound nucleic acids. These are then eluted in water or low salt buffer to detach the nucleic acid.

1.2.3 Amplification

The amount of nucleic acids extracted varies by starting amount of sample, type of sample, the sample preparation technique and the specific extraction protocol, but is on the order of ones to tens of micrograms of DNA from 10^5 - 10^6 starting cells¹⁵. Unfortunately, this extracted number of target molecules is quite often below the detectable level of many analysis methods¹³. For this reason, most molecular diagnostic processes include an amplification step. Many amplification techniques are available, of which the most widely used and most powerful method is polymerase chain reaction (PCR)¹⁵.

POLYMERASE CHAIN REACTION

Polymerase chain reaction is a life sciences technique used to amplify or replicate a specified sequence of deoxyribonucleic acid (DNA) across several orders of magnitude, beginning with a few copies and finishing with hundreds of millions¹³. This is achieved by cycling through three specific temperatures at which the DNA melts, the primers bind

or anneal to the single-stranded DNA template, and the specified sequence is replicated using a DNA polymerase. These replicated portions of the starting DNA strand are then used as a template for the next cycle, allowing amplification to occur exponentially over the course of a few cycles. This “chain reaction” of replication and the DNA polymerase necessary for this reaction to occur provide the name for this technique.

Specifically, PCR can have five steps: an optional initialising step (pre-denaturation), a final step (post-extension), and the three cycling steps which are repeated (denaturation, annealing and extension); one set of three is defined as a “cycle”. The initialising and final steps (if present) are usually on the order of several minutes, cycling steps on the order of tens of seconds, and approximately 25-35 cycles are used.

1. **Pre-Denaturation:** this is an optional initialising step and consists of holding a high temperature (92-98°C) to either heat-activate specific DNA polymerases¹⁶ or to ensure the denaturation of complex DNA molecules.
2. **Denaturation:** the first step of the cycle also consists of holding a high temperature (92-98°C). Here, the hydrogen bonds between the complementary bases of the double-stranded template are broken, denaturing the DNA and producing single stranded DNA.
3. **Annealing:** the second step of the cycle consists of holding a lower temperature (50-60°C) to allow hydrogen bonds to form between the primers and the target region on the DNA template, a process known as annealing. The DNA polymerase then binds to the annealed primer.
4. **Extension:** the third step of the cycle holds a mid-temperature (70-80°C) wherein the DNA polymerase synthesises the product strand by adding bases complementary to the template strand in the 5' to 3' direction of each primer, “extending” the primers. The time necessary to synthesise the target region depends on the DNA polymerase used and the length of the region.

Now, the amount of double-stranded DNA that was present at the beginning of the cycle will be doubled, and will be the template for the next cycle. This allows for exponential DNA synthesis.

5. **Post-Extension:** this is an optional final step and also consists of holding a mid-temperature (70-80°C) to ensure that any remaining single-stranded DNA is extended.

PCR is usually executed in small, sealed reaction tubes using a commercial thermal cycler which heats and cools the tube via a metal holding block and heated lid. Many reagents are required for successful PCR:

- *DNA template* – double-stranded DNA molecules containing the target region to be amplified; the target cannot be synthesised from nothing. In a diagnostic test, the lack of amplified product will then indicate that the target molecule (e.g. viral DNA species) is not present in the patient sample.
- *Two complementary primers* – single-strands of nucleic acid complementary to the ends of the target region to be amplified.
- *DNA polymerase* (most often, Taq polymerase) – the enzyme required to extend the primers and synthesis the new strand of DNA.
- *dNTPs* (deoxynucleoside triphosphates) – the building blocks for the nucleotides to be polymerised by the enzyme.
- *Ionic Aqueous Solution* – this includes the buffer necessary to achieve a stable, suitable chemical environment for the DNA polymerase, and magnesium (Mg^{2+}) and potassium (K^+) ions necessary for DNA synthesis.

1.2.4 Detection

Once enough analyte is present, it must then be detected. The ability to separate and identify specific components and molecules of a sample is a critical requirement for any

type of diagnostic testing. There are a few methods with which to detect genetic information, and electrophoresis is one of the most common methods.

ELECTROPHORESIS

Electrophoresis is the movement of dispersed ionic molecules within an aqueous environment under an applied, uniform electric field. By applying an external electrical field to the ionic molecule contained in the fluidic medium, the charged particle moves towards the opposite pole with velocity:

$$v = \mu_E E \quad \text{EQUATION 1.2-A}$$

where μ_E is the electrophoretic mobility of the species and E is the applied electric field. This creates a counteractive resistive frictional force with the surrounding environment that is dependent on both the physical properties of the particle and the fluidic medium, as defined in the electrophoretic mobility:

$$\mu_E = \frac{q}{6\pi\eta r} \quad \text{EQUATION 1.2-B}$$

where q is the charge, r is the ion's Stokes' radius, and η is the viscosity of the fluidic medium¹⁷. Thus, electrophoresis allows molecules to be separated by their physical characteristics such as size and charge.

Gel Electrophoresis

Upon the discovery of electrophoresis as a separation technique, it was found that the separation efficiency in a buffer or free solution was limited by thermal diffusion and convection. Thus, this analysis technique has conventionally been performed in porous and solid separation media such as polyacrylamide or agarose gel sections and has subsequently been named (slab) gel electrophoresis.

Quite often, ethidium bromide is used to stain DNA molecules when they are placed into the gel. An electric field is then applied to the gel via an electrophoresis chamber,

and the DNA moves through the gel due to the negative charge of the phosphate backbone in the slightly basic pH environment (usually ≈ 8). The gel aids in the separation by size of the DNA molecules as the gel chains restrict the movement of larger molecules more than smaller molecules. Once electrophoresis is completed, the gel is removed from the electrophoresis chamber and a photograph is taken with the gel exposed to ultraviolet light only. This illuminates the DNA via the ethidium bromide, and the distance the DNA travelled through the gel then determines its size.

Capillary Electrophoresis

Like gel electrophoresis, capillary electrophoresis (CE) derives its name from the capillary which is used to contain and separate the analytes. Narrow capillaries have large surface-to-volume ratios and low conductance, allowing for effective heat dissipation. Thus, capillaries can be filled with either a free solution or a gel like the polyacrylamide or agarose used in gel electrophoresis and can make use of high voltages, leading to shorter analysis times and higher performance.

However, in capillary electrophoresis, acidic silanol groups on the capillary wall form a negative charge when in contact with the buffer solution. Cations build up on the surface of the wall to maintain electroneutrality, forming an electric double layer. When the electric field is applied, these cations are attracted to the negative electrode and the solution molecules move with them. This causes the electrolyte to flow along the capillary, as determined by the charge on the capillary (ζ), the electrolyte viscosity (η) and the dielectric constant (ϵ)¹⁸:

$$\mu_{EOF} = \frac{\epsilon\zeta}{\eta} \quad \text{EQUATION 1.2-C}$$

and is called electro-osmotic flow (EOF). This also affects the velocity of the analytes, positively or negatively depending on the analyte charge.

$$v = (\mu_E + \mu_{EOF})E$$

EQUATION 1.2-D

With negatively-charged DNA, the EOF affects the velocity of the DNA negatively as the DNA is moving against the solution flowing with the cations in the opposite direction. This and other capillary wall effects (such as DNA adsorption) can lead to peak broadening, which lowers sample resolution and sensitivity. To counteract this, the channel surfaces are coated to prevent interactions with the reagents and suppress EOF.

In capillary electrophoresis, absorbance and fluorescence optical detection methods are commonly used. Both methods involve placing a source and detector at one place along the capillary – usually near the end – which is optically transparent. The source then illuminates the solution and analyte as it passes, and the detector collects the data with respect to time. This allows for simpler detection than gel electrophoresis and thus, automation.

This leads to an electropherogram or a plot of intensity versus time. Positive or negative peak(s) (depending on whether the detection method is fluorescence or absorbance, respectively) indicate the time the analyte(s) passed the detector. The length of the capillary from the sample's introduction to the detector, the arrival time and applied electric field can then be used to determine the analyte mobility and its physical properties. The height of the peaks can also provide information about the concentration of the analyte.

While absorbance detection is a well-established macro-structure analytic detection system used for conventional capillary electrophoresis and other techniques in diagnostic laboratories, it does not translate well to microfluidic devices. It is severely limited by the short optical paths in microdevices which lead to weak optical absorption competing with high background transmission noise and significantly impacts its sensitivity¹⁹. Conversely, fluorescence detection – specifically laser-induced

fluorescence (LIF) – has become one of the most commonly used detection methods in microchip capillary electrophoresis (μ CE).

LASER-INDUCED FLUORESCENCE

Fluorescent compounds – structurally rigid compounds with unsaturated or aromatic functional groups called fluorophores – emit fluorescence when excited by light or other electromagnetic radiation. The incident energy absorbed by the fluorophore excites an orbital electron to a higher quantum state, where it then relaxes to its ground state by releasing a photon of light. Usually this photon is released with less energy and thus at a longer wavelength than the excitation source. The excitation and fluorescence wavelengths are very specific to each type of fluorophore molecule, allowing target fluorophores to be excited and detected selectively by varying the wavelength of the excitation source.

The sensitivity of fluorescence detection depends on the background signal (i.e. non-fluorescent light collected by the detector) which is made up of impurities in the sample, Rayleigh and Raman scattering. These effects scale down linearly with respect to the detection volume²⁰ and thus fluorescence detection achieves much higher sensitivities at smaller sample volumes. This makes it particularly useful for microfluidic devices, wherein the sensitivities of other detection methods (e.g.: absorbance detection) decrease with the detection volume.

A variety of excitation sources are available including lasers, LEDs and lamps. Lamp sources are less expensive and most flexible in terms of wavelength; however, laser-induced fluorescence (LIF) is most easily adapted to the dimensions of the microfluidic chip as the focal point of the laser is easily positioned onto the microfluidic capillary. Furthermore, low background noise and high irradiation of LIF results in one of the lowest LODs for all optical detection techniques²¹.

However, most samples must be labelled with a fluorescent tag to be detected (few molecules autofluoresce). The disadvantage of this is additional sample preparation

must be executed prior to detection. However, selective labelling followed by selective detection results in significantly lower background noise, making the detection of fluorescently-labelled analytes simpler than absorption techniques.

Numerous fluorescent molecules are commercially available with excited and emission wavelengths for any region in the visible light spectrum. These are often included in kits to bind fluorophores to many different analytes, such as DNA, protein and cells, and added to primers for selective labeling during PCR. Thus, LIF detection can be applied to wide range of applications, including diagnostic genetic analysis processes.

1.2.5 Conclusion

As can be seen from above, much of the diagnostic process is separated into unique steps, most of which require specialised one-function equipment (e.g. thermal cyclers for PCR, electrophoresis chambers for gel electrophoresis) and extensive operator handling between and during steps. This contributes significantly to the cost of the process, the potential for sample contamination and operator error, and impacts workflow.

For these reasons, a single instrument capable of performing all steps from sample preparation to detection with minimal operator intervention using disposable test cartridges is highly desirable. Furthermore, to make this instrument available to point-of-care applications, it must also be portable and inexpensive, unlike most current laboratory systems.

1.3 LAB-ON-A-CHIP SYSTEMS

For LOC systems to replace conventional clinical equipment in the simplest manner possible, they need to have processing techniques similar to protocols molecular biologists are familiar with, and have the same or greater sensitivity and reproducibility of current methods. As described in the previous section, polymerase chain reaction

and electrophoresis are widely-used techniques for amplification and detection in clinical laboratories. Thus, although a number of genetic analysis systems have been demonstrated in the academic literature (for which a number of excellent reviews are available^{22,23,24}), here we will briefly discuss microfluidic chips and instruments built for PCR-(LIF)CE.

1.3.1 Microfluidic Chips for PCR-CE

To enable both PCR and CE techniques on one genetic analysis system, it must first have a single microfluidic chip capable of both PCR and CE. Four elements critically impact the process integration: the material the chip is made of, heater and temperature sensor designs for thermal-cycling during PCR, microvalves for fluid sample partitioning, and transport methods for fluid handling between analytical steps.

The chip material is extremely important as the choice of substrate affects the design, fabrication and operation of the chip. Glass is the most widely used material for genetic analysis microdevices due to its high dielectric strength, transparency for optical detection, and mature surface chemistry manipulation. However, its high material cost and complex fabrication make it unattractive for disposable chip usage. In addition to this, the heating and cooling rates for PCR are quite slow with primarily glass chips due to the large thermal mass. Adequate surface passivation must also be employed to prevent deactivation of the Taq polymerase during PCR²⁵ and attraction of DNA to the micro-channel walls during CE. Conversely, if left unpassivated this same surface allows for EOF desired for many applications and the etching process required to fabricate its channels also cleans the surfaces²⁶.

As discussed previously, PCR requires accurate, and often accelerated, temperature control for thermal cycling of reagents within a micro-containment chamber. Temperature control methods can be broken up into two groups: contact and non-contact heating. Contact heating approaches involves direct contact between the material surrounding the micro-chamber and the heating device, including external heaters such as Peltier heaters and integrated heaters in the form of microfabricated

thin films. Non-contact heating uses electromagnetic induction (e.g.: infrared (IR) irradiation) to heat the contents of the micro-chamber²⁷. While both heating methods are feasible in a laboratory setting, contact heating is more suitable for point-of-care (POC) applications as it is readily miniaturised and integrated onto the microfluidic device.

Microvalves are an essential component in PCR-CE microfluidic chips for isolation of fluids in the micro-containment chamber and fluid partitioning between the integrated PCR and CE functionalities. These miniaturised and integrated valves can be broken into active and passive valves, which can further be classified into mechanical and non-mechanical²⁸. Active non-mechanical valves include materials that undergo a phase change when activated, while passive non-mechanical valves include hydrophobic and gel valves. Electromagnetic, piezoelectric and pneumatic valves are categorised as active mechanical, and are the most common microvalves in PCR-CE microdevices due to their performance²². However, passive mechanical valves (e.g.: flaps, membranes, spherical balls²⁸) are also seen in PCR-CE microchips as they act like a check valve between the viscous separation matrix used for CE and the PCR mixture within the micro-chamber due to their one-way behaviour. Factors such as normal operation mode (open or closed), dead volume, power required for actuation, fabrication complexity and cost must be considered when choosing a microvalve for an integrated PCR-CE chip²⁹.

The seamless transport from one analytical step to another is also crucial to integrated PCR-CE microfluidic chips to remove operator handling steps. Transport methods include the use of active pumps, electric fields, DNA capture-and-carry structures (e.g.: magnetic beads), and capture filters such as solid phase columns³⁰. Active pumps and electric fields are simple, but require timing optimization and volume changes during transport can lead to the dilution or loss of the sample, which is less of an issue with capture methods²².

The Mathies group first demonstrated an integrated PCR-CE device³¹ made of two bonded glass wafers, the first containing the etched channels and chamber for the

fluidic layer, and the second the micro-fabricated thin film Ti/Pt heater and RTD sensor. The PCR chamber was connected directly to the CE separation chamber, with the sieving matrix-PCR mixture interface acting as a passive mechanical valve. Hydrophobic vents and valves were also included on the device to allow for the use of vacuum and positive pressure for active transport of the PCR mixture to the micro-chamber and isolation of the reagents during thermal cycling. These were constructed using latex membranes and o-rings that were applied external to the fabricated chip. Electric fields used for microchip capillary electrophoresis were used to draw the sample from the PCR step into the injection arm of the micro-channels for CE.

Further development³² included the patterning of high voltage electrodes on the second glass wafer for CE, and two glass-PDMS wedges to fit on top of the fluidic glass wafer for valve control. A subsequent design³³ further involved moving the micro-channels to allow for inline injection of the sample for CE.

The Landers group demonstrated a fully integrated microfluidic device that not only performed PCR-CE, but sample preparation (SP) as well²⁷, with the same glass-PDMS-glass-glass layer system as seen in the Mathies chips. Fluidic isolation was accomplished using differential channel flow resistances, elastomeric valves and laminar flow. Infrared thermal cycling was used to amplify the sample, and both electrokinetic mobilization and on-chip pressure injections of product were used to inject the product into the separation micro-channel for CE, with the latter more reproducible.

A fully integrated SP-PCR-CE device was also demonstrated by the Burns group³⁴. This microchip uses a glass substrate to contain the fluidic layer, a silicon substrate with a Ti/Pt thin film heater, and a parylene layer to bond the two substrates. Both pneumatic valves and phase change valves were used for fluid partitioning. These pneumatic valves were also used as active pumps for fluid transport within the device, and channels were etched to allow for mixing between analysis steps.

These microfluidic chips demonstrate the state of the art in terms of integrated functionality and performance in the academic literature; however, these devices are

primarily operated by expensive and bulky systems confined to laboratory benches which do not address the portability and cost-effectiveness required to improve healthcare. For example, while infrared thermal cycling provides a non-contact method for quick heating, it requires large power resources that make it unsuitable as a heating method of LOC devices for POC applications.

1.3.2 Lab-on-a-Chip Systems for PCR-CE

The first fully portable, integrated PCR-(LIF)CE system was demonstrated by the Mathies group for pathogen detection³². It contained electronics for sensing and powering the PCR heater and high voltage supplies for performing CE separations. It also employed an optical system for CE detection, consisting of a frequency-doubled solid-state laser, dichroic beam splitters, confocal optics, and photomultiplier (PMT) detection. Using this system, amplification and detection of *Escherichia coli* and *Staphylococcus* was performed in approximately thirty minutes.

This system was further developed and applied to forensic short tandem repeat typing³³. In addition to the electronics for PCR and CE as the original system, this instrument also contained pneumatics for the on-chip microvalves. The optical system was further outfitted to contain a detection cube made of multiple filters, dichroic beam splitters and lenses, coupled to four PMTs so as to detect four different fluorescence wavelengths. It was operated using two National Instruments DAQ boards.

Another PCR-(LIF)CE system has been developed by the Sandia group for point-of-care detection of biotoxins³⁵. This prototype instrument integrates miniaturized electronics, optical components, fluid-handling elements, and data acquisition software onto one portable, self-contained platform. The optical system was composed of two laser diodes, two mirrors and an aperture-lens pair for delivery of light to the microdevice, two filters and an aspherical lens for light collection, and a PMT for detection³⁶. However, it should be noted that the compact, prototype instrument was not operated with all of these functionalities integrated into the device. Rather, the separate components were operated independently, with the future possibility of integration.

These instruments demonstrate the state of the art in terms of functionality and performance in the academic literature, with efficient PCR-CE analysis times (less than 30 minutes) and small volume manipulation. However, these systems primarily contain complex optical sensing systems comprised of confocal components and PMT-based detection, making them relatively expensive and bulky. Much effort is still necessary to miniaturise, automate, and improve the cost of these systems to make them available for point-of-care applications¹⁹.

Commercially, instruments tend to use very specific and expensive cartridge-like devices which limit the potential for development of microchips for a wide range of applications using those systems for implementation. Furthermore, while CE and PCR systems are available, an integrated PCR-CE system is not yet to be available. Examples are CE analysis systems (Agilent 2100³⁷, Shimadzu MCE-202 MultiNA³⁸, Hitachi SV1100 & SV1210³⁹), RT-PCR (Idaho Technologies' Razor Ex⁴⁰), and PCR with microarray-based detection (ST Microelectronics' In-Check⁴¹).

Thus, to the best of our knowledge, there have been no inexpensive PCR-(LIF)CE instruments demonstrated in the academic literature or commercial products.

1.4 SCOPE OF THESIS

Our lab is exploring what we feel is a necessary step for the actual use of LOC systems in traditional healthcare: the reduction in cost of the infrastructure required to operate the many devices demonstrated by the LOC community and the application of technologies already familiar to healthcare professionals, to attempt a smoother transition from conventional instruments to LOC systems. We do this by continuing to demonstrate systems significantly less expensive than what is currently available commercially and in the literature and attempt to design and build an instrument that can be used for many whole-molecular biology applications.

This thesis addresses the need for inexpensive, portable and integrated systems by contributing to the development of a modularised, less costly version of previous systems developed in the laboratory. System development is divided into four chapters, the first of which describes the architecture of the instrument, while the remaining three explore the implementation of one step in the diagnostic process and how the system was augmented to support and improve the sensitivity of this functionality.

The microfluidic platform design is discussed first in Chapter 2 as the system's main structure is the same for any molecular biology protocol: electronic hardware for controlling and sensing of the chip; and, firmware on a microcontroller and/or software on a laptop computer to control the hardware. Specifically, fluid-handling, temperature control, high voltage, and analyte detection are functionalities necessary for almost any genetic analysis application. To improve the ability to customise these capabilities for multiple molecular diagnostic techniques, update and debug the system without significant overall changes required, and miniaturise these modules for future improved cost and portability, this instrument was redesigned with an emphasis on modularity. Electronic modules are separated into distinct functionalities via separate printed circuit boards and are linked to a microcontroller via a communication bus using a standard serial peripheral interface protocol. The firmware controls and reads in sensing data from the electronics, and with standardised interface protocol, the hardware modules and firmware can be upgraded and improved independently. However, it is difficult for a single microcontroller to be responsible for all of the required system tasks if a high sampling rate is required for sensitive detection (i.e. to remove noise sources). Conversely, it is not recommended to trust precise timing of external equipment to a personal computer where multi-tasking operating systems can lead to erratic timing. With these considerations, in-house software with a graphical user interface was designed to execute logging, processing and interpreting commands required by a molecular diagnostic platform, while time-critical functions that could be performed within the sampling and reporting interval of the microcontroller were included in the

microcontroller's custom firmware. Furthermore, with a set of communication interface rules, the firmware and software are also able to be updated independently. This modularity allows easy integration of new system functionalities without altering the structure of the hardware, firmware and software's interaction. Although written and altered by multiple people, the author of this thesis played a key role in the development of the firmware, and its limitations and operation flow will be discussed here. The command-line interface protocol outlines the interaction between the firmware and the software, and will be detailed next as it was both written and maintained by the author over the course of this project. Furthermore, Chapter 2 will explore the software's modularity and functionality, of which the author was the sole developer.

Once the hardware, firmware and software components of the system were ready, they were combined first as a system outfitted for CE, and subsequently PCR-CE and SP-PCR-CE. In this manner, the author could assess the associated challenges with each step of the biological process, implement required solutions, and determine the system performance of each function, independently.

In Chapter 3, the last step of the molecular diagnostic process is implemented – analyte detection and analysis through the application of capillary electrophoresis. CE has matured as an analytical technique in the decades since it was first scaled onto microfluidic chips and is capable of detecting analytes from a large variety of applications. Unfortunately, microchip CE is limited by the bulky confocal optics and high voltage components required to operate the microfluidic chip, making it not suitable for POC applications due to size, cost and complexity. It is possible to use inexpensive, scalable components in a non-confocal set-up, but to have diagnostically relevant sensitivities, these detection schemes tend to still rely on expensive components. Here we present a non-confocal, inexpensive and scalable system configured for CE that can detect analytes from relevant life science procedures with sensitivity comparable to conventional processing techniques and commercial CE

instruments. In this chapter, the key challenges involved with the system implementation of CE, required protocol developments and the system's subsequent performance are described. In addition to the system level design described in Chapter 2, the software signal processing method developed by the author of this thesis will be described here, and its effectiveness for different types of sample will be explored along with specific challenges these samples introduced. Through extensive testing of the microfluidic platform configured as a CE instrument, the author identified four key optical challenges which dramatically impact the system's limits of detection, and these will also be discussed here. With these factors fixed, the author then demonstrated that the CE instrument was comparably sensitive to gel electrophoresis run routinely in clinical laboratories and only slightly less sensitive than a considerably more expensive commercial CE instrument. System and protocol performance is determined here by the author in terms of DNA mobilities, resolution, run-to-run and load-to-load variability, and sensitivity.

Chapter 4 builds on the previous chapter and the molecular diagnostic process through the implementation of the amplification technique of polymerase chain reaction and its integration into the instrument. A major challenge of developing portable and inexpensive LOC platforms is achieving the precise temperature control and local environment factors necessary for genetic amplification. The academic literature describes other microfluidic instruments capable of PCR-(LIF)CE, but most of these instruments use considerable external infrastructure and/or high power consumption methods for heating that confine these systems to the laboratory bench. Here we improve upon our previous implementations with modularisation, better chip calibration and fabrication, the addition of a heat-sink, and better thermal control. Through extensive verification of the instrument for both PCR and PCR-CE, the author determined the system performance, which was found to be able to detect down to 10^5 /mL of starting template (approximately one copy in the chamber) and had variabilities comparable to the conventional instrument. However, even though the

system amplified and detected all analytes, verifying its reproducibility for the chosen application, the lower efficiency of the amplification process as compared to the commercial instrument was not desirable. Thus, once the system was verified, the thermal control of the system was subsequently analysed by the author, key issues and challenges with the design will be identified here, along with a brief description of how these have been addressed by other members of the group after this thesis project's completion.

The sample used primarily throughout these two chapters is purified BK virus (BKV) template and purified Cy5 end-labelled BKV PCR products. BK virus has been found to cause the rejection of renal transplants when present in high concentrations in transplant patients. Thus, BKV is a clinically relevant sample, and its amplification and detection in this thesis demonstrates this system's capability to be adapted to other PCR-(LIF)CE protocols as well.

When considering how to quantify distribution for experimental variabilities in this thesis, it was noted that: a) it is unknown if all points exhibit a normal distribution due to the small sample sets; and b) some measurements may include unavoidable errors such as longer laser focusing time leading to greater diffusion of ions. For these reasons⁴² and the fact that this technique is much easier to understand than standard deviation, the average absolute deviation (also known as mean deviation) is used to quantify variabilities in this thesis. Mean deviation is the average of a sample set's absolute values from a central tendency of the data set; due to the small data set, the mean was chosen as the central tendency for this work. Microsoft (MS) Excel implements this statistical function as $AVEDEV(num_1, num_2, \dots, num_n)$. Furthermore, since peak strength is given in voltage – a scale dependent on the gain of the amplifier of the optical unit – relative mean deviation (RMD) is used. The RMD is the mean deviation expressed in percentage of the average measurement (e.g. intensity, time), or in MS Excel: $(AVEDEV(num_1, \dots, num_n)/AVERAGE(num_1, \dots, num_n))*100\%$.

Chapter 5 of this thesis briefly discusses the integration of a sample preparation unit developed by other members of the lab to allow the full molecular diagnostic protocols from collection to detection to be performed on our inexpensive, portable instrument. Adhering to our goal of portability and modularity, this module was based on conventional nucleic acid extraction methods using paramagnetic beads and was first developed as a separate unit before its integration. Here, nucleic acids are extracted from buccal cells and a sequence unique to the β 2-microglobulin gene (described further in Section 5.1.3) is amplified and detected via PCR-CE. This chapter's presence is secondary to the previously described chapters, however, as the author was included at the end of the sample preparation project to aid in its integration with the system tested extensively as a PCR-(LIF)CE instrument. In addition to contributing to the SP unit's integration via the command-line interface, software, and established protocols, the author also evaluated the modified system's performance based on previous characterisations.

Modular and Scalable System

CHAPTER 2

2.1 INTRODUCTION

While the LOC community has made significant progress transferring molecular biology protocols onto microfluidic chips, LOC technologies see minimal use outside of the academic laboratory. For these technologies to be more readily adapted in conventional laboratories and used in POC applications, a cost-effective and portable platform must be developed¹⁹. We further believe that this platform should be reconfigurable to enable a wide range of life-science procedures rather than a one- or two-process instrument.

To realise such a system, it is necessary to integrate fluid-handling, temperature control, high voltage, and analyte detection functionalities necessary for many microfluidic diagnostic assay techniques. Towards this goal, our lab demonstrated a \$1000 genetic analysis instrument using discrete components⁴³ shortly before this thesis project began. However, due to limitations with its choice of optical detection system (described further in Chapter 3) and its non-modular design, this system was ultimately neither easily automatable nor suitable for miniaturisation and was still costly.

To improve the ability to customise the instrument for multiple diagnostic techniques, update and debug the system without requiring significant full-system level changes, and shrink these modules to improve portability and cost, this instrument was redesigned with an emphasis on modularity⁴⁴. By developing each of the above functionalities as a separate unit, testing and integrating them into the system, it was possible to build a genetic analysis diagnostic instrument that is inexpensive, portable and miniaturisable. Furthermore, as fluid-handling, temperature control and optical detection are necessary for a wide range of life-science procedures, this system is also customisable.

Modular and Scalable System

In this thesis, the system is customised as a PCR-(LIF)CE instrument as shown in Figure 2.1-A, with a component cost of \$600 and sensitivities comparable to relevant conventional equipment (as described in later chapters). With inexpensive, portable systems similar to the instrument demonstrated here, we believe the continuing transfer of molecular biology protocols to LOC technologies by the wider community will be more readily adapted into clinical laboratories, revolutionising the healthcare system.

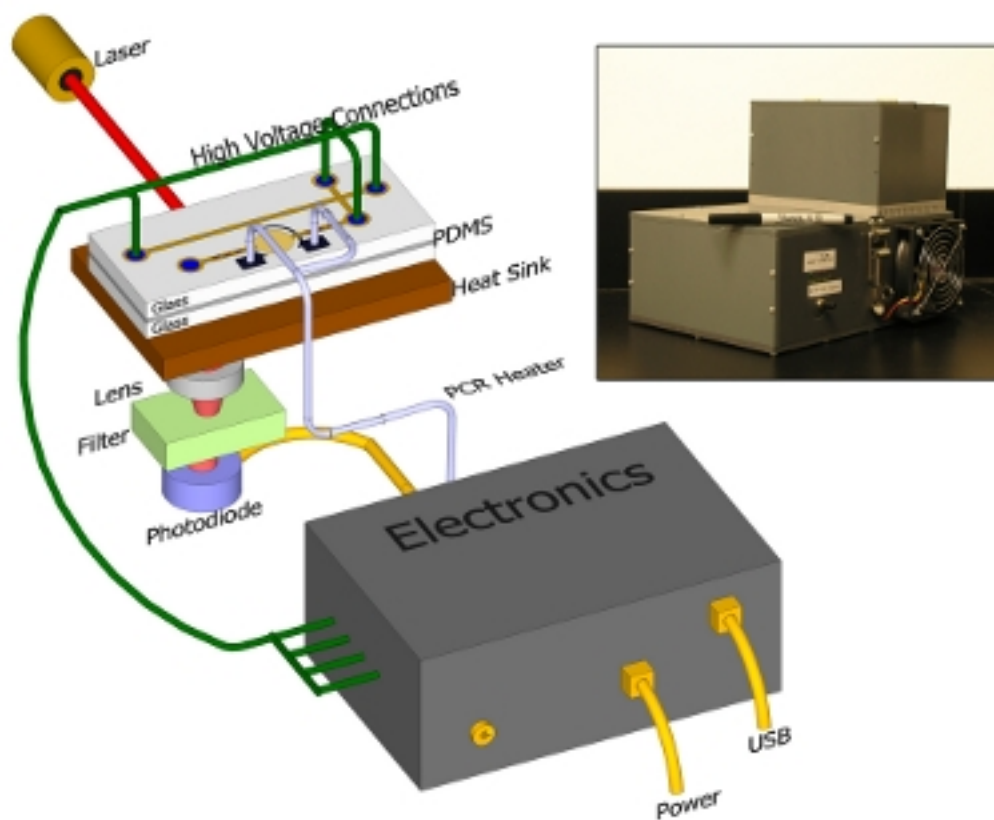


FIGURE 2.1-A: DIAGRAM OF OUR DEVELOPED LAB-ON-A-CHIP TOOLKIT SET-UP AS A PCR-(LIF)CE INSTRUMENT. THE INSET FIGURE IS AN IMAGE OF THE ACTUAL INSTRUMENT, WITH DIMENSIONS OF 30X20X11 CM FOR THE ELECTRONICS BOX, THE TOP BOX CONTAINING THE MICROFLUIDIC CHIP. © THE ROYAL SOCIETY OF CHEMISTRY⁴³, 2010.

This chapter is based on the architecture of the developed microfluidic platform, with testing of the genetic analysis toolkit's molecular diagnostic implementations described in subsequent chapters. Any LOC platform will need electronic hardware for controlling

and sensing of the microfluidic chip and firmware and/or software to control the hardware. Our system’s main structure is made up of three components: electronic hardware for controlling and sensing of the microfluidic chip; firmware on a microcontroller to monitor the hardware and perform time-critical tasks; and software to operate the instrument via the firmware, log collected data, and process, interpret and present the experimental data in a format a molecular biologist can understand. Both firmware and software were implemented due to the high sampling rate found necessary for precise detection of analytes as seen in previous demonstrations by our lab^{45,46}. With the frequent timer interrupts used with high sampling rates, it is difficult for a single microcontroller to take responsibility for and execute all tasks required by the microfluidic platform within a very small time window. However, it is also not advisable to leave operations that require precise timing to software loaded on a desktop/laptop computer, where multi-tasking operating systems (e.g. Windows) can lead to erratic timing. With a timer-interrupt of 10ms for the initial 100Hz optical detection sampling rate (see main.c in Supplementary CD/AML Files/TTK/Firmware), and the knowledge that we may need to increase this rate depending on noise sources of data and for some applications, only time-critical functions that could be performed within this time interval were included in the microcontroller unit’s (MCU) custom firmware. The software was then designed to generate the graphical user interface (GUI) and execute the remaining logging, processing and interpreting commands.

TABLE 2.1-A: DELEGATION OF THE REQUIRED OPERATION TASKS FOR THE GENETIC ANALYSIS SYSTEM BETWEEN THE MICROCONTROLLER AND THE GRAPHICAL USER INTERFACE

Required Tasks	Given to
Collect and store run-specific information from the user	GUI
Initialise electronics	MCU
Read from the electronics during experiment	MCU
Adjust parameters as necessary based on incoming data	MCU
Log read data	GUI
Complete test and return electronics to an idle state	MCU
Process and interpret collected data	GUI
Provide user with run information, collected into a tidy report	GUI

Modular and Scalable System

The software is stored on an external laptop computer, and with input from the user, commands the firmware to set and collect data from multiple hardware modules linked to the microcontroller. In this manner, each system component (hardware, firmware and software) has its own distinct responsibility. This separation of functionality allows for necessary timing and processing tasks to co-exist, and with a set of communication interface rules (as depicted in Figure 2.1-B), further allows each standard module to be updated independently. In this way, optimisation of the firmware code or further development of the optical detection module, for example, can be done with no concern to higher level processes due to the thoroughly documented interface protocols.

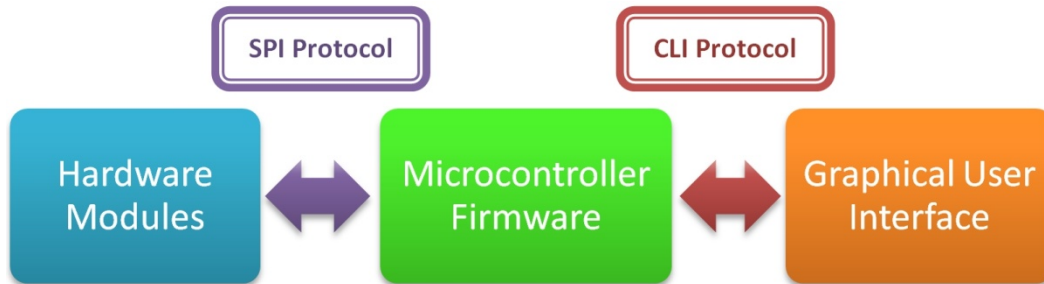


FIGURE 2.1-B: DIAGRAM OF THE THREE SEPARATED FUNCTIONALITIES OF THE INSTRUMENT COMPONENTS AND THEIR INTERFACE PROTOCOLS THAT ALLOW FOR INDEPENDENT UPGRADES OF THE HARDWARE, FIRMWARE AND SOFTWARE.

Although the system hardware units were designed before this thesis project began and thus were not contributed to by the author, they will be described briefly for completeness in Section 2.2. Each of these hardware units addresses one of the aforementioned molecular biology functionalities (e.g. fluid-handling, thermal control) and allows for a custom instrument to be assembled for multiple applications.

Section 2.3 will discuss the specifications of the firmware used on the system's microcontroller. While the author of this thesis played a key role in the development of the firmware, it was written and contributed to by multiple people over the course of this project. As such, emphasis will be placed on the firmware's limitations and

operation rather than on its design. The exception to this is the thermal controller, which will be discussed in detail in Chapter 4 (Section 4.2.1).

Section 2.4 will present the command-line interface protocol and challenges with its design. Its purpose is to outline the software's interaction with the custom firmware, the process flow with which they converse and the commands it uses to control it. This protocol was written and maintained by the author of this thesis.

Following this, Section 2.5 will explore the software, of which the author is the sole developer. The software was written to be modular, much like the firmware, with the majority of its modules called in a class hierarchy format. This allows new features and molecular biology functionality to be added or altered with minimal to no impact on its main routine. Following a brief description of each of the modules and their purpose, the genetic analysis protocol files created by the software will be briefly described. The chapter is then concluded in Section 2.6 with a summary of the issues discussed and suggestions for future work.

2.2 HARDWARE

Electronic modules are separated into distinct functionalities via separate printed circuit boards (PCBs). These modules are then linked to the PIC microcontroller (PIC 18F4550, Microchip Technology Inc., AZ, USA) on a communication bus using standard serial peripheral interface (SPI) protocol. This allows each module to be individually addressable using a set of standardised commands and each system to have customisable functionality. Furthermore, as long as the SPI commands remain unchanged, each module may be significantly improved without affecting the higher levels of instrument (firmware, software, and user).

To minimise the amount of electrical noise delivered to each instrumentation module, the power regulation and distribution unit takes input at 24 V and 3A from a laptop power supply connected to a standard electrical outlet, and then regulates this input

and distributes “clean power” to the other system modules at +24V, ±14V, and +7V. Each system board then regulates the ±14V and +7V supplies into ±12V and +5V to further suppress any noise that may have been picked up from other electronics within the instrument.

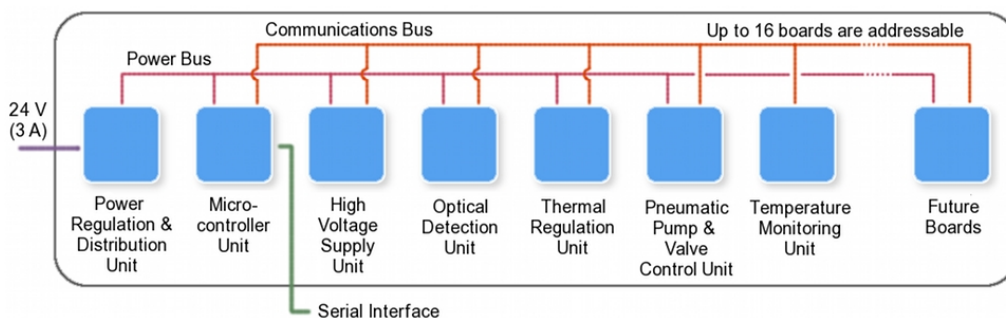


FIGURE 2.2-A: DIAGRAM OF THE MODULAR ARCHITECTURE OF OUR DEVELOPED INSTRUMENTS’ DESIGN. IT IS BASED ON MULTIPLE SINGLE-FUNCTION ELECTRONIC BOARDS WITH COMMON POWER AND COMMUNICATION BUSES, ALLOWING FUTURE BOARDS TO BE ADDED AND/OR CURRENT BOARDS REMOVED AS THE SYSTEM DESIGN AND APPLICATION EVOLVES. © THE ROYAL SOCIETY OF CHEMISTRY⁴³, 2010.

HIGH VOLTAGE SUPPLY UNIT (REV03)

The HV unit is designed to supply the high voltages necessary to perform microchip capillary electrophoresis. Using the power supplied by the regulation and distribution unit, this board uses an EMCO DC-DC converter (C60, Sutter Creek, CA, USA) to generate up to 6 kV. Four relays on this board then control the state of the four platinum electrodes interfaced with the microchip. Three states are possible: fixed voltage, electrical disconnect (so the electrode is effectively floating), and ground.

OPTICAL DETECTION UNIT (REV03)

Discussed in more detail in Section 3.5, this module consists of a laser, photodiode, amplifier and 16-bit analog to digital converter with a lens and interference filter placed in the optical path, external to the PCB. The laser is focused onto the capillary of the microchip, and fluorescence is collected by the photodiode through the lens and filter

and converted to a current. This analog current is then digitised and transferred as data across the SPI bus to the microcontroller, and subsequently, the GUI.

THERMAL REGULATION UNIT (REV03)

This module simultaneously injects current (as specified by the MCU) into two pins interfacing with the microchip's thin-film heater and measures the voltage across the heater. This value is returned to the MCU, and the firmware then uses this information to determine the temperature of the heater. This design allows this module to act as both an actuator and a sensor, and the firmware to control the temperature of the on-chip micro-chamber using this single module. Further detail will be described in Section 4.4.

PNEUMATIC PUMP AND VALVE CONTROL UNIT (REV02)

The valve/pump unit consists of seven three-way valves capable of switching up to 30 psi in differential pressures which are used to control the on-chip valves for fluid handling. These valves can be addressed and actuated individually for fluid isolation, or sequentially in groups of three for fluid transport.

TEMPERATURE MONITORING UNIT (REV01)

As the temperature within the micro-chamber is affected by shifts in heatsink and ambient temperature, both of these are monitored by the temperature module using K-type thermocouples.

2.3 FIRMWARE

While the author of this thesis did not directly write the firmware, she played a key role in its development in terms of what functions were included, its specifications, process flow, and its contributions to the CLI.

The firmware is written in the C programming language and is executed by the PIC microcontroller on the MCU module. The microcontroller handles the initialisation,

communication, control, and data acquisition from each of the hardware modules using industry standard SPI protocol. While all boards, board addresses and the firmware adhere to this, upgrades and optimisation can be done on individual modules and the firmware, with no concern of the two interfacing incorrectly.

The microcontroller also communicates with an external laptop computer via a universal serial bus USB serial link. To increase its versatility, a developer may communicate with the microcontroller using a terminal program on the external computer for debugging purposes, while a user operates the system using the custom-built graphical user interface. Both the terminal program and software interact with the firmware using a standardised set of commands in a specific operation sequence, referred to as the command-line interface protocol (CLI). While the CLI is adhered to, successive versions of the firmware may be significantly improved without affecting higher levels of the instrument architecture (software and user).

When the firmware is initialised, the SPI is opened with a data rate of 750 kHz, the laser is turned off and the chip selects (shift registers) are set to ensure the high voltage module supplies are set to zero, all of the optical components are off, and all valves and relays in the system are open. This ensures the system always powers up into its “reset” state.

Once this is completed, the firmware then enters its idle state, also known as Command-Line Mode (CL mode). It is named as such because the firmware remains in CL mode until one of three states is initiated by the receipt of a command from the terminal program or software. All received characters are collected into the command buffer and commands are executed one at a time (a semicolon designates the end of a command), except for the Esc key which ends the currently running process.

The first state is Execute Command, the only state used by the software and used most often by the terminal program for board debugging. This state is initiated by the firmware upon receipt of any command other than the EEPROM and reset commands,

wherein the command specifics are executed and the firmware returns to CL mode once execution has finished or is aborted. More detail on the process flow of the Execute Command state is detailed in the CLI (Appendix B) and Section 2.4.1.

The remaining two states are used to write a script to the external EEPROM (Microchip 25AA512) included on the MCU module and run the written script: Load Script to EEPROM and Run Script on EEPROM, respectively. These states and the external EEPROM were included in the system design to allow for testing of new molecular biology protocols (such as optimal magnetic bead movement) to later be automated by the firmware via a defined CLI command. Load Script to EEPROM is initiated with one specific command, that then writes all further characters onto the external EEPROM until the end-of-script or abort character is received, returning the firmware to CL mode. Run Script on EEPROM is initiated with one specific command that then reads and executes commands line-by-line from the loaded script. Once the script is finished or aborted, the firmware returns to CL mode.

If the initiated state is aborted, all flags are zeroed, relays and valves are opened, high voltages are zeroed and the laser is turned off before returning to CL mode. All other settings are retained. If the command completes without being aborted, only the settings associated with that command are returned to their initial state. The reset command returns the firmware to its initial state wherein it repeats the power up initialisation and all settings are returned to their default values.

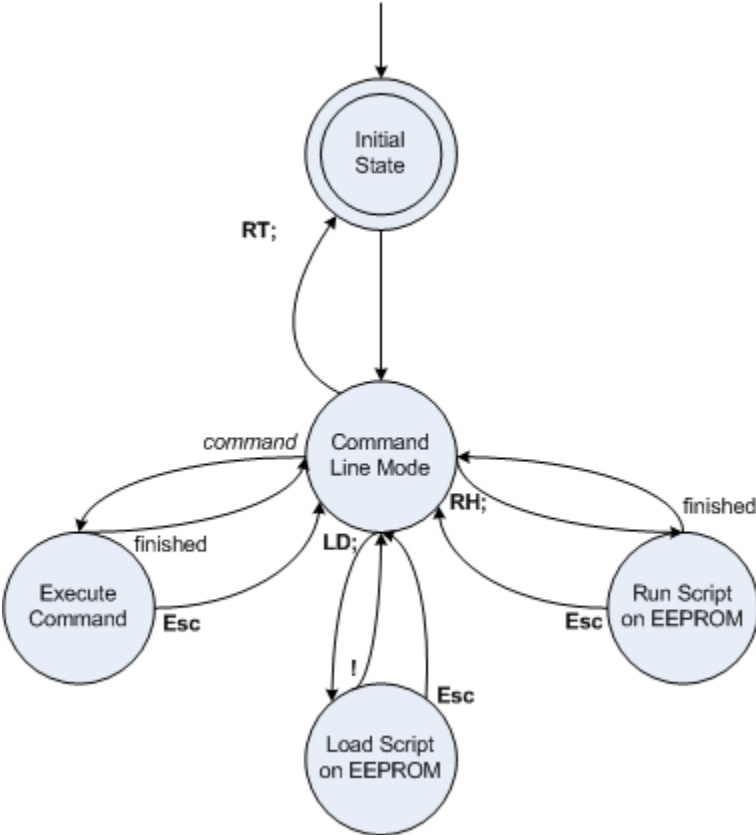


FIGURE 2.3-A: OPERATION FLOW CHART OF THE FIRMWARE STATES AS DESCRIBED ABOVE. THE ESC CHARACTER IS THE ABORT CHARACTER.

2.4 COMMAND-LINE INTERFACE PROTOCOL

The command-line interface protocol is an important element in the system as it is what describes the communication between the software and firmware, allowing for independent improvements to these modules. Furthermore, it provides the specification for a developer wishing to work directly with the firmware using a terminal program rather than the software. The author of this thesis wrote the CLI protocol and updated it as necessary throughout the system’s development (Appendix B).

2.4.1 Hardware and Firmware Structure

The first part of the specification details the firmware process flow and the data flow across the virtual serial port via the USB link from the firmware to the external laptop computer. While in the main event loop, the firmware routinely checks if a command has been received from the terminal program/software. If it has, the firmware echoes this command so the developer/software can ensure the command was received correctly. The firmware then determines if it received a valid command. If the command is defined by the CLI and formatted correctly, the firmware then executes the command as appropriate (Figure 2.4-A) and sends a notification message when the Execute Command state is exited (successfully or with error).

TABLE 2.4-A: EXAMPLE OF THE DATA FLOW ACROSS THE FIRMWARE-SOFTWARE INTERFACE

Received	Sent	Description
<i>XX(para1);</i>		- process command, terminated with ;
	<i>XX(para1);</i>	- command (as received) is echoed - firmware checks command to ensure legality - if defined, command is executed
	#0XX Status Message	- execution complete; ready for next
or	#5XX Error Message	- execution aborted; ready for next - ready for next command to be received

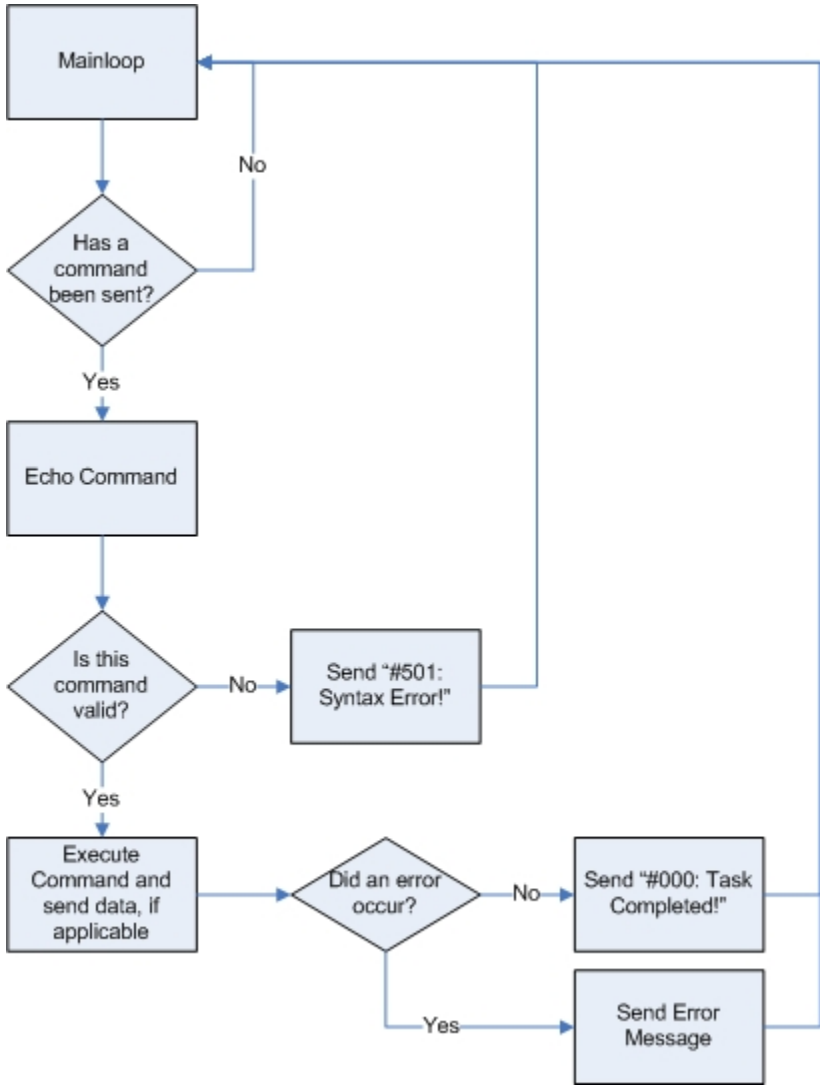


FIGURE 2.4-A: SIMPLIFIED PROCESS FLOW OF THE FIRMWARE PERTAINING TO THE FIRMWARE-SOFTWARE INTERFACE.

2.4.2 Commands and Messages

The second part of the specification details the format commands and messages must take, and further describes each command individually.

COMMANDS

All commands are written like functions for readability, with two upper-case letters “XX” designating the command, followed by an open bracket “(“ and the command parameters separated with commas “parameter1,parameter2”, and finishing with a closing bracket “)” and a semi-colon “;”. E.g. *XX(parameter1,parameter2);* All characters are ASCII and case-sensitive. Furthermore, all values sent are decimal integers unless otherwise stated, to avoid requiring the firmware to execute floating point calculations. Once the semi-colon character is found, the firmware then echoes, processes and executes the command as described in the previous section.

While deciding the commands to be included in the firmware, it was important to know:

- what hardware functions and information need to be accessed directly by the developer and software/user;
- which system functions need to be executed within a specific time period;
- what data needs to be passed between the system components; and,
- how that data should be formatted.

The default reporting frequency (how often data is passed across the serial port to the external computer) was set at 10 Hz, as 10 samples per second provides enough information for most processes. Thus, it was also important from a firmware perspective to know which functions would need a shorter reporting period.

Furthermore, necessary commands were designed by categorizing overall system needs, individual module functionalities to be accessed, and specific molecular biological protocols specific to certain combinations of modules. These CLI commands are presented below in their specific categories.

System Information & Testing

System information commands set or read information specific to the microcontroller unit; as such, they are contained within the firmware rather than within the software.

TABLE 2.4-B: SYSTEM INFORMATION & TESTING CLI COMMANDS

Description	Command	Returns
System Reset	RT;	Message #005
Set System Information	SI (type, value) ;	Message #000
Read System Information	RI (type)	Requested Information
Set DAC	SD (num, value) ;	Message #000
Read ADC	RA (num, value) ;	Requested Information
Send Byte Over SPI	SB (addr, value) ;	Message #000

The system reset command performs a full reset as described in Section 2.3. Set system information is a command performed upon compilation of the firmware onto the microcontroller and is used to store system-specific information such as system name, firmware compilation date, board version numbers, and the loaded firmware version. This command is also used by the software to store the name of the system's last user. Read information is used by the software to read the system-specific information for logging and reporting purposes. System and user information commands are necessary to allow the software to automatically detect which system it is connected to and who last used the system, so this information can be recorded in all experiment logs and provided in all reports.

System testing commands allow the digital-to-analog- and analog-to-digital-converters (DACs/ADCs) to be set/read directly, and a specified byte to be sent to a board over the SPI. These commands are necessary for individual board and system characterisations and testing. As such, they are included in the firmware and specified in the CLI protocol.

External EEPROM

These commands are used only if an external EEPROM is connected the microcontroller and scripts are used to control the firmware rather than the software.

TABLE 2.4-C: EXTERNAL EEPROM CLI COMMANDS

Description	Command	Returns
Load File to EEPROM	LD ;	Message #001
Print EEPROM Content	DS ;	Requested Information
Run File from EEPROM	RN ;	Message #002
Wait	WT (time) ;	N/A

These self-explanatory commands are useful for testing of next-generation commands, as described in Section 2.3.

High Voltage Supply & Optical Detection

These commands are used with the high voltage supply and optical detection modules specifically. Also categorised here is the process command for capillary electrophoresis which requires both high voltage and optical detection modules to be included in the system to perform this molecular biology technique.

TABLE 2.4-D: HIGH VOLTAGE SUPPLY & OPTICAL DETECTION UNIT CLI COMMANDS

Description	Command	Returns
Select HV Relays	RS (num , state) ;	Message #000
Set Laser State	SL (state) ;	Message #000
Set Detection Mode	DM (type) ;	Message #008
Capillary Electrophoresis	CE (injt , injv , sept , sepv) ;	Running Information

Selecting the high voltage relays is a testing command used for checking the High Voltage Supply Unit, and is included here because it is board specific. The laser state command is used both for board testing and by the user to toggle for chip alignment prior to capillary electrophoresis (see Chapter 3). The detection mode is used to define if a photodiode optical detection unit is present in the board and photodiode voltage is to be read from the ADC, or if a charge-coupled device (CCD) camera is present and only timing and current information should be reported on.

The capillary electrophoresis command is a molecular biology process command that sets all of the required system components based on the experiment needs specified by

the user and returns the experiment specific data to the user. This is included in the firmware to allow for precise timing of applied voltages and electrophoresis data collection.

In the parameters of the command, the user provides a time and voltage for both the injection and separation steps of CE in seconds and volts (the system is limited to 1kV), respectively. The firmware then calculates the required HV unit DAC values before the run commences and initiates the run by setting the appropriate flags, relays and voltages. While electrophoresis is performed, the firmware reads the ADCs for electrophoretic current and photodiode voltage, checks to ensure the current is not beyond the maximum limit, and returns these values. ADC values are transmitted across the serial link to the software/terminal program so floating point calculations that could potentially exhaust the reporting interval required for a high sampling frequency are unnecessary. Thus, the system returns time in terms of clock count, photodiode voltage as a decimal ADC value and electrophoretic current as a decimal ADC value, separated by tabs and next-line characters.

Count \t PD_ADC \t Current_ADC\r\n → Time(s) \t PD(V) \t Current(uA) \n

The software reads this information and formats the data into seconds, voltage and microamperes (see TtkCalc.py), respectively. These comprehensive values are then printed to the screen for the user and saved in the log-file as standard units. These value conversions are done by the software using the following equations. The voltage equation is a simple 16-bit ADC calculation, while the current is dependent on the resistor value used in conjunction with the ADC (in this case, 100kΩ).

$$I = \frac{50 \cdot ADC}{65536} \text{ } [\mu\text{A}] \quad \text{EQUATION 2.4-A}$$

$$V_{PD} = \frac{5 \cdot ADC}{65536} \text{ } [\text{V}] \quad \text{EQUATION 2.4-B}$$

Thus, in this manner the firmware and software work together to achieve both proper timing for CE and comprehensible data for the system operator. If the reporting interval (currently set to 10ms) is exhausted, the clock count will return values larger than a count of 10 between. This can be seen when the relays are changing between injection and separation (takes approximately 2 seconds). The software could (in future) be modified in the genetic analysis module (CE/PCR/MCA) to compare the time-stamps on each report line to ensure only 10ms is between reported data and to note any discrepancies within the final generated report. This could be achieved in the “format” function, using a class variable that retains the previous clock value and compares to the current value before it formats it. This “format” function to common to all genetic analysis modules.

Thermal Regulation and Temperature Monitoring

These commands are used with the thermal regulation and temperature monitoring modules specifically. Also categorised here is the process command for polymerase chain reaction which requires both thermal regulation and temperature monitoring modules to be included in the system to perform this molecular biology technique.

TABLE 2.4-E: THERMAL REGULATION & TEMPERATURE MONITORING UNIT CLI COMMANDS

Description	Command	Returns
Read Wheatstone Bridge	ZB;	Requested Information
Read Temperature	TE(time);	Requested Information
Set Chip Characteristics	CC(type,res,slope);	Message #000
Set PCR Parameters	PP(num,time,temp);	Message #000
Execute PCR	DP(cycles,Troom);	Running Information
Execute MCA	TM(Tstart,Tend,ramp);	Running Information

Reading the Wheatstone bridge, reading the room temperature and providing the firmware with chip-specific characteristics are all tasks that need to be performed by the user and system prior to executing an on-chip PCR or melt-curve analysis (MCA) experiment (see Chapter 4). For the firmware to control and sense the on-chip thin film

heater, the potential resistor in the Wheatstone bridge must be set to match the resistance of the heater (described further in Section 4.4.2). This requires the user to place the microfluidic chip into the system and balance the bridge by hand. To do this, the firmware injects a small current into the bridge so the thin film is not heated (i.e. DAC = 300, ~15mA) and an ADC (voltage) value of zero should be read when the bridge is balanced. When this command is sent, the ADC on the Wheatstone bridge is reported until the user has effectively zeroed the bridge and manually cancels the command. To avoid the user having to set the DAC (injected current) and read the ADC using the system testing commands, this is a built-in command in the firmware.

The temperature of the thermocouples connected to the system via the temperature monitoring unit must also be read to provide the firmware with the temperature the Wheatstone bridge was zeroed at (described further in Chapter 4). Historically, the temperature board and thermocouples were “optional” and the room temperature was something estimated by the user. At the completion of this project, the software was altered to read the thermocouple for a two-second period using the read temperature command (while displaying the data for the user), average the collected values and then store this value in the room temperature field on the GUI. The firmware is then sent this temperature value when the experiment is initiated. The firmware cannot read and calculate this value itself at the beginning of the experiment as the heater could have been zeroed a number of minutes prior to initiation and at a different temperature.

The set PCR parameters command is also necessary to provide the firmware with the step temperatures required for PCR prior to execution. This was separated from the execute PCR function to limit the length of the command (otherwise it would have needed to pass 14 parameters) and thus, limit confusion.

The polymerase chain reaction and melt curve analysis commands are molecular biology process commands associated with the thermal regulation and temperature monitoring units. During PCR, the firmware reports on the system state every 100ms. Included in

this information is the clock count; the cycle and step number (see Section 4.2.1 for more information on steps); the decimal DAC value (current) calculated by the controller to achieve the correct temperature; the decimal ADC value (voltage) measured across the heater; the effective heater temperature in Celsius (T_h) as calculated by the controller; and the temperature monitoring unit (T_r) and thermocouple readings (T_{c1} , T_{c2} , and their average, T_{ave}) in Celsius. All values are separated by tabs and the report for that period ends with a next-line character. The software reads in this information, formats the clock time into seconds, prints the data to the screen for the user and saves it in the log-file.

```
Time(s) \t Cycle \t Step \t DAC \t ADC \t Th( °C) \t Tr( °C) \t Tc1( °C) \t Tc2( °C) \t Tave( °C)\n
```

The DAC and ADC values for temperature control (described in more detail in Chapter 4) are logged for development purposes, along with the heater temperature for plotting and user comprehension purposes (an ADC value means nothing to a user unfamiliar with the system). The remaining temperature values are included so the temperature at specific locations in the system can be monitored and logged over the course of the experiment.

An interrupt service routine in the firmware tracks the system timing in terms of a clock count. However, the firmware also includes floating point calculations and these may introduce variations in the processing time required during CE or temperature control. Specifications for the times required for these floating point calculations do not seem to be available for our present compiler, however an earlier compiler (CCS C) specified times of on the order of 100 microseconds for floating point multiplications and divisions. Using this as a metric, this means that for a 10 ms interval during either CE or PCR, we estimate that we have time for about 100 floating point calculations. It is likely that we are below this number of calculations per time step. As a result, we presently believe that this processing time requirement is not causing a problem in system timing but have not yet verified this. Such variations could lead to missing data points in CE, or

erratic temperature control during PCR. However, there is no obvious problem in the data produced from CE runs. This timing stability will need to be further assessed in future work.

Pneumatic Pumping and Valving

These self-explanatory commands are specific to the pneumatic pump and valve unit, and include board addresses so multiple pneumatic boards may be added to the system as necessary for new protocols/chip designs. As they directly manipulate the pneumatic board and require no specific timing (none are molecular biology process commands), they are included in the firmware.

TABLE 2.4-F: PNEUMATIC PUMP & VALVE UNIT CLI COMMANDS

Description	Command	Returns
Set Valve	VL(addr, value);	Message #000
Set Pump	SP(addr, v1, v2, v3, period);	Message #000
Perform Pumping	PM(cycles);	Messages #300,#000

NOTIFICATION MESSAGES

When the firmware has finished executing the command (finished setting values, gathering/displaying data) or the command is aborted (run error, cancellation), the firmware sends a notification to the software/user, also demonstrating that it is ready for another command.

Notification messages all begin with a hash (#) symbol so the software can differentiate messages from other data the firmware may be transmitting. This is followed by three numbers, the first designating the type of message being transmitted and the following two identifying the individual message. Status messages all begin with the number 0, error messages with 5, and processing messages with 3. This leaves a wide range for more notifications to be included as the system continues to develop.

This number is followed by the user message, or the English equivalent notifying the user of the number's meaning. User messages need not be character limited as

messages are not sent during time critical operations and only the first four characters must be received correctly by the software. With this convention, the software can easily differentiate between status, process and error messages while also enabling a developer to use a terminal program.

TABLE 2.4-G: FIRMWARE SYSTEM STATUS MESSAGES SPECIFIED BY THE CLI PROTOCOL

Num	Message	Occurrence
#000	Task Completed!	Successful completion of requested task
#001	Program Downloaded!	Program downloaded onto EEPROM successfully
#002	End of Program!	EEPROM script finished running
#003	System Reset!	System was successfully reset
#004	Program Successfully Aborted!	Program was successfully aborted
#005	Operating Mode Changed!	Operating mode changed (EEPROM/CL)
#006	Task Aborted!	Current task aborted successfully
#007	Ready To Load Program!	EEPROM program will load begin loading on next loop
#008	Optical Detection Mode Changed!	Indicates the user has successfully set the optical detection mode (CCD/PD)
#300	Working....	Processing message
#500	Error: Program Exceeds Memory!	The EEPROM is full, but the firmware has not yet received the '!' character
#501	Error: Syntax Error!	First two letters of sent command does not match any known commands
#502	Error: Current Exceeded Limit!	High voltage current exceeds 45 μ A during a CE run or setting/reading of the HV board
#503	Error: Invalid Relay Number!	Number in relay command is invalid (> 4)
#504	Error: Unknown Board is Selected!	Invalid board chosen when reading/writing to ADC/DAC
#505	Danger: Unsafe Operation!	Heater chamber temperature exceeded 200°C
#506	Error: Not Implemented!	Required board is not present

2.5 SOFTWARE

Allocating all time-critical functions to the embedded microcontroller allows the use of external consumer-grade external laptops (or desktop computers) for data logging and processing without concern for erratic timing due to multi-tasking operating systems (OS) or overwhelming the bandwidth of the virtual serial link. With the current implementation, approximately 1.1% of the bandwidth is used during a typical CE experiment (~16kbit/s with a capacity for 1.5 Mbit/s). Python was chosen for the programming language of the software due to its OS platform independence.

In addition to commanding and collecting data from the microcontroller, the software collects run information from the use and logs this with the incoming raw data in a time-stamped text file (.txt). After the completion of the run, the software processes this data and plots both the raw and processed data as image files (.png). It then combines the run-specific information, user notes and images into a report in standard HTML format which can then be printed.

The software code follows a modular approach itself, with a class hierarchy used to separate functionalities. This allows new features to be added to the software with minimal to no impact on its main routine.

The author of this thesis was the sole developer of the software. The most recent exe installer and py files can be found in Supplementary CD/AML Files/TTK/Software (v3.47).

2.5.1 Software Modules

AMLGUI

This is the top level of the software's class hierarchy and contains all of the code pertaining to the creation and appearance of the graphical user interface (GUI). Tkinter was chosen as the GUI programming toolkit as it is Python's de-facto standard and one of the most commonly used GUI packages; thus, extensive documentation exists for it.

Tkinter is a thin object-oriented layer on top of Tcl/Tk (a combination of Tcl and the Tk GUI toolkit) and is implemented by translating Tkinter calls into Tcl commands, which are then fed into a complete Tcl interpreter embedded into the Python interpreter. This allows Tcl and Python to exist in a single application, with Tcl being used to create the appearance of the GUI and Python executing the functionality.

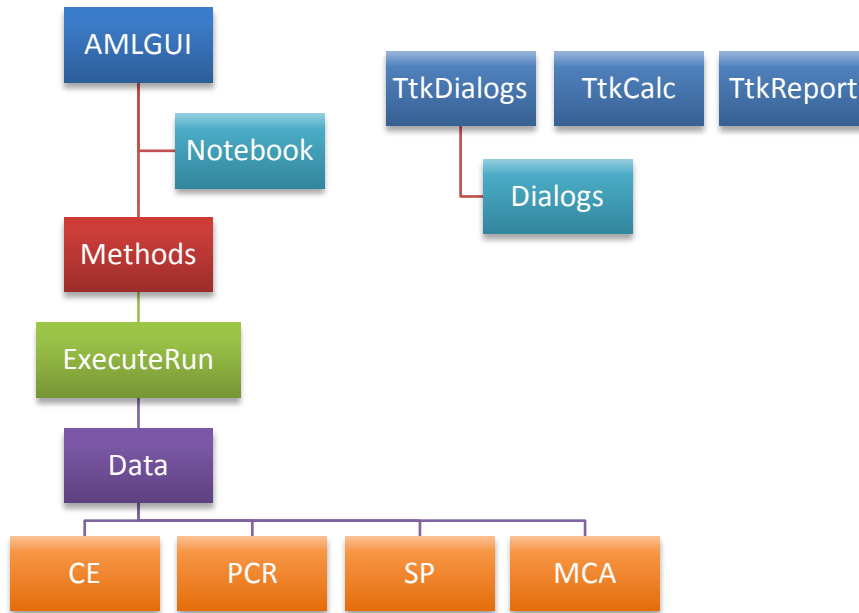


FIGURE 2.5-A: CLASS HIERARCHY OF THE SOFTWARE

The main routine of the software initialises Tkinter by creating a Tk root widget on an ordinary window with its appearance specified by the OS’s window manager. An instance of the AMLGUI class – the class containing all of the widgets to create the appearance of the GUI – is created, and the Tkinter event loop is then entered. The application remains in this event loop until the application window is closed, thus terminating the software program.

Initialisation of the AMLGUI class defines all of the Tkinter variables to be used by the application, reads and sets the default settings for these definitions (saved upon last

exit), and creates all of the widgets of the application. It also contains the functionality for the menu bar (e.g. Load, Save, Exit) and changes in the read-only state of entries, as these are all main window and appearance related.

All entry-field widgets containing run-specific information are AMLGUI class variables as these parameters must be accessible to lower-level classes so that user entered values can be included in commands to be sent the firmware, log files for molecular biology processes, and reports. When lower-level classes are initiated, the calling module passes a reference to itself so that these higher-class variables are always accessible.

This class was chosen to be the highest level as the appearance of the GUI is constant throughout the application's use, while other modules are only used when the system is in use. In this manner, the GUI can remain open even when the system is not connected.

METHODS

The Methods class contains all of the code pertaining to the functionality of the GUI's buttons and events. The functionality of the GUI's widgets was separated from the appearance for two reasons: a) to cut down on the length of the GUI module and improve readability of the code; and b) defined CLI commands are contained in the functionality of the buttons so that the user may execute a run without needing to be aware of the interface protocol. Thus, if it is necessary to alter any CLI-specified command names or parameters, all CLI command usage in the software is clearly separated from the rest of the code.

An instance of the Methods class is created in the initialisation of the AMLGUI class, and this is the sole instance created throughout the application's use because it is essentially an extension of the GUI appearance and AMLGUI class. When the Methods class is initialised, it saves a reference to the main application instance and creates the reporting run variables that must exist outside of individual run executions (such as CE run counts). These variables are also set as class variables so they can be the Data

module's "memory" as this lower-level class is initiated before/terminated after the serial link to the instrument is opened/closed via the ExecuteRun module.

EXECUTERUN

This class module executes the run once a defined CLI command has been sent from Methods via a button callback or "enterkey" (terminal window) event. Thus, all serial information and code pertaining to the data flow across the firmware-software interface (see Figure/Table 3.4-A) is contained here, while CLI defined commands are not. Any changes in the data flow principle across the interface would need to be reflected here.

An instance of the ExecuteRun class is created in every button callback function that is required to communicate with the system. Upon initialisation, the buttons on the main application are disabled (so no further commands may be issued) and the serial port is opened. The callback method then sends as many CLI defined commands as necessary and the data flow process is followed for each of these commands. Once all necessary commands have been sent or the run has been cancelled, the callback method closes the serial port and re-enables all buttons on the application. The ExecuteRun instance is then terminated.

The ExecuteRun class was created as a separate module to allow the GUI to be opened without it requiring it to be connected to the serial port. This allows the system to be disconnected from the external computer and reconnected between runs (or swapped for another system) without needing to close the GUI and re-open. Furthermore, there is no real need for the port to be open when the system and software are not communicating with one another.

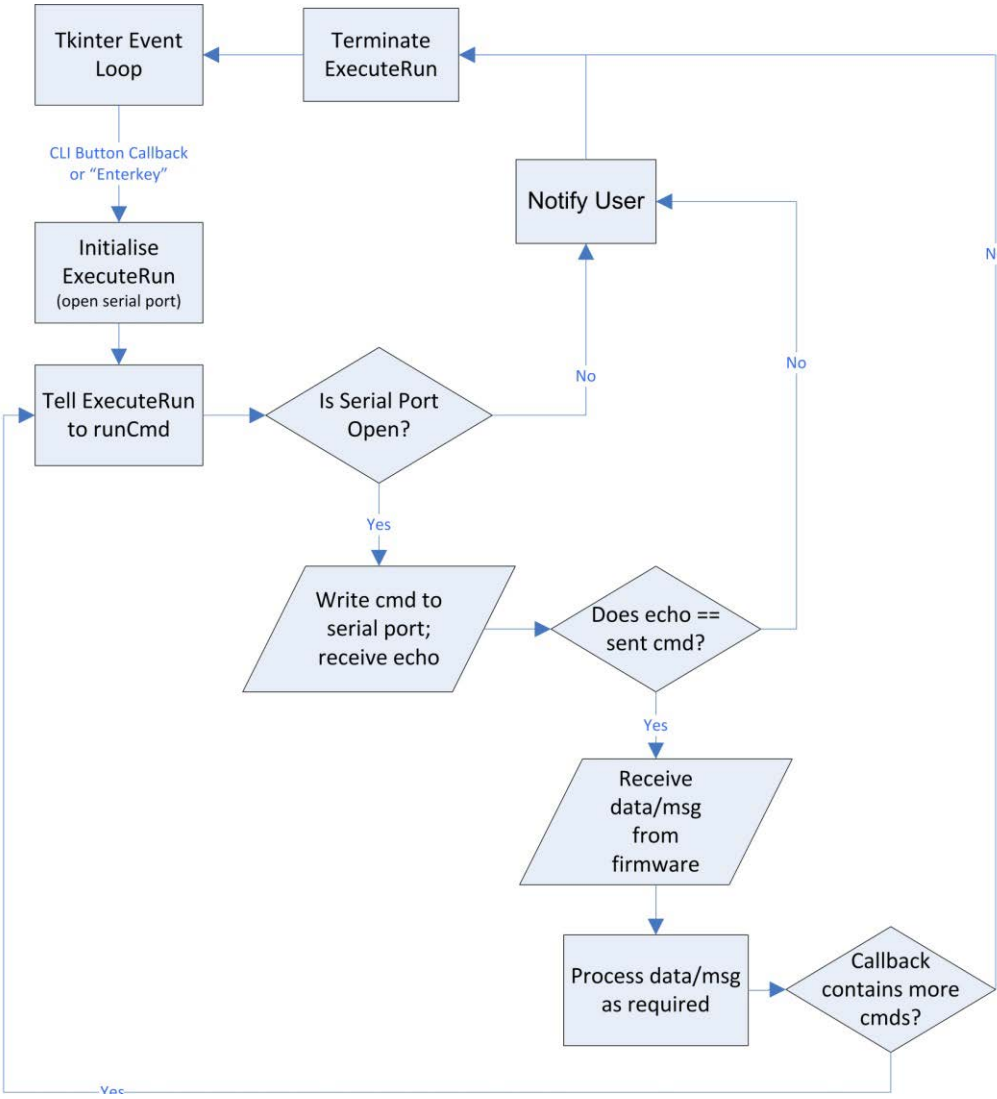


FIGURE 2.5-B: SIMPLIFIED PROCESS FLOW OF THE SOFTWARE PERTAINING TO THE FIRMWARE-SOFTWARE INTERFACE

DATA

After the CLI command is sent to and echoed back by the firmware, the firmware writes either a message (task completed/error) or data to the virtual serial port. ExecuteRun receives this “status” and creates an instance of the Data class. This class module determines what is being sent (data or message) and acts appropriately.

If messages are being sent, they are printed to the application screen to notify the user. The Data class instance is then terminated, and the button callback can subsequently send another command or terminate the ExecuteRun instance.

If data is being sent, this class module must determine if this data requires a report to be created (molecular biology processes) or any other special action to be taken (update info parameters or room temperature). It determines this based on the defined CLI command that was written to the serial port; thus, any changes to CLI defined commands may also need to be reflected in this module. If special actions are required, these are executed and the Data class instance is terminated. Any other data is printed to the application screen until a message is received. This message is then treated as above.

CE/PCR/MCA/SP

Molecular biology processes require the incoming raw data to be logged in a time-stamped text file (.txt) while it is being collected. In some cases, it also requires this data to be formatted for readability prior to logging (e.g. converting clock count to seconds). Furthermore, this data may need to be processed, plotted, and an HTML report file must then be created specific to the type of genetic analysis process being executed. To improve readability of the code and enable easy integration of new molecular biology techniques into the software, all code pertaining to each process is contained in its own class module.

Once the Data instance determines a molecular biology process is being executed, it creates a respective instance. During initialisation of this instance, the current time is

saved and the time-stamped text file for logging is created with the experimental parameters as a header of the file. Time-stamped logging is necessary both for record keeping of experiments and to ensure that if an error occurs with the system and the report is not created, the raw information up to the time of error is recorded.

The Data instance then enters a data-collection loop that reads in the data, formats it using the run experiment instance, prints it to the application screen and saves it in the log file. This loop is repeated until a message designating an error or run completion is received. Formatting the data as it is printed and saved is important to make some data – such as capillary electrophoresis, as described in Section 2.4.2 – comprehensible.

If the run is completed successfully, the Data instance then calls the respective run experiment instance to process and/or plot the data (as necessary) and create/append to the HTML report. Once this is completed, both the run experiment and Data instances are terminated.

OTHER MODULES

Notebook

This module contains the code for the functionality of the notebook on the main application window. This is an important module as it allows system functionality (e.g. run experiment types) to be separated on the main application window, and provides an easy way to add further system functionality to the GUI without needing to alter the rest of the appearance code. As it is more of a template class than part of the process flow of the software, it is not directly part of the class hierarchy.

TtkDialogs & Dialogs

The TtkDialogs module contains all of the code pertaining to the pop-up dialogs seen during the use of the GUI. Each dialog is separated into its own class, and these classes are all built from the Dialogs template class, except for the Run Notes dialog. This ensures all pop-ups behave in the same manner, with similar appearance and blocking

use of the main application until the user provides the required input. The Run Notes dialog is special in that it must remain open for the entirety of the run without restricting the user's access to the main application (i.e. the user must be able to provide run-specific information but still be able to see the incoming data and cancel the run if necessary). Thus, it has its own application window and provides data to the main application upon its termination.

TtkCalc & TtkReport

The TtkCalc module contains hardware-specific system calculations so that they may be changed or referenced easily. This includes converting ADC values for current and photodiode voltage into physical values, and the comparison calculation between the calibration and DMM data (Chapter 4). The TtkReport module contains all the common HTML report text and functions used by the run experiment class modules (e.g. report stylisation). These are helper files to hold calculations and stylisation so they may be consistent everywhere and easily altered as necessary.

Setup & AMLGUIexe

To standardise distributions of the software on windows machines for our collaborators, the software was compiled into an exe file using the Python module py2exe and an installer using Nullsoft Scriptable Install System (NSIS). Some issues arose in creating the exe with the matplotlib module used by software for plotting purposes due to the inability of the glob module to determine which files are necessary and which are not. Thus, by excluding backends not being used by the software and manually copying the matplotlib-data files needed to a folder within the distribution files, a functioning exe is created using setup.py. The AMLGUIexe.nsi file then packages the exe and distributable files into an installer. The installer and exe files have been used for multiple versions of the software, and used successfully on both Windows XP and Vista operating systems.

To create the installer and exe, one must have all of the files necessary for the software (all modules described here and supporting text files) and must have the same

environment as used during the software's development. This consists of the following standard Python modules, in Supplementary CD/AML Files/TTK/Software/Installer Modules:

- ❖ Python 2.5.4 Windows Installer (and included modules)
- ❖ Numpy 1.0.4 Win32
- ❖ Scipy 0.6.0 Win32 Python 2.5
- ❖ PySerial 2.2 Win32
- ❖ Matplotlib 0.91.2 Win32 Python 2.5
- ❖ PyWin32 210 Win32 Python 2.5
- ❖ Py2Exe 0.6.9 Win32 Python 2.5
- ❖ NSIS 2.46

Using a command window, the user navigates to the folder containing the software files and types: `python setup.py py2exe`. The distribution folder and exe are then created. Once this has completed, NSIS should be opened and "run script" should be chosen. Dragging the AMLGUI.exe.nsi file onto this window or navigating to the file will then create the installer. For successive versions, the AMLGUI.exe.nsi file should be edited so the installer reflects the software version number.

2.5.2 Software Output Files

TEXT LOG FILES

When the run is initiated by the operator, the software creates a text file in which to log the collected run data as it is received. This is done so that if something were to occur to the system or the software/computer while the run is executing, causing the system to stop, the run to quit prematurely with an error message, or the computer to freeze, not all of the data of the experiment would be lost.

All log files are created beginning with the acronym of the function being executed, followed by the date and the time the run was initiated. The run specific information is

then included at the head of the log, containing all of the experimental parameters and a header for the data to follow. Once the data is finished being received, the log file is closed without any additional information added. However, if the experiment is cancelled before its' completion, a "Run Cancelled!" line is added at the foot of the data that was received.

Example Log-file: CE10.03.09_17h50m04.txt

```
{Experimental Parameters}
{Researcher: Allison}
{Device Name: Belle}
{Run Number: 234}
{Previous User: Allison}
{Date (yy/mm/dd): 10.03.09}
{Time (hh:mm:ss): 17h50m04}
{Sample: 0.5uL TC+}
{Sizer: none}
{Polymer: 4% LPA}
{Buffer: 1xTTE}
{Chip: 0904C16}
{Injection Voltage (v): 200}
{Injection Time (s): 80}
{Separation Voltage (v): 600}
{Separation Time (s): 300}
{Detection Position (mm): 13mm}
Time (s)      Signal (V)  Current (uA)
0.85  1.58683776  0.0
0.86  1.58843994  0.0
...      ...      ...
```

The device name and previous system user parameters are read from the system by the software using the System Information command described previously. The date and time are collected from the operating system on the computer. Sample and experiment specific information are collected from the user before beginning the experiment.

Run numbers are system specific and are used to catalogue how many and which experiments have been performed on the system. Although it was included into the commands described previously, System Information values from the previous firmware programmed onto the microcontroller (e.g. run number, system name, last user name) cannot be preserved through the next programming. Thus, the run number is randomly assigned. During testing and development where the firmware was changed sometimes

quite frequently, this would have resulted in many occurrences of random and possibly large number gaps between successive runs. To keep testing data sets more comprehensive, users were responsible for assigning run numbers to all testing experiments performed on each system using the field on the GUI. This could have been avoided with a command to manually set the run number, but this command was discouraged to prevent users from manually resetting the run number as they saw fit. With the system developed to a state where the firmware rarely needs to be updated, the run number field on the GUI needs only to be changed to read-only and the run number system command included into the “Update System Information” callback in the Methods module to effectively use this feature.

PROCESSED IMAGES

Once the experiment and logging is completed, the software re-opens the log file and reads in all of the data so that it can plot and, if necessary, process it. For CE, this involves plotting the raw photodiode voltage (optical) and current data versus time. The software then processes the raw optical data (described in Section 3.2) and plots this processed electropherogram. For PCR, this involves plotting the heater temperature versus time and re-plotting the first 20% of the PCR experiment for a zoomed in picture of transition times and potential noise. The plots are saved as soon as they are created, for inclusion into the HTML report. In this manner, all images are processed and appear in the HTML reports in the same format, not selectively processed.

HTML REPORTS

After any necessary plots are drawn and saved, the software then creates the HTML report. Reports were chosen to be given in HTML as this allows the report to be viewable on any operating system platform with any HTML viewing program. Furthermore, comments can easily be added post-experiment based on the analysis provided by the software (as opposed to PDF). These files can then easily be printed or saved as a PDF file with any number of Print-to-PDF programs.

The HTML reports include:

- ❖ the experimental parameters as provided by the user and included in the log;
- ❖ run-specific notes entered by the user over the course of the experiment (e.g. Condensation observed in the chamber at cycle 5);
- ❖ drawn plots; and,
- ❖ in the case of CE, an analysis of the electropherogram, providing a standard calculation of the noise and timing, intensities, and signal-to-noise ratios (SNRs) of all located peaks (see Chapter 3).

An example HTML report for a PCR-CE experiment with positive control (TC+) electropherograms and on-chip PCR product (OT118) electropherograms can be seen on the next four pages. Please ignore the Comments and Notes sections as these are running notes taken by the author while conducting the experiment and are not relevant for what this section is trying to present.

Belle PCR-CE Report - Chip Load #118

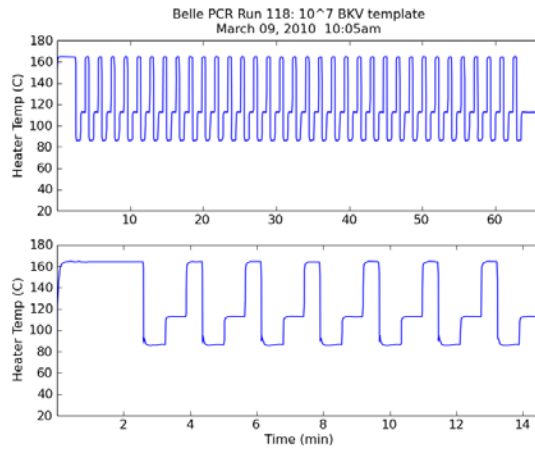
PCR Information:

<i>User</i>	Allison		Temp (C)	Time (s)
<i>Date</i>	March 09, 2010	Rev. Transcription	94	0
<i>Time</i>	10:05am	Pre-Denaturation	94	120
		Denaturation	94	15
<i>Sample</i>	10 ⁷ BKV template	Annealing	58	25
<i>Protocol</i>	TTK PCR CE	Extension	70	25
<i>Chip</i>	PCR-CE4[0901C14]	Post-Extension	70	120
<i>Heater</i>	67.0Ω 0.1453 1/Ω	Cycles	35	

Notes:

- added 5 s to each step due to increased add times for the new firmware
- chip bonded by Abraham in RIE, on *Mar 5th* with SigmaCote
- no evap or bubbles apparent in the chip after loading
- ambient temperature rose ~1C during the run
- flushed out with 0.01xTTE

Temperature Plots:



CE Information:

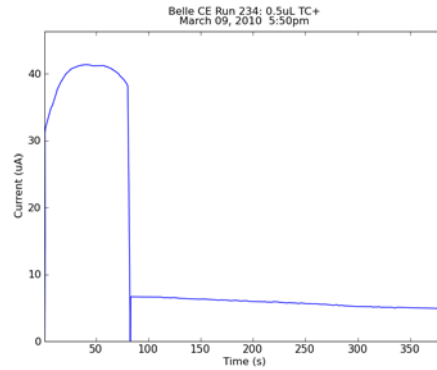
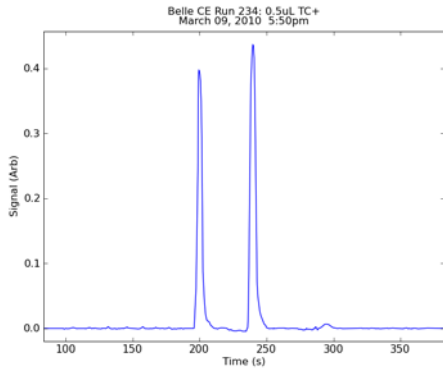
Run 1

<i>User</i>	Allison	<i>Protocol</i>	TTK PCR-CE
<i>Date</i>	March 09, 2010	<i>Chip</i>	0904C16
<i>Time</i>	5:50pm		
<i>Sample</i>	0.5uL TC+	<i>Injection Time</i>	80 s
<i>Polymer</i>	4% LPA	<i>Injection Voltage</i>	200 V
<i>Buffer</i>	1xTTE	<i>Separation Time</i>	300 s
		<i>Separation Voltage</i>	600 V

Notes:

- positive thermocycler control
- was slow beginning injection due to user error

Electropherogram & Current Profile:



Peak Information:

Std. Dev. of Noise : 0.000613273484869

Peak (#)	Time (s)	Voltage (V)	SNR
Peak 1:	195.95	0.397761090371	648.586805372
Peak 2:	235.86	0.437710442958	713.727975785
Peak 3:	291.51	0.00680563767385	11.0972312382

Run 2

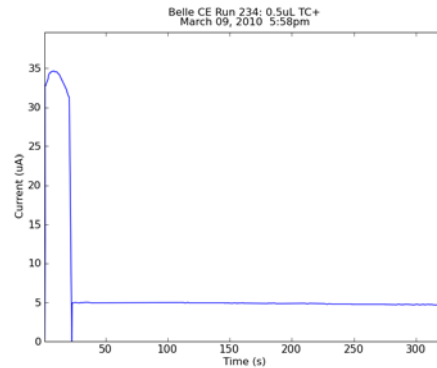
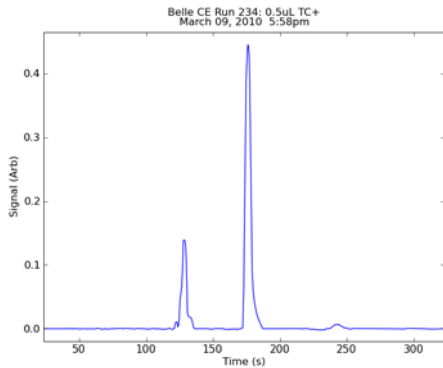
User Allison
 Date March 09, 2010
 Time 5:58pm

Protocol TTK PCR-CE
 Chip 0904C16

Sample 0.5uL TC+
 Polymer 4% LPA
 Buffer 1XTTE

Injection Time 20 s
 Injection Voltage 200 V
 Separation Time 300 s
 Separation Voltage 600 V

Electropherogram & Current Profile:



Peak Information:

Std. Dev. of Noise : 0.000260267386128

Peak (#)	Time (s)	Voltage (V)	SNR
Peak 1:	121.23	0.140057748508	538.130230574
Peak 2:	172.22	0.4457389148	1712.61916997
Peak 3:	237.86	0.00655650446412	25.1914178017

Comments:

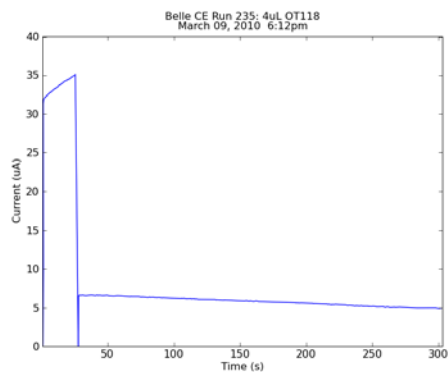
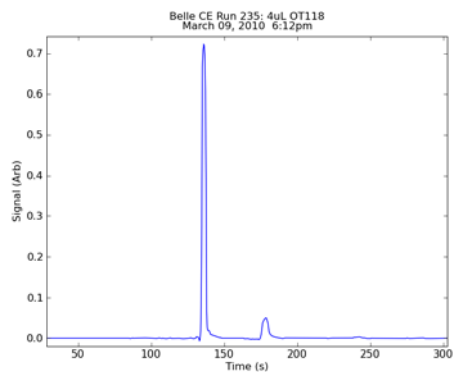
The positive control peaks look weaker than usual, likely due to the slowly dying laser. To give an estimation, the baseline fell by about 10-15%.

Run 1

<i>User</i>	Allison	<i>Protocol</i>	TTK PCR-CE
<i>Date</i>	March 09, 2010	<i>Chip</i>	0904C16
<i>Time</i>	6:12pm		
<i>Sample</i>	4uL OT118	<i>Injection Time</i>	25 s
<i>Polymer</i>	4% LPA	<i>Injection Voltage</i>	150 V
<i>Buffer</i>	1xTTE	<i>Separation Time</i>	275 s
		<i>Separation Voltage</i>	600 V

Notes:

- current limit after 55s of injection

Electropherogram & Current Profile:**Peak Information:**

Std. Dev. of Noise : 0.000255775482176

Peak (#)	Time (s)	Voltage (V)	SNR
Peak 1:	130.79	0.722247632331	2823.75631232
Peak 2:	174.81	0.0504913696118	197.405041258
Peak 3:	237.81	0.00305945474456	11.9614855909

Run 2

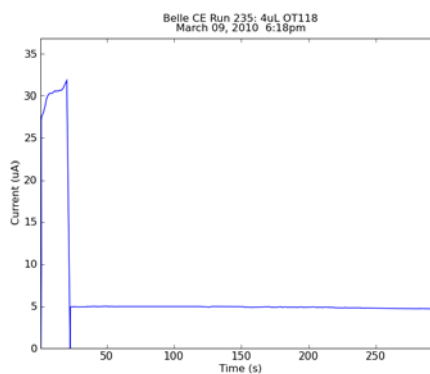
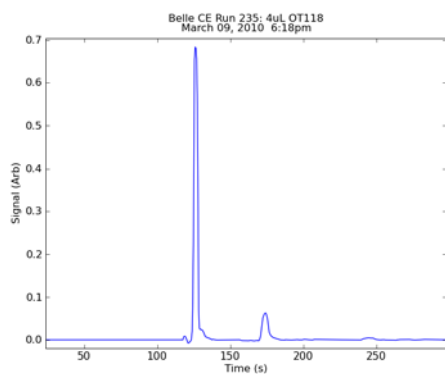
User Allison
Date March 09, 2010
Time 6:18pm

Protocol TTK PCR-CE
Chip 0904C16

Sample 4uL OT118
Polymer 4% LPA
Buffer 1XTTE

Injection Time 20 s
Injection Voltage 150 V
Separation Time 275 s
Separation Voltage 600 V

Electropherogram & Current Profile:



Peak Information:

Std. Dev. of Noise : 0.000245209101584

Peak (#)	Time (s)	Voltage (V)	SNR
Peak 1:	117.5	0.684066255393	2789.72620092
Peak 2:	170.03	0.06315452122	257.553740102
Peak 3:	240.31	0.00446200106226	18.1967187737

2.6 CONCLUDING REMARKS

The microfluidic platform presented here is 'shoebox-sized' with a component cost of less than \$600 and contains similar functionality to considerably more expensive commercial systems. Its modularity allows individual modules to undergo significant development without requiring a redesign of the overall system; provides a customisable, inexpensive and portable LOC platform for POC applications; and, enables further development of progressively less expensive and more compact systems.

The divided responsibility between the firmware and software allows for time-critical functions to execute on time as necessary, while still enabling the automatic data logging, processing, and report generation required of a diagnostic system. The command-line interface protocol is crucial to this separation of tasks and to future improvements to both firmware and software. Modularity of the software components further allows easy integration of new system functionalities and simple appearance and usage changes without altering the software's interaction with the firmware. With improved automation in the microfluidic component of the system, simple changes to the callback events of the Methods class in the GUI will allow for system automation. Furthermore, the hardware of the system may continue to be improved and miniaturised, and with a new firmware that adheres to the CLI protocol, the same software may also be used for these future systems.

Crashes of the software have been reported by other users after the completion of this thesis project, and this could be due to, among other things, a driver problem or data corruption during transmission. The author used a model IBM Thinkpad Lenovo T60 computer running the operating system Windows XP and with the win2k_winxp CDCInif driver. With this computer, software versions leading up to 3.41 and version 0.3.4 of the firmware, the author did not experience any software crashes in approximately 250 PCR and CE runs.

The author of this thesis played a key role in the development of the firmware, wrote and maintained the CLI protocol, and was the sole developer of the software. Once the hardware, firmware and software components of the system were ready, they were combined first as a system outfitted for CE, and subsequently PCR-CE and SP-PCR-CE. In this manner, the author could assess the associated challenges, implement solutions, and determine the system performance of each function, independently. This will be further discussed in the following chapters.

One aspect of the software that was not explored within the duration of this thesis project was real-time plotting. This is not an entirely necessary functionality as the data is displayed to the user during the run and plotted for the user at its completion (both raw and processed). However, users tend to like to be able to see that the program or system they are using is working and a list of data is not as comprehensive as an image. While this functionality was explored to some extent, it requires the implementation of threads or a similar multi-process tool (e.g. forks) as the software needs to be able to update the plotting image simultaneously with its reporting/logging tasks, and more debugging was required to implement real-time plotting than the author of the thesis had time for.

One ideal solution for would be to remove the platform independence functionality of the software and instead load a distributable version of an OS such as Linux onto a USB key and run the software off there. This way, the software would not need to be tested on every distribution of every operating system to ensure its functionality, as it could be booted from the USB key. Furthermore, it allows the lab to directly control which software version is being used with each system, without needed to assign a specific computer to each system.

Another aspect of the software that could not be explored was re-plotting of imaging using different signal processing methods. In the next chapter, two variations on the software's current signal processing method and an alternative method developed by

Modular and Scalable System

another member of our group will be discussed. This would be useful to allow users to subsequently re-process their data using a different, lab-approved method or to zoom in on plotted data.

In the next chapter, the key challenges involved with the system implementation of CE and its performance will be described.

Microchip Capillary Electrophoresis

CHAPTER 3

3.1 INTRODUCTION

One of the greatest advantages of capillary electrophoresis as an analytical technique is its wide range of applications, including the separation and detection nucleic acids, proteins, amino acids, chiral drugs, vitamins, pesticides, and even whole cells. This coupled with the fact that CE is easily scaled onto a microchip and automated makes it a key element of lab-on-a-chip devices. Since it has become available on microfluidic platforms almost 20 years ago⁴⁷, microchip CE has significantly improved in performance and standardisation. This includes the development of coatings to control electro-osmotic flow and limit channel-reagent interactions^{48,49} and online pre-concentration techniques to improve the sensitivity of CE^{50,51}, for which a number of excellent reviews are available.

Many detection schemes exist for LOC devices^{52,53}. Of these, laser-induced fluorescence (LIF) detection is the most commonly used technique due to its high sensitivity (able to detect low volume to one molecule samples well) and its simple coupling with microfluidic devices. In recent years, many CE instruments have been developed both commercially and academically using this detection method. However, these conventional systems are not suitable for POC applications due to their size, cost and complexity. LIF detection is primarily achieved using a confocal configuration which almost completely suppresses scattered light to provide high signal-to-noise ratios (SNR) and excellent sensitivity. Unfortunately, the components used in confocal detection systems consist of bulky optics which are both expensive and not easily scalable. Furthermore, these systems also tend to rely on external HV power supplies, contributing to their confinement to the laboratory where it is difficult for them to compete with traditional diagnostic methods.

A non-confocal detection approach requires fewer optical components and is advantageous in its miniaturisation and cost. However, this approach also tends to be several orders of magnitude less sensitive⁵⁴. This is often in part due to the increased collection of scattered excitation light which leads to high baselines that are sensitive to even minute laser intensity fluctuations. Although some non-confocal detection schemes with comparable sensitivity have been demonstrated in the literature^{55,56}, these still consist of expensive and large optical components; specifically, photomultiplier tubes (PMTs).

Before this thesis project began, our lab demonstrated a non-modular PCR-(LIF)CE instrument with a simplified detection system⁴³. Rather than relying on expensive and bulky gas lasers, microscope objectives, dichroic mirrors, and/or PMTs, this system consisted of an inexpensive laser diode and a charge coupled device (CCD) for optical detection. CCDs are advantageous as they have very low dark current and result in sensitivities comparable to confocal CE instruments. However, while less expensive than a PMT, the CCD was still costly, quite large, and limited in its rate of data collection. Furthermore, it was not possible to easily automate the PCR-CE experiment due to the external software required to capture images from the CCD.

Thus, we replaced the CCD camera with a photodiode-based system consisting of an inexpensive laser diode, GRIN lens, interference filter and photodiode. Photodiodes are inexpensive, compact, and can be patterned onto microfluidic chips or incorporated into microelectronic chip designs (i.e. CMOS). Lasers diodes are advantageous over their light-emitting diode (LED) counterparts because they provide a collimated, spectrally pure light source. The GRIN lens is used to collect the fluorescence emission from analytes passing the detection point and the interference filter to remove collected excitation source light.

This chapter is based on the configuration of the modular system presented in the previous chapter as a CE instrument. Specifically, the challenges associated with

implementing the optical detection scheme and required protocol developments to increase the overall system sensitivity to sufficient diagnostic levels are discussed, along with a verification of the system performance as a microfluidic CE platform.

In Section 3.2, the system level and challenges associated with the optical components will be detailed configuration beyond what was described in the previous chapter. Where in the previous system, the CCD-associated software performed some unknown processing on the images and intensity was determined from the pixel brightness, here white noise from the electronics and slow baseline drift needed to be removed from the sampled signal. This was done using a low-pass filter designed by the author followed by median subtraction as discussed further in the signal processing section. Furthermore, during verification of the non-confocal set-up, the author observed and determined four factors that contributed to a well-focused excitation beam on the CE channel, and thus, ultimately, to the sensitivity of the system. These factors are proper alignment of the laser, power of the laser output, stability of the laser intensity, and microfluidic chip characteristics. With each of these four factors controlled, a reproducible sensitivity could be achieved.

The next section discusses the CE protocol, its development by the author to increase the sensitivity of the system, and the resultant performance characteristics which directly rely on this protocol (DNA mobilities, resolution, run-to-run variability and buffering capacity). Overall system performance which includes both protocol and the system optical detection are subsequently discussed in Section 3.4 (load-to-load variability and the limit of detection). These values are then compared to the commercial CE PMT-based confocal instrument (Microfluidic Toolkit (μ TK), Micralyne, Edmonton, Alberta) available in our laboratory, and are found to be comparably sensitive (within 2-3 times) with a system approximately 100 times the cost. All performance characteristics were determined through extensive testing by the author. This chapter is then concluded in Section 3.5 with a summary and suggestions for future work.

3.2 SYSTEM

To perform CE on the instrument, two modules must be included as described in Section 2.2: the high voltage supply unit for generating the voltages necessary to perform capillary electrophoresis and sensing the current; and, the optical detection unit to toggle the laser, read the light intensity data from the photodiode, and perform the hardware filtering on the signal (described more in Section 3.2.3). These components are connected to both the power and communications buses.

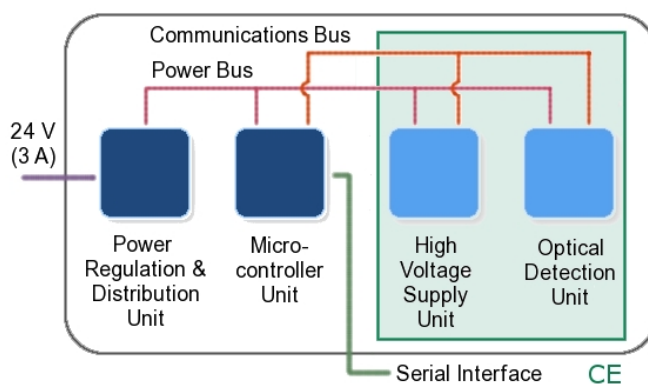


FIGURE 3.2-A: A DIAGRAM OF THE SYSTEM MODULES NECESSARY FOR CE, ADAPTED FROM⁴³.

The microfluidic chip used in this thesis is the same microfluidic chip demonstrated in earlier work⁴³. The fabrication procedure can be found there, and improvements here⁴⁴. It consists of two glass layers (1.1mm Borofloat, Schott AG, Germany) with a PDMS membrane between to create the valves necessary for PCR, as further described in Section 4.2.2. The CE channels are etched 45 μ m deep (100 μ m in width).

We specifically chose to work with the same microfluidic chip so the system could be verified and characterised with a known microfluidic device. However, to demonstrate the scalability of the instrument (using smaller distance separations) and in attempt to automate this integrated chip (described in Section 4.5), the detection point was moved from the end of the separation channel to 13mm from the intersection.

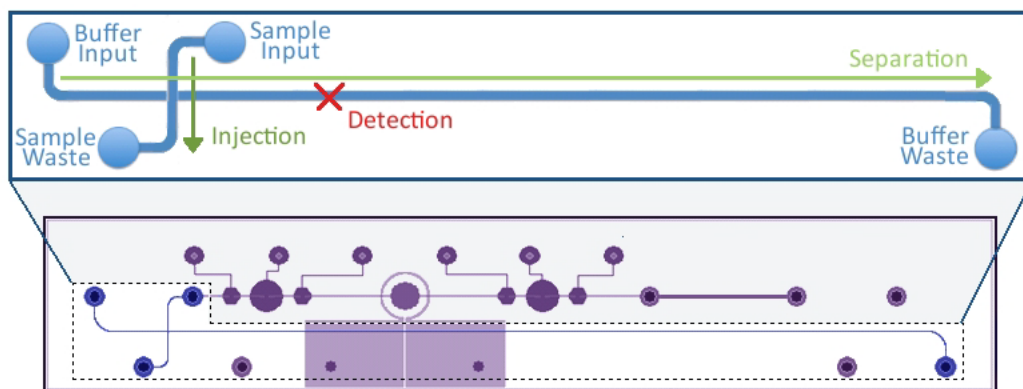


FIGURE 3.2-B: DESIGN OF THE MICROFLUIDIC CHIP, EMPHASISING THE CE SECTION OF THE MICRODEVICE CONTAINING THE SAMPLE AND BUFFER INPUT/WASTE WELLS AND THE DETECTION POINT 13MM FROM THE INTERSECTION OF THE INJECTION AND SEPARATION CHANNELS (LABELLED PARTS ARE NOT DRAWN TO SCALE).

3.2.1 Optical Design

In addition to the modules, a simple red (635nm) laser diode with built-in driver circuit (M635-5; US Lasers, Hazlehurst, GA, USA), an interference filter (HQ669LP, Chroma Technology Corp., VT, USA), a gradient index (GRIN) lens (LGI630-6, Newport, CA, USA) and a photodiode (NT57-506, Edmund Optical, NJ, USA) are included in our non-confocal detection set-up as depicted in Figure 3.2-B and described in a previous publication⁵⁷. A detailed diagram drawn to scale can be found in Figure 3.2-C.

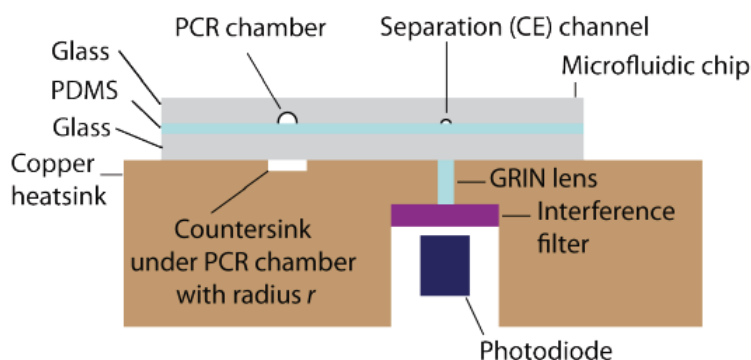


FIGURE 3.2-C: A DIAGRAM OF THE NON-CONFOCAL SET-UP IN THE CUSTOM-BUILT INSTRUMENT³⁹. THE LASER IS FOCUSED ONTO THE SEPARATION CHANNEL OVER THE GRIN LENS/INTERFERENCE FILTER WHEREIN THE PHOTODIODE COLLECTS THE LIGHT INTENSITY (NOT DRAWN TO SCALE). © THE ROYAL SOCIETY OF CHEMISTRY⁴³, 2010.

Due to the small dimension of the channel as compared to the optical set-up, the fluorescence spot (the object) will be modeled here as an isotropic point source. The object is located 1.35mm from the GRIN lens; however, they are separated by glass and PDMS and the provided lens equations^{58,59} model the GRIN lens in air. Using basic trigonometry and Snell's Law, we can build an equation for the effective object distance:

$$d = \alpha_2 = \beta_2 / \tan \left\{ \sin^{-1} \left[n_1 \sin \left(\tan^{-1} \frac{\beta_1}{\alpha_1} \right) / n_2 \right] \right\} \quad \text{EQUATION 3.2-A}$$

where α is the adjacent edge of the triangle, β is the opposite edge and n is the index of refraction. As we are trying to calculate the effective distance from glass to air, subscript 1 denotes glass distances and subscript 2 denotes air. Using this equation, $\alpha_1 = 1.35\text{mm}$ and $\beta_1 = \beta_2 = 0.9\text{mm}$, we get an object distance in air of 0.6mm. The PDMS, Borofloat glass and interference filter are approximated to have refractive indices of 1.5.

The Newport GRIN lens specifications sheet gives the effective focal length in terms of the diameter and numerical aperture of the lens, which can be used with the general form of the effective focal length equation^{58,59} to determine n_0 , the index on axis of the lens:

$$f = \frac{\phi}{2 \cdot NA \cdot \sin(L\sqrt{A})} = \frac{1}{n_0 \sqrt{A} \sin(L\sqrt{A})} \rightarrow n_0 = \frac{2 \cdot NA}{\phi \sqrt{A}} \quad \text{EQUATION 3.2-B}$$

$$\sqrt{A} = \frac{2\pi p}{L} \quad \text{EQUATION 3.2-C}$$

Where the numerical aperture ($NA = 0.46$), diameter ($\phi = 1.8\text{mm}$), pitch ($p = 0.29$) and length of the lens ($L = 5.37\text{mm}$) are provided by the specifications sheet to give the gradient-index constant ($A^{1/2} = 0.339 \text{ mm}^{-1}$) and $n_0 = 1.51$.

The image distance can then be found using the fundamental ABCD matrix for GRIN lens⁵⁹, arranged as the following equation⁵⁸:

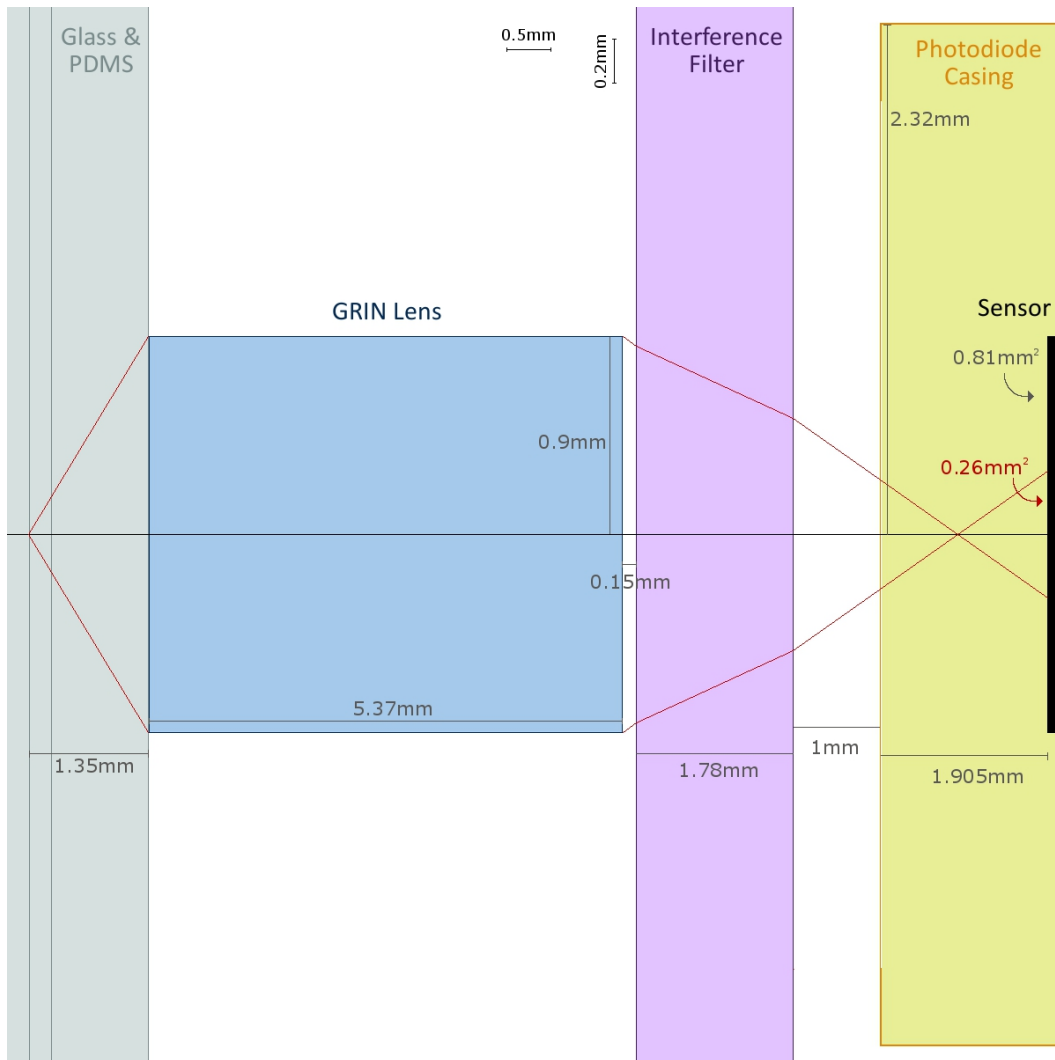


FIGURE 3.2-D: RAY DIAGRAM WITH THE LENGTHS AND DISTANCES OF THE OPTICAL COMPONENTS (TO SCALE).

$$d' = \frac{1}{n_0\sqrt{A}} \cdot \frac{n_0\sqrt{A}d \cos(L\sqrt{A}) + \sin(L\sqrt{A})}{n_0\sqrt{A}d \sin(L\sqrt{A}) - \cos(L\sqrt{A})} \text{ [mm]} \quad \text{EQUATION 3.2-D}$$

The image distance in air was calculated to be 3.2mm. However, the interference filter is ~0.15mm from the end of the GRIN lens, and the change in refractive index will also affect the image distance. Again, using basic trigonometry and Snell’s Law (Eq. 3.2-A), the image was found to be 3.82mm from the end of the GRIN lens or 1.02mm from the

surface of the photodiode sensor. The rays then diverge again from this image point, reaching the sensor with an effective radial area of 0.26mm^2 as compared to the 0.81mm^2 detection area of the photodiode. This means 100% of the filtered light reaches the detector. In the canister version designed later for subsequent systems by C.Bargen⁶⁰, the photodiode casing is flush with the filter, placing the image directly on the sensor.

However, it should be noted that the Newport GRIN lens specifications sheet provides a graph for the object and image distances for 0.29 pitch lens, and the image distance found with the fundamental equation does not match with the provided graph. Setting the object distance, d , to 0.1mm and 0.5mm using the fundamental equation, n_0 was varied in attempt to achieve image distances of 5mm and 3mm as respectively provided by the graph. This required two separate values for n_0 : 1.68 and 1.82, respectively. Thus, the graph on the Newport specifications sheet does not match the fundamental ABCD matrix equation and the optical diagram shown here should be considered a preliminary finding.

3.2.2 Anomalous Intensity Spikes

The author discovered that anomalous intensity spikes appeared in the electropherogram when the power regulation and distribution unit was included in the system. Whereas previously each board in the system was powered individually by a standard, regulated bench-top supply unit, with its inclusion into the box, ribbon cables distributing power from the power module now supplied multiple boards within. On-board regulators suppress pickup noise from the supply cable connected directly to each module. However, no method to isolate pickup noise from adjacent cables was in place and due to the contained nature of the electronics box, power cables passed across and near the optics module. This led to bit errors in the ADC, which manifested themselves as anomalous intensity spikes as seen in Figure 3.2-D. Table 3.2-A demonstrates the isolated nature of these spikes.

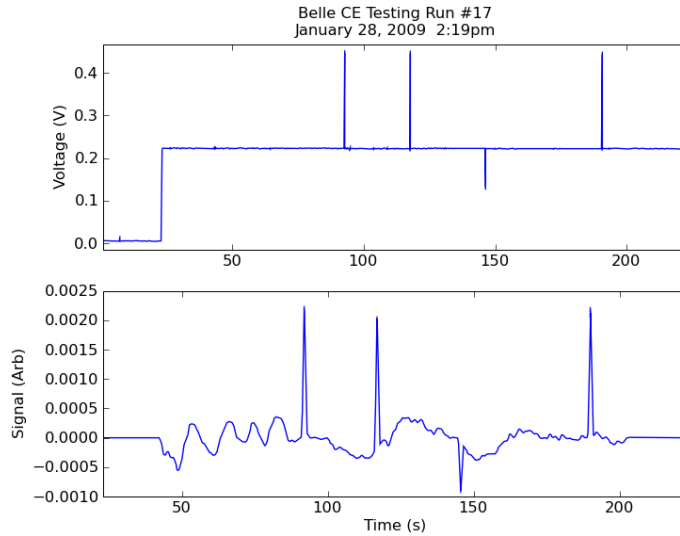


FIGURE 3.2-E: EXAMPLE OF ISOLATED, ANOMALOUS INTENSITY SPIKES IN THE ELECTROPHEROGRAM DUE TO POWER CABLES TO OTHER MODULES PASSING OVER THE OPTICAL DETECTION UNIT. THE BOTTOM PART OF THE FIGURE IS THE PROCESSED SIGNAL (SEE SECTION 3.2.4), LEADING TO THESE ISOLATED POINTS APPEARING TO BE PEAKS.

TABLE 3.2-A: DATA FROM THE ELECTROPHEROGRAM SEEN IN FIGURE 3.2-D. THE PHOTODIODE SIGNAL IS AUTOMATICALLY CONVERTED FROM AN ADC VALUE TO A VOLTAGE SIGNAL VIA THE SOFTWARE (CHAPTER 2).

Time (s)	Photodiode Signal (V)	Current (μA)
92.74	0.22300720	3.621
92.75	0.22224426	3.671
92.76	0.22338867	3.689
92.77	0.44662475	3.469
92.78	0.22239685	3.607
92.79	0.22270202	3.457
92.80	0.22270202	3.665

These anomalous intensity spikes were most likely a random sampling of voltage transient spikes on the power distribution ribbon cables due to the switching power supply⁶¹. Thus, an aluminum Faraday cage was built to surround the optics module and protect the optical signal. Once the cage was included in the system, the optics module

was effectively isolated from any pickup noise and these anomalous spikes no longer occurred. The noise was otherwise not characterised prior to this point.

This was a crucial step to achieving sensitive CE as signal processing can transform these spikes into peak-like formations that would make the integrity of our true peaks questionable. Due to the optical module's location (on the underside of the metal heatsink), it should be noted that the introduction of the Faraday cage subsequently grounded the heatsink as well.

SOFTWARE

The sampled signal from the optical module is saved into a time-stamped text file with the run parameters and graphed by the GUI. This allows the user to see the intensity data pre-signal processing if anomalies are seen in the electropherogram (processed data plot), such as artifacts of sudden laser variations. Furthermore, it allows all collected data to later be processed by alternative methods. The sample signal is then processed (as described in Section 3.2.5) and plotted along with the current information, which are attached to the report along with the run parameters and information as detailed in Chapter 2.5.

3.2.3 Signal Processing

A standard transimpedance photovoltaic op-amp (OPA129U, Texas instruments) amplifier is built into the hardware optics module in a high-gain (10^9 V/A), low bandwidth configuration designed to suppresses frequency components higher than ~ 1.5 Hz, as described elsewhere⁵⁷. This amplified signal is then sampled at 100Hz as the passage of DNA peaks take several seconds.

Semiconductor photodiode signals have two main categories of noise: shot noise and thermal noise. Shot noise sources encompass the dark current noise and shot noise from the current source, while thermal noise includes the build-up of resistance in the junction and bond contact, also called Johnson or Johnson-Nyquist noise⁶².

The photodiode datasheet specifies a dark current of 0.01nA, and with our $\sim 10^9$ A/V gain, this approximates to 10mV (as can be seen in Figure 3.2-F). The noise in this signal includes the shot and thermal noise inherent to the photodiode and electronics (excluding the laser), and white noise from the electronics.

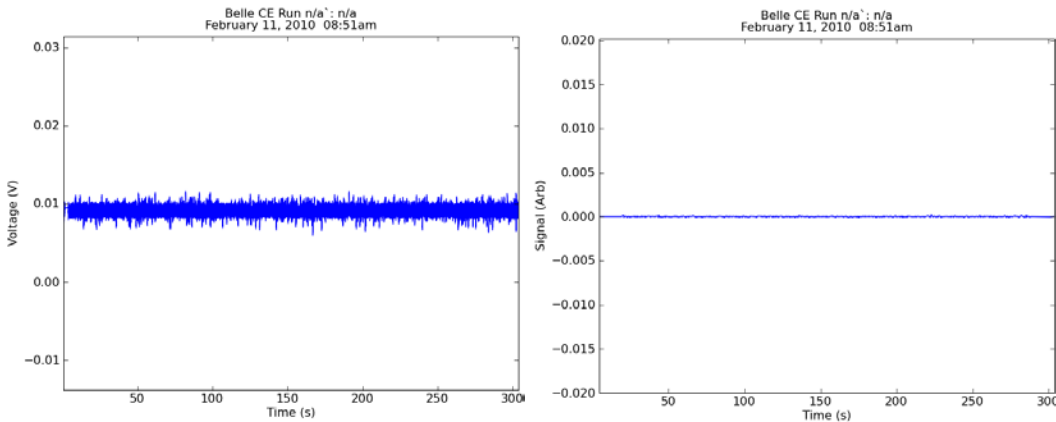


FIGURE 3.2-F: THE RAW, COLLECTED DARK PHOTODIODE SIGNAL DEMONSTRATING THE NOISE SOURCES INHERENT TO THE PHOTODIODE AND DETECTION CIRCUITRY (LEFT) AND THE SAME SIGNAL AFTER SIGNAL PROCESSING (RIGHT).

As seen on the right of Figure 3.2-F, the signal processing described in this section removes most of the noise sources inherent to the photodiode and detection circuitry. This signal processing method was based on the signal processing method used previously for this optical detection set-up (60-point moving average and 117-point median subtraction)⁵⁷. Post-processing, the standard deviation of the first 50 seconds (the noise) of our dark signal was found to be $\sim 5 \times 10^{-5}$ V. Excitation source noise will be described in detail in the next section (3.2.4).

To obtain a smooth signal, the collected photodiode data is subsequently processed using a low-pass software filter (LPF). A standard low-pass finite impulse response (FIR) equiripple filter with attenuation initiated at 1.2Hz and a cut-off frequency of 1.5Hz was designed by the author using MATLAB's filter design and analysis tool (FDA-Tool). Peaks are slowly varying with respect to our sampling frequency, and so the filter was

designed to remove all frequencies above 1.5Hz. Furthermore, as sample peaks in an electropherogram often increase sharply in intensity, the impulse response of the filter is as important as its magnitude response. The oscillations in the sinc impulse response function (see Figure 3.2-G) can create unreal “dips” before dramatically increasing sample peaks and so focus was placed on minimising these oscillations during design.

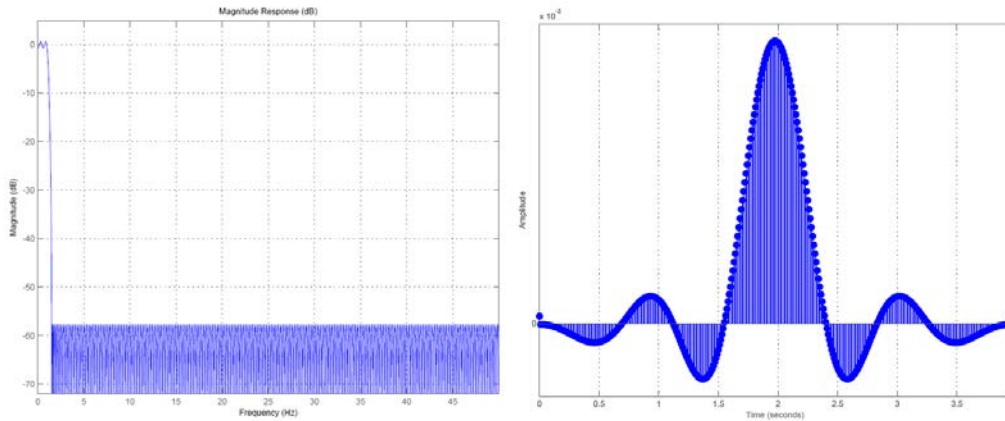


FIGURE 3.2-G: MAGNITUDE (LEFT) AND IMPULSE RESPONSE (RIGHT) OF THE SOFTWARE FILTER.

To remove the baseline and any intensity drift from the excitation source (as seen in Figure 3.2-H) due to slow, minute changes in temperature, the signal then undergoes a moving median subtraction, a standard processing tool for suppressing slow varying baselines. The length used for the median subtraction is important as too small of a window will significantly reduce the peak intensities, but too large of a window will not suppress the drift as effectively. The author investigated various widths during development of the signal processing method. 1500 points (15s) in each direction from the point being processed was found to effectively retain peak intensities, but did not remove decreasing intensity drifts occurring immediately prior to peaks (see below). 400 points (4s) was found to sufficiently suppress this type of baseline drift while minimally affecting the height of the DNA peaks, and so is more favourable than 1500 points if this is a re-occurring problem. However, as the scales on Figure 3.2-H demonstrate, there is still some intensity loss.

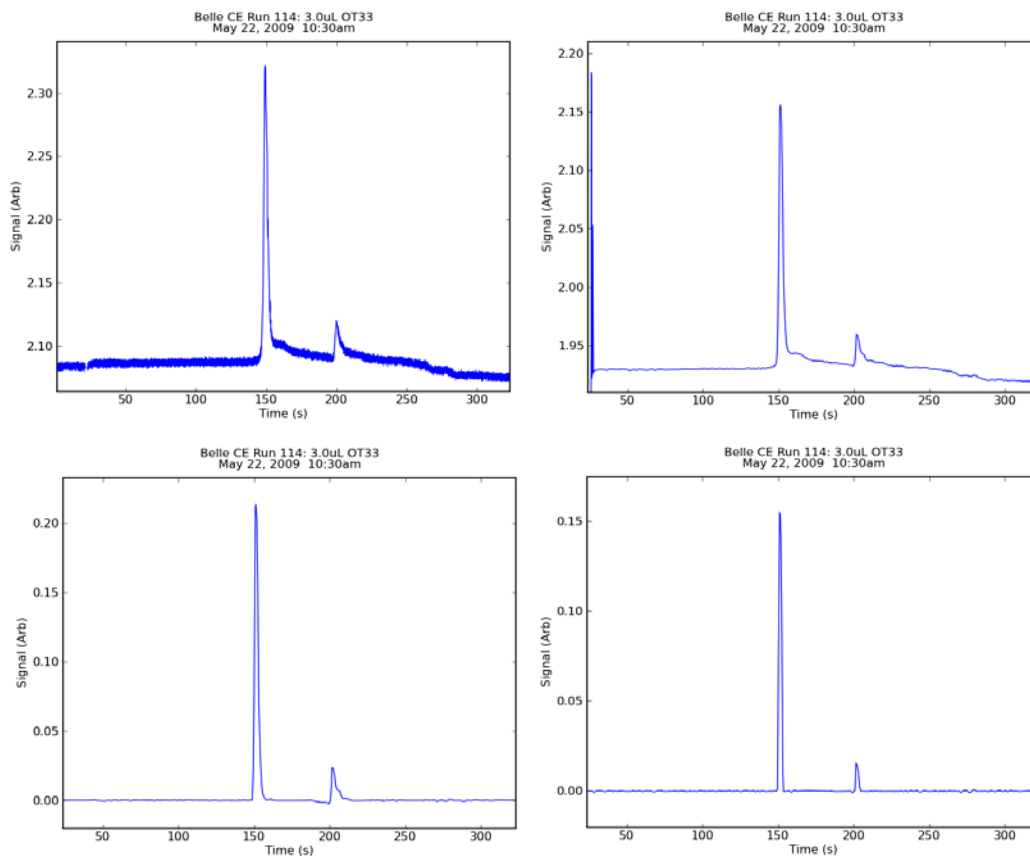


FIGURE 3.2-H: A DIAGRAM OF THE SIGNAL PROCESSING FLOW FROM THE RAW DATA (TOP LEFT), AFTER THE LOW-PASS FILTERING (TOP RIGHT), AND POST MEDIAN SUBTRACTION WITH TWO DIFFERENT WIDTHS: 1500 POINTS (15 SECONDS, BOTTOM LEFT) AND 400 POINTS (4 SECONDS, BOTTOM RIGHT)

This processing method reliably gives electropherograms with clearly detectable, isolated peaks corresponding to the primer and product peaks. However, when two peaks occur close to one another, the small median subtraction length leads to large, negative (unreal) intensity artifacts proportional to the intensity of the surrounding peaks. This can be seen in Figure 3.2-I with a double-labelled sample (the fluorescent tagging of both the forward and reverse primers in our protocol led to two closely spaced peaks, corresponding to either both individual primers or the primers and an artifact).

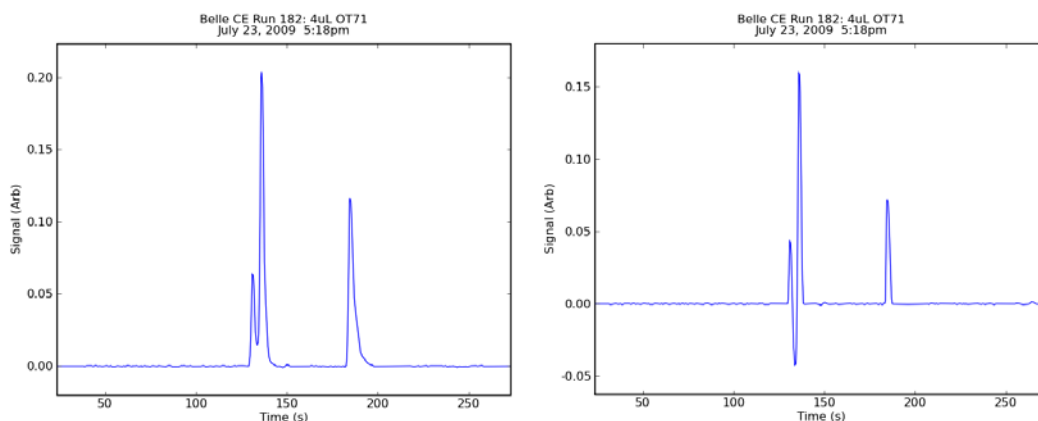


FIGURE 3.2-I: DEMONSTRATION OF HOW SMALLER MEDIAN SUBTRACTION LENGTHS LEAD TO UNREAL ARTIFACTS WHEN PEAKS ARE CLOSE TOGETHER; 1500 POINTS WAS USED ON THE LEFT AND 400 POINTS ON THE RIGHT.

While this is not a significant concern for this sample as the product peak is unaffected, when the area of interest has closely spaced peaks, this can lead to an unclear electropherogram. Performing CE and detection on a DNA ladder (a solution of known different DNA molecule lengths used to estimate the size of unknown products) is the perfect example of this (Figure 3.2-J, left image). It is not possible for the intensity of the signal to drop below zero as if in anticipation for the upcoming peak, as shown in the final processed image using the low-pass filter and median subtraction method. This coupled with the significant noise on either side of the red ladder peaks makes this electropherogram very questionable.

These challenges and concerns with laser stability (described in Section 3.2.4), led to the investigation of an alternative robust signal processing method that could be applied to a range of samples. S. Choi led this project, and with input from the author of this thesis, developed a signal processing algorithm using wavelet transform de-noising, peak region detection, iterative polynomial baseline fit, and parametric Jansson's deconvolution. More information on the exact process can be found in his thesis⁶³. This developed method was found to not only resolve the unreal artifacts and intensity loss brought about by the median subtraction, but also further reduced baseline variations,

leading to an improved signal-to-noise (SNR) ratio and an improved limit of detection (Section 3.3.1). While a moving, median subtraction can remove slowly varying baselines that are longer than its width, it cannot remove peak-like variations that are shorter. Preliminary results suggest the iterative polynomial baseline fit may be better equipped to remove these peak-like variations that occur from bursts in the laser (Section 3.2.4). S. Choi's method applied to a sample of AlfaExpress DNA ladder can be seen in Figure 3.2-J (right) and addresses the aforementioned problems.

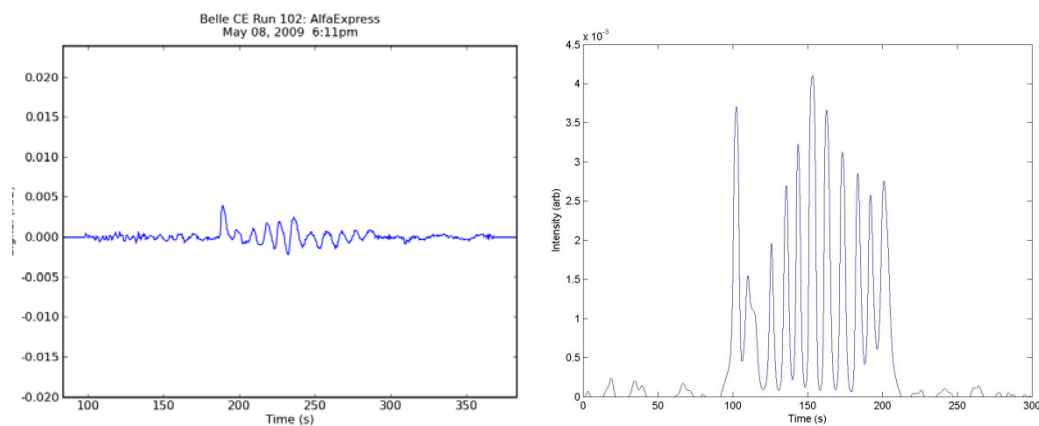


FIGURE 3.2-J: COMPARISON OF THE TWO DESCRIBED SIGNAL PROCESSING METHODS FOR AN ALFAPRESS DNA LADDER SAMPLE; LPF AND MEDIAN SUBTRACTION (1500S) ON THE LEFT, S.CHOI'S METHOD ON THE RIGHT.

The general signal processing method developed by the author was included in the software (as described in Section 2.5), and it is also possible to process data collected from the custom-built microfluidic instrument using an executable developed by S. Choi. However, it must be noted that the experiments must have been performed under the same running conditions of this thesis (i.e. CE protocol and optical detection set-up). The 32-bit version (Supplementary CD/AML Files/TTK/Choi Executable) includes three files: MCRInstaller.exe, ceSignalProcessing_standalone.exe and readme.txt. The MCR exe file installs MATLAB Compiler Runtime 7.10 so the shared libraries necessary for the signal processing exe work. The path environment variable must then be changed as described in the readme file. Once this is finished, the Signal Processing executable can

be run directly with no installation. The program will first ask which file is to be processed and then it will output a 1200x900 pixel jpeg image showing the processing steps from raw signal to deconvolved (seen in Figure 3.2-K) and a text file containing the location and heights of peaks found in the processed image.

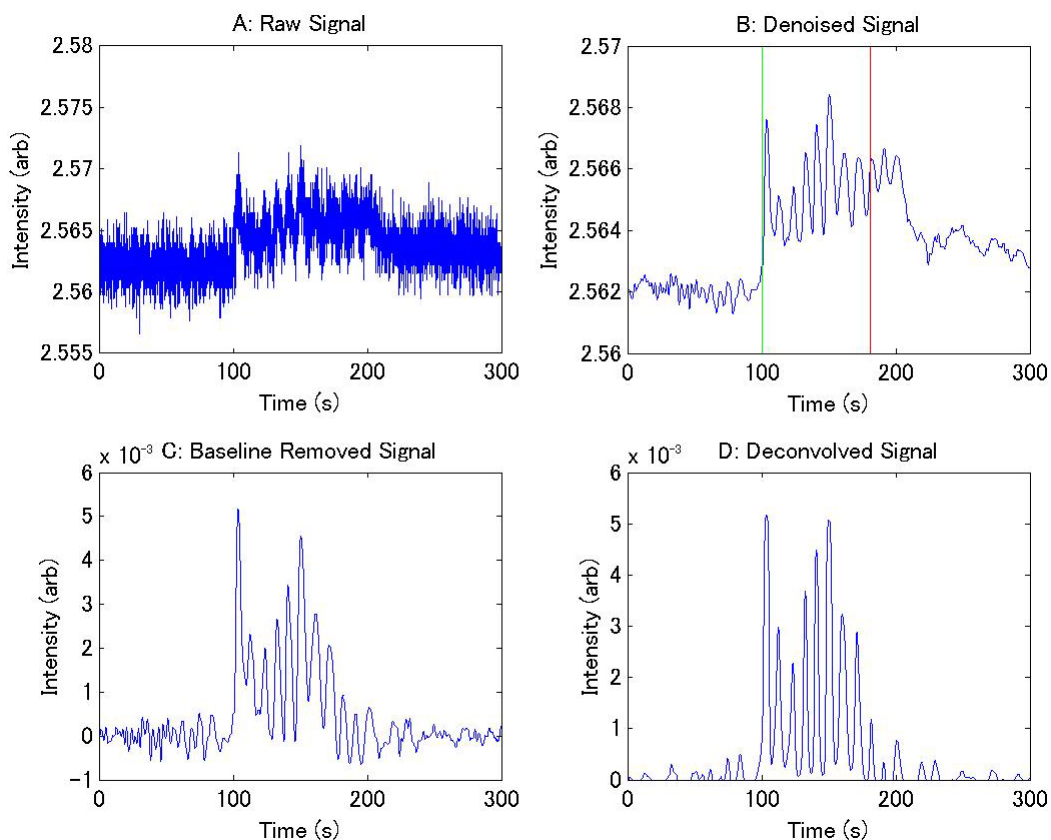


FIGURE 3.2-K: AN EXAMPLE OUTPUT JPEG IMAGE OF THE STAND ALONE SIGNAL PROCESSING EXECUTABLE AS DEVELOPED BY S. CHOI. THE ORIGINAL DATA FILE WAS COLLECTED FROM THE CUSTOM INSTRUMENT SET-UP AS DESCRIBED IN THIS THESIS AND WRITTEN BY THE SOFTWARE, AS SEEN IN FIGURE 3.2-J.

This should not be confused with the executable S.Choi also created for processing data from Micralyne's μ TK system, which only involves performing wavelet transformation. The author of this thesis has not tested this executable and thus only describes the processing developed for the custom-built microfluidic instrument described in this thesis.

3.2.4 Detection Factors

The disadvantage of most non-confocal systems is their high baselines. The baselines seen with the laser focused on polymer-filled CE channels in this thesis were typically ~1.5-2V..

Through thorough testing of the non-confocal set-up, the author determined that there were four factors that contributed to a well-focused and stable excitation beam spot on the separation channel, and thus, a good baseline. Improvements to each of these factors further improved the sensitivity of the system to achieve a low limit of detection, as described in Section 3.4.

LASER ALIGNMENT

If the laser is not focused well on the separation channel (the channel is illuminated by the laser from the side of the microfluidic chip), less excitation light can lead to less fluorophore light emission from the same amount of sample and thus, less sensitivity.



FIGURE 3.2-L: DIAGRAM ILLUSTRATING THE LASER BEAM'S POSITION IN RELATION TO THE GRIN LENS AND THE CHIP HOLDER, AND WHICH DIRECTIONS ARE DEFINED AS X, Y, AND Z.

When a laser is first placed in the system, the lens included in its packaging is adjusted so the focal point is above the GRIN lens in the detection path (Figure 3.2-L). This is accomplished by holding a flat, black background (i.e. black vinyl electrical tape on a

microscope slide) above the GRIN lens and rotating the included laser lens until the smallest point is seen on the background ($\sim 100\mu\text{m}$). Although this is done in air, the subsequent placement of the glass chip does not significantly affect the focal point. In this manner, the laser is fixed in an x-y position once it is installed. The chip is then placed reproducibly in a y position by centring the separation channel over the GRIN lens and in an x position via markings on the heatsink (notably, the countersink used for PCR as shown in Figure 3.2-B).

Unfortunately, microfluidic chip thicknesses were found to vary slightly (likely due to varying PDMS thicknesses of $\pm 10\%$, i.e. $\pm 25\mu\text{m}$) and with the CE fluidic channel etched into the bottom of the top plate; this required the laser to be adjusted in a z direction prior to beginning a CE (or PCR-CE) run. If multiple CE experiments (multiple chip loads of sample) are to be run on the same thickness of microfluidic chip, this only needs to be adjusted once. To set the z position of the laser, the clean, unfilled microfluidic chip is positioned on the heatsink as described and the laser holder is slowly adjusted until the brightest spot possible is seen refracting from the CE channel above the GRIN lens. There is a larger refractive index difference between air and glass than the separation matrix and glass; thus, using an unfilled chip creates a very distinguishable, bright spot where the focused laser light is scattered off of the channel wall when the laser is aligned correctly.

The baseline can then be used as a reference for how well a chip is focused and was experimentally found to be reproducible within $\sim 10\%$ for the same chip by the author. However, baselines were found by the author to vary by $\sim 25\%$ between good chips due to minor fabrication differences (i.e. varying the amount of scattered light) and the operator must be careful to ensure the laser is correctly focused on the channel (not that the baseline comes primarily from scattered light off other areas of the chip).

LASER OUTPUT

As with laser alignment, if the laser is not emitting enough excitation light into the channel, less fluorescent light will emit from tagged analytes, leading to lower sensitivity. Furthermore, for inexpensive laser diodes used under constant current conditions (as in this thesis), reduction in output power is indicative of degradation of the laser⁶⁴ due to a decrease in injected carrier lifetimes, increase in internal cavity loss, or problems in the laser driver circuitry. Thus, a decrease in the laser output power impacts its reliability.

A laser's output power should be measured at the time of installation using the optical power meter set to the wavelength (635nm) and recorded in its respective system binder (along with the note of its installation). The author of this thesis kept one microfluidic chip that was well-known for CE in her possession at all times so that if doubt about the laser power or focusing arose, she could use it as a reference and compare. If the laser's output power becomes suspect, it should be re-tested with the optical power meter (this can be done by adjusting the z axis of the laser holder, without needing to remove it) to ensure the laser output has not decreased.

LASER STABILITY

Stability is important as oscillations and step-like responses in intensity can obscure peaks and increase the noise, reducing SNRs and sensitivity.

As the brass casing of the laser diode is +5V when the laser is powered, the laser holder is made of brass, and the heat-sink is made of aluminum and grounded (due to the Faraday cage built for the optical system as described previously), the laser needed to be electrically insulated from the holder where it did not in the previous system. This was done by placing thin sheets of mica between the laser and the holder. However, as was determined through extensive testing, this also unexpectedly thermally insulated the laser and its casing. As the laser was toggled on only for separation times and was off between runs and during injection, the laser temperature was never allowed to equilibrate and this led to variations in the temperature of the laser casing for every

separation. This is detrimental to the laser light both in terms of wavelength and intensity, as these can be nonlinear functions of the operating temperature of the laser⁶⁵. These temperature variations manifested into dramatic oscillations coupled with mode-hopping behaviour as described elsewhere⁶⁵. While the magnitude of these variations were only $\sim 1.5\%$ from the mean of the baseline, they were comparable to or larger than sample product peak sizes (i.e. 20-30mV).

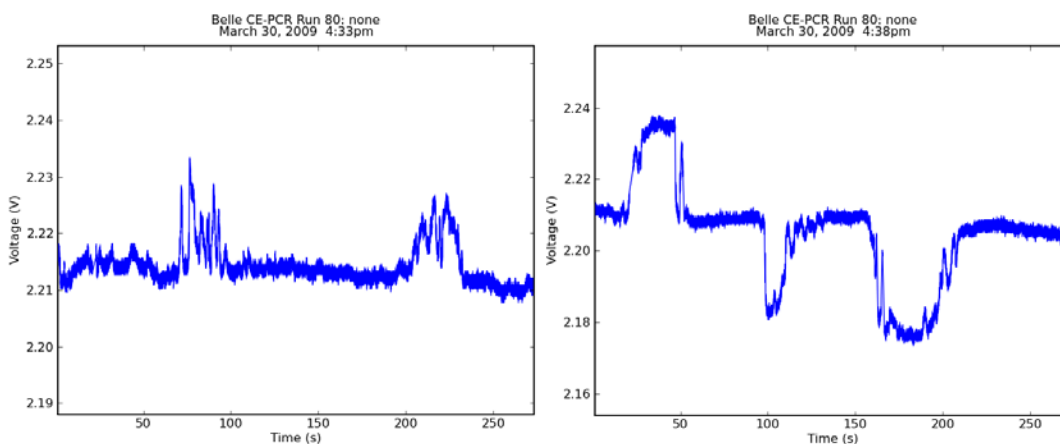


FIGURE 3.2-M: IMAGES OF RAW DATA COLLECTED AFTER THE LASER WAS ELECTRICALLY INSULATED FROM THE HOLDER BUT ALSO UNEXPECTEDLY THERMALLY INSULATED THE LASER. ERRATIC CHANGES IN INTENSITY GIVE THE DRAMATIC OSCILLATIONS AND MODE-HOPPING BEHAVIOUR SEEN HERE.

Thus, as others have previously described⁶⁶, our laser diode needed to be temperature controlled to achieve a beam quality sufficient for sensitive capillary electrophoresis. To provide a means of stabilizing the temperature, a new laser holder was built with a larger thermal mass and a larger area of contact with the $\sim 40\text{g}$ heatsink used for on-chip PCR. Furthermore, the post connecting the laser to the heatsink was changed from brass to ceramic so Mica film could be removed. With this new laser holder and warm-up times to bring the laser to thermal equilibrium, it was possible to reduce the variation of the baseline to less than 0.5% (measured from the minimum to maximum values on the raw signal of $\sim 5\text{min}$ in length). The remaining variation was contributed to

mostly by very slow variations likely due to minor temperature fluctuations that could be removed with our signal processing (Section 3.2.3).

Unfortunately, the laser manufacturer builds their laser diodes to a specification of ~5% of variation at operating temperatures between 21-24°C, it has been found that not all purchased lasers are capable of achieving the stability described in this thesis. Thus, to determine if a laser is sufficiently stable, a characterization program was built into the software by the author. This consists of placing a chip filled with water and sealed to limit evaporation into the system (air would cause too much refraction and saturate the photodiode), and collecting data from the optical system for the first 2.5 hours of the laser's life (i.e. when it is first installed). Upon placement of the chip in the system, the laser is toggled on ("Laser On" button) and the "Characterise" button on the CE panel of the GUI is pressed. Thirty CE runs with 0s of "injection" and 5min of "separation" each are then collected and processed using the low-pass filter and median subtraction method built into the software. This provides both a thermal equilibrium time and a representation of the laser's stability. The standard deviation of the first 50 seconds of data for each 5 minute interval is determined automatically and recorded in the report. After the 20-25 minute intervals, the standard deviation should be less than 0.0002V to achieve CE sensitivities comparable to the ones established in this thesis.

Figure 3.2-N demonstrates a typical laser characterisation, with the signal being very noisy when it is first switched on (with peaks of more than 15x the average standard deviation of this laser when stable), illustrating the need for a warm-up period. This tapers off in the first 5 minutes and lower frequency wobbles do not appear after the first 15 minutes. After 20 minutes, the standard deviation of the first 50s of data is 6.81×10^{-5} V. This warm-up behaviour was found to be consistent between the two or three lasers tested by the author of this thesis.

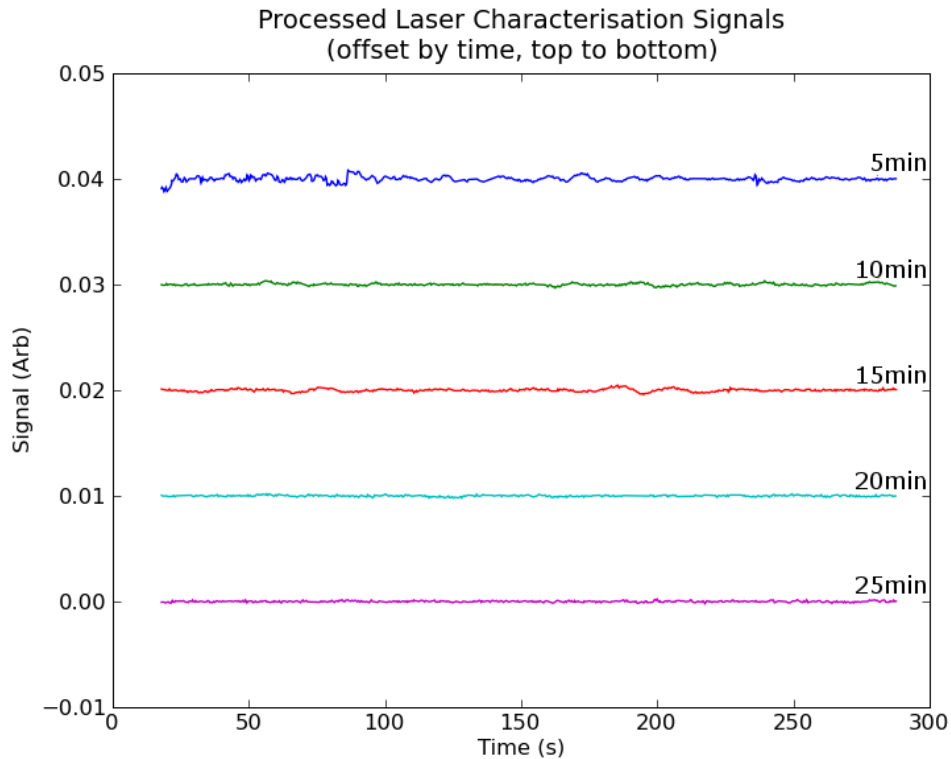


FIGURE 3.2-N: AN IMAGE OF THE FIRST 25 MINUTES OF A NEW LASER BEING CHARACTERISED BY THE SOFTWARE. THE FIRST FIVE MINUTES ARE VERY NOISY, BUT AFTER ABOUT 15 MINUTES OF WARM-UP, THE SIGNAL STABILISES.

Unfortunately, as shown to some extent in Figure 3.2-O, the signal is not constant and small bursts of noise can be seen. These can be due to small fluctuations in temperature or noise coming off the wall power, and are seen even in the best characterised lasers. Unfortunately, these small bursts cannot be removed with the simple signal processing method described in this thesis and are often on the order of 4-5x ($\sim 0.2\text{-}0.5\text{mV}$) the average standard deviation of the stable laser. This is larger than our specified limit of detection (3x the standard deviation) and so all CE experiments are run in duplicate or triplicate on the same chip load to ensure weak peaks are not the product of laser variations. Peaks seen on all runs are considered to be true diagnostic products. A typical on-chip PCR product (as discussed in the next chapter) using our standard protocol was approximately 40mV and ranged from $\sim 5\text{mV}$ -70mV.

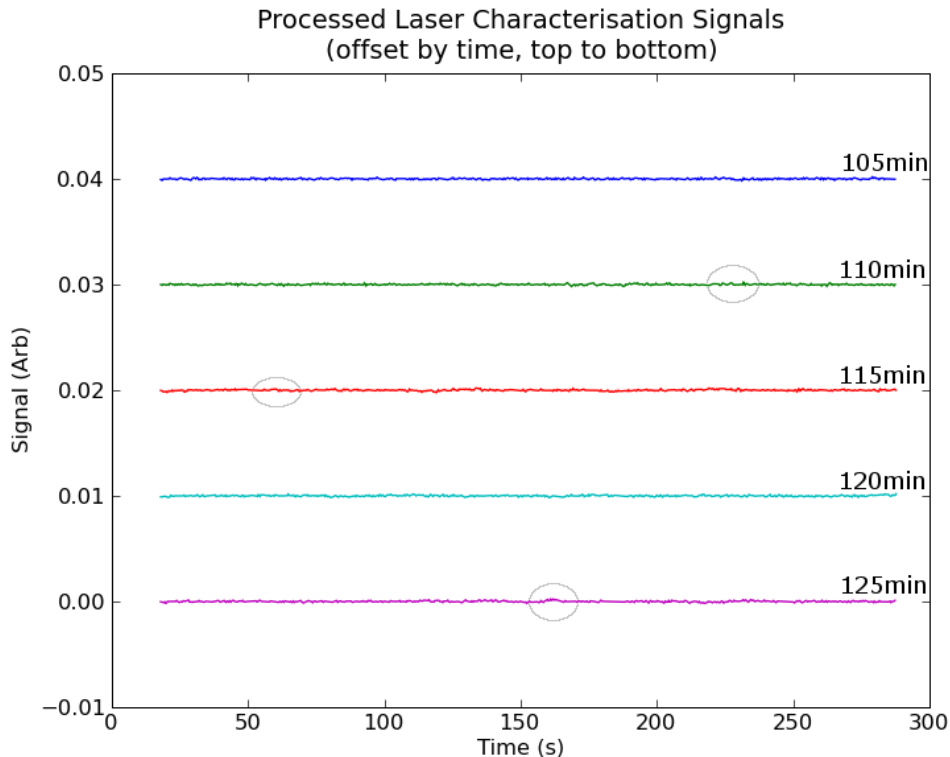


FIGURE 3.2-O: AN IMAGE AFTER 100 MINUTES OF THE SAME LASER IN THE PREVIOUS FIGURE BEING CHARACTERISED BY THE SOFTWARE. SMALL BURSTS OF NOISE CAN BE SEEN IN THE 110, 115 AND 125MIN TRACES.

These bursts of noise were part of the motivation for an alternative robust signal processing method led by S. Choi. His preliminary results were briefly presented in Section 3.2.3, but unfortunately they were not able to address this issue.

CHIP CHARACTERISTICS

Partway through the verification process, the author discovered that the laser could not be focused on the CE channel at the detection point on most microfluidic chips. Rather than a bright focal spot of approximately $200\mu\text{m}$, the excitation light was scattered across the channel and a focal point could not be reached. For a period of experiments, the author was required to perform the CE experiments of all PCR-CE runs on two “magic chips”. Through multiple batches of newly assembled microfluidic chips, the author managed to collect 5 of these “magic chips”. She then compared them with

another 5 chips that were unfocusable, all of which were built in the laboratory by Abraham Jang. It should be noted that the CE channels themselves were etched cleanly on all 10 chips. The author discovered two points of commonality between all of the chips.

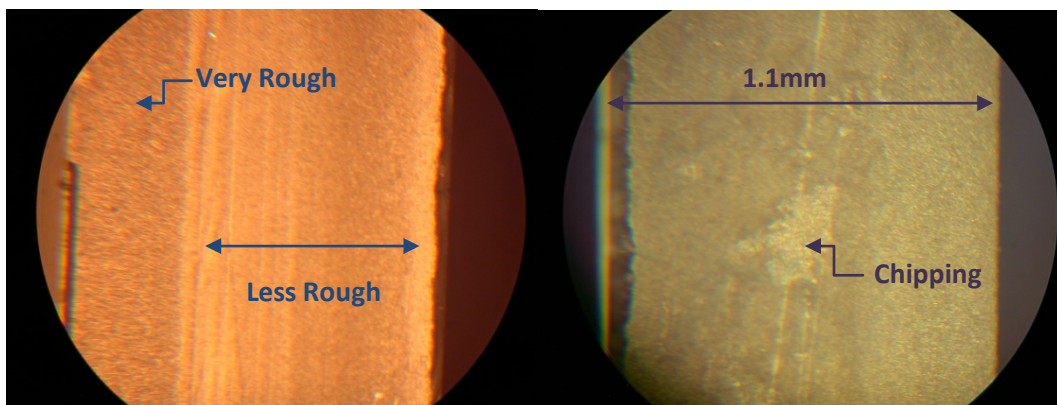


FIGURE 3.2-P: IMAGES TAKEN BY A. JANG DEMONSTRATING THE INCREASED ROUGHNESS ON THE DICED SURFACES OF THE GLASS PLATES. ON THE LEFT, THE TOP PLATE SHOWS THE 1/3 ROUGH AND 2/3 SMOOTH SURFACE AS DESCRIBED; ON THE RIGHT, THE ENTIRE DICED FACE IS CONSIDERABLY ROUGHER THAN THE CLEANER SURFACE ON THE LEFT.

First, all glass plate sides had a bi-roughness pattern with $\sim 1/3$ of the 1.1mm depth considerably more rough than the remaining $2/3$ where they were diced. On well-focused chips, the rougher surface was at the top of the glass plate; on poorly-focused chips, the rougher surface was at the bottom of the plate, or the interface between the PDMS and top plate (where the laser passes through). Once this was discovered, it was found other plates had entire surfaces which were considerably rougher than the well-focused chips, even with some chipping (Figure 3.2-P). However, on much older chips, the etched features could be seen through the side of the chip and they did not have this “frosted” quality. Thus, it was eventually determined by other members of the group that this roughness was due the use of a different dicing saw.

Second, the author discovered that on well-focused chips, the top plate was slightly dislocated from the bottom and was slightly over-hanging the PDMS and bottom plate

on the detection face. On poorly-focused chips, the bottom-plate was slightly overhanging the top plate and PDMS. This means when the top-plate/PDMS interface was flush, the beam could not be focused on the chips; when they were staggered (specifically, when the glass was closer to the excitation beam than the PDMS face), the beam could be focused. Even though the channel is etched into the bottom of the top plate, for the beam to be focused on the channel, a large area of the beam must first pass through the air/glass and air/PDMS interfaces. As the PDMS tears even when sliced with a clean scalpel, the PDMS surface is considerably rougher than the glass surface and leads to light scattering. Furthermore, the scalpel chips at the glass surface while slicing the PDMS: if the top glass plate was overhanging, the bottom plate was chipped and if the bottom plate was overhanging, the top plate was chipped. These chips in the top plate also contributed to increased scatter. For these reasons, M.Behnam moved the beam from a 0° angle (parallel with the x-y plane) to a 5° angle (downwards) and version 3 PCRCE4 chips were designed to have larger top plates than bottom plates (this was also done to improve the alignment).

This was an important discovery as the sensitivity of the CE detection is very dependent on how much light can be focused onto the channel; i.e. how many fluorophores could be excited. Thus, this was a significant challenge identified by and solved with the help of the author.

3.3 PROTOCOL

3.3.1 On-chip Procedure

The CE separation matrix used to separate the analytes of interest was 4% linear polyacrylamide (LPA) as in previous work⁶⁷ and was prepared as described elsewhere^{43,32}. To minimise analyte adsorption to the glass walls and electro-osmotic flows, the CE channels were also coated as in prior demonstrations⁶⁷. A stock 10xTTE buffer made of 500mM Tris-base, 500mM TAPS and 10mM Na₂EDTA was made with a pH of 8.3 ± 0.3 from which all subsequent dilutions originated from. The pH was

measured using the Accumet BASIC AB15 pH Meter by first standardising the reading using the manual instructions (press the “std” button and submerge the electrode into the pH 4, 7 and 10 buffers as instructed, washing with distilled water and drying with a Kim-wipe between buffers) and then measuring the pH. The 10xTTE buffer was measured upon mixing and before new 1xTTE dilutions were made. It was not possible to measure the pH of the 1xTTE buffer before all CE experiments due to its small volume, so the LPA and 1xTTE were mixed fresh from stock monthly (before their expected lifetimes were expired).

The channels are filled with LPA via a fitted syringe applied to the buffer waste well. The excess polymer is removed and 4 μ L of 1xTTE buffer is then pipetted into each CE well, except for the sample input well. 1.0 μ L of sample is then added to the sample input well with 3.0 μ L (for a total of 4 μ L) of 0.01xTTE. The DNA sample is then electrokinetically injected into the injection channel using 200V (~222 V/cm) for 80s and separated using 600V (~67 V/cm) for 250s. Subsequent injections also use 200V, but are only 20s in length.

In this thesis, “chip load” refers to the loading of the channels with matrix, wells with buffer, and sample well with sample. Multiple injections following the protocol described above are defined as “runs”.

3.3.2 Sample Stacking

Using a lower ionic concentration buffer than that of the background buffer (matrix and buffer/waste wells) when executing CE promotes a phenomenon called sample stacking. As the lower ionic buffer concentration region has lower conductivity, when an electric field is applied the sample accelerates through this region due to its enhanced electrophoretic mobility. Once the sample crosses the boundary to the higher conductivity region or higher concentration buffer (where the sample has a lower electrophoretic mobility) the sample slows, creating a traffic jam effect and stacking the sample together^{68,50}.

Ideally, this would mean the sample stacking effect is limited only by the impurities in the channel and if water is placed in the well with the sample, the highest stacking effect should be achieved. However, diffusion will happen over the boundary between the low and high ionic concentration regions. Furthermore, due to the differences in electroosmotic velocity between the two concentration buffers and the bulk velocity of the fluid in the capillary, laminar flow will occur⁶⁹. This will go against the flow of the DNA, and will work to broaden or de-concentrate the sample stacking at that boundary. The higher the concentration difference between the two buffers, the greater the rate of diffusion and laminar flow will be. Thus, there exists a trade-off and an optimal sample buffer concentration for greatest sample stacking effect.

Here, the lower concentration buffer is mixed with the sample in the sample well while the channels and other wells are filled with the higher concentration buffer. In this manner, the sample stacks between the sample input well and the injection channel (as it moves from lower ionic concentration to higher), and capillary electrophoresis proceeds as standard with a higher concentrated sample. The author determined experimentally how the peak height increases as the sample ion concentration decreases with the previously described protocol (Section 3.3.1). The buffer used in the CE channels and all wells, excluding the sample well, is 1xTTE. Thus four buffers (0.1x, 0.01x, 0.001x, and 0.0001xTTE) were run to find the “optimal” concentration that would provide the strongest and most reproducible peaks (see Table 3.3-A). For each buffer concentration, two runs were performed on multiple chip loads using the commercial CE instrument (μ TK). A factor for relative peak height was determined in relation to 0.1xTTE as this was the sample buffer used in previous work⁶⁷.

TABLE 3.3-A: VARIABILITY AND AVERAGE INTENSITY INCREASE FOR DIFFERENT MAGNITUDES OF SAMPLE BUFFER CONCENTRATION TO DETERMINE THE OPTIMAL CONCENTRATION FOR DESIRED SAMPLE STACKING.

Sample Buffer Concentration	Run	Avg. Primer Peak		Avg. Product Peak		Average Intensity Ratio
		RMD	Intensity Ratio	RMD	Intensity Ratio	
0.1xTTE	1	0.19	Ref	0.20	Ref	Ref
	2	0.17	Ref	0.21	Ref	
0.01xTTE	1	0.07	2.45	0.01	1.80	2.03
	2	0.26	1.90	0.31	1.96	
0.001xTTE	1	0.37	2.73	0.11	3.02	2.46
	2	0.63	2.20	0.62	1.87	
0.0001xTTE	1	0.07	1.58	0.23	1.46	1.57
	2	0.02	1.84	0.17	1.42	

The lowest concentrated buffer, 0.0001xTTE, was found to have the lowest average intensity ratio of the three tested, most likely due to the diffusion and laminar flow effects described previously being much stronger than the stacking effect. The buffer with the best average ratio was 0.001xTTE, at 2.46 times stronger in intensity than using 0.1xTTE. However, the average intensity of the product peak for the first run is almost twice that of the second run and the variability of the second run is quite large with an RMD of 62%. This drop in intensity and increase in variability is likely due to diffusion of the higher concentrated buffer into the lower concentrated sample buffer over time, leading to considerably different, time-dependent ionic conditions for the second run of the experiment as compared to the first.

For these reasons, 0.01xTTE was chosen as the “optimal” buffer concentration to be mixed with the sample rather than 0.001xTTE, even though the average intensity ratio for the latter is higher. The second run of 0.01xTTE is half as variable as 0.001xTTE (31% vs. 62%), only slightly more variable than the standard buffer, and does not suffer the dramatic decrease in intensity that the second run of 0.001xTTE did. This is important for low concentration peaks where multiple runs are performed to ensure products are not the result of laser instabilities.

3.3.3 Mobilities and Resolution

An analyte's velocity during electrophoresis was described in Section 1.2.4, and this can further be re-arranged to find the analyte mobility:

$$\mu_E + \mu_{EOF} = \frac{v}{E} \quad \text{EQUATION 3.3-A}$$

While the EOF mobility can be measured experimentally using neutrally-charged analytes, here we are interested more in the analyte apparent mobility (μ_a), or the algebraic sum of the EOF mobility (μ_{EOF}) and the electrophoretic mobility (μ_e).

The apparent mobility can be determined from the migration time of the analyte (time taken for the analyte to move from the intersection to the detection point, t), the applied voltage (V), the effective length of the capillary (migration distance, l), and the total length of the capillary (L)⁷⁰:

$$\mu_a = \frac{lL}{tV} \quad \text{EQUATION 3.3-B}$$

Using this equation, the apparent mobilities for a conventionally thermal-cycled BK virus (BKV) primer and product (see Section 4.2.3) with a length of 26 bases and 299bps in length were $\sim 0.015 \text{ mm}^2/\text{V}\cdot\text{s}$ and $\sim 0.011 \text{ mm}^2/\text{V}\cdot\text{s}$, respectively.

This means with a detection point at 13mm and an applied voltage of 600V on our microfluidic chip using the previous described protocol, the BKV primer appears at ~ 150 s of separation and the 299bps product at ~ 200 s. Peak arrival times were found to vary by about 2%. This was likely due to minor variations in buffer concentration and electro-osmotic flow.

As demonstrated in a previous publication⁷¹, we define the resolution in bps using:

$$R_{s,bp} = \frac{(w_1 + w_2) \Delta M}{2 \Delta t} \quad \text{EQUATION 3.3-C}$$

where w_1 and w_2 are the full width at half the maximum (FWHM) of the preceding peak and the peak under investigation, respectively; ΔM is the bp size difference; and Δt is the time difference between the two peaks passing the detector, centre to centre. The resolution in bps defines how well the CE protocol and microfluidic chip resolve similarly sized analytes. Two peaks that met at their half-widths could still be resolved while any closer would be assumed to be one peak.

The resolution was found first using BKV PCR product and then compared with the resolution determined using a size standard due to the extremely poor signal processing of the red ladder (Section 3.2.3), and was found to be ~ 12 bps. This agreed with results found using a DNA ladder on both the custom and commercial (μ TK) systems, indicating the resolution is determined by the CE protocol and the microfluidic chip, and is not contributed to negatively by the instrument's detection system. However, the signal processing can also play a factor in the resolution, depending on which method is used. As demonstrated in Section 3.2.3, the median subtraction step in the signal processing can affect the peak shape/height if its width is smaller than the width of the peak. This ~ 12 bps resolution was determined from using a 400 point (4s) median subtraction, which is smaller than the average product peak width. For comparison, the resolution was re-calculated from the electropherograms using 1500 points (15s), a value which is much wider than the product peak widths. Here, the resolution was found to be ~ 16 bps.

This resolution is more than sufficient for our applications. However, if a higher resolution were required, it would be possible to adjust the CE protocol (such as a more viscous or alternate separation medium or possibly lower voltages) and/or move the detection point further down the channel to allow peaks closer in size to be resolved. It should be noted that single bp resolution is possible and has been achieved using these techniques: the Mathies' group demonstrated single-base resolution through extension of their separation channel⁷², and our group showed near-single-base resolution using a different CE protocol/chip for a different application⁷³.

3.3.4 Run-to-Run Variability

As the limit of detection experiments were run multiple times at each concentration on both the μ TK and our custom-built instrument, it is convenient to also use these runs to determine the variation of peak intensities present in our CE procedure.

There are multiple types of variabilities that can be explored for CE. In this thesis, we will discuss the run-to-run variability of one chip load, demonstrating the optimisation of the CE protocol, and the load-to-load variability on one chip, demonstrating the repeatability of achieving the same peak height upon separate sample loadings (Section 3.4.2). To separate the run-to-run variability from the load-to-load variability, successive runs of each load are compared to one another and averaged.

With a well-optimised CE protocol, the peak intensities for successive injections of the same chip sample load should be reproducible. Buffer effects and improper timing of injections can lead to varied amounts of the sample in the intersection, and subsequently, passing by the detector during separation. Furthermore, variances in electro-osmotic flow (EOF) velocity can also lead to different migration times. As the previous are a result of the CE protocol and capillary, run-to-run variability should be system independent.

For the LOD experiments, the average RMD for the three concentrations gave a run-to-run variability of 6.9%. To ensure this variability wasn't attributable to the primers alone, a conventionally thermal-cycled BKV product was also compared. The product or "diagnostic" peak was found to have average RMD run-to-run variability of 5.9%.

3.3.5 Buffering Capacity

The buffer ensures a constant pH environment during capillary electrophoresis. However, over time the finite volume of the wells and electrode reactions will deplete the buffer ions, allowing the pH to possibly change and damage the DNA sample. Brask⁷⁴ defines the following equation to provide a rough estimate on depletion time:

$$t_{dep} = \frac{cvF}{I} \text{ [s]}$$

EQUATION 3.3-D

where c is the buffer concentration in the well, v is the volume of the well, I is the electric current and F is the Faraday constant. The maxima of injection and separate currents during average CE experiments were determined to be about $30\mu\text{A}$ and $4\mu\text{A}$, respectively.

Using this method for the conditions in our sample input well suggests the injection time expected to deplete the buffering capacity of Tris in the sample well for the first run is approximately 40 seconds, or half of the injection time specified in our protocol. However, in spite of this, we reliably obtained results with variabilities similar to those with higher concentrations of sample input buffer (see Section 3.3.2). This is likely due to the fact that Brask's method does not consider our sample stacking environment in his rough equation. While the sample input well has a Tris concentration of only 2.5mM, the channels and other three wells have concentrations of 50mM. Thus, diffusion will replenish depleting ions due to electrode reactions, leading to considerably longer depletion times. As expected, the separation depletion times were calculated at approximately 4800 seconds (~80 minutes).

3.4 SYSTEM PERFORMANCE

3.4.1 Limit of detection

The system's optical sub-system was characterised by determining the limit of detection. This was done using three known concentrations of end-labelled DNA (Cy5 end-labelled reverse primer). For the standard PCR mixture (Section 4.2.3), these primers are diluted from stock using PCR grade water to an initial concentration of $10\mu\text{M}$ or 1xRevPrimer. Further dilutions of this 1xRevPrimer with PCR grade water gave three primer solutions at 0.3x, 0.2x, and 0.1xRevPrimer, or $3\mu\text{M}$, $2\mu\text{M}$, and $1\mu\text{M}$, respectively. Our standard PCR mixture (Section 4.2.3) was then mixed using these three primer concentrations rather than the specified $10\mu\text{M}$ and substituting forward primer,

template DNA and platinum Taq with water, to form what we refer to as 0.3x, 0.2x and 0.1xLODmix. These three samples have final concentrations of 0.749 ng/ μ L, 0.498 ng/ μ L, and 0.249 ng/ μ L of end-labelled DNA, respectively. The detailed protocol can be found in Appendix D.

This mixture includes all of the standard PCR reagent concentrations to avoid an unrealistic LOD value brought about with sample stacking effects, while excluding the DNA template, unlabelled primer and Taq polymerase to avoid different CE characteristics brought about with high levels of excess DNA and enzyme that would otherwise be mostly consumed during the PCR reaction. This provided the author with a known fluorescently tagged DNA concentration with the same ionic components and strength as the standard PCR product in use.

Once the three different concentrated samples are prepared, CE was then performed using 1 μ L of the LODmix of interest and 3 μ L of 0.01xTTE as specified in Section 3.3.1. Each concentration had duplicate or triplicate chip loads, with duplicate runs on each load. All electrophoresis runs had identical electrophoretic conditions, reagents and were run on the same microfluidic chip (flushed thoroughly with autoclaved water between each load). This resulted in average SNRs of 363, 229, and 194 for the concentrations of 0.749 ng/ μ L, 0.498 ng/ μ L, and 0.249 ng/ μ L of end-labelled DNA, respectively. An example electropherogram for each concentration can be seen in Figure 3.4-A.

The data was then processed as described in Section 3.2.3 by the software and all peak intensities were plotted versus the primer concentration. The noise was determined by taking the standard deviation of the first 50s of separation data (sufficient for the primer arrival time) for all runs and averaging these values, and was found to be 1.14×10^{-4} V. As standard procedure⁷⁵, a linear regression was performed on the intensity vs. concentration plot to extrapolate the concentration of a peak with intensity 3 times the average noise level.

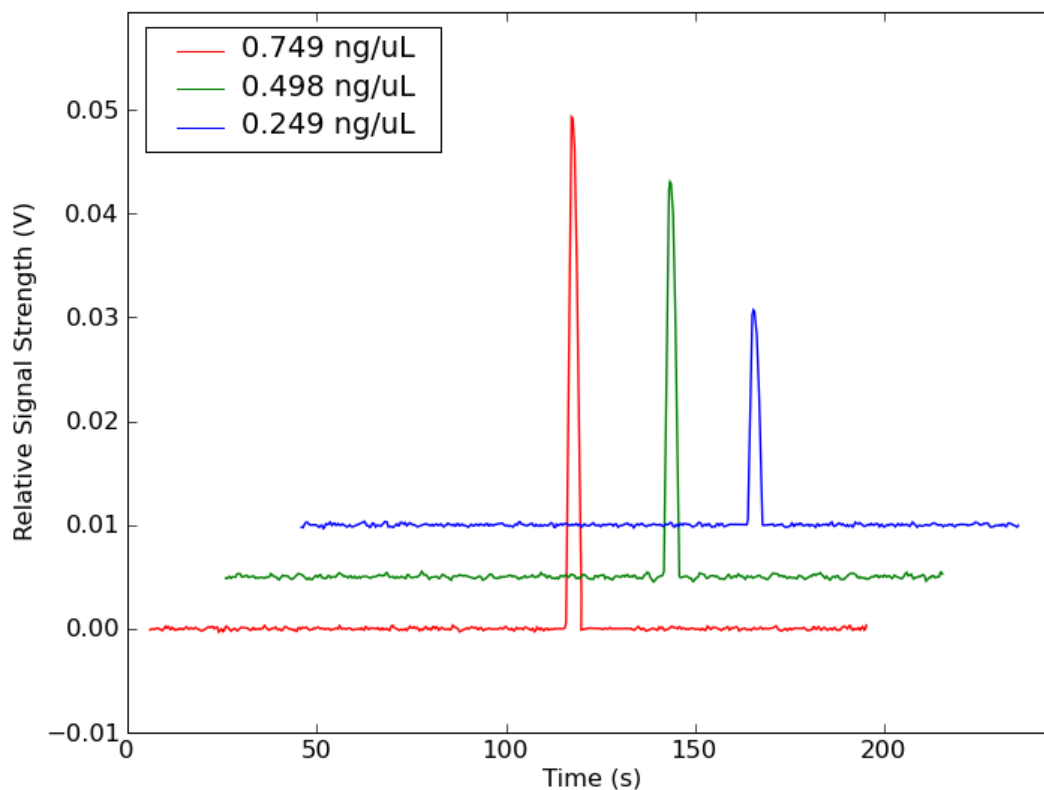


FIGURE 3.4-A: LIMIT OF DETECTION ELECTROPHERORAMS FOR 0.749 ng/ μ L, 0.498 ng/ μ L, AND 0.249 ng/ μ L OF END-LABELLED BKV REVERSE-PRIMER DNA. © THE ROYAL SOCIETY OF CHEMISTRY⁴³, 2010.

The LOD was estimated to be 700pM (7.0×10^{-16} mol/ μ L) of Cy5 fluorophores, corresponding to 5.8pg/ μ L of Cy5-end-labelled (25 base) BKV primer DNA or approximately 60pg/ μ L of double-Cy5-end-labelled, double-stranded 250bps PCR product. If intercalators were used instead of end-labelled primers, we would expect a LOD of 1.2pg/ μ L of double-stranded 250bps PCR product, assuming labelling of 1 fluorophore per 3 bases. Whichever labelling technique is used, this system is orders of magnitude more sensitive than expected to detect a standard, single-labelled PCR product.

It is also important to note that the LOD represents the concentration loaded into the CE sample well of the microfluidic chip, not the actual concentration of the sample in

the separation channel over the detection point. This means the LOD value is very specific to the CE protocol, which determines how much DNA is loaded into the intersection and separated at which resolution. The actual amount of reverse-primer detected in these electropherograms is expected to be $\sim 10^{-4}$ of the amount of the sample loaded into the sample well, estimated roughly from the chip dimensions (intersection volume/sample volume = $4.5 \times 10^{-13} \text{ m}^3 / 4.0 \times 10^{-9} \text{ m}^3 \cong 1 \times 10^{-4}$).

In conventional diagnostic laboratories, gel electrophoresis is most often used as described in Section 1.2.4 using ethidium bromide as an intercalator, which has a limit of detection of approximately $20 \text{ pg}/\mu\text{L}$ – $20 \text{ ng}/\mu\text{L}$ of DNA⁷⁶. Applying the same LOD protocol to the μTK resulted in an LOD of $2.8 \times 10^{-16} \text{ mol}/\mu\text{L}$ of Cy5 fluorophores or $2.3 \text{ pg}/\mu\text{L}$ of Cy5-end-labelled BKV primer DNA. This means our system is comparably sensitive to the conventional method currently used in clinical laboratories now. Furthermore, it is only ~ 3 times less sensitive than a commercial, confocal-based approach using a PMT detector, which is approximately 100 times as expensive as our system!

Unfortunately, instabilities in the laser intensity as described in Section 3.2.1 occasionally results in burst of noise that can affect the SNR of the peaks in the electropherogram, reducing the LOD to about $120 \text{ pg}/\mu\text{L}$ of Cy5-end-labelled (26 bases) BKV primer DNA. For this reason, duplicate and triplicate runs are always performed. Preliminary results using S.Choi's method, as discussed in Section 3.2.3, was found to improve the limit of detection from $5.8 \text{ pg}/\mu\text{L}$ to $1.7 \text{ pg}/\mu\text{L}$. This is approximately 3.5 times more sensitive and certainly able to detect the PCR products shown in this thesis, even with rare laser instabilities.

3.4.2 Sensitivity

From the LOD data, the sensitivity of the system can also be determined. Using Figure 3.4-A, the sensitivity for primers is estimated to be $67 \text{ mV} \cdot \mu\text{L}/\text{ng}$. Likewise, the sensitivity of a 250 bps, single-labelled PCR product would be $7 \text{ mV} \cdot \mu\text{L}/\text{ng}$.

3.4.3 Load-to-Load Variability

As the same chip was used for all LOD experiments to eliminate chip-to-chip variabilities, the calculated load-to-load variability is chip independent. But it is not CE protocol independent due to small changes in ion concentrations of the sample well from pipetting errors and pre-run timing differences; still, these contributions to the variability are expected to be small. The largest portion of the load-to-load variability is expected to be the x-y-z alignment of the confocal optical system in the μ TK and the z-axis alignment of the custom-built system laser.

For the LOD experiments, the average RMD for the three concentrations gave a load-to-load variability on the custom instrument of 20.3% and on the μ TK of 23.6%. To ensure this variability wasn't a result of the primers alone, a conventionally thermal-cycled BKV product was also compared. The product peak (our "diagnostic" peak) was found to have average RMD run-to-run variability of 23.1% on the μ TK, validating the previous procedure.

Load-to-load variability is important because large variability can lead to a higher limit of detection (or lower sensitivity) if it is considerably variable. Here, our LOD was found to be $\sim 6\text{pg}/\mu\text{L}$ of primer as determined by the averaged peak intensities of multiple chip loads. However, considering the load-to-load variability the LOD is more correctly $5.8 \pm 1.16\text{pg}/\mu\text{L}$. Likewise, it can also contribute to errors in the quantification of PCR products. Acceptable variabilities vary with the diagnostic test, and this variability was acceptable for our application.

3.5 CONCLUDING REMARKS

Using an inexpensive laser diode, GRIN lens, interference filter and photodiode, we have demonstrated the ability to build a portable, cost-effective optical detection system capable of detecting clinically relevant viral PCR product samples. In addition to the system level design related to CE described in Chapter 2, the software signal processing

method described here was also developed by the author of this thesis and its effectiveness for different types of sample was compared. Through extensive testing of the microfluidic platform configured as a CE instrument, the author also identified four key challenges in the optical detection set-up that could lead to dramatically worse limits of detection. With these factors fixed, the author determined that the CE instrument was comparably sensitive to gel electrophoresis run routinely in clinical laboratories and only 2-3x less sensitive than the available commercial CE instrument which is 100x the cost! System and protocol performance determined by the author were also discussed in terms of DNA mobilities, resolution, run-to-run and load-to-load variability, and sensitivity.

In future work, further improvement to sensitivity could possibly be achieved by turning the laser to strike the chip surface at a 45° angle in the x-y plane rather than at a 90° angle. In a demonstration by Fu et al.⁵⁶, light scatter from their excitation source was almost entirely removed by changing the angle of their detector. Thus, although our detector is where their excitation source is and vice versa, it may be possible to achieve the same effect through angling of the laser diode beam.

Sensitivity could also be improved through the implementation of a different lens for fluorescence collection. Our interference filter is a high-pass optical filter designed to pass the fluorescence wavelength and reflect the excitation wavelength. However, we still see high baselines of refracted/scattered excitation light characteristic of non-confocal systems. This is likely due to the GRIN lens not passing collimated light to the interference filter, as the efficiency of interference filters dramatically decreases when the incident light is at an angle to the surface⁷⁷. This could effectively limit the high baselines seen in this thesis and suppress erratic instabilities in the laser, improving the limit of detection.

To avoid the need to adjust the laser before each new chip load, our PDMS spinning protocols should be investigated more thoroughly to achieve more reproducible

thicknesses and/or it might be possible to move the CE fluidic layer could be moved to the top layer of the bottom layer of glass. Replacing the laser diode with an LED could also further improve the cost of the system and remove the need for extensive pre-focusing and laser characterising.

In the next chapter, the key challenges involved with the system implementation of PCR, integrated PCR-CE and its performance will be described.

Microchip Polymerase Chain Reaction and Integrated PCR-CE

CHAPTER 4

4.1 INTRODUCTION

One of the major challenges of developing portable and cost-effective microfluidic platforms is the integration of thermal modules that can control temperature precisely and efficiently. Biochemical reactions are the backbone of many diagnostic tests and their efficiency strongly depends on local environment factors of which temperature is one critical concern. Polymerase chain reaction (PCR) is one such reaction.

A number of commercial systems exist for performing PCR in conventional laboratories (e.g. Applied Bioystems⁷⁸, Eppendorf⁷⁹). In these systems, large reaction volumes (tens to hundreds of microlitres) and large thermal masses are typically used, often hampering the rate of heating and leading to long cycle times. Furthermore, they typically lack any analysis capability and integration with other analysis processes is unfeasible. Microfluidic devices have the ability to handle much smaller sample volumes which can be thermal-cycled by a microfluidic platform, thereby reducing expensive reagent costs, shortening processing times, and allowing for the integration of a detection method such as (LIF)CE.

PCR is a key technology for LOC devices as it rapidly replicates small numbers of nucleic acids (DNA) to concentrations necessary for detection by analysis techniques such as capillary electrophoresis and melting curve analysis. LOC devices are also important for PCR as their large surface-to-volume ratios allow for rapid temperature changes⁸⁰, decreasing cycling time from an hour to minutes. Rapid transitions, precise temperature control and uniform temperature distribution are critical for efficient PCR⁸¹.

There are two methods for implementing PCR on microfluidic devices: continuous-flow or stationary. The continuous flow PCR approach cycles the sample through three separate, distinct temperature zones with integrated heaters/sensors using a serpentine channel. This allows for rapid cycling times as temperature transition times are limited by the sample flow-rate rather than thermal inertia and for variable volumes from a few microlitres to several tens of microlitres. The stationary PCR approach consists of a micro- or nanolitre chamber and one heater/sensor system to cycle this fixed volume through the three necessary temperatures. By reducing the volume of the sample, rapid thermal equilibration of the sample when heating/cooling may also be achieved, such as the 9 minute PCR achieved using IR-mediated heating⁸².

Using resistive heaters and nanolitre volume chambers which require less device area, fluid transport infrastructure and power, we believe portable and inexpensive microfluidic platforms can be more readily realised. Unlike a IR heating⁸³ with Extrinsic Fabry-Perot Interferometric (EFPI) sensing system⁸⁴ or Peltier heating systems^{85,86} which require extensive external infrastructure and/or considerable power and do not lend themselves to miniaturisation well, we believe resistive heating is suitable for POC applications. Furthermore, we use a single element for both heating and sensing (as opposed to two separate ones⁸⁷), which simplifies the electronic interface and uses less device area. Our chip also consists of three layers built using standard microfabrication technologies to assemble microvalves which can be operated with low-power mini-pumps, removing the external infrastructure required by many four-layer chips.

This chapter illustrates how the fluid-handling and thermal control modules described in Chapter 2 (section 2.2) can be used to implement genetic amplification via PCR, and furthermore, be integrated with the previously described model to form an integrated, portable, inexpensive PCR-(LIF)CE system capable of both amplification and detection. To demonstrate the improvement in the system's performance over the earlier report⁴³, the same microfluidic chip design is used here. Although the principle of our thermal control has changed little from the lab's previous demonstration⁴³, re-designing the

system in a modular approach has enabled improvements in performance, illustrated by using the same microfluidic chip design as reported previously.

In Section 4.2, the system level configuration beyond what was described in the previous chapter, challenges associated with its implementation and the thermal controller will be detailed. Where in the previous system a proportional integral derivative was used, it was re-designed in this work as a proportional integral (PI) controller so as to not overshoot the requested temperature and the derivative term is used primary for stabilising overshoots. It was done in this manner because the primary objective here was to verify and evaluate the system performance for PCR, rather than focusing on rapid temperature transitions. This section also describes the PCR-CE on-chip protocol, which was based on other lab protocols and improved by the author through experimentation and observation of the system.

The next section discusses the performance of the system. 25 PCR-CE runs were executed by the author on the system during its verification (not including many other PCR runs with commercial CE analysis), all of which were positive. Furthermore, all product peaks appeared at times corresponding to the expected size of the amplicon, as determined by a DNA sizer. Two negative controls were also run to ensure the peaks were not the result of contamination. The variability of this system was determined both in PCR relative yield (or the PCR variability, defined in subsequent sections) and the load-to-load peak intensity variability of unique on-chip PCR products (or the PCR-CE variability). These variabilities were found to be comparable to the commercial thermal cycling and capillary electrophoresis equipment. However, while the variabilities of the custom-built and commercial instruments were comparable, the amount of amplified on-chip product was considerably lower than expected based on the conventional product. All performance characteristics were determined through extensive testing by the author.

Possible reasons for this discrepancy are explored in Section 4.4, through the identification of errors in the calibration and operation procedures used in the previous two sections and past work. This entire section is based on a system analysis report written by the author at the end of the thesis project.

First the thermal control system as it was designed by other members of the lab before the start of this thesis project began and how the system was calibrated for the experiments done in this thesis is described. This is broken into four sections: the system hardware (measuring the heater resistance), obtaining the heater temperature from its resistance via the chip heater calibration, how the firmware uses this calibration to determine the change in heater temperature, and finally how the system was calibrated to determine the relationship between heater and chamber temperature.

Troubleshooting of the heater resistance to heater temperature steps of the thermal control design is explored next. The author describes the chip calibration procedure as modified during the time of this thesis project due to erratic results as seen by our collaborators. Investigating this, the author analysed ten months worth of PCR experiments done on two fabrication batches of heaters. It was found that occasionally the heater resistance changes so that it no longer matches its calibration data due to defects in the heater rather than a problem with the calibration procedure, as suspected by our collaborators. This prompted the author to include a verification step in the software to ensure all heaters used on the system still adhere to their calibration data. Furthermore, an automated temperature button was built into the software to remove any user error in entering the ambient temperature (e.g. using a wall thermometer).

Next, troubleshooting of the system calibration performed by other members of the lab after the completion of this thesis project is briefly described. The work done with thermochromic liquid crystals (TLCs) before this thesis project began allowed us to reasonably determine the chamber temperature by controlling a specific heater temperature; however, the TLC colour was determined by eyesight, which is neither

quantitative nor reproducible. Furthermore, the amount of TLCs in the chamber, their distribution, and the differences in thermal conductivities between TLCs and water (PCR mixture) were not considered. This and other possible error sources in the system calibration and predictive function are explored.

Lastly, using the new experimental predictive function for the system calibration determined after this thesis project's completion, the author backwards calculated what the expected chamber temperatures were for the experiments described in Section 4.3. This chapter is then concluded in Section 4.5 with a summary and suggestions for future work.

4.2 SYSTEM INTEGRATION

To integrate PCR with the CE instrument, three modules must be included as described in Section 2.2: the thermal regulation unit for heating and sensing; the pneumatic pump and valve unit for actuation of the on-chip valves; and the temperature monitoring unit for logging the ambient temperature. These components are connected to both the power and communications buses. With the integration of these units, our modular system is easily customised from a CE to a PCR-CE instrument.

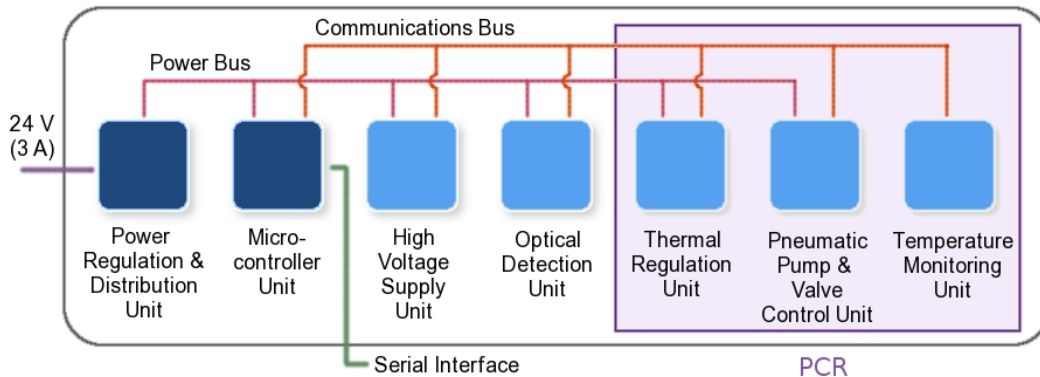


FIGURE 4.2-A: A DIAGRAM OF THE SYSTEM MODULES NECESSARY FOR PCR AND PCR-CE, ADAPTED FROM⁴³.

The PCR chamber temperature is controlled via the heater temperature and this heater-chamber relationship is determined by initial system calibration using thermochromic liquid crystals⁸⁸ (TLCs). As the heater temperature is determined by resistance measurements of the thin film heater, the resistance-temperature relationship (established during chip calibration) is as important as the heater-chamber temperature relationship. The microfabrication was improved from the previous demonstration by limiting the platinum thickness variation with a stricter fabrication protocol and our chip calibration procedure was refined for more reliable measurements through automation and an improved fitness criteria developed by R.Johnstone⁸⁹. Furthermore, a heat-sink was also added to improve the speed of cooling and reliability of the chamber temperature without affecting the rate of heating, as described in other work⁸¹. (More detail on the current system will be given in Section 4.4).

4.2.1 Thermal Controller

A customised, proportional integral (PI) thermal controller was written into the new system firmware by R.Johnstone, designed similarly to that of past work⁹⁰ to ensure rapid and stable thermal transitions. A PI controller, rather than a PID (proportional integral derivative), was chosen because the controller was not designed to overshoot the requested temperature. The primary objective of this work was to verify and evaluate the system performance for PCR. Thus, known and stable temperatures for all PCR steps were of the utmost importance, while fast transitions for short PCR cycles were secondary. As the derivative term is mainly used to stabilise the oscillations produced by a large integral overshoots, a PI controller was appropriate.

The open loop gain of the controller PI was measured to be 0.045°C/DAC increment by placing a chip into the system, setting a DAC value, measuring the voltage and calculating the change in heater temperature via the equations described in Section 4.4. The system time constant is 2.54 seconds (according to the comments in the firmware; the location of the report with this information is unknown). Knowing these values, the

PI constants were then determined by R.Johnstone to be $K_p = 73.2$ and $K_i = 0.13$, where K_i is dependent on the PCR sample period.

The firmware controls multiple temperatures by moving through the PCR cycle, or the series of heater setpoints, via nine states as illustrated in Fig 4.2-B. In state 0, the PCR state is immediately set to 1 (or 3, if reverse transcription has 0 seconds in length) and the required heater temperature for the upcoming step is made the setpoint. When changing the setpoint, the DAC value for the previous setpoint divided by the integral constant is removed from the error sum, the DAC value for the new setpoint is calculated, and this value divided by the integral constant is added to the error sum. This anticipates the change in error sum that should occur with the heater at steady state and the setpoint being changed, accelerating transitions.

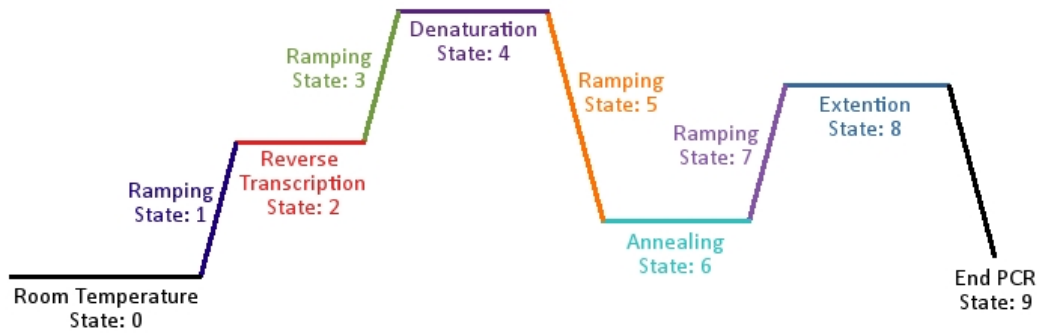


FIGURE 4.2-B: DIAGRAM OF THE THERMAL CONTROLLER STATES FOR PCR. PRE-DENATURATION AND POST-EXTENSION, IF INCLUDED, HAVE THE SAME STATES AS DENATURATION AND EXTENSION, RESPECTIVELY.

At the next state (ramping state), the controller then ramps the temperature until the heater is within 1°C of the required temperature. To ensure the ramps are as fast as possible (without overshoot), the DAC (injected current) is set to maximum/minimum if the temperature is ramping up/down, until the temperature is within 6°C of required temperature (or $\text{abs}(\text{error}) < 6^\circ\text{C}$). Once the temperature is within 6°C, the error (the difference between heater setpoint and measured temperature) is then accumulated in the error sum and the output (DAC value) is calculated using:

$$output = K_p \cdot error + K_i \cdot error_sum \quad \text{EQUATION 4.2-A}$$

To avoid integral windup (overshooting the setpoint), the integral term is removed from the error sum if the output is calculated to be larger than the maximum DAC value, and the output is set to the maximum.

Once the setpoint is within 1°C, the firmware counts the time required to be at this temperature (with the PI controller holding the temperature stable via the unchanged setpoint), and increments the state to the next ramping state when the time is finished. This continues, with state 8 moving on to state 3 and increasing the cycle count, until the last cycle is reached. When all cycles are completed, the PCR state moves to state 9, wherein the DAC (current) is set to zero and the PCR state variable is reset in preparation for the next experiment.

The controller described above was the final controller used in the system, labeled as firmware version 0.5.0. It should be noted that this controller performs temperature control every 10ms, although it only reports every 100ms, while the previous version (0.3.4) performed temperature control every 100ms. Furthermore, the previous version did not rail the temperature when it was more than 6°C off the set point and did not anticipate the DAC value, leading to much softer ramp rates and longer PCR times. Transition times for a PCR cycle of 56°C, 70°C and 94°C are approximately 43s and 14s on version 0.3.4 and 0.4.0, respectively. Typical steady-state decimal DAC values for these temperatures are approximately 53900, 17200 and 29400, respectively. All firmware versions can be found in the firmware repository in the AML laboratory (S.Groendahl's computer).

The author of this thesis provided feedback on the design of the controller and assisted with its development in terms of its specifications. She also aided with determining how the necessary PCR tasks would be split between the firmware and software. The author then wrote the associated software components and report generation tasks, enabling independent PCR experiments and integrated PCR-CE experiments.

4.2.2 Anomalous Temperature Spikes

With the integration of the thermal regulation unit with the other boards already present in the system, the author observed the appearance of anomalous temperature spikes in the sensing of the heater temperature. M.Behnam found this was due to the sensing unit being in close vicinity of the power regulation and distribution leading to noise on the board and anomalous values. On-board regulators suppress pickup noise from the supply cable connected directly to each module. However, there was no method to isolate pickup noise from two boards placed face to face, and due to the contained nature of the electronics box, the power unit and thermal regulation were practically on top of each other. These anomalous intensity spikes were most likely a random sampling of voltage transient spikes on the power distribution ribbon cables due to the switching power supply⁶¹. This led to bit errors in the ADC, which manifested themselves as anomalous and isolated temperature “spikes”. Table 4.2-A demonstrates the isolated nature of these spikes.

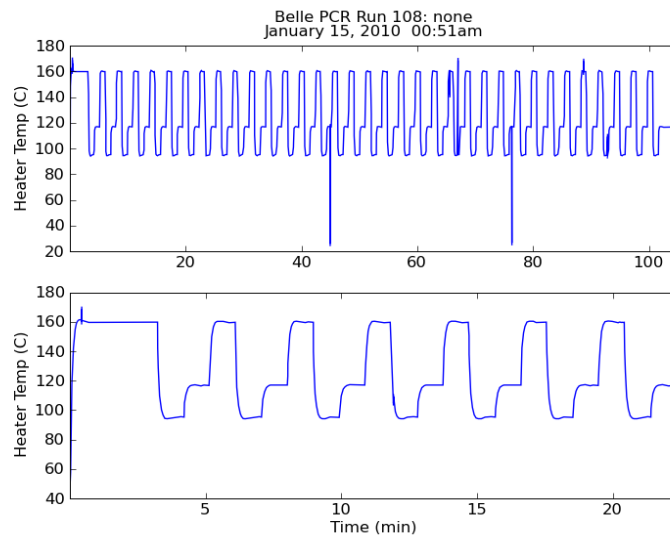


FIGURE 4.2-C: EXAMPLE OF ISOLATED, ANOMALOUS TEMPERATURE SPIKES DUE TO ENVIRONMENT NOISE

TABLE 4.2-A: DATA FROM THE ELECTROPHEROGRAM SEEN IN FIGURE 4.2-B. TIME IS RECORDED IN THE LOG FILE IN SECONDS BUT WAS CONVERTED INTO MINUTES HERE FOR EASIER INTERPRETATION WITH FIGURE 4.2-C.

Time (min)	DAC	ADC	Heater Temp (°C)
44.9351	2793	33494	116.9
44.9368	2792	33476	116.9
44.9385	2793	33471	116.8
44.9402	2792	1415	26.2
44.9419	2793	33492	116.9
44.9436	2792	33476	116.9
44.9453	2793	33493	116.9

Thus, the power unit was removed from inside the main electronics box and attached to the outside of the box, within a Faraday copper casing. While this solved most spikes, the occasional PCR temperature profile (approximately 1 in 30 experiments) would show similar spikes, as illustrated in Figure 4.2-C. Due to its random occurrence and appearance in specific locations (for example, spikes were not seen in the MDG laboratory but were seen in the Glerum laboratory), the author attributed these spikes to noisy wall power and/or interference from other systems in the vicinity. However, it was communicated to the author by S.Groendahl that a poor power adaptor can have the same effect, which led to S.Groendahl specifying the AED100US24 power supply for the systems with $\pm 2\%$ load regulation. Previously, any 24V/2A power supply as was used previously and not documented.

In the previous version of the firmware (0.3.4), as shown in the table above, the error sum term and the soft ramp rates insulated the DAC value from deviating too quickly based on one incorrect temperature reading. As the table shows, both the DAC and subsequent ADC readings are not affected by this isolated, unreal temperature value. In the current version of the firmware, the output is slew rate limited, which should likewise hold the real temperature relatively constant despite one isolated spike. This information is based on communication with R.Johnstone, the designer of both versions of the controller.

4.2.3 Microfluidic Chip

The microfluidic chip consists of two glass layers (1.1mm Borofloat, Schott AG, Germany) with a PDMS membrane between, based on previous demonstrations^{91,92} by the Mathies group. This tri-layer glass-PDMS-glass chip allows for the integration of microvalves and pumps while maintaining a relatively simple chip fabrication technology. The top glass layer acts as the fluidic layer, containing the 90 μ m deep, 600nL PCR reaction chamber and 45 μ m deep fluidic channels. The bottom glass (control) layer contains the deposited Pt heater thin film and the etched valve ports. More details on the fabrication procedure can be found in our earlier report⁴³, and improvements here⁴⁴. The PCR chamber is comparatively larger than other demonstrations to make it suitable for clinical samples with low concentrations of target DNA, as our lab demonstrated before this thesis project with the detection of BKV from urine⁶⁷.

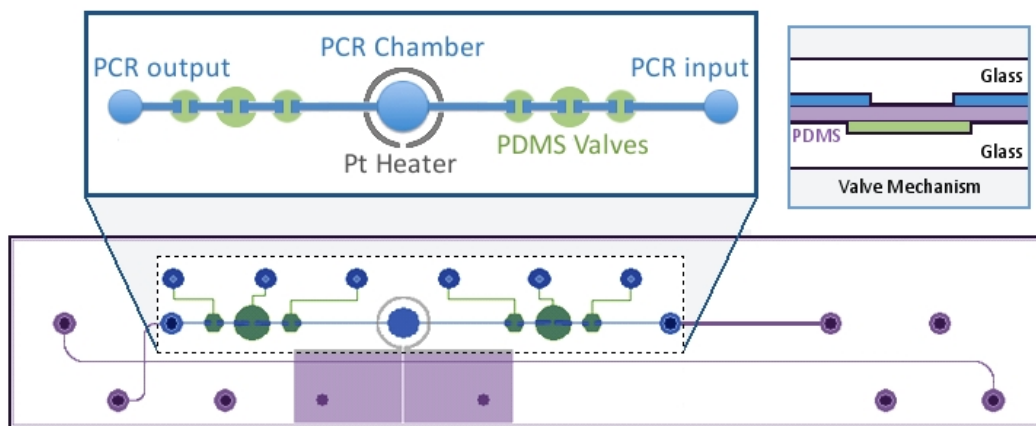


FIGURE 4.2-D: DESIGN OF THE INTEGRATED PCR-CE CHIP, EMPHASISING THE PCR SECTION OF THE MICRODEVICE CONTAINING THE PCR CHAMBER, VALVES, FLUIDIC CHANNEL AND WELLS, AND THE HEATER RING OF HEATING/SENSING ELEMENT (LABELLED PARTS ARE NOT DRAWN TO SCALE).

A side view of an on-chip valve is inset on Figure 4.2-D to illustrate its operation. When positive pressure is applied to the control layer, the PDMS membrane is in contact with the un-etched sections of the fluidic layer, effectively closing the valve; when negative

pressure is applied, the PDMS membrane is deflected away from the fluidic layer, creating a path for the fluid to flow through. The actuation of three consecutive valves creates a peristaltic pumping motion that can be used to transport fluid within the PCR channel.

The glass plates in this thesis are named for lab use as PCRCE4 chips. Version 1 can be seen above; version 2 top plates have the CE separation channel extending to the upper right corner instead of lower right (shown in Section 5.2.2); and, version 3 has a larger top plate than bottom plate for more reliable alignment. Version 1 chips were used for all PCR-CE experiments in this thesis and version 2 chips for SP-PCR-CE experiments (Chapter 5). Version 3 chips were never run by the author. All glass plates were fabricated by A.Jang. Furthermore, all chips in this thesis were bonded by A.Jang using the PDMS bonding protocol⁹³.

Issues with the PDMS forming bonds with the top plate of glass instead of being suspended as in Figure 4.2-D led to the inclusion of 30psi of N₂ air being blown through the PCR section of the chip just after bonding and again at 15min, 30min, 1hr and 2hr after bonding. Bonding to the bottom plate is prevented by coating the valve pad with a green marker. Once this was included into the protocol, stuck valves were only seen by the author in one set of chips which had been left on the shelf for three weeks after bonding and were not blown through with N₂ (an irreversible bond between glass and PDMS can also be formed if the two materials are left in contact for extended periods of time, without an oxygen plasma step).

Delamination, or the lack of a bond between the glass and PDMS, was seen on many chips over the course of this thesis project which at times made for slow production. As delamination around the PCR and CE sections of the chip can make it unusable, bonding quality was incorporated into the quality control on the chip before it was passed to the author. Details on the quality control can be found in the bonding protocol⁹³.

4.2.4 On-Chip Procedure

The PCR and PCR-CE protocol was written by the author based on previous lab protocols and improved by the author through experimentation and observation of the system. The full PCR-CE protocol can be found in Appendix E.

POLYMERASE CHAIN REACTION

Prior to the beginning of the experiment, a mixture of PCR reagents and template is prepared. This volume is used to perform simultaneous on-chip and off-chip conventional thermal cycler (positive control) experiments. This mixture is made up of 1xPCR buffer (20mM Tris-HCl, 50mM KCl, pH 8.4), 4mM MgCl₂, 200μM dNTPs, 5U of Platinum Taq polymerase (all included in Pt Taq DNA kits from Invitrogen, Burlington, Ontario), 0.02% BSA (Sigma-Aldrich, Oakville, Ontario), 4% DMSO (Fisher Scientific, Ottawa, Ontario), each BKV specific primer (200nM of unlabelled forward: 5'-GTGACCAACACAGCTACCACAGTGT-3', 300nM of Cy5-labelled reverse: Cy5-5'-TCAAACACCCTAACCTTCTTACCTG-3'; Integrated DNA Technologies, Coralville, IA) and 2x10²copies/μL of BK virus DNA. This reference sample was graciously provided by Dr. Xiao-Li Pang (of the Provincial Laboratory for Public Health (Microbiology), Edmonton, Canada).

10μL of this mixture is reserved as a positive PCR control and the remaining volume is used to perform multiple on-chip PCR-CE experiments (the mixture is stored on ice between PCR runs). The positive control is then run on commercial thermal cycler (GeneAmp PCR System 9700, Applied Biosystems, Foster City, CA) with the same thermal settings as the on-chip experiment. If a negative control is included, the PCR mixture is prepared without the template and a 10μL aliquot is also thermal cycled on the conventional system at this time.

Once the chip is positioned in the system, 5μL of PCR mixture is added to the PCR input well. The on-chip pumps are then activated by using the sequential actuation of three consecutive valves and keeping the remaining three open. Typically, 3-4 cycles are

sufficient to fill the PCR section of the chip with mixture; any more is indicative of problems associated with the microfluidic chip (extreme hydrophobicity as seen before quality control was included into the protocol), system-chip interface (poor valve/pneumatic coupling) or system (incorrect air/vacuum pressures) and further testing is not performed on this chip (see Section 4.3.3). All valves are subsequently closed and the remaining mixture is removed from the PCR sample well.

On-chip thermal cycling is performed based on parameters set by the GUI: pre-denaturation at 94°C for 120s; 35 cycles of 94°C for 10s, 56°C and 72°C for 20s each; and post-extension at 72°C for 120s. When completed, 5µL of flush-out buffer (0.01xTTE) is placed into the PCR input well, and the valves are actuated in a pumping motion for 8 cycles at which point this well is empty. At this time, 4.5-5µL of diluted PCR product (0.6µL of which is the thermal-cycled chamber contents and approximately 0.2µL of which is non-thermal-cycled PCR mix that was present in the PCR channels) is present in the PCR output well (doubling as the CE sample well).

As with loading the chip, problems associated with the microfluidic chip (delamination not noted in quality control), system-chip interface (poor valve/pneumatic coupling) or system (incorrect air/vacuum pressures) could result in the mix evaporating or being pushed out of the PCR chamber during cycling. Thus, if less than 4µL was recovered after flush-out with buffer, this was determined to be an experimental error and further testing was not performed on this chip. This was only seen in two PCR experiments performed by the author.

ANALYSIS (µCE)

The CE separation matrix, CE and flush-out buffer are 4% linear polyacrylamide (LPA), 1xTTE and 0.01xTTE, respectively. The analysis section of these experiments is identical to past work (described in Section 3.2.3), and the detailed procedure and CE reagent compositions can be found there.

As seen previously, the CE section of the microfluidic chip is passivated prior to analysis to minimize EOF and DNA binding to the channel walls. The CE microchannels are then filled with CE separation matrix and 4µL of 1xTTE buffer is placed into the remaining three CE wells (not the sample well). 1µL of the 5µL of diluted PCR product from the CE sample well is reserved, and DNA from the remaining 4µL is electrokinetically injected into the injection channel using an electric field of 222V/cm for 80s, followed by a separation of 67V/cm for 300s. Detection is performed at 13mm from the cross intersection.

Likely due to variability in the unloading procedure, the author observed on-chip PCR samples had injection currents that showed notable run-to-run variability. If the injection current exceed 40µA (typical conventional products have injection currents of ~30µA; section 3.3.5), the injection voltage was reduced to 150V for the remaining injection time. Either way, the primer and product peak reliably reached the intersection of the CE channels and was separated successfully (with the mobilities found in Section 3.3.3, it takes approximately 22s for the product to reach the intersection on the first injection and we perform 80s on the first injection).

TABLE 4.2-B: CONVERSION TABLE FOR PEAKS ON THE CUSTOM-BUILT INSTRUMENT TO THE EXPECTED PEAKS ON THE COMMERCIAL SYSTEM AS DETERMINED FROM THE LOD RESULTS (WHICH WERE RUN WITH A PMT GAIN OF 0.7).

TTK Peak	µTK Peak	PMT Gain
10 mV	0.12 V	@ 0.6
10 mV	0.34 V	@ 0.7
10 mV	0.69 V	@ 0.8

Analysis is also performed on the µTK as a reference (Epsilon’s detection module, various voltage systems), with the same electrophoretic conditions as the custom-built instrument and a PMT gain setting of 0.8. A conversion table from peak intensity on the custom-built instrument to the expected peak size on the commercial instrument can be see in Table 4.2-B. This table was determined from the LOD experiments (Section 3.4.1)

which were performed at a PMT gain of 0.7. The expected peak at other PMT gains were then estimated based on the estimated factors of intensity between gains (3x from 0.6 to 0.7 and 2x from 0.7 to 0.8). To run the on-chip PCR sample on this system, the reserved 1 μ L was further diluted with 3 μ L of flush-out buffer (0.01xTTE) and placed into the CE sample well. The rest of the chip was prepared the same as previously described.

The conventionally thermal-cycled PCR positive control was also run on the custom-built system or the commercial CE system. In this case, 0.5 μ L of the positive control is mixed with 3.5 μ L of flush-out buffer (0.01xTTE) and placed into the CE sample well. All other CE conditions are as previous described. These volumes were chosen as they allow the conventional product dilution to be compared to the on-chip product (12.5% dilution as compared to 12% dilution of 0.6 μ L of on-chip product in 5 μ L of flushed-out volume).

To size the amplified product, CE was performed with 1 μ L of DNA ladder (ALFExpress, Amersham Biosciences, New Jersey) and 3 μ L of flush-out buffer (0.01xTTE) in the sample well, and the same CE protocol as the product. The arrival times of the ladder peaks were recorded and interpolated to estimate the size corresponding to the arrival time of the product peak and they agreed within approximately 20bps. The sizing was performed separately as the signal processing is designed for isolated peaks (see Section 3.2.4).

4.3 SYSTEM PERFORMANCE

4.3.1 System Level PCR-CE Results

As the system was tested and improved, 125 PCR-CE experiments (see Appendix A) were performed by the author on the system described in this thesis, named "Belle". However, not all of these experiments will be discussed in this section. The first 31 experiments were done with microfluidic chips that were not calibrated using the new, stricter method as developed by R.Johnstone and so were not included in the system performance. Experiments that did not follow the protocol above (e.g. less than 4 μ L

was collected, PCR chambers were filled with mix more than once, etc.), negative controls, non-SigmaCoted microfluidic chips, training experiments, varied concentrations of starting DNA template, and SP-PCR-CE experiments are also not included in this section.

Thus, to establish a timeframe where the system and protocols were kept as constant as possible, for system performance we will discuss 24 PCR-CE runs executed by the author with minor variations in the PCR and CE protocols between May and August 2009 in preparation for a subsequently published paper⁴⁴ (see Appendix A). All of these experiments were positive. Three consecutive PCR-CE runs are shown in Figure 4.3-A, demonstrating that the system clearly resolves the samples. Two negative controls were performed on chip and found to be negative, demonstrating the on-chip product peaks were not the result of contamination.

The 26-base primer arrives at ~130s of separation and a second peak arrives at ~180s, corresponding to 300 bps as interpolated from a size standard (not shown). A BLAST prediction⁹⁴ of viral genomes resulted in matches (for our primers) for BK virus variants, all with an expected product size of 299 bps, verifying that this second peak is the product peak. A third, broad, low-intensity peak centred at ~250s of separation is seen in approximately 50% of the on-chip experiments and all conventional thermal-cycler experiments. This peak was attributed to non-specific amplification and its appearance in half of the on-chip electropherograms may be due to variations in injection characteristics (Section 4.2.3). However, a Basic Local Alignment Search Tool (BLAST) search of all available sequences (non-redundant) found potential matches in the human genome of near 700bps, the interpolated size of this third peak. Thus, this intermittent, on-chip behaviour could also be due to statistical effects expected of low-concentrated human target DNA.

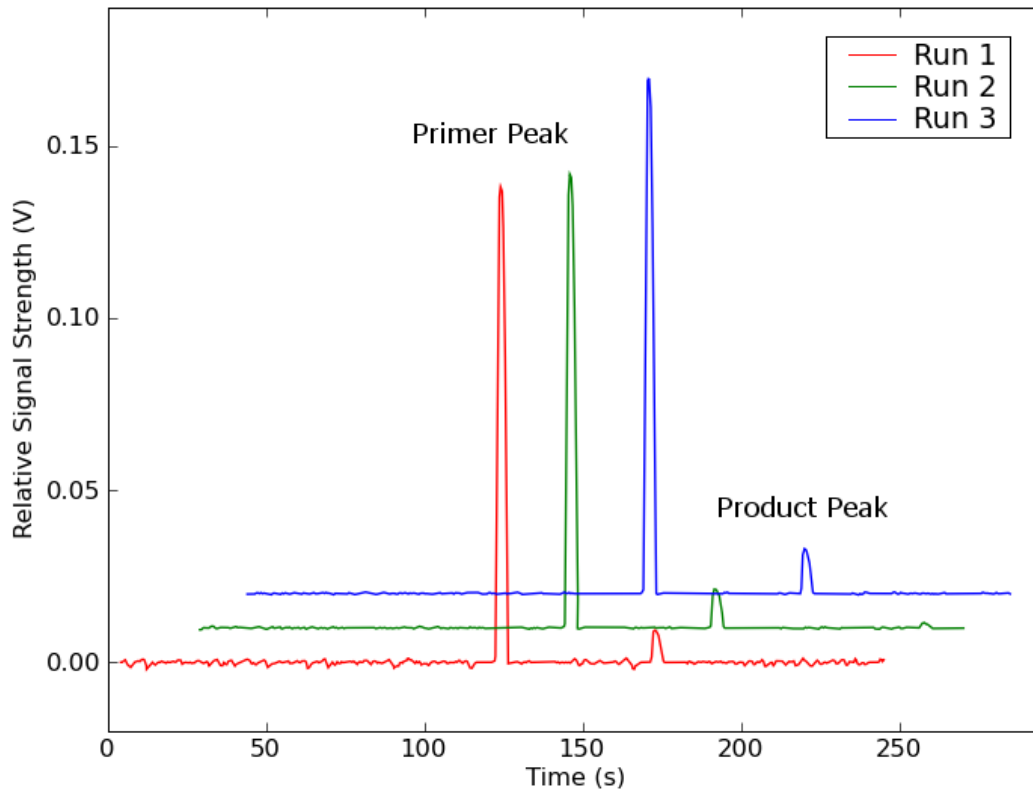


FIGURE 4.3-A: THREE CONSECUTIVE MICROCHIP-BASED PCR-CE RESULTS. FOR EACH RUN, THE PRIMER PEAK IS ON THE LEFT AND THE PRODUCT ON THE RIGHT, REPRESENTING THE PRESENCE OF BK VIRUS IN THE SAMPLE.

With a starting template concentration of 2×10^2 copies/ μL , approximately 120 copies are expected to be in the PCR chamber. Using the same protocol described in Section 4.2.3, starting template concentrations were diluted to 2 copies/ μL to expect 1 copy in the PCR chamber and two experiments were performed. One of these experiments was negative and one experiment was positive, which reflects the expected statistical behaviour of 1 copy of DNA in the chamber. As in previous work⁶⁷, these preliminary results suggest our PCR-CE protocols and system are able to detect at or near the single copy level. More experiments were not run at this concentration as this dilution was unintentional. Quantification of our product after the fact later revealed the correct starting concentrations of sample, which are the values used in this thesis.

4.3.2 Variability

All PCR products in this thesis (both conventional and on-chip) are analysed using capillary electrophoresis. In attempts to separate the CE contribution to the PCR-CE variability from the PCR variability, RMDs are given from both the mean PCR relative yield and mean product peak intensity in this section.

MEAN PCR RELATIVE YIELD (PCR VARIABILITY)

Unlike gel electrophoresis, capillary electrophoretic analysis allows us to evaluate the primer to product ratio, indicating how much of the primers have been consumed during the reaction and how well the PCR reaction has been driven towards completion. This can indicate to the user qualitatively how well the PCR conditions have been optimized and the PCR amplification efficiency⁹⁵. As the PCR efficiency is often used in the life sciences as a means of determining the percent increase in final PCR product from the initial starting template⁹⁶, here we define the PCR relative yield as the percentage of the starting amount of primers (or total fluorescence) that have been used to create the amplicons (or product peak fluorescence). Ideally, the area of the peaks should be used, but given that both our primer and product peaks are the same shape:

$$PCR\ Relative\ Yield = \frac{V_{product}}{V_{primer} + V_{product}} [\%] \quad \text{EQUATION 4.3-A}$$

where V_{primer} is the height of the primer peak and $V_{product}$ is the height of the product peak. The PCR amplification efficiency is dependent on the PCR conditions, including the reaction components and concentrations, temperatures, and environment. As the same PCR mixture (reaction components and concentrations) is used for all experiments on both the custom-built instrument and the conventional thermal cycler, the relative yield can be used as a means of determining the reliability of our on-chip PCR temperatures and surface passivation (environment).

First, as CE variabilities were given in peak intensity Section 3.3.4, the CE protocol and chip loading effects must first be looked at with respect to the PCR relative yield. As described there, the CE run-to-run variability is protocol dependent and system independent. This is true when considering the variability in intensity and the variability in the PCR relative yield, and thus these two variabilities should be comparable. The CE load-to-load variability is system dependent when considering the intensity, but is expected to be mostly system independent when considering the PCR relative yield as the relative intensities are important, not the absolute intensities. Thus, the variation in PCR relative yield from load-to-load is expected to be negligible. As expected, when the data in Section 3.3.4 was re-analysed for PCR relative yield, the run-to-run variability was found to have an RMD of 5.4% from the mean (as compared to 5.9% for the mean product peak intensity), and the load-to-load variability, an RMD of 2.4% (as compared to 23.5%). Thus, the load-to-load variability of the PCR relative yield essentially negates the variability of the analysis technique and is the best method with which to analyse only the PCR variability in both the conventional and on-chip methods.

Before determining the variability associated with our on-chip PCR products, the variabilities inherent to the molecular biology of conventional PCR and associated pipetting effects were first established by the author. A standard 50 μ L PCR mixture as described in Section 4.2.3 was prepared and separated into five 10 μ L aliquots. These aliquots were thermal-cycled simultaneously, using the same commercial instrument and then run on the commercial CE instrument. The variability of these five aliquots was found to have a RMD of 6.2% from the mean sample relative yield. This value is the dispersion of PCR efficiencies, or variability, inherent to the molecular biology of the mixture and its conventional thermal-cycling (set #1). Five 10 μ L aliquots of PCR mixture prepared on different days (and stored at 4°C until the final day) were also analysed to determine if pipetting errors contributed to the variability of the PCR (set #2). These aliquots were found to have an RMD of 8.3% from the mean sample relative yield. Thus, pipetting errors seem to have minimal effects on conventional PCR.

Microchip PCR and Integrated PCR-CE

To determine the variability of our on-chip PCR, a 50µL mixture (Section 4.2.3) was prepared, of which 10µL was run as a positive control on the conventional thermal-cycler while the remaining 40µL was kept on ice. Using this same mixture, four PCR-CE runs were performed successively. However, as the DC coat was did not effectively coat the channels for the CE of one of these experiments (characterised by the product peak broadening into a right-angle triangle rather than an isosceles peak due to analyte-surface interactions), only three of the four on-chip PCR-CEs were considered for the variability. The RMD of the mean sample relative yield was found to be 9.5%, slightly larger than that of the conventional thermal-cycler. Thus, the dispersion of on-chip PCR is similar to that of the conventional relative yield (note that this does not mean that the efficiencies themselves are comparable).

When analysing the averaging the variability in all the performed PCR-CE experiments (rather than those just performed on one day), the average RMD was found to be 22.2% from the average relative yield. However, if this variability is broken into the first half of experimentation and the following half (only considering single labelled BKV PCR runs completed using firmware version 0.3.4 over the span of four months), the average variabilities in relative yield are found to be 53.2% and 7.5%, respectively.

TABLE 4.3-A: AVERAGE PCR RELATIVE YIELDS AND AVERAGE VARIABILITY FOR GROUPS OF ON-CHIP PCR RUNS RAN USING V0.3.4 OF THE FIRMWARE, USING THE SAME CALIBRATION PROTOCOLS, SINGLE-LABELLED REVERSE PRIMER, AND 10⁷ BKV TEMPLATE; GROUPED BY MINOR VARIATIONS IN TEMPERATURES (2°C) AND FLUSH-OUT BUFFER.

Run #s	Average Yield	Average RMD	
32,33,36,40	11.5%	31.7%	= 53.2%
38,39	10.4%	68.2%	
42,43,45,47	21.8%	59.6%	
67,76	15.7%	9.8%	= 7.5%
68,69	19.9%	1.9%	
72,73	25.8%	8.7%	
74,75,77	21.7%	14.3%	
85,86,88	8.1%	9.5%	

As the same PCR protocols run in the first two months were run again in the second two, the same fabrication protocol for the glass top and bottom plates were followed, the bonding protocol was the same protocol, the same calibration for all heater rings were used, and the system was unaltered in terms of PCR for the full testing period, the chip assembly and system operators would be suspect for this variability. However, as A.Jang built and assembled all of the chips used and the author ran all the experiments, this suggests the knowledge gained through repetition of the chip protocols and operation of the system, and an increased understanding of all working parts of the equipment, improved the repeatability of the runs. In other words, the users developed “good hands”. This demonstrates that a high level of training is required to assemble the microfluidic chips and operate the custom-built system, and while the system is inexpensive and portable, much work must still be done to remove the user from the diagnostic tests and fully automate chip manufacturing and the instrument itself.

MEAN PRODUCT PEAK INTENSITY (PCR-CE VARIABILITY)

In Section 3.4.3, the CE load-to-load variability on the conventional (μ TK) and custom-built instruments were found to have RMDs of 23.5% and 20.3% from the mean peak height, respectively. As described previously, this variation is primarily attributable to the optical detection set-up; or, more specifically, the reproducibility of the laser focus on the microchannel. When the sample from load-to-load is a unique on-chip PCR product (rather than the same sample loaded multiple times), the load-to-load variability of product peak intensity is effectively the combined PCR-CE variability.

The variability of the conventional PCR-CE (commercial thermal cycler and CE instrument) was found to have an RMD of 21.4% and 28.5% from the mean for set #1 and set #2 (the products used to determine the inherent molecular biology and contribution of pipetting errors, respectively, as described above). These sets were found to have approximately the same variance when considering the PCR variability alone (6.2% vs. 8.3%). As these sets were analysed using the same conventional CE system, one might expect approximately the same variance when considering their PCR-

CE variabilities. However, the high variability in the CE could either work to create a worse dispersion in the product peaks (the strongest product has the best optical alignment and the weakest has the worst) or a seemingly “better” dispersion (the strongest product has the worst optical alignment, making it appear weaker, and the weakest has the best, making it appear stronger).

When analysing two sets of multiple on-chip PCR-CE experiments run on the same day (from the second half of experimentation, as described in the previous section), these two extremes can be seen. For the first set (a), the PCR-CE variability was found to have an RMD of 13.8%, even though the PCR variability for this set was 9.5% and the CE variability is 23.5%. Conversely, the second set (b) had an RMD of 27.2% for the PCR-CE variability, with a PCR variability of 8.1% and CE of 23.5%. In this manner, the first set seems to have a considerably better variance than the second set, when in actuality they have similar PCR and CE variabilities.

TABLE 4.3-B: COMPARISON OF THE VARIABILITIES FROM THE MEAN PCR RELATIVE YIELD (EFFECTIVELY THE PCR VARIABILITY) AND THE MEAN PRODUCT PEAK INTENSITY (EFFECTIVELY THE PCR-CE VARIABILITY).

Variability Experiment	RMD (rel. yield) [%]	RMD (product intensity) [%]
Conventional CE (load)	2.4	23.5 (μTK)
On-chip CE (load)	--	20.3 (<i>custom</i>)
Conventional PCR (set #1)	6.2	21.4 (μTK)
Conventional PCR (set #2)	8.3	28.5 (μTK)
On-chip PCR (set a)	9.5	13.8 (<i>custom</i>)
On-chip PCR (set b)	8.1	27.2 (<i>custom</i>)

Thus, the PCR-CE variability for our custom-built instrument was found to be comparable to that of the conventional instrument, although this variability really has minimal importance. The PCR and CE variabilities themselves have more bearing on the performance of the instrument. The PCR variability especially important when starting with a low number of DNA targets that may not be able to be amplified to detectable levels by our CE detection. Thus, the importance of the variability is diagnostic test specific, and for the application used here, these variabilities were sufficient.

4.3.3 Relative Yield

The PCR on the conventional thermal-cycler had an average amplification relative yield of 68.1% while the three successive on-chip PCRs shown in Figure 4.3-A had an average amplification relative yield of 8.1%.

If poorly passivated, the high surface to volume ratio of the PCR chamber increases the chances of necessary PCR enzymes sticking to the surfaces of the chamber⁹⁷ and not participating in the amplification. As the literature suggests the effects of PDMS are small or negligible relative to the effects of the glass^{98,99} for large surface area to volume ratios, only the glass surfaces of the PCR chamber were passivated with SigmaCote in this work. However, as the efficiencies achieved with on-chip PCR experiments are considerably lower than the conventional products, this suggests either the environment (i.e. the chip passivation method) or the PCR temperatures must be improved.

While improved PCR temperatures will be discussed in the next section, evidence of poor chip passivation can be seen when the PCR chamber of the same chip is filled multiple times with PCR mix before running. Poor coupling of the valve ports to the chip (user error as described previously) led the PCR chamber being filled with bubbles rather than mix. To try and salvage the chip, the author first dried the PCR channels and chamber with the CDA gun, and re-loaded the chip. Double loading of the same chip with only a drying step led to many large unspecific peaks characteristic of a poor PCR recipe (i.e. reagent saturation) and a very weak product, as seen in Figure 4.3-B. When a similar problem occurred due to user error, the author soaked the PCR chamber and channels with PCR grade water for 45 minutes before rinsing and drying with the CDA gun, to determine if this would help dilute any residual PCR reagents that were otherwise dried to the surface in the previous chip. However, an electropherogram almost identical to the first was seen, indicating some reagent(s) of the mix is sticking to the surface and cannot be removed with a simple flush-through step. Thus, preliminary results suggest our chip passivation methods could possibly be improved.

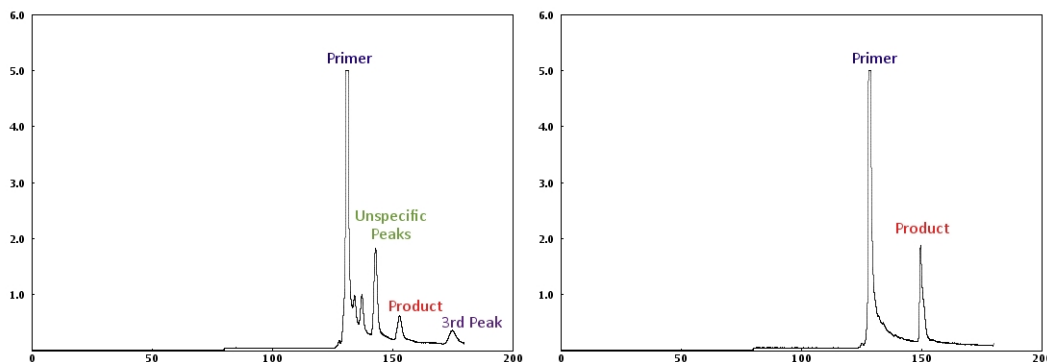


FIGURE 4.3-B: ON THE LEFT: AN EXAMPLE OF A CHIP LOADED MULTIPLE TIMES WITH PCR MIX (LARGER VOLUME OF MIX IN CONTACT WITH THE SAME SURFACE AREA). ON THE RIGHT: A CHIP LOADED ONCE WITH PCR MIX. BOTH ON-CHIP PRODUCTS WERE ANALYSED ON THE CONVENTIONAL CE SYSTEM (SAME MIX USED FOR BOTH EXPERIMENTS).

4.4 SYSTEM ANALYSIS

Heating of the thin film resistive element on the control layer of the microfluidic chip is designed to heat the chamber volume in the fluidic layer of the chip. Measurement of the element's steady-state temperature is then used to predict the chamber volume's steady-state temperature using the heater-chamber temperature relationship determined through calibration of the system. Because the PCR chamber temperature cannot be measured directly, the resistive element acts as both a heater and a sensor. The advantage to this is a simple electronics interface to the device, less chip area used for heating and sensing, and a simple microfabrication process. However, the disadvantage of this indirect "sensing" is any errors determination of the heater-chamber temperature relationship and the accuracy with which the heater temperature is measured could potentially introduce multiple, compounding errors into the chamber temperature prediction.

This section first describes the system's thermal set-up as designed by previous lab members and how the system was calibrated for all the experiments in this thesis. It then identifies errors in the calibration and operating procedures and describes methods with which they could be (or have recently been) controlled and/or accounted

for. While the design of the system was developed prior to this thesis project, this section is based on a system analysis report written by the author at this thesis project's completion.

4.4.1 System Hardware: Measuring the Heater Resistance

The heater temperature is not sensed directly by the system as temperature; rather, the heater is made from a material with a linear resistance-temperature relationship (platinum) and the resistance is measured by the system to determine the heater temperature. Resistance measurements of the heater are taken by the firmware through the Wheatstone bridge by injecting a known, fixed current determined by the thermal controller and measuring the resultant voltage. R_1 and R_2 are selected to be 100 times larger than the resistors in the heater branch so most of the current flows through the heater. Conversely, R_3 is chosen to be small. The user manually balances the bridge before operation using the variable resistor R_2 , allowing the heater resistance R_h to be broken up into two parts:

- ❖ $R_{h,WB}$ – the resistance of the heater when it was zeroed before operation
- ❖ ΔR_h – the change in heater resistance during operation

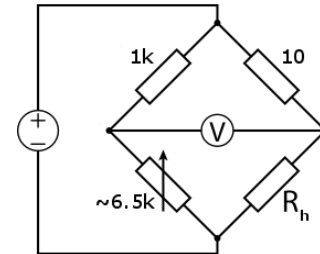


FIGURE 4.4-A: WHEATSTONE BRIDGE CIRCUIT DIAGRAM.

which leads to the following equations:

$$\Delta R_h = \frac{V_b \left(\frac{R_1}{R_3} + 1 \right) (R_{h,WB} + R_3)}{I_b R_1 - V_b}$$

$$= \frac{101V_b (R_{h,WB} + 10)}{1000I_b - V_b} \text{ } [\Omega] \qquad \text{EQUATION 4.4-A}$$

$R_{h,WB}$ cannot currently be measured by the system, so it must be either be measured and entered by the user (60-70Ω) or calculated from the chip calibration (next section) using

the temperature of the heater at the time of zeroing. The former method was chosen by the previous lab members who designed this system, presumably out of convenience. I_b is the fixed current flowing into the Wheatstone bridge set by the DAC on the thermal regulation board (on the order of ~100-150mA) and V_b is the voltage measured by the ADC (on the order of ~10-50mV). Thus, the measured voltage term in the denominator is significantly smaller than the $1000I_b$ term and can be approximated as zero. Furthermore, considering a fixed, injected current, the change in heater resistance (ΔR_h) is directly proportional to any change in measured voltage (ΔV_b) or any change in entered zeroed Wheatstone bridge resistance from the actual value ($\Delta R_{h,WB}$). The DAC to current and ADC to voltage equations are as follows:

$$I_b = 49.6 \cdot DAC - 1.95 \text{ } [\mu\text{A}] \quad \text{EQUATION 4.4-B}$$

$$V_b = \frac{0.05 \cdot ADC}{65535} \text{ } [V] \quad \text{EQUATION 4.4-C}$$

4.4.2 Chip Calibration: Heater Resistance & Temperature

The heater's temperature-resistance relationship is inherent to the physical properties of the element, such as the thin film thickness, deposition rate and level of impurities present. As the sputtering technique is not precisely reproducible for every chip, initial chip calibration considers slight variations in the physical characteristics of the individual heater elements and provides an individual relationship for that specific element.

Newly fabricated heater elements must be annealed before calibration⁸⁹. Annealing involves heating the resistive heater to speed up the process of diffusion, relieving internal stresses and ensuring that material properties of the heater will not change during normal operation. This must be performed on un-bonded control layers of multilayer chips as PDMS melts at 200°C.

Calibration is also done solely on the bottom plate, or control layer. This process involves using a water bath to bring the resistive heater up to temperature, and

measuring its resistance at that temperature via a four-wire (or Kelvin) resistance measurement. This allows wire resistances to become negligible, but still incorporates any contact resistance from the pogo pins on the heater element. Resistance measurements are taken three times at each temperature of 25°C, 40°C, 60°C, 70°C, 80°C, and 25°C (the final temperature should match the initial temperature). R.Johnstone wrote software to automate this process, and at the end of the temperature measurements, it automatically logs all recorded data in a *.csv file. More details on the calibration set-up and process can be found in the protocol⁸⁹. The software files can be found in Supplementary CD/AML Files/TTK/Chip Calibration.

The resistance with respect to temperature for conductors can be represented as follows, and further simplified for a reference temperature of 0°C:

$$R = R_{ref} \left(1 + \alpha(T - T_{ref}) \right) = R_0 \alpha T + R_0 [\Omega] \quad \text{EQUATION 4.4-D}$$

As both the temperature coefficient of resistance (TCR), α , and the element's resistance at 0°C, R_0 , are constants for platinum, our resistance-temperature relationship is linear. Thus, a least squares regression on the collected data is then performed to determine the calibration coefficients and their uncertainty. A propagation of uncertainty analysis is also performed to determine the temperature uncertainty when the heater is 170°C (approximately 94°C in the PCR chamber, typically the highest temperature during a PCR experiment). To limit uncertainties to $\pm 1^\circ\text{C}$ in the chamber temperature, the calibration data must be able to predict the heater temperature at 170°C within $\pm 2^\circ\text{C}$ at a 99% confidence level.

An Excel spread sheet also made by R.Johnstone is used to perform the necessary calculations for the propagation of uncertainty (Supplementary CD/AML Files/TTK/Chip Calibration/chip-tcr-calibration.r37). Rearranging Equation 4.4-D for temperature and replacing the constants with m and b for slope and intercept as determined by the least squares regression, the propagation of uncertainty is as follows:

$$T = \frac{1}{m}(R - b) \text{ [}^\circ\text{C]} \quad \text{EQUATION 4.4-E}$$

$$\sigma_T^2 = \frac{(R - b)^2}{m^4} \sigma_m^2 + \frac{1}{m^2} \sigma_b^2 + 2 \frac{(R - b)}{m^3} \sigma_{bm}^2 \text{ [}^\circ\text{C}^2\text{]} \quad \text{EQUATION 4.4-F}$$

The following parameters are then copied from the Excel sheet into the database log file of all calibrated chips. If the thin film heater is extrapolated to be within $\pm 2^\circ\text{C}$ of 170°C at a 99% confidence level, it is then bonded. If the bonding passes the quality control specified in the bonding protocol⁹³ (described previously), the microfluidic chip is then given to the user with the calibration information.

TABLE 4.4-A: EXAMPLE CALIBRATION COEFFICIENT DATA GIVEN TO THE USER FOR A RESISTIVE ELEMENT

Chip	m ($\Omega/^\circ\text{C}$)	σ_m	b (Ω)	σ_b	Conf. 25°C	Conf. 170°C
0904C1	0.1498	0.0004	61.65	0.02	0.3 $^\circ\text{C}$	1.3 $^\circ\text{C}$

4.4.3 System Firmware: Determining Heater Temperature

Once the resistance is measured, entered, the Wheatstone bridge zeroed and the PCR experiment started, the change in heater resistance, ΔR_h , is then used to determine the heater temperature:

$$T_h = T_{am} + \frac{\Delta R_h}{m} \text{ [}^\circ\text{C]} \quad \text{EQUATION 4.4-G}$$

m is the slope of the resistive element given by the element calibration and T_{am} is the ambient temperature of the resistive element (or heat sink) *at the time of calibration*. Thus, if the ambient temperature has not changed and the heater temperature has not been raised, ΔR_h will be zero and $T_h = T_{am}$, as expected. Furthermore, the change in heater temperature (ΔT_h) is directly proportional to heater resistance (ΔR_h).

4.4.4 System Calibration: Heater & Chamber Temperature

The relationship between steady-state heater temperature and steady-state chamber temperature is dependent on many factors, such as the physical heat-sink and microfluidic chip material properties and dimensions. Initial system calibration considers these properties while incorporating system specific variations (e.g. component precision errors) and chip-specific factors (e.g. minor dimension variations) to provide an individual relationship or predictive function for that system.

Direct thermal measurement of micro-PCR systems is challenging as the introduction of temperature sensors into the PCR microchamber can have a significant effect on both the temperature distribution⁸⁰ and the average chamber temperature. Furthermore, these probes read only a restricted point temperature and provide limited information on the average or distribution of temperature. For these reasons, we use microfluidic chips with narrowband thermochromic liquid crystals (TLCs) contained within the PCR chamber to indicate the chamber volume's temperature, as developed in previous work^{81,88}. TLCs are compounds that react to temperature by continuously changing colour (red → green → blue) over a specific range to provide a qualitative image of a two-dimensional field of temperature. As temperature changes of 1-2°C are significant enough to affect PCR, the TLCs used for calibration in this work were custom-synthesized to have 3°C colour bands. Outside of this narrowband, the TLCs are a milky-white colour. Three different TLCs are used in this project, each one centred about the temperature typical of each PCR step (58°C for annealing, 70°C for extension, and 93°C for denaturation; R58C3W, R70C3W, and R93C3W, respectively; Hallcrest, Glenview, USA), and three calibration chips for each TLC temperature are assembled.

TABLE 4.4-B: COLOUR OF THERMAL LIQUID CRYSTALS (TLC) AT SPECIFIC TEMPERATURES

TLC	Start of Red	Start of Green	Maximum Green	Start of Blue
R58C3W	58.0	58.6	59.7	60.8
R70C3W	69.7	70.6	71.7	72.8
R93C3W	92.4	93.6	94.7	95.8

CALIBRATION CHIPS AND TLCS

Calibration chips are unbounded microfluidic chips as described in Section 4.2.3 that have PCR chambers filled with dried TLCs. Initially, to build calibration chips the TLC slurry was applied to the PCR chamber of an unbonded fluidic glass top layer with a pipette tip and air-dried for 15 minutes¹⁰⁰. The PDMS membrane and control layer were then placed on top of the fluidic layer, creating a reversible bond rather than using the oxygen plasma activation step. To perform the initial calibration of the system (or determine the experimental heater-chamber temperature relationship), calibration chips were loaded into the instrument as normal. Calibration experiments were then performed in a dark room using a controlled light source and the user's vision. The room temperature was kept constant within 0.5°C and the heater temperature was slowly varied, allowing time for thermal equilibrium. Unlike previous work^{81,88}, green was used to indicate the temperature rather than blue as it is closer to our target temperatures. Furthermore, the start of green (where the TLC just begins to turn green from red) was used as it is difficult to ascertain between maximum green and green-blue (start of blue) by eye. When the desired colour was reached, the temperature corresponding to that colour and the heater temperature (DAC value; see Section 4.4.2) were recorded. S.Poshtiban repeated these steps for each of the nine chips; three chips at three temperatures, first for Belle (the system described in this thesis, report unknown) and subsequently for Winnie¹⁰¹. A least squares regression on the collected data was then performed to determine the experimental predictive function coefficients for that system.

PREDICTIVE FUNCTION

Due to the time-critical nature of the thermal control for PCR, the thermal controller is contained in the firmware of the system. However, the firmware does not control the chamber temperature directly. Instead, it determines the heater temperature(s) necessary to achieve the defined chamber temperature(s) using the predictive function prior to the PCR run commencing, and subsequently controls the heater temperature

over the course of the run. This is done to limit the number of required double calculations from 1-6 for each run (depending on the number of PCR steps) to 1-6 for each heater temperature measurement instance (for every 100ms this is 10 calculations per second). The predictive function is of the following form:

$$T_h = \alpha T_c + \beta \text{ [}^\circ\text{C]} \quad \text{EQUATION 4.4-H}$$

where T_h is the heater temperature, T_c is the chamber temperature, and α and β are fitted constants using the previously described calibration method. This relationship takes this form because in steady-state conduction, temperature varies linearly along the direction of heat transfer. In this case, the heater temperature is our source and the chamber is one point on the spatial gradient, with the amount of heat entering the chamber equal to the amount leaving once equilibrium has been reached.

To simplify upgrades, only one firmware program using one predictive function and one software program were written for all systems of all possible configurations. The predictive function included in the firmware was the initial experimental calibration curve done on the instrument used in this work, determined to have values of $\alpha = 2.15$ and $\beta = -37.96$ by S.Poshtiban.

SOFTWARE ADD TIMES AND CALIBRATION VERIFICATION

While not responsible for time-critical functions, the software also plays a role in the thermal control. As the firmware controls the heater temperature, it begins counting the PCR step time when the heater becomes stable at the appropriate temperature (Section 4.2.1). However, it takes time for the heat to transfer from the heater to the chamber and the chamber contents to reach thermal equilibrium. This time is referred to as an “add time”, or the time that needs to be added to the PCR step so that the chamber is at the user-defined temperature for the specified length of time.

Add times are dependent on chip and heat sink dimensions and controller specifications. If the controller overshoots the temperature before stabilizing, the add

time will be shorter than if the temperature ramps very quickly but doesn't overshoot. These times are determined by timing how long it takes for the TLC chips to reflect the desired colour after the firmware says it is stable. The software was chosen to hold the add time information as the firmware is written to be system/chip independent while the software collects chip- and system-specific information from the user for reporting purposes.

Firmware version 0.3.4 was determined through TLC testing to need 10s additional time for each step, bringing the transition time from 43s to 53s for a PCR cycle of 56°C, 70°C and 94°C; version 0.4.0 was determined to need 15s for each step, bringing the transition time from 14s to 29s. Modifying the controller to overshoot the heater setpoint (as described in Section 4.2.1) could keep the transition time at ~14s without the need for add times and shorten the PCR by ~25min for a 35 cycle, 3 step PCR.

Verification of the system temperatures post-calibration were initially made with TLC-filled calibration chips and the firmware controller by defining the chamber temperature via the GUI and determining by eye if the TLCs to changed to the expected green. This method introduced further errors due to: a) the temperature resolution is limited to 1°C (the system will only take integer values) while the DAC has a resolution of 0.04°C; and b) the firmware allows the heater temperature to drift by 1°C while holding it "stable". This drift corresponds to approximately 0.5°C in the chamber – significant enough to be the difference between the start of red and green. It should be noted that this verification method could introduce an additional 1°C chamber temperature error.

4.4.5 Troubleshooting: Heater Resistance & Temperature

MEASURING THE HEATER RESISTANCE

All room-temperature resistance measurements were initially performed by the author using a Fluke 179 DMM and clean probes. The probes were contacted together prior to heater measurement to ensure the starting resistance was 0Ω (i.e. no offset resistance);

if this was not the case, the probes were re-cleaned and/or changed. The heater on the bonded chip was contacted with the probes at right angles to the pad, with minimal pressure, two-three times to ensure the measured resistance was within 0.1Ω (the resolution of the DMM) each time. Discrepancies between multiple measurements were found to be user error in the contact angle of the probes, and these measurements were repeated.

However, one thing was not considered with this method: the contact resistance could be different with the probes than with the pogo-pins used by both the system and the element calibration hardware for reliable, good electrical contact. The author saw a systematic shift of $0.5\text{-}0.6\Omega$ between measuring the DMM probes directly in contact with the element and attaching DMM probes to the wires leading to the pogo-pins via alligator clips. Thus, measuring the heater resistance with DMM probes in direct contact with the thin film, an error of approximately 0.5°C at denaturation (94°C) would be observed in the chamber for a heater of 65Ω room temperature resistance.

To correct for this, an extra connection was added between the pogo-pins and the sensing board near the end of this thesis project, to allow for the Wheatstone bridge resistance to be measured with the DMM connected directly to the pogo-pins rather than via the probes. The author tested for electrical contact variations by re-loading the same chip multiple times and measuring the resistance seen by the pogo-pins via three U1252A portable DMMs. As these resistance measurements had a standard deviation of 0.025 and a variation of approximately $\pm 0.03\Omega$, electrical contact effects were considered negligible.

CHIP CALIBRATION

Our collaborators found significant variation in both their PCR products using a similar protocol (from no product to a very strong product) and the slopes of resistive heaters that had been re-calibrated after use. When the author reviewed their data, she discovered they were missing the annealing step of heater fabrication, causing the thin

film properties to change during heating of the ring. Furthermore, in her own data, she found that requiring the user to measure the element resistance before zeroing illustrated that the ambient-temperature resistance seems to occasionally shift, after a random number of PDMS de-bonding and re-bonding processes.

To investigate this, the author analysed 27 chips run over the course of 10 months (May '09 to March '10) for a total of 46 experiments (see Appendix A). The majority of bottom plates (or control layers) used over these ten months came from two fabrication batches: April '09 and June '09. For this reason – and the fact that changes in resistance over time were only observed with control layers from these batches – only these elements are considered in the following analysis. This amounts to 27 chips between May 13, 2009 and Mar 9, 2010, 11 of which were de-bonded, re-bonded with new PDMS and run again, to make a total of 46 PCR experiments. All chips run with positive BKV and β 2M (see Section 5.1.3) controls had successful PCR products. The calibration data for the April '09 and June '09 batches were collected between May 5-15, 2009 and Jun 24-Jul 16, 2009, respectively.

Using the values provided for each heater calibration (as shown in Table 4.4-C), the calibration resistance, R_{cal} , at ambient temperature and its error limits were calculated using Eq. 4.4-I with slope substituted for $R_0\alpha$ and a propagation of error on Eq. 4.4-J, respectively, with ambient temperature taken to be 22.5°C:

$$R_{cal} = Tm + R_0 [\Omega] \quad \text{EQUATION 4.4-I}$$

$$\sigma_R^2 = \sigma_{R_0}^2 + T^2 \sigma_m^2 + 2T \sigma_{R_0 m}^2 [\Omega^2] \quad \text{EQUATION 4.4-J}$$

$$R_{cal} \pm 3\sigma_R [\Omega] \quad \text{EQUATION 4.4-K}$$

These values were then compared with the DMM measured resistance using Eq. 4.4-K and the datasheet equation:

$$\text{FLUKE 179:} \quad R_{DMM} \pm (0.2 + 0.009R_{DMM}) [\Omega] \quad \text{EQUATION 4.4-L}$$

$$\text{U1252A:} \quad R_{DMM} \pm (0.1 + 0.0005R_{DMM}) [\Omega] \quad \text{EQUATION 4.4-M}$$

For more precise measurements, the U1252A portable DMM should be used for resistance measurements as its error is approximately 0.25% at 65 Ω (the average accepted room temperature heater resistance) as opposed to the Fluke179 at 1.21%.

Over the PCR experiments run with the April and June '09 batches, the ambient-temperature resistance measured with the DMM was found not to be within error limits of the estimated resistance from the calibration data in 7 experiments (7 of 27 chips). Two of these seven chips shifted in resistance after what appeared to be the first bonding process; the remaining five appeared to have undergone at least two to four bonding processes before shifting. A systematic shift of about 0.5 Ω can be seen between the calibration resistance and the DMM resistance. This is a result of contact resistance differences between pogo pin and probe measurements (discussed previously).

TABLE 4.4-C: CALIBRATED ROOM TEMPERATURE RESISTANCES VS. MEASURED DMM RESISTANCES AND THEIR ERROR LIMITS. IF THE LIMITS OVERLAP, THE MEASURED HEATER RESISTANCE WAS WITHIN ERROR AND THE INITIAL CALIBRATION WAS UNCHANGED. ONLY CHIPS THAT EXPERIENCED SHIFTED RESISTANCES ARE SHOWN.

Chip Name	Date Run	R _{cal} @22.5°C [Ω]	Error Window Overlap [Ω]	R _{DMM} [Ω]
0904C14	27-May-09	62.1 ± 0.1	0.5	62.4 ± 0.8
0904C14	15-Jul-09		0.6	62.3 ± 0.8
0904C14	2-Oct-09		- 0.5	63.4 ± 0.8
0904C15	25-May-09	65.7 ± 0.1	0.6	66.0 ± 0.8
0904C15	11-Jun-09		0.6	66.0 ± 0.8
0904C15	24-Jul-09		0.4	66.2 ± 0.8
0904C15	19-Aug-09		- 0.7	67.3 ± 0.8
0904C16	27-May-09	64.0 ± 0.2	0.9	64.1 ± 0.8
0904C16	24-Feb-10		- 0.4	65.4 ± 0.8
0904C17	28-May-09	60.7 ± 0.1	0.4	61.1 ± 0.7
0904C17	20-Aug-09		- 0.5	62.1 ± 0.8
0906C5	20-Jul-09	62.7 ± 0.1	- 1.6	65.2 ± 0.8
0906C7	21-Jul-09	62.8 ± 0.1	0.3	63.3 ± 0.8
0906C7	21-Jan-10		1.3	62.3 ± 0.8
0906C7	9-Mar-10		- 0.3	63.9 ± 0.8
0906C14	20-Jul-09	65.0 ± 0.1	- 1.2	63.0 ± 0.8

Three of the seven chips that changed in resistance were observed under a high powered microscope and the following scratches on the heater rings were documented by A.Jang. The other four chips could not be located for inspection.

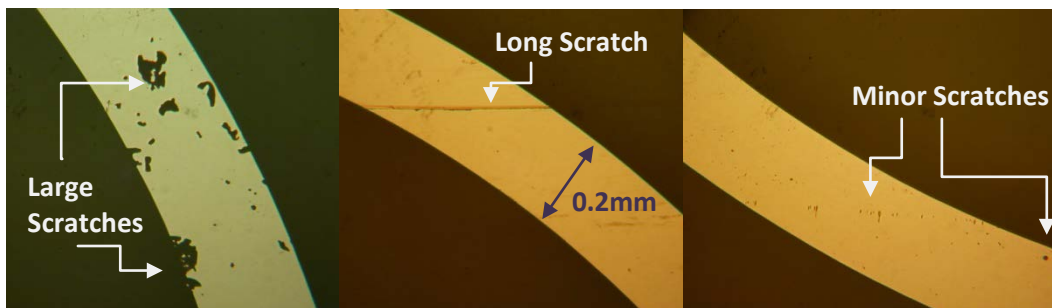


FIGURE 4.4-B: 0904C15 (LEFT): INITIAL RESISTANCE CHANGED FROM 66.0Ω TO 67.3Ω AT ROOM TEMPERATURE AFTER WHAT APPEARED TO BE THE 4TH BONDING PROCESS; 0904C16 (MIDDLE): 64.1Ω TO 65.4Ω AFTER WHAT APPEARED TO BE THE 2ND BONDING PROCESS; 0906C7 (RIGHT): AFTER WHAT APPEARED TO BE THE 3RD BONDING PROCESS.

These chips should not have been used for PCR. At least, scratches change the resistance of the thin film heater in a variable amount depending on the size and location of the imperfection, and make the heater calibration data invalid. At most, they can create localised hotspots such as the scratches on the inside of the ring as seen in Figure 4.4-C (0904C15) that will alter the properties of the thin film.

0906C7 and 0904C16 could potentially be reused even with defects as localised hotspots should not be present. However, the calibration data would need to be corrected. The slope of the linear heater resistance-temperature line is the product of the Pt thin-film TCR, α , and the initial resistance of the chip at 0°C, R_0 (Eq. 4.4-B). One might assume the TCR should not change as it is an inherent property to the thin film and is known from the initial calibration of the element (pre-defects). If this were true, the change in initial resistance could potentially be determined from a DMM measurement and the previous calibration data could be “scaled” for the above chips without needing to re-calibrate the chips.

To determine if this was true, re-calibration was performed on these three chips by F.Hejazi, and the propagation in error of the TCR of these heater elements was performed by the author using the following:

$$\alpha = \frac{m}{R_0} \text{ [}^\circ\text{C}^{-1}\text{]} \quad \text{EQUATION 4.4-N}$$

$$\sigma_\alpha^2 = \frac{m^2}{R_0^4} \sigma_{R_0}^2 + \frac{1}{R_0^2} \sigma_m^2 - \frac{2m}{R_0^2} \sigma_{R_0 m}^2 \text{ [}^\circ\text{C}^{-2}\text{]} \quad \text{EQUATION 4.4-O}$$

TABLE 4.4-D: CALIBRATION DATA BEFORE/AFTER AMBIENT-TEMPERATURE RESISTANCE CHANGES WERE OBSERVED.

Chip	Date	m	sig_m	b	sig_b	Conf. 170°C	CoVar
0904C15	2009-May-05	0.1514	0.0004	62.25	0.03	1.31	0.004
0904C15	2010-Apr-23	0.1538	0.0002	64.37	0.01	1.01	0.002
0904C16	2009-May-05	0.1486	0.0007	60.69	0.04	2.02	0.007
0904C16	2010-Apr-23	0.1481	0.0008	61.65	0.04	4.05	0.008
0906C7	2009-Jul-07	0.1454	0.0001	59.54	0.01	0.80	0.002
0906C7	2010-Apr-23	0.1529	0.0001	59.45	0.00	0.46	0.001

TABLE 4.4-E: CALCULATED TCR AND THE ERROR IN THE TCR FOR CHIPS EXPERIENCING CHANGES IN AMBIENT-TEMPERATURE RESISTANCE.

Chip	Date	TCR	sig_TCR
0904C15	2009-May-05	0.002431	0.000007
0904C15	2010-Apr-23	0.002389	0.000003
0906C7	2009-Jul-07	0.002443	0.000002
0906C7	2010-Apr-23	0.002572	0.000001

The re-calibration of the second chip (0904C16) is not valid as the calibration failed at the confidence interval of 170°C. For the other two heaters, both calibrations passed and showed changes in the TCR of the heater: one increasingly by ~5% and the decreasingly by ~2%. This result is statistically significant and not unexpected because the TCR changes in thin films as the thickness changes¹⁰², unlike in bulk material where it is constant. This means that scratched or damaged areas of the thin film heater will have different TCRs than that of the rest of the heater and the overall TCR of the heater will appear to change. Thus, chips that are found to have room temperature resistances not matching their calibration data cannot be scaled, but instead must be inspected for defects and re-calibrated as appropriate.

To ensure the heater’s ambient temperature resistance matches the calibration for every run and to add another layer of control (beyond chip assembler and operator inspection), the author built a “check calibration” function into the software. The DMM resistance value measured via pogo-pin contact is entered into the GUI along with the calibration values and DMM type (Fluke 179 or U1252a). Prior to PCR, or if the “Check Calibration” button is pressed, the software performs a propagation of errors and the

expected ambient temperature resistance from the calibration is compared to the DMM resistance measurement. The error limits for the calibration resistance are determined using Eq. 4.4-I and for the DMM resistance, datasheet accuracy values are used (Eq. 4.4-J or 4.4-K).

The GUI will then state if these values are within error. If the two values do not agree within error, the calibration data is no longer valid and the initial resistance of the chip has either changed from the time of calibration or the user is doing something incorrectly. For the former, the heater element needs to be re-calibrated and inspected for holes or defects on the heater ring. If holes or defects are present, this control layer should no longer be used.

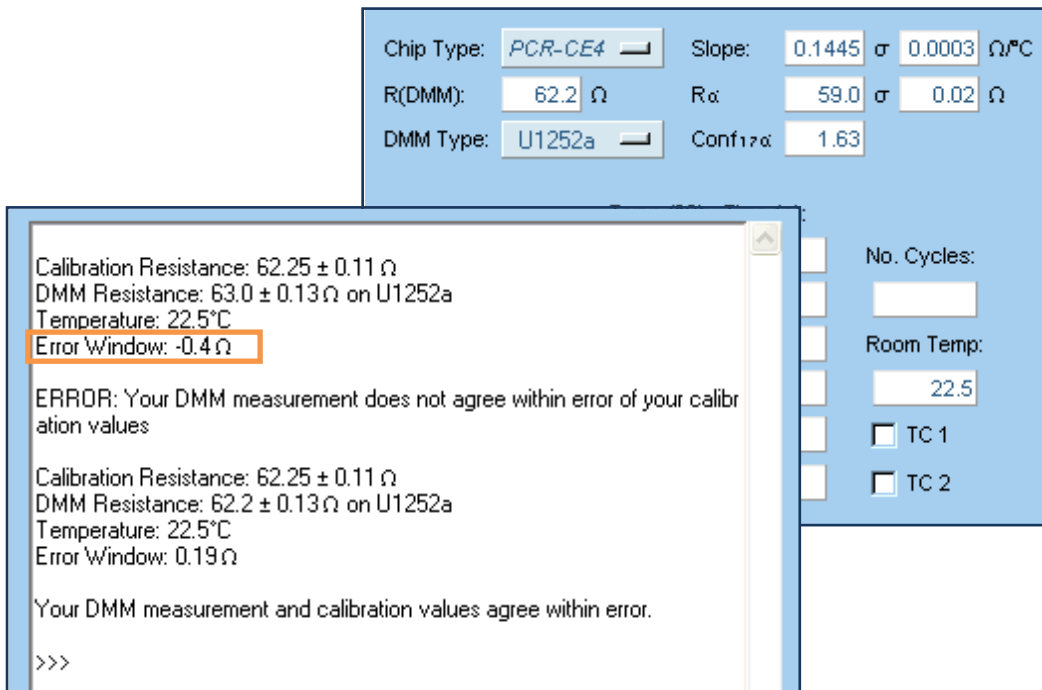


FIGURE 4.4-C: IMAGES OF THE CALIBRATION DATA ENTERED INTO THE GUI FOR THE VERIFICATION OF THE HEATER CALIBRATION, AND EXAMPLES OF THE CALIBRATION DATA AGREEING WITH THE DMM RESISTANCE AND NOT.

There was a lot of speculation at this time that some DMMs were incorrect and others were correct. To remove any possibility for error, much work was done by M.Behnam and S.Groendahl to characterise all of the DMMs in the lab. The author then built the ability to choose from these characterised DMMs and the option to add more DMMs via a textfile “driver” system into the GUI. When performing the verification, the GUI first corrects the measured resistance from the DMM characterisation, then calculates the error limits based on the datasheet accuracy values (included in the driver) and compares it to the calibration resistance at ambient temperature as described before.

Similarly, M.Behnam and S.Groendahl characterised the thermocouples used to measure the ambient temperature and included these curves in the firmware. They also characterised the waterbath using new and sensitive resistive thermal devices (RTDs).

SYSTEM FIRMWARE: DETERMINING HEATER TEMPERATURE

$$T_h = T_{am} + \frac{\Delta R_h}{m} \text{ [}^\circ\text{C]} \quad \text{EQUATION 4.4-G}$$

With the inclusion of the heatsink temperature into the predictive function by other members in the group (as described in the next section), two thermocouples were placed at the edges of the microfluidic chip and the average of their temperatures is used as the heatsink temperature. Likewise, the ambient temperature at the time of zeroing should be measured by the system via the same method as it measures it for the predictive function, but only measured once: at the time of zeroing. After the Wheatstone bridge has been zeroed, any changes in the ambient temperature will result in a change in resistance and will be accounted for.

To automate this, the author included a button on the GUI that reads the averaged temperature of these two thermocouples for three seconds, and then places the average of the received heatsink temperature data in the ambient temperature field.

4.4.6 Troubleshooting: Heater & Chamber Temperature

After the system analysis report written by the author of this thesis and this thesis project's completion, solutions to the identified problems associated with the previous procedure were implemented by other members in the lab. For completeness, they are included here.

CALIBRATION CHIPS AND TLCS

With the method described in Section 4.4.4, errors in the system-specific predictive function would be the result of inaccuracies associated with: a) chip-to-chip variations of glass dimensions and material properties affecting the thermal response; b) measuring the heater temperature; c) thermal contact variations between the microfluidic chip and the ambient temperature; and, d) quantifying the chamber temperature. Chip variations as described in (a) are expected to be quite small due to strict fabrication standards and effectively compensated for by calibrating the system using three chips at each temperature. The accuracy with which the heater temperature can be measured (b) will be left for later sub-section discussions (see Section 4.4.5). Thermal contact variations described in (c) were tested for by S.Postiban¹⁰¹ by re-loading the same chip multiple times, setting the same heater temperature and observing the colour of the TLCs; as the colour appeared to be the same after each chip load, these variations contribute minimally as in (a).

The key challenge in determining the heater-chamber temperature predictive function is the assessment of the chamber temperature. While TLCs excel in qualitative two-dimensional information, their use for quantitative measurements is restricted by the need to translate the TLC surface "colour" into a measurable scalar¹⁰³. This is usually accomplished using either a hue-based or intensity-matching method where the Hue-Saturation-Value/Intensity or Red-Green-Blue colour space is first calibrated to determine its relationship with temperature¹⁰⁴. In this manner, it is possible to obtain a quantitative measurement for colour. With the previously described method, a scalar value is not reliably obtainable as it is impossible to calibrate one's eye to give a

quantifiable result, colour is very subjective from one individual to another¹⁰⁵, and illumination effects are more significant as a user cannot clamp his head at one specific angle and distance from the TLCs. Considering that each band of green is $\sim 2^{\circ}\text{C}$ wide from start of green to start of blue, the operator’s perception of colour, angle and distance could perceive start of green or maximum green to $\sim 1^{\circ}\text{C}$ inaccuracy.

Removing the user from what is supposed to be a quantitative process was crucial. M.Behnam and S.Groendahl developed a method to overcome this through the use of a spectrometer and a blue illumination source¹⁰⁶. Some reflection from the source on the top layer of the glass will result in a peak at $475\ \mu\text{m}$. The green colour of the TLCs at the specified temperatures will result in another peak at $510\ \mu\text{m}$. When the ratio of these two peaks is a minimum (i.e. the green is as strong as the blue being reflected), the chip is considered to be at maximum green. Maximum green is used for this process instead of the start of green as it is easier to quantify.

TLCs also have a “wet film thickness” and a “dry film thickness”. The “wet” corresponds to when the slurry is initially applied to the chamber and the “dry” to when the slurry has dried. In the previous process, neither the wet nor dry thicknesses were quantified (the slurry is too viscous to pipette accurately). This means the air-TLC volume ratio and TLC distribution within the chamber were unknown, and the differences in the thermal conductivities of the PCR chamber contents (air-TLCs vs. water) were not considered. In this manner, both the temperature distribution across the chamber (affecting the colour seen) and the extra heat required to bring the TLC-filled PCR chamber up to temperature could contribute to $\sim 3\text{-}4^{\circ}\text{C}$ inaccuracy, as determined by J.Martinez-Quijada¹⁰⁷.

TABLE 4.4-F: THERMAL CONDUCTIVITIES OF PCR CHAMBER CONTENTS¹⁰⁵

Material	Thermal Conductivity
Water	0.58 W/mK
Air	0.0252 W/mK
TLCs	0.3 W/mK

To control the distribution of the TLCs, M.Behnam developed a method where small amounts of the TLC slurry are added to the PCR chamber and dried at a time¹⁰⁶. This is repeated until a uniform film of 55-60 μm is built up. This 30-35 μm insulating air gap reduces the rate of heat transfer to the TLCs, and through simulation, was found to limit the heat distribution across the TLC thickness. This is important as it raises the entire TLC thickness to one temperature, so not only the surface of the TLCs are changing colour and making the colour more apparent. Simulation of this chamber condition, as determined by J.Martinez-Quijada, also provides the air-TLC vs. water relationship so the respective temperature of the PCR mix-filled chamber when the TLCs change green is known and used to establish the experimental predictive function¹⁰⁷.

PREDICTIVE FUNCTION

While the system calibration procedure states the room temperature must be held stable for $\pm 0.5^\circ\text{C}$ ¹⁰⁰, it a) specifies nothing about the ambient temperature surrounding the chip, and b) does not specify at which temperature it should be held stable. Heat flow and thermal conductivity are analogous to electrical current and conductivity, respectively. Due to the higher thermal conductivities of glass, PDMS and the heat sink as compared to the large thermal resistance of the junction separating the top glass layer and the air, the heat primarily flows from the chamber down into the heat sink temperature is effectively the ambient temperature of the chip.

The heat sink temperature is not only affected by the room temperature, but also the system components. The author has observed that the heat sink temperature will rise approximately 1°C in the first 20 minutes after power up, an additional 0.5°C when a PCR run is executing, and can vary by 1°C over a $\sim 1\text{hr}$ PCR experiment. These variations were not noted in the previous calibration procedure, and measurements could have been taken at a time when the heat-sink temperature was varying but the room temperature was not. Furthermore, the average heat sink temperature is important as less input to the heater is required to raise the chamber temperature at 25°C than at 20°C .

The previously described approach also did not account for changes in heat sink temperature. A 1°C shift in heat sink temperature as described above could shift the chamber temperature by approximately 0.5°C; similarly, a 2°C increase in heat sink temperature due to the room temperature rising could give a 1°C error in the chamber temperature.

Since the heat sink temperature was not included in the predictive function, it contains an assumption of its state; that all PCRs will be run at the same heatsink temperature the system calibration was performed at. Furthermore, when the heater is steady-state at room temperature, the chamber temperature should be as well. For the system calibration equation determined experimentally by S.Poshtiban, entering a value of 22°C for heater temperature gives a chamber temperature of 28°C; likewise, solving for when heater and chamber temperature equate gives $T_h = T_c = 33^\circ\text{C}$. As laboratory room temperature usually lies between 20-25°C and heat sink temperature between 21-26°C, this equation certainly contains errors. This is likely due to a combination of the TLC errors (eyesight and thermal conductivity/distribution) described previously and the average/variations in heat sink temperature not being considered.

Thus, the system was re-calibrated by M.Behnam and S.Groendahl using the previously described method and considering the heat sink temperature at the time of measurements. The following experimental equation for the system was found^{106,108}:

$$T_h = 2.032T_c - 1.015T_{hs} - 0.484 \text{ [}^\circ\text{C]} \quad \text{EQUATION 4.4-P}$$

Before, a heater temperature of 22°C gave a chamber temperature of 28°C. With this equation, a heater and heat sink temperature of 22°C gives a chamber temperature of 22°C, as expected.

PREDICTIVE FUNCTION IMPLEMENTATION

The experimental predictive function takes discrete component errors in the thermal hardware module and system variations such as heat sink size into consideration. The same system calibration procedure was performed by S.Groendahl on a second system (named “Winnie”, with the same configuration and heat sink design) and its predictive function was found¹⁰⁹.

$$T_h = 2.032T_c - 1.015T_{hs} - 0.484 \text{ [}^\circ\text{C]} \quad \text{EQUATION 4.4-Q}$$

These two system functions can be seen in Figure 4.4-D with T_{hs} values of 23°C.

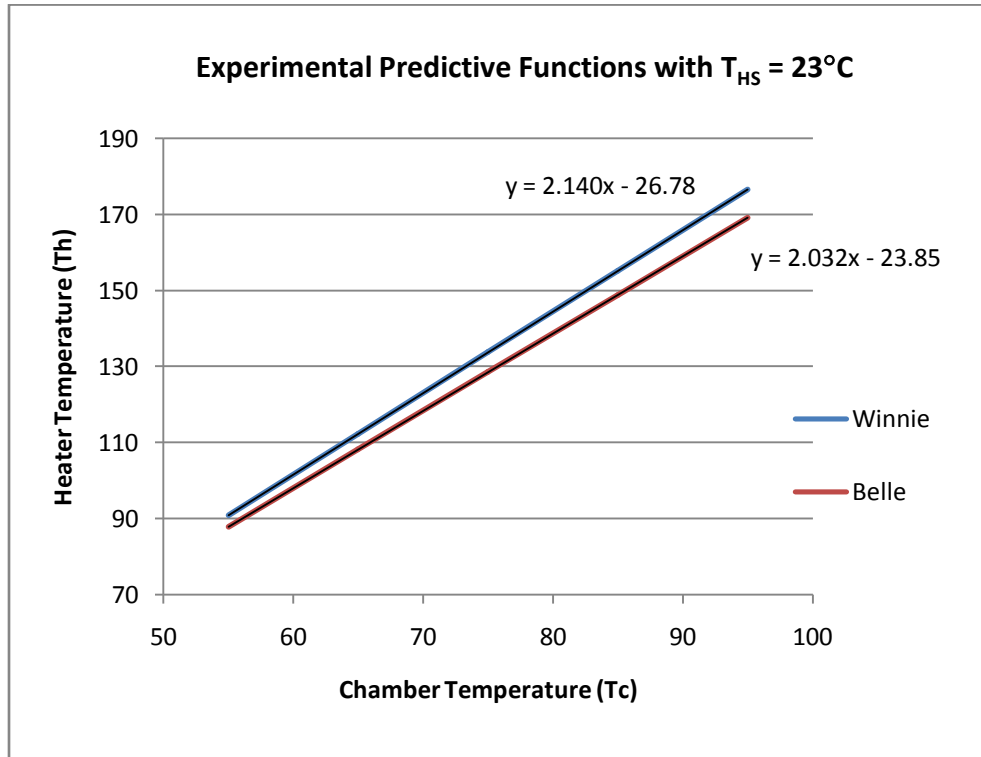


FIGURE 4.4-D: EXPERIMENTAL PREDICTIVE FUNCTIONS DETERMINED FROM TWO DIFFERENT SYSTEMS BY S.GROENDAHL, WITH A GIVEN HEATSINK TEMPERATURE OF 23°C FOR COMPARISON PURPOSES.

At 94°C, the heater temperature difference between the first system achieving the temperature and the second is approximately 7°C. Thus, using the predictive function of one system for the other would result in an ~3.5°C difference in chamber temperature. However, it is unlikely for component precision errors and minor system variations to be the sole culprit for such a large system-to-system discrepancy. In R.Johnstone's thermal report¹¹⁰, he calculates a worst case scenario of 3.5°C in the heater temperature (~1.8°C in chamber) due to component variations and uncertainty in the heater resistance measurement, Wheatstone bridge, voltage measurement and noise. The remaining 3.5°C variation likely comes from other system to system variations such as minor changes in the heatsink manufacturing and soldering of components.

To remove the error associated with using one system's calibration for all systems, the predictive function determined during initial system calibration is now treated as system-specific data and is specified when compiling the firmware onto the system's microcontroller. Furthermore, to fully account for varying heat sink temperatures, the required heater temperatures are calculated at the beginning of every cycle rather than only at the beginning of all (35) cycles.

4.4.7 On-Chip PCR Results Revisited

As the heat sink temperature varied between ~21°C and 26°C over the PCR experiments run by the author, these two limits were entered into equation determined in the previous section to determine how the heater temperatures would compare to the function used for the experiments in this thesis.

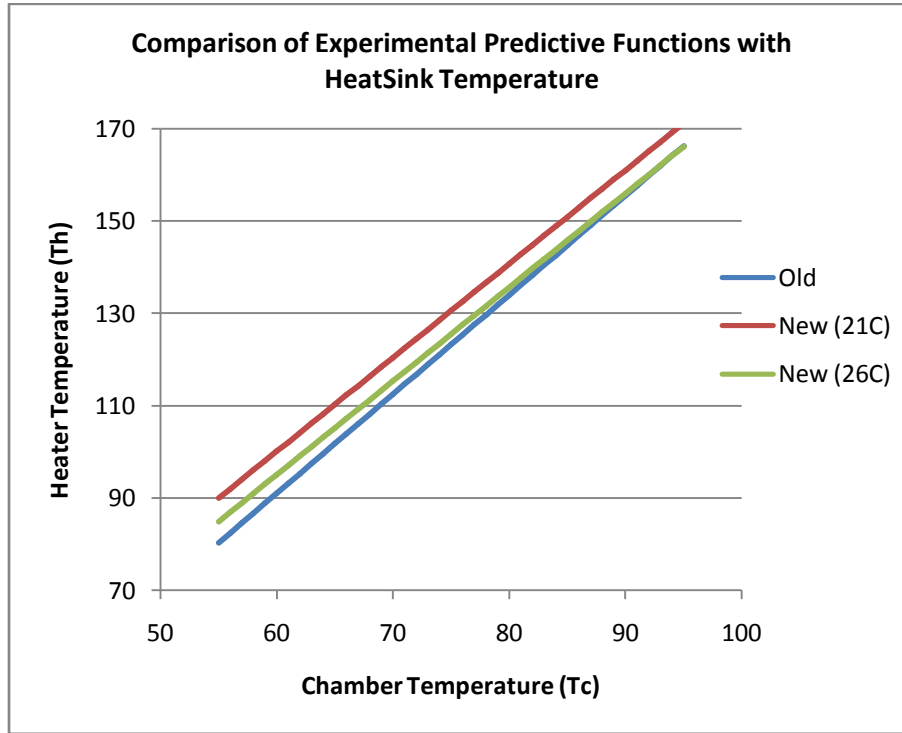


FIGURE 4.4-E: A COMPARISON OF THE SYSTEM'S EXPERIMENTAL PREDICTIVE FUNCTION BEFORE HEAT SINK TEMPERATURE WAS INCLUDED AND AFTER, WITH SET POINTS OF 21°C AND 26°C.

At 26°C, the new line almost overlaps the previous function, with the required heater temperature to reach 58°C for the new function 4°C hotter than the predictive function used in this work (Old). This suggests the previous function did not reach the required annealing temperature (cooler by at least ~2°C). At 21°C, the heat sink temperature effect is even more pronounced, with the heater temperature 5°C hotter to reach 94°C and 9°C hotter to reach 58°C for the new function. This suggests the previous function had chamber temperatures too cold for all PCR steps when the heat sink was at 21°C.

Using Eq. 4.4-P (the new experimental predictive function including heat sink temperature), considering for the contact resistance and the 0.5°C added to the ambient temperature entered into the GUI (due to the rise in temperature from system standby to operation), the chamber temperatures achieved were calculated as follows:

$$T_h \text{ aim: } T_h = 2.15T_c - 37.96 \text{ [}^\circ\text{C]} \quad \text{EQUATION 4.4-R}$$

$$T_h \text{ achieved: } T_{h,act} = T_h - \frac{0.5}{R_{wb} + 10} (T_h - T_{am}) - 0.5 \text{ [}^\circ\text{C]} \quad \text{EQUATION 4.4-S}$$

$$\text{Respective } T_c: T_c = \frac{T_h + 1.015T_{hs} + 0.484}{2.032} \text{ [}^\circ\text{C]} \quad \text{EQUATION 4.4-T}$$

Using these equations, the average chamber temperatures for the three successive PCR-CE experiments with heat sink temperatures of 22.1-22.5°C were found to be 90.4°C for denaturation, 53.2°C for annealing, and 65.9°C for extension (should be 94°C, 56°C, and 70°C, respectively). These inaccuracies in temperature likely reduced the relative yield of the PCR (found to be 8.1%). For a less robust sample, a product may not have been seen at all.

The best efficiencies were seen for two successive samples which had higher heat sink temperatures (23.8°C for both) and the annealing/denaturation temperatures entered into the GUI at 2°C, giving 93.3°C for denaturation, 54.9°C for annealing, and 67.9°C for extension. This average relative yield was 25.8.

These results suggest the loss in relative yield was at least in part due to incorrect chamber temperatures, rather than passivation as initially expected. To determine if passivation also contributes to this, experiments would need to be re-performed with the correct temperatures to determine if a loss in relative yield still exists.

4.5 CONCLUDING REMARKS

This custom-built, integrated PCR-CE system demonstrates performance comparable to commercial systems that are much larger than a shoe-box size and cost magnitudes more than ~\$600. In terms of PCR, the author has shown this inexpensive, portable system can reproducibly detect the presence of BK virus samples. Although the relative yield could be improved with better thermal control and/or passivation, this system has performed both several and possibly single molecule amplification.

As demonstrated with the large number of variable PCR-CE experiments performed by the author, this custom-built instrument is a standard tool in our laboratory due to its repeatable performance and integration. Higher levels of integration will be seen in the next chapter, allowing for sample-in-to-answer-out diagnostics, and in the near future, these will be further scaled down into even more inexpensive systems. However, even though this system can continue to be improved upon, in its current state it clearly demonstrates LOC infrastructure does not need to be expensive and can further the development of LOC devices for POC applications.

Increasingly accurate, inexpensive and faster thermal control methods are ongoing investigations in our group. Now that our group is becoming even more confident with the PCR chamber temperature, the thermal controller could be modified to overshoot the set point temperature, eliminating the need for add times in the software. Furthermore, it's possible the PCR step time lengths could be shortened to even further reduce the PCR cycle time.

Another major area of future work is to automate the PCR-CE process. While PCR and CE are certainly integrated in this system in terms of electronics, firmware, software and microfluidic chip, the ability to seamlessly transition from amplification to detection with no interference from the operator is not possible. The polymer used in this work for CE is dry before the amplification is completed and the buffers evaporated. Furthermore, small air bubbles often appear at the PCR output well which often introduces bubbles into the CE channels, invalidating or inhibiting the analysis step. Thus, a new microfluidic chip design is a must even though the electronics, firmware and software are all prepared to perform automated PCR-CE.

A new microfluidic chip would need to address the following limitations:

- During lengthy PCR run times (i.e. on the order of an hour or more), heating of the thin film causes the PDMS to deflect slightly as the area between the heater and the un-bonded PDMS (it bonds to the glass, not the metal) heats to incredibly high

temperatures. The author speculates that it is this flexing of the PDMS that contributes to the migration of air within the PDMS and the appearance of air bubbles in the CE wells and/or channel that is detrimental to the subsequent CE process. One potential solution to this could be incorporating a Parylene-PDMS or Parylene-PDMS-Parylene membrane (air does not diffuse through Parylene).

- Capping the CE wells with oil to prevent evaporation of the buffer and polymer is cumbersome and not reproducible; furthermore, it requires the user to do this with a microscope to ensure the buffer is fully covered. Modifications of the gantry to contain electrodes with an o-ring type setup would seal the wells containing buffer, removing the need for oil.
- In the current set-up, 1 μ L of flush-out buffer needs to be present in the PCR output/CE sample well to prevent introduction of air into the CE channel. Over the course of the experiment, diffusion from the higher concentration matrix will alter the concentration of this 1 μ L of buffer. Furthermore, introduction of the flush-out buffer post-PCR by the operator does not allow for automation. A reservoir for the flush-out buffer to be loaded prior to the PCR-CE run would remove the need it to be added mid-experiment by the operator.
- The separation channel of the CE portion of the chip passes over the heater, drying the polymer during the PCR run so that detection may not be done beyond 13mm. Thus, there is little point in the channel being as long as it is in the current design. Furthermore, this long length leads to low electric field strengths and lengthy migration times (detection of a 299bps product takes on the order of 3min). Thus, it would be more beneficial for the CE portion of the microfluidic chip to adapt more of a 4-port-mini (as named in the AML lab) configuration.
- Lastly, although a minor point, one of the valves on the current design is directly in the path of the laser, contributing to increased scatter of excitation light reflected back towards the GRIN lens. Careful attention should be paid in the new design to

limit features in the detection path to parallel channels which should scatter less excitation light.

In the next chapter, the key challenges involved with the integration of the in-house developed sample preparation protocol and its performance will be described.

Integrated Sample Preparation-PCR-CE

CHAPTER 5

5.1 INTRODUCTION

Current commercial genetic analysis equipment is limited to performing assays which require many procedural steps and several hours to days in processing time, the majority of which is contributed to the preparation of samples prior to amplification/analysis¹¹¹. Furthermore, expensive reagent kits and allocated space for single-function instruments and operator handling augment the cost and complexity of diagnostic tests. While reliable and reproducible on the macroscale¹¹², integration of these expensive and time consuming conventional sample preparation techniques onto microfluidic devices remains a key challenge¹¹³. To realise genetic analysis systems of POC applications, a simple and generic sample preparation technology is necessary for the development of portable, fully-integrated platforms capable of implementing complete molecular diagnostic protocols¹¹⁴.

In previous chapters, emphasis has been placed on developing an inexpensive, portable instrument and microchip for genetic amplification and analysis/detection. However, genetic testing of biological samples requires the nucleic acids (DNA) of interest to be separated from other cellular components and raw sample debris that could reduce the sensitivity of subsequent processing steps. Like many LOC devices that have been developed for medical diagnostics¹¹⁵, in its PCR-CE form our custom-built system still requires substantial off-chip preparation of the raw sample in a well-equipped facility with trained operators before it can be amplified. In this respect, it is not truly portable (aside from its shoe-box size and standard power requirements) as it remains tied to conventional sample preparation (SP) infrastructure.

To enable full portability and increase the functionality of this instrument, a sample preparation module was designed based on conventional nucleic acid extraction

methods using paramagnetic beads and integrated into the modular system⁵³. With this unit, system is able to perform magnetic particle immobilisation and transport, fluidic movement and isolation, temperature control, and analyte detection using high voltages. In this thesis, the sample preparation unit is used to extract nucleic acids from buccal cells, and then amplify and detect the β 2-microglobulin gene via PCR-CE.

This chapter is based on the architecture of the sample preparation unit, its integration into the system and its subsequent performance. However, its presence in this thesis is secondary to what was described in previous chapters. The development and validation of the bead-based SP process overviewed here was A. Olanrewaju's project and more detail on it can be found in his thesis¹¹⁶. The author of this thesis was included at the end of this project to aid in the integration of the SP module with the extensively tested system described in the rest of this thesis via CLI, software, and previously refined protocols. A brief background of the literature will be provided for overview in the rest of this section, and subsequently system additions and modified protocols will be described. The system performance will then be evaluated by the author in Section 5.3 based on the previous characterisation of the PCR-(LIF)CE system, with conclusions to follow.

5.1.1 Sample Preparation Techniques

The development of on-chip nucleic acid extraction techniques has resulted in extraction efficiencies comparable to those achieved by conventional methods¹¹⁷ and can utilise many approaches (including chemical, optical, thermal and electrical), as recently reviewed for bacteria analysis and detection¹¹⁸.

Of these developed techniques, solid-phase extraction (SPE) using silica or glass with chaotropic salts has been demonstrated to be the most efficient¹¹⁴ but is not easily adapted to on-chip methods. For example, while μ SPE was successfully demonstrated on a credit-card sized platform with an integrated isothermal method for genetic amplification and detection for the analysis of human cervical fluid¹¹⁹, this complex

system consisted of attached pre-concentration, silica filters, membranes, 2 syringe pumps, multiport valves and heaters that are not scalable, and used a chip that was assembled by hand from various components. In another demonstration¹²⁰, a disposable microfluidic chip isolated infectious bacteria DNA from spiked whole blood samples with performance comparable to standard sample preparation kits. However, the employed μ SPE process required the 450 μ L sample mixture (containing buffer and detergent) to be applied to the microfluidic chip with a syringe and tubing, and subsequent SPE-channel rinses with ethanol to enhance cell lysis and DNA extraction. The system also required off-chip amplification/detection via real-time PCR and approximately an hour processing time for only the DNA extraction step.

Magnetic particles are capable of extracting nucleic acids in minutes and alone do not inhibit subsequent PCR unlike the chaotropic salts and solvents used in previously described SPE methods, while still retaining high efficiency¹¹⁷. Magnetic beads are also commercially available and are capable of transporting the sample from high volumes (mL) to small volumes (μ L), effectively concentrating the nucleic acids. However, like other SPE methods, they are also difficult to fabricate and integrate on-chip. A recent demonstration showed the SPE extraction of DNA from whole blood was more effective with magnetically controlled silica beads than packed beads¹²¹. Magnetic bead-based sample preparation has been integrated in related work with real-time and Taqman-based PCR^{122,123}; however, these demonstrations required substantial external instrumentation.

5.1.2 SP Integrations with PCR and CE

Less development emphasis has been placed on SP integrations with PCR and CE as compared to realtime-PCR-Taqman. However, CE is advantageous in that it not only detects the sample, but also provides the sample size, allowing for corroboration of the diagnosis. Furthermore, PCR-CE is the basis of many standard laboratory biological protocols, allowing for easier portability or many applications.

A powerful SP-PCR-CE demonstration²⁷ presented a fully integrated microfluidic system with sample-in-answer-out capability in 24 minutes with SP of raw bodily fluids via a silica bed. More recently¹²⁴, a microdevice with on-chip silica bead-based SP, on-chip PCR using a conventional thermal cycler and external CE was described. However, both of these presentations required extensive external infrastructure, the first including an Ar ion laser and IR thermal cycling apparatus, and the second, commercial PCR and CE systems. Likewise, other demonstrations^{32, 33, 125} have shown high functionality systems with also high cost, often external instrumentation.

In a recent review¹²⁶ of current state-of-the-art nucleic acid-based pathogen detection using integrated LOC systems, commercial developments by ACLARA Biosciences, Affymetrix, Agilent Tech., Alderon, Cepheid, Fluidigm, Motorola, Roche Molecular Diagnostics and others were described. However, these are characteristically expensive and not portable, confined to a laboratory like the equipment they are intended to replace.

Here, the functionality and versatility developed in previous chapters is increased through the integration of a sample preparation unit. This enables our system to process raw samples, providing a sample-in-to-answer-out diagnostic platform while performing cell lysis, nucleic acid transport and delivery, particle trapping for purification, mixing, isolation of fluid, thermal cycling, and optical detection. A miniaturised paramagnetic bead-based approach based on widely-used conventional methods was chosen for SP to allow for easy portability from traditional to microfluidic methods. To the best of our knowledge, this is the first demonstration of an inexpensive, portable instrument capable of performing SP-PCR-CE in one microchip.

5.1.3 Bead-based Nucleic Acid Extraction

ChargeSwitch® gDNA Buccal Cell Kits (Invitrogen, Calsbad, CA) are commercially available kits that can be used to perform bead-based nucleic acid extraction. Included in these kits are ChargeSwitch beads, Proteinase K and lysis, purification, wash, and

elution buffers. Nucleic acids are extracted from cellular debris using ChargeSwitch® magnetic beads by controlling the surface charge on the bead using the pH of the surrounding liquid. In low pH conditions (<6.5pH), the positive surface charge attracts the negatively-charged backbone of nucleic acids. The nucleic acids can then be removed from unwanted cellular components using a magnetic field. Once the nucleic acid is extracted with the bead, the pH is raised (>8.5) to remove the surface charge from the beads, eluting the RNA/DNA.

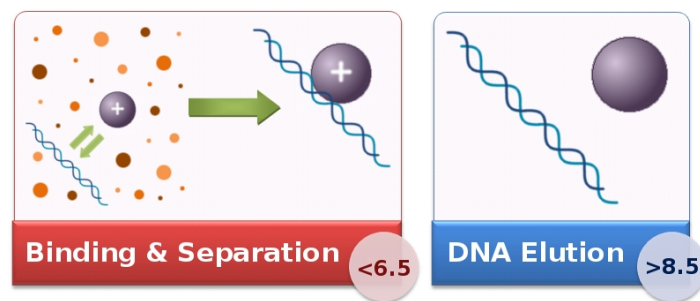


FIGURE 5.1-A: ILLUSTRATION OF THE PRINCIPLE OF THE CHARGESWITCH BEADS

Buccal smears are used as the verification sample in this work as they are a convenient source of genomic DNA for non-invasive genotyping, and are safer and easier to obtain than blood. β 2-microglobulin (β 2M), a housekeeping gene found in all nucleated human cells (including buccal cells), is tested for and provides a proof-of-concept for many other applications. Buccal smears are conducted on healthy volunteers with informed consent using a 15cm sterile swab (AMG Medical, Montreal, QC). After applied to the volunteer's inner cheeks, the swab is incubated for 15min in 500 μ L of lysis buffer and 10min in 5 μ L of Proteinase K to lyse the collected cells and denature the histones, respectively. Proteinase K aids in releasing nucleic acids for improved access by the primers during genetic amplification. Post-incubation, 25 μ L of purification buffer, 5 μ L of CST beads (stored in 10mM MES, ph 5.0, 10mM NaCl, 0.1% Tween20) and 12 μ L of 10% Tween20 (Sigma Aldrich, USA) are added. This mixture is referred to as the SP lysate mixture.

The off-chip nucleic acid extraction protocol is modified from the manufacturer's recommended approach and simplified for development of the on-chip protocol. It involves replacing the wash and elution buffers with our SP separation matrix (25% sucrose and 1% Tween20 in wash buffer) and PCR mixture, respectively. Tween20 and sucrose are used to increase the density and viscosity of the wash buffer, enhancing the washing effect. Once the beads are separated from cellular debris and immobilised using an external magnet, the supernatant is removed and the PCR mixture is added, eluting the DNA. Specific procedure details on the developed off-chip sample preparation technology can be found elsewhere¹¹⁶.

5.2 SYSTEM INTEGRATION

5.2.1 Instrument

The sample preparation module consists of two parts to be integrated into the PCR-CE instrument: the "stage" consisting of the required mechanical components and the circuit board consisting of the drive electronics to be connected to the microcontroller unit via the communication bus (see Section 3.2). Both of these components are connected to the power bus regulated and distributed by the power module. With the integration of this unit, our modular system is easily customised from a PCR-CE to an SP-PCR-CE instrument.

Two computer-controlled motors (26DBM10D2U-K, Portescap, USA), encoders, infrared transceivers (OPB390, OPTEK Technologies, USA), and a neodymium-iron permanent magnet are included in the SP module. The two motors provide X-Y translation of the machined 2mm diameter permanent magnet in a range of 25mm x 25mm, and the encoders and transceivers are used for position sensing and auto-zeroing. This set-up allows the SP module transport the magnetic beads within the SP microchannel and deliver them to the PCR input well.

TABLE 5.2-A: SAMPLE PREPARATION CLI COMMANDS

Description	Command	Returns
Direct XY Movement	$XY(x_{pos}, y_{pos}) ;$	Message #000
Circle XY Movement	$CM(x, y, rad, cyc, dir) ;$	Message #000
Wiggle XY Movement	$WM(x, y, rad, cyc, dir) ;$	Message #000
Perform SP	$PS ;$	Message #300,#000

Integration of the SP module into the system required it to be integrated into the firmware, CLI, and software as well. Direct, circle and wiggle movements were built into the firmware to allow for protocol testing. The functional SP command executes the optimised set of motion commands determined for the SP channel in the chip to be described in Section 5.2.2. In this manner, the user has the option to transport and deliver the beads automatically via one button on the GUI, or to manipulate the magnet (and thus the beads) in various one- and two-dimensional ranges of motion. The GUI collects the actions performed by the user and saves them in a log-file and HTML report like described in Section 2.3.2.

The author of this thesis aided with determining how the necessary SP tasks would be split between the firmware and software, included the interface requirements into the CLI, and then wrote the associated software components and report generation tasks, enabling independent SP experiments and integrated SP-PCR/SP-PCR-CE experiments.

5.2.2 Microfluidic chip

The microfluidic chip used in this work is the same tri-layer glass-PDMS-glass chip as described in previous chapters (see Section 4.2.2), except for one minor variation: the CE separation channel was shortened by 5mm to connect to BW-2 rather than BW-1 (version 2 top plate; Figure 5.2-A). This change was made to facilitate easier loading of the CE separation matrix into the CE microchannels, and has a minor impact on the electric field strength due to the overall length of the separation channel.

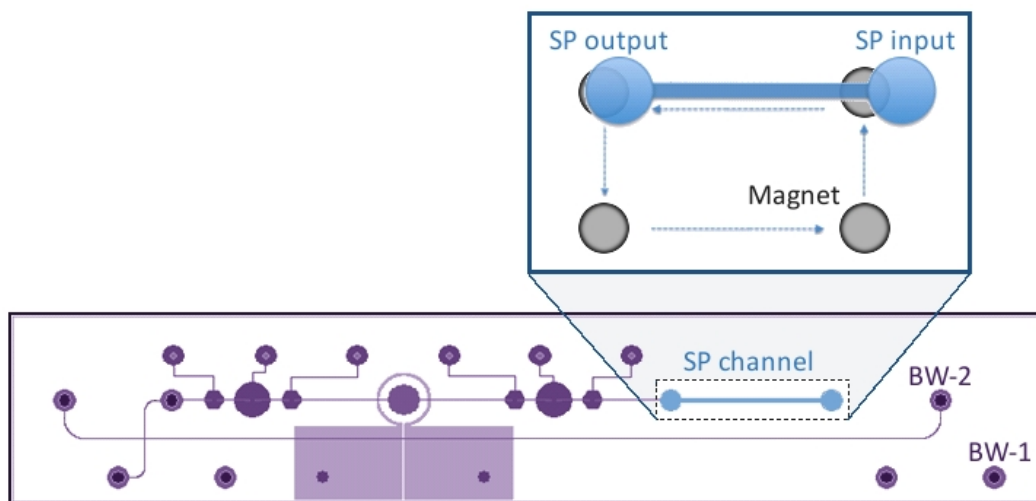


FIGURE 5.2-A: DESIGN OF THE INTEGRATED SP-PCR-CE CHIP, EMPHASISING THE SP SECTION OF THE MICRODEVICE. THE PERMANENT MAGNET MOVES BENEATH THE MICROFLUIDIC CHIP ALONG PRE-DEFINED PATHS SET BY THE SP MODULE, MANIPULATING THE MAGNETIC BEADS WITHIN THIS SECTION OF THE CHIP (NOT DRAWN TO SCALE).

The SP section of the integrated SP-PCR-CE chip consists of a microchannel etched into the bottom face of the top glass layer (100µm deep x 500µm wide) with two wells on either side of the channel. The right well is the SP input and the left well doubles as the SP output and PCR input, minimizing sample transport.

5.2.3 On-chip Procedure

The SP-PCR-CE protocol was written by the author based on developed lab SP protocols by A.Olanrewaju and G.Kaigala, and improved through experimentation and observation of the system. The full SP-PCR-CE protocol can be found in Appendix F.

SAMPLE PREPARATION

The SP separation matrix and SP lysate mixture used in the on-chip method were developed along with the off-chip method (described in Section 6.1.3), and descriptions of their compositions can be found there.

First, the output well is filled with SP separation matrix and drawn into the SP microchannel using a custom-fitted syringe applied to the SP input well until the channel is completely filled. Once this is completed, the syringe and any excess separation matrix are removed from the SP input well. The system then positions the magnet primarily under the microchannel to the left of the SP input well with a small area of the magnet under the well itself. 4 μ L of the SP lysate mixture (containing the sample) is added to the input well, the placement of the magnet drawing the beads immediately to the entrance of the channel. The magnet then moves down the channel, pulling the beads through the separation matrix at 140 μ m/s. It is believed that the dense, viscous separation matrix improves the nucleic acid extraction by isolating the unwanted cell components, effectively “washing” the NA-bound beads from cellular debris. Once the magnet reaches the output well, it immobilizes the beads in the centre of the well so the SP separation matrix can be removed from the well without removing the sample. The lysate mixture is also removed from the input well at this time to minimize pressure-driven flow of more separation matrix into the output well, and the magnet is moved away by the system, leaving the sample in the well. At this time, the nucleic acids are extracted from the cell debris and the sample preparation is complete; the next step is amplification.

GENETIC AMPLIFICATION (PCR)

Prior to the beginning of the experiment, a 24 μ L mixture of PCR reagents is prepared. This volume is used to perform simultaneous on-chip and off-chip conventional thermal cycler (positive control) experiments. This mixture is made up of 1xPCR buffer (20mM Tris-HCl, 50mM KCl, pH 8.4), 4mM MgCl₂, 200 μ M dNTPs, 2.5U of Platinum Taq polymerase (all included in Pt Taq DNA kits from Invitrogen, Burlington, Ontario), 0.02% BSA (New England Biolabs, Ipswich, MA), 4% DMSO (Fisher Scientific, Ottawa, Ontario),

and 200nM of each β 2M specific primer (forward: 5'-CCAGCAGAGAATGGAAAGTC-3', reverse: Alexa647-5'-ACTTA ACTATCTTGGGCTGTGAC-3'; Integrated DNA Technologies, Coralville, IA). These primers are designed to amplify a 236 bp segment of the β 2M gene. A BLAST search by the author with these primers resulted in the intended target as the only exact match; 13 potentially unintended templates were also found with various sequence mismatches.

19.2 μ L of this mixture is combined with approximately 76ng of human gDNA (purified from whole blood; FlexiGene DNA kit, Qiagen, Mississauga, Ontario) to form a 20 μ L positive PCR control, while the remaining 4.8 μ L is reserved for the on-chip experiment. The positive control is then run on commercial thermal cycler with the same thermal settings as the on-chip experiment. (If a negative control is included, a larger volume of PCR mixture is prepared and the extra volume is also thermal cycled on the conventional system at this time.)

Once the sample preparation is completed, the remaining 4.8 μ L of PCR mixture is added to the SP output well (now the PCR input well) and mixed with the beads. The pH of the PCR mixture is approximately 8.8, sufficiently basic enough (>8.5) to release the sample from the magnetic beads without the need for an intermediate solution. As described in Section 4.2.3, 3-4 pump cycles of sequential valve action loads the PCR section of the chip with the sample mixture. Once the chamber is filled, the valves are closed, any remaining mixture is removed from the PCR input well and this well is then washed with water to remove any residual concentrate.

On-chip thermal cycling is performed based on parameters set by the GUI: pre-denaturation at 94°C for 120s; 35 cycles of 94°C, 60°C, and 72°C for 30s at each temperature; and post-extension at 72°C for 120s. When completed, 5 μ L of flush-out buffer is placed into the PCR input well, and the valves are actuated in a pumping motion until this well is empty. At this time, approximately 5 μ L of diluted PCR product is present in the PCR output well (doubling as the CE sample well).

ANALYSIS (μ CE)

The CE separation matrix, CE and flush-out buffer are 4% linear polyacrylamide (LPA), 1xTTE and 0.01xTTE, respectively. The analysis section of these experiments is identical to past work (described in Section 3.2.3), and the detailed procedure and CE reagent compositions can be found there.

As seen previously, the CE section of the microfluidic chip is passivated prior to analysis to minimize electro-osmotic flow and DNA binding to the channel walls. The CE microchannels are then filled with CE separation matrix and 4 μ L of 1xTTE buffer is placed into the remaining three CE wells (not the sample well). 1 μ L of the 5 μ L of diluted PCR product from the CE sample well is reserved, and DNA from the remaining 4 μ L is electrokinetically injected into the injection channel using an electric field of 222V/cm for 80s, followed by a separation of 67V/cm for 250s. Detection is performed at 13mm from the cross intersection.

5.3 SYSTEM PERFORMANCE

5.3.1 System Level SP-PCR-CE Results

To test the system, 6 SP-PCR-CE runs were performed, all of which were positive. However, two of these runs were unable to have the CE performed on the same chip due to bonding weaknesses between the top layer of glass and the PDMS around the CE portion of the chip. Thus, only four of the SP-PCR-CE runs are shown in Figure 5.3-A.

The 26-base primer arrives at \sim 100s of separation and a second peak arrives at \sim 140s, corresponding to 250 ± 20 bps as interpolated from a size standard (not shown here; see Section 4.2.3). A BLAST prediction⁹⁴ of human genomes resulted in matches (for our primers) for B2M variants, all with an expected product size of 236 bps, verifying that this second peak is the product peak.

A third, broad, low-intensity peak centred at \sim 180s of separation is occasionally seen in both the on-chip experiments and all conventional thermal-cycler experiments. This

peak was attributed to non-specific amplification and may have only appeared in half of the on-chip electropherograms due to variations in injection characteristics (Section 3.2.4).

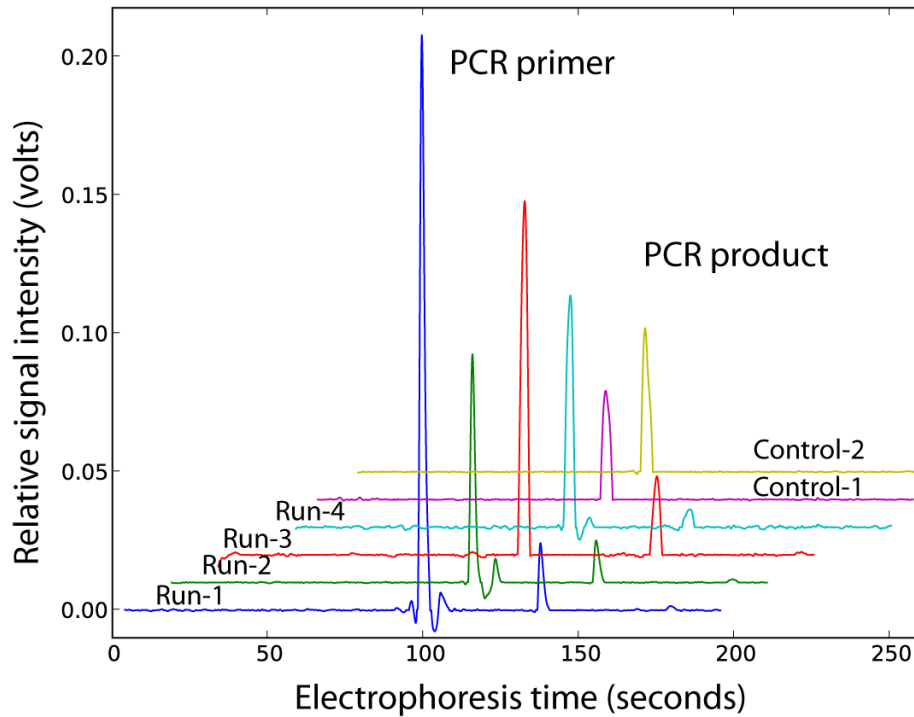


FIGURE 5.3-A: THIS ELECTROPHEROGRAM DEMONSTRATES THE SUCCESSFUL RESULT OF THE INTEGRATED SP-PCR-CE INSTRUMENT. FOUR CONSECUTIVE RUNS ARE SHOWN HERE TO DEMONSTRATE REPEATABILITY WITH TWO NEGATIVE CONTROLS TO RULE OUT CONTAMINATION.

On occasion, a brief decrease in the processed signal intensity appears before/after the primer peak. This is a result of our processing (Median subtraction, specifically) and does not affect the limit of detection.

Several negative controls were performed to confirm the microfluidic chips, process reagents and laboratory environment were not contaminated. First, the sample

preparation step was skipped and a PCR-CE negative was performed, replacing the sample-beads portion of the mixture with PCR-grade water. This control was designed to ensure no contamination was introduced during microchip fabrication or reagent pipetting with respect to PCR-CE and was found to be negative. Second, the entire on-chip SP-PCR-CE process was performed by replacing the buccal cell and lysate buffer volume with water. This control was designed to ensure no contamination was introduced during the microfabrication process or SP reagents for the entire SP-PCR-CE process, and was also found to be negative. This suggests the product peaks observed from our SP-PCR-CE process were not the result of contamination.

5.3.2 Variability

All SP-PCR products in this thesis (both conventional and on-chip) are analysed using capillary electrophoresis. As seen in the previous chapter, in attempts to separate the CE contribution to the SP-PCR-CE variability from the SP-PCR variability, RMDs are given from both the mean PCR relative yield and mean product peak intensity in this section.

MEAN PCR RELATIVE YIELD (SP-PCR VARIABILITY)

The PCR relative yield is the ratio of product peak height (product-labelled fluorophores) to the primer and product peak combined (total fluorophores); or, the efficiency with which the PCR was executed. It is dependent on the PCR conditions, including the reaction components and starting concentrations (i.e. SP performance), environment, and temperatures. In this case, the relative yield will be used as a means of determining the reliability of our on-chip SP-PCR process, PCR temperatures, surface passivation (environment) and the repeatability of the amount of DNA recovered.

To determine the variability of our on-chip SP-PCR, all 6 SP-PCR-CE were considered for the variability. The RMD of the mean sample relative yield was found to be 28.4%, much larger than that of the conventional PCR thermal-cycler variability seen previously.

Thus, it is expected the amount of DNA recovered from our SP process – or rather, the number of beads present in the PCR input well – is not strictly controlled, resulting in a large dispersion of PCR efficiencies. However, this could also be a result of operator handling. As seen previously, a high level of training is required to operate this custom-built system, and this variability may be improved with knowledge gained through operation of the system and an improved understanding of the process.

MEAN PRODUCT PEAK INTENSITY (PCR-CE VARIABILITY)

In section 3.2.2, the load-to-load variability of the conventional (μ TK) and on-chip CE were found to have RMDs of 23.5% and 20.3% from the mean peak height, respectively. As described previously, this variation is primarily attributable to the optics in the system; or, more specifically, the reproducibility of the laser focus on the microchannel. Thus, the variability of product peak intensity is effectively the SP-PCR-CE variability. When analysing the on-chip SP-PCR-CE runs, the variability was found to have an RMD of 50.3% (PCR-CE variability was found to have an RMD of 27.2%). However, as described in Section 4.3.2, the high variability in the CE could either work to create a worse dispersion in the product peaks (i.e. the strongest product has the best optical alignment and the weakest product has the worst) or a seemingly “better” dispersion when determined experimentally. Thus, the variance in the SP-PCR relative yield is more applicable.

5.3.3 Relative Yield

As found in the previous chapter, the average PCR amplification relative yield of three successive on-chip SP-PCR-CE experiments was determined to be 9.8%. As described in Section 4.4, this decrease in relative yield was at least in part due to incorrect chamber temperatures.

5.4 CONCLUDING REMARKS

One of the major challenges limiting current LOC systems from use in POC applications is the complexity involved in the processing of raw samples. Here, a sample preparation module designed based on the developed off-chip protocol was integrated into the portable, inexpensive system. This module performs nucleic acid extraction with bead manipulation techniques, removing the need for complex fluid handling and potentially reducing sample handling variabilities.

Although buccal cells were used as the raw sample in this preliminary demonstration, the genetic analysis instrument and its sample preparation module can be used for a wide range of applications including DNA/RNA extraction from yeast, bacteria, living tissues and forensic samples (all of which have commercially available beads). The simple integration of the sample preparation module further illustrates the modularity of the system and its importance, and due to its scalable, inexpensive, portable nature and sample-in-to-answer-out capability, this instrument represents a significant advancement for the use of LOC technologies in POC applications.

However, the large variability in the SP-PCR efficiencies suggests the process is quite variable and the automation of this process to minimise operator intervention has the potential to considerably improve this variability. Furthermore, a re-evaluation of the experiments could be done with the improved temperature control as described in Section 4.4 to see if this improves the relative yield and possibly the variability as well.

Conclusions

CHAPTER 6

6.1 SUMMARY OF WORK

The work detailed in this thesis has contributed to the LOC community by augmenting the development of an inexpensive, portable and integrated genetic analysis system through contributing to the design of, extensive testing, debugging and verifying the newly modularised and photodiode-based system.

In Chapter 2, the 'shoebox-sized' microfluidic platform is presented with a component cost of less than \$600 and functionality comparable to considerably more expensive, one-function commercial systems. Modularity is emphasised as it allows development to continue without an entire system redesign, the instrument to be customisable and enables the development of progressively smaller, less expensive, more sensitive systems. The divided responsibility between the firmware and software allows for time-critical functions to execute as necessary while retaining automatic data-logging, processing, and report generation functionalities required of a diagnostic system. The command-line interface protocol developed by the author is crucial to this separation of tasks and to future improvements to both firmware and software. Furthermore the modularity of the software components further allows easy integration of new system functionalities and simple appearance and usage changes without altering the software's interaction with the firmware.

Chapter 3 described how an inexpensive laser diode, GRIN lens, interference filter and photodiode were used to build a portable, cost-effective optical detection system capable of detecting clinically relevant viral PCR product samples. Through extensive testing of the microfluidic platform configured as a CE instrument, the author developed the signal processing method and identified four key challenges in the optical detection set-up that could lead to dramatically worse limits of detection. CE protocol and

performance were then discussed it was determined that the sensitivity of the CE instrument had improved so it was comparable to gel electrophoresis run routinely in clinical laboratories and only 2-3x less sensitive than the available commercial CE instrument which is 100x the cost!

Building on this, Chapter 4 adds the amplification step the molecular diagnostic process through the implementation of polymerase chain reaction and its integration with the CE instrument. Improvements to our lab's previous implementation were discussed and through extensive verification of the instrument for both PCR and PCR-CE, the author determined the system performance. This customisable platform was found to have several and possibly single molecule amplification sensitivity and detected all on-chip PCR products, verifying its reproducibility through the application of a clinically relevant sample. It was also found to be comparable to that of commercial instruments confined to the laboratory in terms of variability; however, the lower relative yield of the amplification process as compared to the commercial instrument was not desirable. Thus, once the system was verified, the thermal control of the system was discussed.

Chapter 5 of this thesis briefly discussed the integration of the sample preparation unit based on conventional nucleic acid extraction methods using paramagnetic beads and developed by other members of the lab. This allowed full molecular diagnostic protocols from sample-in to answer-out to be performed on our inexpensive, portable instrument. The author was included at the end of the sample preparation project to aid with its integration into the system and help evaluate the system's application to the extraction of nucleic acids from buccal cells and the subsequent amplification and detection of the β 2-microglobulin gene.

6.2 FUTURE WORK

Several interesting supplementary projects to this work could not be explored due to time constraints, and some of these are described here.

Real-Time Plotting and Software Portability

Real-time plotting wasn't a necessary functionality of the GUI so it was omitted due to time constraints when difficulty was experienced with integrating the real-time drawing of the graph using matplotlib and the TkAgg backend. However, system operators often prefer the ability to see the program/system working and scrolling data is not understood as easily as an image. Thus, it would be useful for the real-time plotting functionality to be re-explored in the future. If more time were available for this project, more information on the backend and employing threads in the code for simultaneous updating of the plot and writing/showing data could be collected and the issues the author was experiencing likely be resolved.

Re-Plotting and Alternative Processing of Images

Re-plotting of saved data in software generated text files to allow the application of alternative signal processing methods and/or the ability to zoom in on plotted data (not possible on an image file).

Improvements in CE Sensitivity

Two possible improvements to the optical detection scheme could increase the sensitivity of capillary electrophoresis. One is to angle the laser to strike the chip at 45° in the x-y plane, rather than at 90° . In another demonstration⁵⁶, it was found that light scatter from the excitation source on the CE channel was almost completely removed by angling the detector; with our similar (but reversed) set-up, angling the laser may achieve the same effect. Second, an alternative lens that would collimate the collected light rather than focusing it could improve the efficiency of our interference filter, which decreases severely when the light is not collimated. This could effectively reduce the high baselines observed in this thesis and suppressed instabilities in the laser, improving the sensitivity. Another option would be to have a filter designed with the half-cone angle of the focused light⁷⁷, although this would likely be quite costly.

Faster Thermal Control

Now that our group is becoming even more confident with our ability to set temperature, the next step to improving on-chip PCR would be increase the processing time. The thermal controller could be modified to re-include a derivative term and overshoot set point temperatures, further eliminating the need for add times in the software.

New Microfluidic Chip Design

Finally, but possibly most important, an alternative microfluidic chip design needs to be explored. This could benefit CE by removing the need to adjust the laser before each chip load by, for example, moving the fluidic layer to the bottom plate. However, even more important is the necessary automation of the PCR-CE and SP-PCR-CE processes. Operators need to be extensively trained to operate this equipment and enabling their automation should remove much of the operator error and contamination possibilities seen even in conventional healthcare. It could also significantly improve the variability of the SP process as witnessed in Chapter 5.

Bibliography

1. Manz, A., Graber, N. & Widmer, H. Miniaturized total chemical analysis systems: A novel concept for chemical sensing. *Sensors and Actuators B: Chemical* **1**, 244-248 (1990).
2. Terry, S., Jerman, J. & Angell, J. A gas chromatographic air analyzer fabricated on a silicon wafer. *Electron Devices, IEEE Transactions on* **26**, 1880-1886 (1979).
3. Vilkner, T., Janasek, D. & Manz, A. Micro Total Analysis Systems. Recent Developments. *Analytical Chemistry* **76**, 3373-3386 (2004).
4. Lee, S. & Lee, S. Micro total analysis system (μ -TAS) in biotechnology. *Applied Microbiology and Biotechnology* **64**, 289-299 (2004).
5. Harrison, D.J. et al. Micromachining a Miniaturized Capillary Electrophoresis-Based Chemical Analysis System on a Chip. *Science* **261**, 895-897 (1993).
6. Kopp, M.U., Crabtree, H.J. & Manz, A. Developments in technology and applications of microsystems. *Current Opinion in Chemical Biology* **1**, 410-419 (1997).
7. Reyes, D.R., Iossifidis, D., Auroux, P. & Manz, A. Micro Total Analysis Systems. 1. Introduction, Theory, and Technology. *Analytical Chemistry* **74**, 2623-2636 (2002).
8. Auroux, P., Iossifidis, D., Reyes, D.R. & Manz, A. Micro Total Analysis Systems. 2. Analytical Standard Operations and Applications. *Analytical Chemistry* **74**, 2637-2652 (2002).
9. Dittrich, P.S., Tachikawa, K. & Manz, A. Micro Total Analysis Systems. Latest Advancements and Trends. *Analytical Chemistry* **78**, 3887-3908 (2006).
10. Dittrich, P.S. & Manz, A. Lab-on-a-chip: microfluidics in drug discovery. *Nature Reviews Drug Discovery* **5**, 210-218 (2006).
11. Applied Biosystems 3500 Genetic Analyzer at <https://products.appliedbiosystems.com/ab/en/US/adirect/ab?cmd=catNavigate2&catID=606262&tab=TechSpec>

12. Agilent 7100 Capillary Electrophoresis System. (2009) at <<http://www.chem.agilent.com/Library/datasheets/Public/5990-3962EN.pdf>>
13. Huang, Y., Mather, E., Bell, J. & Madou, M. MEMS-based sample preparation for molecular diagnostics. *Analytical and Bioanalytical Chemistry* **372**, 49-65 (2002).
14. Boom, R. et al. Rapid and simple method for purification of nucleic acids. *J Clin Microbiol* **28**, 495-503 (1990).
15. Grody, W.W., Nakamura, R.M. & Kiechle, F.L. *Molecular Diagnostics: Techniques and Applications for the Clinical Laboratory*. (Academic Press: London, 2009).
16. Sharkey, D.J., Scalice, E.R., Christy, K.G., Atwood, S.M. & Daiss, J.L. Antibodies as Thermolabile Switches: High Temperature Triggering for the Polymerase Chain Reaction. *Nat Biotech* **12**, 506-509 (1994).
17. Altria, K.D. *Capillary Electrophoresis Guidebook*. (Springer: Totowa, 1996).
18. Altria, K.D. *Capillary electrophoresis guidebook: principles, operation, and applications*. (Humana Press: Totowa, 1996).
19. Myers, F.B. & Lee, L.P. Innovations in optical microfluidic technologies for point-of-care diagnostics. *Lab Chip* **8**, 2015-2031 (2008).
20. Dittrich, P.S. & Manz, A. Single-molecule fluorescence detection in microfluidic channels—the Holy Grail in μ TAS? *Analytical & Bioanalytical Chemistry* **382**, 1771-1782 (2005).
21. Kuswandi, B., Nuriman, Huskens, J. & Verboom, W. Optical sensing systems for microfluidic devices: A review. *Analytica Chimica Acta* **601**, 141-155 (2007).
22. Liu, P. & Mathies, R.A. Integrated microfluidic systems for high-performance genetic analysis. *Trends in Biotechnology* **27**, 572-581 (2009).
23. Yan, H., Zhang, B. & Wu, H. Chemical cytometry on microfluidic chips. *Electrophoresis* **29**, 1775-1786 (2008).
24. Lien, K. & Lee, G. Miniaturization of molecular biological techniques for gene assay. *Analyst* **135**, 1499 (2010).

25. Ferrance, J.P. et al. Developments toward a complete micro-total analysis system for Duchenne muscular dystrophy diagnosis. *Analytica Chimica Acta* **500**, 223-236 (2003).
26. McDonald, J.C. et al. Fabrication of microfluidic systems in poly(dimethylsiloxane). *Electrophoresis* **21**, 27-40 (2000).
27. Easley, C.J. et al. A fully integrated microfluidic genetic analysis system with sample-in-answer-out capability. *Proceedings of the National Academy of Sciences* **103**, 19272-19277 (2006).
28. Oh, K.W. & Ahn, C.H. A review of microvalves. *J. Micromech. Microeng.* **16**, R13-R39 (2006).
29. Zhang, C., Xing, D. & Li, Y. Micropumps, microvalves, and micromixers within PCR microfluidic chips: Advances and trends. *Biotechnology Advances* **25**, 483-514 (2007).
30. Long, Z., Shen, Z., Wu, D., Qin, J. & Lin, B. Integrated multilayer microfluidic device with a nanoporous membrane interconnect for online coupling of solid-phase extraction to microchip electrophoresis. *Lab Chip* **7**, 1819 (2007).
31. Lagally, E.T., Emrich, C.A. & Mathies, R.A. Fully integrated PCR-capillary electrophoresis microsystem for DNA analysis. *Lab Chip* **1**, 102-107 (2001).
32. Lagally, E.T. et al. Integrated Portable Genetic Analysis Microsystem for Pathogen/Infectious Disease Detection. *Analytical Chemistry* **76**, 3162-3170 (2004).
33. Liu, P. et al. Integrated Portable Polymerase Chain Reaction-Capillary Electrophoresis Microsystem for Rapid Forensic Short Tandem Repeat Typing. *Analytical Chemistry* **79**, 1881-1889 (2007).
34. Pal, R. et al. An integrated microfluidic device for influenza and other genetic analyses. *Lab Chip* **5**, 1024-1032 (2005).
35. Meagher, R.J., Hatch, A.V., Renzi, R.F. & Singh, A.K. An integrated microfluidic platform for sensitive and rapid detection of biological toxins. *Lab Chip* **8**, 2046-2053 (2008).

36. Fruetel, J.A. et al. Microchip separations of protein biotoxins using an integrated hand-held device. *Electrophoresis* **26**, 1144-1154 (2005).
37. Agilent | 2100 Bioanalyzer. at <<http://www.chem.agilent.com/en-US/products/instruments/lab-on-a-chip/2100bioanalyzer/pages/default.aspx>>
38. Shimadzu Biotech - Products. at <<http://www.shimadzu-biotech.net/pages/products/0/index.php>>
39. Umemoto, Y. et al. Sequential analysis of RNA synthesis by microchip electrophoresis. *Analytical Biochemistry* **388**, 161-163 (2009).
40. Idaho Technology Inc. - RAZOR EX, BioThreat Detection System at <<http://www.idahotech.com/RAZOREX/>>
41. STMicroelectronics - ST In-Check Platform Technology at <<http://www.st.com/stonline/products/technologies/labonchip/technolo.htm>>
42. Gorard, S. Revisiting a 90-year-old debate: the advantages of the mean deviation. *British Journal of Educational Studies* **53**, 417-430 (2005).
43. Kaigala, G.V. et al. An inexpensive and portable microchip-based platform for integrated RT-PCR and capillary electrophoresis. *Analyst* **133**, 331-338 (2008).
44. Kaigala, G.V. et al. A scalable and modular lab-on-a-chip genetic analysis instrument. *Analyst* **135**, 1606-1617 (2010).
45. Bliss, C.L., McMullin, J.N. & Backhouse, C.J. Rapid fabrication of a microfluidic device with integrated optical waveguides for DNA fragment analysis. *Lab Chip* **7**, 1280 (2007).
46. Bliss, C.L., McMullin, J.N. & Backhouse, C.J. Integrated wavelength-selective optical waveguides for microfluidic-based laser-induced fluorescence detection. *Lab Chip* **8**, 143 (2008).
47. Harrison, D.J., Manz, A., Fan, Z., Luedi, H. & Widmer, H.M. Capillary electrophoresis and sample injection systems integrated on a planar glass chip. *Analytical Chemistry* **64**, 1926-1932 (1992).
48. Righetti, P.G., Gelfi, C., Verzola, B. & Castelletti, L. The state of the art of dynamic coatings. *Electrophoresis* **22**, 603-611 (2001).

49. Horvath, J. & Dolník, V. Polymer wall coatings for capillary electrophoresis. *Electrophoresis* **22**, 644-655 (2001).
50. Osbourn, D.M., Weiss, D.J. & Lunte, C.E. On-line preconcentration methods for capillary electrophoresis. *Electrophoresis* **21**, 2768-2779 (2000).
51. Lin, C. & Kaneta, T. On-line sample concentration techniques in capillary electrophoresis: Velocity gradient techniques and sample concentration techniques for biomolecules. *Electrophoresis* **25**, 4058-4073 (2004).
52. Mogensen, K.B., Klank, H. & Kutter, J.P. Recent developments in detection for microfluidic systems. *Electrophoresis* **25**, 3498-3512 (2004).
53. Baker, C.A., Duong, C.T., Grimley, A. & Roper, M.G. Recent advances in microfluidic detection systems. *Bioanalysis* **1**, 967-975 (2009).
54. Kamei, T. et al. Microfluidic Genetic Analysis with an Integrated a-Si:H Detector. *Biomed Microdevices* **7**, 147-152 (2005).
55. Wang, S., Fan, X., Xu, Z. & Fang, Z. A simple microfluidic system for efficient capillary electrophoretic separation and sensitive fluorimetric detection of DNA fragments using light-emitting diode and liquid-core waveguide techniques. *Electrophoresis* **26**, 3602-3608 (2005).
56. Fu, J., Fang, Q., Zhang, T., Jin, X. & Fang, Z. Laser-Induced Fluorescence Detection System for Microfluidic Chips Based on an Orthogonal Optical Arrangement. *Analytical Chemistry* **78**, 3827-3834 (2006).
57. Kaigala, G. et al. Inexpensive, universal serial bus-powered and fully portable lab-on-a-chip-based capillary electrophoresis instrument. *IET Nanobiotechnol.* **3**, 1-7 (2009).
58. Melles Griot Gradient-Index Lenses at https://www.cvilaser.com/products/Documents/Catalog/Gradient-Index_lenses.pdf
59. Damask, J.N. *Polarization optics in telecommunications*. (Springer: New York, 2005).
60. Bargen, C. USB-SP_PCR_CE Chip Sizing and Alignment Tolerances. (2009).

61. Pressman, A.I., Billings, K.H. & Morey, T. *Switching power supply design*. (McGraw Hill Professional: New York, 2009).
62. Brillant, A. *Digital and analog fiber optic communications for CATV and FTTx applications*. (SPIE Press: Hoboken, 2008).
63. Choi, S. Signal Processing Methods for Inexpensive Genetic Analysis Instruments. MSc Thesis to be Submitted, Department of Electrical & Computer Engineering, University of Alberta. (2011).
64. Fukuda, M. *Optical semiconductor devices*. (Wiley-IEEE: Hoboken, 1999).
65. Petermann, K. *Laser diode modulation and noise*. (Springer: Dordrecht, 1991).
66. Johnson, M.E. & Landers, J.P. Fundamentals and practice for ultrasensitive laser-induced fluorescence detection in microanalytical systems. *Electrophoresis* **25**, 3513-3527 (2004).
67. Kaigala, G.V. et al. Automated screening using microfluidic chip-based PCR and product detection to assess risk of BK virus-associated nephropathy in renal transplant recipients. *Electrophoresis* **27**, 3753-3763 (2006).
68. Fanali, S. *Handbook of capillary electrophoresis*. (CRC Press Inc.: Boca Raton, 1996).
69. Burgi, D.S. & Chien, R.L. Optimization in sample stacking for high-performance capillary electrophoresis. *Analytical Chemistry* **63**, 2042-2047 (1991).
70. Chankvetadze, B. *Capillary electrophoresis in chiral analysis*. (John Wiley and Sons: Hoboken, 1997).
71. Sieben, V.J. & Backhouse, C.J. Rapid on-chip postcolumn labeling and high-resolution separations of DNA. *Electrophoresis* **26**, 4729-4742 (2005).
72. Blazej, R.G., Kumaresan, P. & Mathies, R.A. Microfabricated bioprocessor for integrated nanoliter-scale Sanger DNA sequencing. *Proc Natl Acad Sci U S A* **103**, 7240-7245 (2006).
73. Footz, T., Somerville, M.J., Tomaszewski, R., Elyas, B. & Backhouse, C.J. Integration of combined heteroduplex/restriction fragment length polymorphism analysis on an electrophoresis microchip for the detection of hereditary haemochromatosis. *Analyst* **129**, 25 (2004).

74. Brask, A., Kutter, J.P. & Bruus, H. Long-term stable electroosmotic pump with ion exchange membranes. *Lab Chip* **5**, 730 (2005).
75. MacDougall, D. & Crummett, W.B. Guidelines for data acquisition and data quality evaluation in environmental chemistry. *Anal Chem* **52**, 2242-2249 (1980).
76. Pelt-Verkuil, E.V., Belkum, A.V. & Hays, J.P. *Principles and technical aspects of PCR amplification*. (Springer: Dordrecht, 2008).
77. Reichman, J. *Handbook of Optical Filters for Fluorescence Microscopy*. (Chroma Technology Corp: Brattleboro, 2007).
78. 60-Well and 0.5 ml Tube GeneAmp® PCR System 9700 at <<https://products.appliedbiosystems.com/ab/en/US/adirect/ab?cmd=catNavigate2&catID=600964&tab=Overview>>
79. Eppendorf Canada - Products - Mastercycler® ep realplex, real-time thermal cycler - Overview at <<http://www.eppendorf.ca/int/index.php?l=211&sitemap=2.5.1.3&action=products&contentid=1&catalognode=22330>>
80. Noh, J. et al. In situ thermal diagnostics of the micro-PCR system using liquid crystals. *Sensors and Actuators A: Physical* **122**, 196-202 (2005).
81. Hoang, V.N., Kaigala, G.V., Atrazhev, A., Pilarski, L.M. & Backhouse, C.J. Strategies for enhancing the speed and integration of microchip genetic amplification. *Electrophoresis* **29**, 4684-4694 (2008).
82. Legendre, L.A., Bienvenue, J.M., Roper, M.G., Ferrance, J.P. & Landers, J.P. A Simple, Valveless Microfluidic Sample Preparation Device for Extraction and Amplification of DNA from Nanoliter-Volume Samples. *Analytical Chemistry* **78**, 1444-1451 (2006).
83. Giordano, B.C., Ferrance, J., Swedberg, S., Hühmer, A.F.R. & Landers, J.P. Polymerase Chain Reaction in Polymeric Microchips: DNA Amplification in Less Than 240 Seconds. *Analytical Biochemistry* **291**, 124-132 (2001).

84. Easley, C.J. et al. Extrinsic Fabry–Perot Interferometry for Noncontact Temperature Control of Nanoliter-Volume Enzymatic Reactions in Glass Microchips. *Analytical Chemistry* **77**, 1038-1045 (2005).
85. Jia, G. et al. A low-cost, disposable card for rapid polymerase chain reaction. *Colloids and Surfaces B: Biointerfaces* **58**, 52-60 (2007).
86. Khandurina, J. et al. Integrated System for Rapid PCR-Based DNA Analysis in Microfluidic Devices. *Analytical Chemistry* **72**, 2995-3000 (2000).
87. Liu, P. et al. Real-time forensic DNA analysis at a crime scene using a portable microchip analyzer. *Forensic Science International: Genetics* **2**, 301-309 (2008).
88. Hoang, V.N., Kaigala, G.V. & Backhouse, C.J. Dynamic temperature measurement in microfluidic devices using thermochromic liquid crystals. *Lab Chip* **8**, 484-487 (2008).
89. Jang, A. & Johnstone, R.W. Ti/Pt Resistive Element Annealing and Calibration, V2.1 Protocol 11P. (2010).
90. Kaigala, G.V., Jingbo Jiang, Backhouse, C.J. & Marquez, H.J. System Design and Modeling of a Time-Varying, Nonlinear Temperature Controller for Microfluidics. *IEEE Transactions on Control Systems Technology* **18**, 521-530 (2010).
91. Grover, W.H., Skelley, A.M., Liu, C.N., Lagally, E.T. & Mathies, R.A. Monolithic membrane valves and diaphragm pumps for practical large-scale integration into glass microfluidic devices. *Sensors and Actuators B: Chemical* **89**, 315-323 (2003).
92. Toriello, N.M., Liu, C.N. & Mathies, R.A. Multichannel Reverse Transcription-Polymerase Chain Reaction Microdevice for Rapid Gene Expression and Biomarker Analysis. *Analytical Chemistry* **78**, 7997-8003 (2006).
93. Jang, A. Bonding PDMS and Glass using RIE System, V2.1 Protocol 10P-a. (2010).
94. Karlin, S. & Altschul, S.F. Applications and statistics for multiple high-scoring segments in molecular sequences. *Proc Natl Acad Sci U S A* **90**, 5873-5877 (1993).

95. Butler, J.M., Ruitberg, C.M. & Vallone, P.M. Capillary electrophoresis as a tool for optimization of multiplex PCR reactions. *Fresenius' Journal of Analytical Chemistry* **369**, 200-205 (2001).
96. Ruijter, J.M. et al. Amplification efficiency: linking baseline and bias in the analysis of quantitative PCR data. *Nucleic Acids Res* **37**, e45-e45 (2009).
97. Kim, J.A. et al. Fabrication and characterization of a PDMS-glass hybrid continuous-flow PCR chip. *Biochemical Engineering Journal* **29**, 91-97 (2006).
98. Prakash, A., Amrein, M. & Kaler, K. Characteristics and impact of Taq enzyme adsorption on surfaces in microfluidic devices. *Microfluidics and Nanofluidics* **4**, 295-305 (2008).
99. Kolari, K., Satokari, R., Kataja, K., Stenman, J. & Hokkanen, A. Real-time analysis of PCR inhibition on microfluidic materials. *Sensors and Actuators B: Chemical* **128**, 442-449 (2008).
100. Poshtiban, S. TLC Chip Preparation Protocol. (2010).
101. Poshtiban, S. Thermal Calibration of Winnie using Thermal Liquid Crystal. (2009).
102. Warkusz, F. The size effect and the temperature coefficient of resistance in thin films. *J. Phys. D: Appl. Phys.* **11**, 689-694 (1978).
103. Hay, J.L. & Hollingsworth, D.K. Calibration of micro-encapsulated liquid crystals using hue angle and a dimensionless temperature. *Experimental Thermal and Fluid Science* **18**, 251-257 (1998).
104. Abdullah, N., Abu Talib, A.R., Mohd Saiah, H.R., Jaafar, A.A. & Mohd Salleh, M.A. Film thickness effects on calibrations of a narrowband thermochromic liquid crystal. *Experimental Thermal and Fluid Science* **33**, 561-578 (2009).
105. Neitz, J. & Jacobs, G.H. Polymorphism of the long-wavelength cone in normal human colour vision. *Nature* **323**, 623-625 (1986).
106. Groendahl, S. Tricorder Toolkit Thermal Calibration Using Thermochromic Liquid Crystals. (2010).
107. Martinez-Quijada, J. Effect of Filling the PCR chamber in PCR-4 with Water, Oil, TLC and Air on TLC temperature measurements – Steady State Analysis. (2010).

108. Groendahl, S. TTK Thermal Calibration Certificate Belle (T4-0.4).
109. Groendahl, S. TTK Thermal Calibration Certificate Winnie (T4-0.4).
110. Johnstone, R.W. Temperature Control in TTKs. (2009).
111. Lagally, E.T. & Mathies, R.A. Integrated genetic analysis microsystems. *J. Phys. D: Appl. Phys.* **37**, R245-R261 (2004).
112. Tan, S.C. & Yiap, B.C. DNA, RNA, and Protein Extraction: The Past and The Present. *Journal of Biomedicine and Biotechnology* **2009**, 10 (2009).
113. Chen, L., Manz, A. & Day, P.J.R. Total nucleic acid analysis integrated on microfluidic devices. *Lab Chip* **7**, 1413-1423 (2007).
114. Dineva, M.A., Mahilum-Tapay, L. & Lee, H. Sample preparation: a challenge in the development of point-of-care nucleic acid-based assays for resource-limited settings. *Analyst* **132**, 1193-1199 (2007).
115. Mariella, R. Sample preparation: the weak link in microfluidics-based biodetection. *Biomedical Microdevices* **10**, 777-784 (2008).
116. Olanrewaju, Ayokunle. Towards a portable and inexpensive lab on a chip system for point of care applications. MSc Thesis to be Submitted, Department of Electrical & Computer Engineering, University of Alberta. (2011).
117. Kim, J., Johnson, M., Hill, P. & Gale, B.K. Microfluidic sample preparation: cell lysis and nucleic acid purification. *Integr. Biol.* **1**, 574-586 (2009).
118. Bao, N. & Lu, C. Microfluidics-Based Lysis of Bacteria and Spores for Detection and Analysis. *Principles of Bacterial Detection: Biosensors, Recognition Receptors and Microsystems* 817-831 (2008).
119. Baier, T. et al. Hands-free sample preparation platform for nucleic acid analysis. *Lab Chip* **9**, 3399-3405 (2009).
120. Mahalanabis, M., Al-Muayad, H., Kulinski, M.D., Altman, D. & Klapperich, C.M. Cell lysis and DNA extraction of gram-positive and gram-negative bacteria from whole blood in a disposable microfluidic chip. *Lab Chip* **9**, 2811-2817 (2009).
121. Duarte, G.R.M. et al. Characterization of dynamic solid phase DNA extraction from blood with magnetically controlled silica beads. *Analyst* **135**, 531 (2010).

Bibliography

122. Lien, K., Liu, C., Kuo, P. & Lee, G. Microfluidic System for Detection of α -Thalassemia-1 Deletion Using Saliva Samples. *Analytical Chemistry* **81**, 4502-4509 (2009).
123. Hua, Z. et al. Multiplexed Real-Time Polymerase Chain Reaction on a Digital Microfluidic Platform. *Analytical Chemistry* **82**, 2310-2316 (2010).
124. Bienvenue, J.M., Legendre, L.A., Ferrance, J.P. & Landers, J.P. An integrated microfluidic device for DNA purification and PCR amplification of STR fragments. *Forensic Science International: Genetics* **4**, 178-186 (2010).
125. Toriello, N.M. et al. Integrated microfluidic bioprocessor for single-cell gene expression analysis. *Proceedings of the National Academy of Sciences* **105**, 20173-20178 (2008).
126. Lui, C., Cady, N.C. & Batt, C.A. Nucleic Acid-based Detection of Bacterial Pathogens Using Integrated Microfluidic Platform Systems. *Sensors* **9**, 3713-3744 (2009).
127. Pang, X.L., Doucette, K., LeBlanc, B., Cockfield, S.M. & Preiksaitis, J.K. Monitoring of Polyomavirus BK Virus Viruria and Viremia in Renal Allograft Recipients by Use of a Quantitative Real-Time PCR Assay: One-Year Prospective Study. *J. Clin. Microbiol.* **45**, 3568-3573 (2007).
128. Pang, X.L., Martin, K. & Preiksaitis, J.K. The use of unprocessed urine samples for detecting and monitoring BK viruses in renal transplant recipients by a quantitative real-time PCR assay. *Journal of Virological Methods* **149**, 118-122 (2008).

References aside from textbooks can be found in Supplementary CD/Thesis Library.

Appendices

A. TABULATED EXPERIMENTS

Chip Information		PCR Information		CE Information			Data Sets			
Load	SigmaCote?	Protocol	Chip	System	Buffer	Errors, if any	Heater	PCR-CE	SP-PCR-CE	
1-31	<i>Experiments performed before R. Johnstone's calibration method as described in this thesis</i>							(46)	(24)	(6)
32	Yes	Recipe A1	4PM/PCRCE4	uTK/TTK	0.01xTTE		*	*		
33	Yes	Recipe A1	4PM/PCRCE4	uTK/TTK	0.01xTTE		*	*		
34	Yes	Recipe A1	4PM/PCRCE4	uTK/TTK	0.01xTTE	Multiple loadings	*			
35	Yes	Recipe A1	4PM/PCRCE4	uTK/TTK	0.01xTTE	Multiple loadings	*			
36	Yes	Recipe A1	4PM/PCRCE4	uTK/TTK	0.01xTTE		*	*		
37	Yes	Recipe A1	4PM/PCRCE4	uTK/TTK	0.01xTTE	Multiple loadings	*			
38	Yes	Recipe A1	4PM/PCRCE4	uTK/TTK	0.01xTTE			*		
39	Yes	Recipe A1	4PM/PCRCE4	uTK/TTK	0.01xTTE		*	*		
40	Yes	Recipe A1	4PM/PCRCE4	uTK/TTK	0.01xTTE		*	*		
41	Yes	Recipe A1	4PM/PCRCE4	uTK/TTK	0.01xTTE	<4 μ L recovered	*			
42	Yes	Recipe A2	4PM/PCRCE4	uTK/TTK	0.01xTTE		*	*		
43	Yes	Recipe A2	4PM/PCRCE4	uTK/TTK	0.01xTTE		*	*		
44	Yes	Recipe A2	4PM/PCRCE4	uTK/TTK	0.01xTTE	<4 μ L recovered	*			
45	Yes	Recipe A2	4PM/PCRCE4	uTK/TTK	0.01xTTE		*	*		
46	Yes	Recipe A2	4PM/PCRCE4	uTK/TTK	0.01xTTE	Multiple loadings	*			
47	Yes	Recipe A2	4PM/PCRCE4	uTK/TTK	0.01xTTE		*	*		

CLI Protocol

48	Yes	Recipe A2	4PM/PCRCE4	uTK/TTK	0.01xTTE	Bad DC coat	*	
49	Yes	Recipe A2	4PM/PCRCE4	uTK/TTK	0.01xTTE	Bad DC coat	*	
50	No	Recipe A2	4PM	uTK	0.01xTTE	Bad DC coat		
51	No	Recipe A2	4PM	uTK	0.01xTTE	Bad DC coat		
52	No	Recipe A2	4PM	uTK	0.01xTTE	Bad DC coat		
53	No	Recipe A2	4PM	uTK	0.01xTTE	Bad DC coat		
54	Yes	Recipe A3	4PM	uTK	0.01xTTE	Bad DC coat		
55	Yes	Recipe A3	4PM	uTK	0.01xTTE	Bad DC coat		
56	Yes	Negative	PCRCE4	uTK/TTK	0.01xTTE		*	
57	Yes	Negative	PCRCE4	uTK/TTK	0.01xTTE			
58	Yes	Negative	PCRCE4	uTK/TTK	0.01xTTE			
59	Yes	Negative	PCRCE4	uTK/TTK	0.01xTTE			
60	Yes	Recipe A1	PCRCE4	TTK	0.01xTTE	Products/Chips aged >2-3 weeks		
61	Yes	Recipe A1	PCRCE4	TTK	0.01xTTE	Products/Chips aged >2-3 weeks		
62	Yes	Recipe A1	PCRCE4	TTK	0.01xTTE	Products/Chips aged >2-3 weeks		
63	Yes	Recipe A1	PCRCE4	TTK	0.01xTTE	Products/Chips aged >2-3 weeks	*	
64	Yes	Recipe A1	PCRCE4	TTK	0.01xTTE	Positive Control failed	*	
65	Yes	Recipe A1	PCRCE4	TTK	0.01xTTE	Positive Control failed	*	
66	Yes	Recipe A1	PCRCE4	TTK	0.001xTTE	Multiple loadings	*	
67	Yes	Recipe A1	PCRCE4	TTK	0.001xTTE		*	*
68	Yes	Recipe A3	PCRCE4	TTK	0.01xTTE		*	*
69	Yes	Recipe A3	PCRCE4	TTK	0.01xTTE		*	*
70	Yes	Recipe A2b	PCRCE4	TTK	0.01xTTE		*	*
71	Yes	Recipe A2b	PCRCE4	TTK	0.01xTTE		*	*
72	Yes	Recipe A1	PCRCE4	TTK	0.01xTTE		*	*

CLI Protocol

73	Yes	Recipe A1	PCRCE4	TTK	0.01xTTE		*	*
74	Yes	Recipe A1	PCRCE4	TTK	0.01xTTE		*	*
75	Yes	Recipe A1	PCRCE4	TTK	0.01xTTE		*	*
76	Yes	Recipe A1	PCRCE4	TTK	0.001xTTE			*
77	Yes	Recipe A1	PCRCE4	TTK	0.01xTTE		*	*
78	No	Recipe A1	PCRCE4	uTK	0.01xTTE		*	
79	No	Recipe A1	PCRCE4	uTK	0.01xTTE			
80	No	Recipe A1	PCRCE4	uTK	0.01xTTE			
81	No	Recipe A1	PCRCE4	uTK	0.01xTTE		*	
82	Yes	B2M	PCRCE4	uTK	0.01xTTE		*	
83	Yes	B2M neg	PCRCE4	uTK	0.01xTTE			
84	Yes	B2M neg	PCRCE4	uTK	0.01xTTE			
85	Yes	Recipe A1	PCRCE4	uTK/TTK	0.01xTTE		*	*
86	Yes	Recipe A1	PCRCE4	uTK/TTK	0.01xTTE			*
87	Yes	Recipe A1	PCRCE4	uTK/TTK	0.01xTTE	CE error	*	
88	Yes	Recipe A1	PCRCE4	uTK/TTK	0.01xTTE		*	*
89	Yes	Recipe A1	PCRCE4	uTK	0.01xTTE	Testing [DNA] as suspect		Magic Chip Solved
90	Yes	Recipe A1	PCRCE4	uTK	0.01xTTE	Testing [DNA] as suspect	*	
91	Yes	Recipe A1	PCRCE4	uTK	0.01xTTE	Testing [DNA] as suspect	*	
92	Yes	Recipe A1	PCRCE4	uTK	0.01xTTE	Testing [DNA] as suspect	*	
93-105					<i>Training experiments</i>			
106	Yes	B2M neg	PCRCE4	uTK	0.01xTTE		*	
107	Yes	B2M neg	PCRCE4	uTK/TTK	0.01xTTE		*	
108	Yes	B2M neg	PCRCE4	uTK/TTK	0.01xTTE		*	
109	Yes	SP-PCR-CE	PCRCE4	TTK	0.01xTTE	Negative Control failed		
110	Yes	SP-PCR-CE	PCRCE4	TTK	0.01xTTE	Negative Control failed		

CLI Protocol

111	Yes	SP-PCR-CE	PCRCE4	TTK	0.01xTTE	Negative Control failed		
112	Yes	SP-PCR-CE	PCRCE4	TTK	0.01xTTE		*	*
113	Yes	SP-PCR-CE	PCRCE4	TTK	0.01xTTE			*
114	Yes	SP-PCR-CE	PCRCE4	TTK	0.01xTTE		*	*
115	Yes	SP-PCR-CE	PCRCE4	TTK	0.01xTTE			*
116	Yes	SP-PCR-CE	PCRCE4	TTK	0.01xTTE			*
117	Yes	SP-PCR-CE	PCRCE4	TTK	0.01xTTE			*
118	Yes	Recipe A1	PCRCE4	TTK	0.01xTTE	Testing new firmware		
119	Yes	Recipe A1	PCRCE4	TTK	0.01xTTE	Testing new firmware		
120	Yes	Recipe A1	PCRCE4	TTK	0.01xTTE	Testing new firmware		
121-125						<i>Training experiments</i>		

B. COMMAND-LINE INTERFACE PROTOCOL

B.1 Firmware Operation

Compiler

MPLAB c18 compiler version 320; firmware version 0.5.0 compiles to 30078 bytes (91%).

Power Up Initialization

- SPI: close SPI
open SPI w/ parameters: data rate = 750 kHz
mode 11
- Turn off laser
- Set chip selects (shift registers) to zero HV, turn off all optics, open all valves and relays
- Set Detection Mode = Photodiode
- Set Operating Mode = Command Line Mode

Operation Flow

Single commands, or line-by-line commands, are sent and executed by the firmware as they are received.

If the user would rather load a script to an external EEPROM (Microchip 25AA512), this is also possible, using the EEPROM commands. Once loaded, the script can be run. Once a run has begun, each command in the script is then executed in sequential order.

Operation Control Characters

- ! end of script character
signals firmware to cease writing commands (entered characters) onto external EEPROM
- Esc abort the current process
zero all flags, open all relays and valves, zero high voltage, turn off laser

any other settings (i.e. detection mode) are retained

Please note, the Esc character corresponds to 0x1B

Limitations

USB low speed data transfer rate 1.5 Mb/s (as per PIC18F4550 spec sheet)

Board Addresses

Slot 1: High Voltage Board	-->	0: Relays
		1: ADC
		2: DAC
Slot 2: Optic Board	-->	3: Laser Buffer
		4: ADC
		5:
Slot 3: SMU Board	-->	6: DAC
		7: ADC
		8:
Slot 4: Valve Board	-->	9: Valve Board 1
		10: Valve Board 2
		11:
Slot 5: XY Motorized Stage Board	-->	12:
		13:
		14: Stage Board
Slot 6: Temperature Board	-->	15: Future Temperature Board
<i>(Slots 7-10, addresses 16-29) Not defined</i>		
Slot 11:	-->	30: on board external EEPROM
		31:

B.2 Process Commands Summary

System Information Commands

Display System Information	ID;
Wait	WT(time);
System Reset	RT;
Set System Information	SI(type,value);
Read System Information	RI(<i>type</i>);
Set Username	SU(name);
Set PID controller parameters*	RP();
Set PID controller parameters*	PI();

External EEPROM Commands

Load File to EEPROM	LD;
Print EEPROM Content	DS;
Run File from EEPROM	RN;

Set Chip Parameters

Chip Parameters	CC(type, resistance, slope);
Room Temperature*	RM(R_{RT} , slope);

System Testing Commands

Select High Voltage Relays	RS(relay_number, on/off);
Set Laser	SL(on/off);
Set DAC	SD(num, value);
Read ADC	RA(num, time);
Zero Wheatstone Bridge	ZB;
Send Byte Over SPI	SB(board_address, value);
Setting and Reading Heater	RH(DAC_value, time);

CE/PCR/MCA Commands

Set Optical Detection Mode	DM(<i>type</i>);
Capillary Electrophoresis	CE(<i>time_{inj}</i> , <i>volt_{inj}</i> , <i>time_{sep}</i> , <i>volt_{sep}</i>);
Set PCR Parameters	PP(<i>step</i> , <i>time</i> , <i>temperature</i>);
Do PCR	DP(<i>cycles</i> , <i>T_{Room}</i>);
Melting Curve Analysis	TM(<i>start_temp</i> , <i>end_temp</i> , <i>ramp_rate</i>);
Open-loop Test *	OL(<i>time1</i> , <i>DAC1</i> , <i>time2</i> , <i>DAC2</i>);
Read Temperature	TE(<i>time</i>);
Set LED (MCA)	TL(<i>on/off</i>);

Pumping and Valve Commands

Set Valves	VL(<i>board_address</i> , <i>value</i>);
Perform Pumping	PM(<i>cycles</i>);
Setup Pumping	SP(<i>board_address</i> , <i>v1</i> , <i>v2</i> , <i>v3</i> , <i>period</i>);

Sample Preparation Commands

Perform SP with Micro-Servo	PW(<i>start</i> , <i>end</i> , <i>speed</i> , <i>last_speed</i> , <i>cycles</i> , <i>wait</i>);
Zero Micro-Servo Magnet	AC(<i>value</i>);
Perform SP with XY Stage	PS;
Direct XY Movement	XY(<i>x_pos</i> , <i>y_pos</i>);
Circle XY Movement	CM(<i>x_{center}</i> , <i>y_{center}</i> , <i>radius</i> , <i>cycles</i> , <i>CW/CCW</i>);
Wiggle XY Movement	WM(<i>x_{center}</i> , <i>y_{center}</i> , <i>radius</i> , <i>cycles</i> , <i>CW/CCW</i>);
Set XY Stage Velocity	SV(<i>frequency</i>);

** Indicates commands that are not functional with the V0.5.0 firmware release; these commands may either be artifacts from previous versions or beginnings of new commands.*

Note: There is only one version of the firmware; thus, all these commands are technically contained in all systems. However, a Sample Preparation command will not work on a system that does not contain the hardware needed to perform Sample Preparation. This means if the required hardware is added to a PCR/CE/MCA system, it could do SP/PCR/CE/MCA with no extra programming.

PROCESS COMMAND NOTES

- Commands are written like functions
 - first two upper-case letters and brackets are ASCII characters, and are *case sensitive*
 - all values sent and received are in DECIMAL integers unless otherwise stated
- Every command is terminated with a ';' character
 - '\r' and '\n' characters are not required – if succeeding the ';' character, they are ignored
- ✓ Once the ';' character is found, the firmware then echoes, processes and executes this command
- ✓ When firmware has finished executing the command (i.e. finished setting values, gathering/displaying data), and is ready for another command, it sends '#000 Task Completed!'

B.3 Process Commands in Detail

SYSTEM INFORMATION COMMANDS

Display System Information **ID;**

- Returns a text string: *“Applied Miniaturization Laboratory
Tricorder Toolkit
DATE”*

Where the *DATE* is not necessarily the last date the MCU board was programmed, but the date that the firmware was compiled.

Wait **WT(time);**

- *time* = time in [ms] to wait before executing the next command (rounds up to the nearest clock cycle – i.e. 10[ms])

System Reset **RT;**

- Performs a full system reset; all processes are interrupted and hardware set to initial states.

Set/Read System Information **SI(type, value); RI(type);**

- *type* = selects which system information will be set
 - 1 – system name
 - 2 – firmware compilation date
 - 3 – MCU board version
 - 4 – High Voltage board version
 - 5 – Optics board version
 - 6 – SMU board version
 - 7 – Wheatstone Bridge board version
 - 8 – Sample Preparation board version (relevant for XY stage systems only)
 - 9 – Firmware version (the three digit identifier, i.e. *SI(9,272);*)
 - 100 – Optical Detection Mode (photodiode = 0, CCD = 1)
 - 101 – Sample Preparation Mode (XY = 0, MicroServo = 1)
 - 200 – Set last username
 - 201 – PCR run count
 - 202 – CE run count
 - 203 – Laser on during CE flag
 - 300 – Set TC1 slope (enter in integer format; i.e. 1.234 x 1000 = 1234)*
 - 301 – Set TC1 offset (enter in integer format)*
 - 302 – Set TC2 slope (enter in integer format)*
 - ❖ 303 – Set TC2 offset (enter in integer format)*
- *value* = value or name to be set

**as described in Section 4.4.6 after new system calibrations were included*

Set Username **SU(name);**

- *name* = is self explanatory

EXTERNAL EEPROM COMMANDS

Load File to EEPROM **LD;**

- Writes all entered characters into external EEPROM until the “ ! ” character is received, or the EEPROM runs out of memory which would draw an error message.

Print EEPROM Content **DS;**

- Print current EEPROM contents

Run File from EEPROM **RN;**

- Executes each command currently loaded in the EEPROM as if it were receiving them line-by-line.

SET CHIP CALIBRATION PARAMETERS AND THERMAL MODULE CALIBRATION

Linear Relationship Command **CC(type, resistance, slope);**

- *type* = the characteristic to be set
- *slope, offset* = integer values from chip and board calibrations – examples below

Type	Slope	Offset
1 – PCR Chip	Room temp resistance (Ω)	TCR ($1/\Omega$)
Chip calibration	Default = 60 To enter: $60.0 = 600$	Default = 0.14 To enter: $0.14 = 1400$
3 – SMU Board	Temp vs. DAC linear relationship	Temp vs. DAC linear relationship
Thermal board calibration	Default: 0.0496 To enter: $0.0496 = 496$	Default: 0.0195 To enter: $0.0195 = 195$

SYSTEM TESTING COMMANDS

Select High Voltage Relays **RS(relay_number, on/off);**

- *relay_number* = the relay to be switched
 - RL1 (CB2) – Injection Waste Well

- RL2 (CB3) – Separation Waste Well
 - RL3 (CB0) – Injection Sample Well
 - ❖ RL4 (CB1) – Separation Buffer Well
- *on/off* = “ 1 “ for on, “ 0 “ for off

Set Laser **SL(on/off);**

- *on/off* = “ 1 “ for on, “ 0 “ for off

Set DAC **SD(num, value);**

- *num* = the board with the DAC to be set
 - 1 – SMU board channel one
 - 2 – SMU board channel two*
 - 3 – High Voltage board
- *value* = DAC value to be set

Read ADC **RA(num, time);**

- *num* = the board with the ADC to be read
 - 1 – SMU board channel one
 - 2 – SMU board channel two*
 - 3 – High Voltage board
 - 4 – Optics board
- *time* = the length of time to read the instantaneous ADC value (sampling rate = 10[Hz])
- returns: *'time[ms]: <TAB> ADC value: \r\n'*

Zero Wheatstone Bridge **ZB;**

- sets SMU channel 1 DAC to 300, injecting ~15mA, and reads the ADC so that the user may zero this value, effectively balancing the Wheatstone bridge

Send Byte over SPI **SB(board_address, value);**

- *board_address* = the address of the board to send command to (0-31; see Board Addresses page 12)
- *value* = the decimal equivalent of the byte register to be set (i.e. to set the byte register to 101010 = 42 in decimal)

Setting and Reading Heater **RH(DAC_value, time);**

- It is imperative that all PCR/MCA and chip parameters be set prior to executing this command.
- *DAC_value* = sets the SMU board channel 1 DAC (if *DAC_value* = 0 can be used to measure room temperature)
- *time* = length of time to read instantaneous data at a sampling rate of 10 [Hz]
- returns:

'0 <TAB> *time*[ms] <TAB> *DAC* <TAB> *ADC* <TAB> T_{Heater} <TAB> T_{Room} <TAB> T_{TC1} <TAB> T_{TC2} \r\n'

- *DAC* – SMU board channel 1 setting
- *ADC* – SMU board channel 1 reading
- T_{Heater} – Calculated heater temperature based on entered chip parameters
- T_{Room} – Measured room temperature from the Temperature board
- T_{TC1} – Measured value from thermocouple 1 (attached to copper heat-sink)
- T_{TC2} – Measured value from thermocouple 2 (attached to exterior of TTK)

CE/PCR/MCA COMMANDS

Set Optical Detection Mode **DM(type);**

- *type* = photodiode mode = 0; CCD mode = 1;
- default mode is for photodiode detection
- returns: '#008 Optical Detection Mode Changed!\r\n'

Capillary Electrophoresis

CE(time_{inj}, voltage_{inj}, time_{sep}, voltage_{sep});

- *inj_time* = length of time for injection step
- *inj_voltage* = high voltage for injection step
- *sep_time* = length of time for separation step
- *sep_votage* = high voltage for separation step
- high voltage is limited to 1000 [V]; entered values of greater than 1 [kV] are treated as equal to 1[kV]
- sampling rate = 100 [Hz]
- returns at 100 [Hz]: *'Clockcount<TAB> Optic Signal [ADC] <TAB> Current [ADC] \r\n'*
- the Clockcount is effectively the time in ms; ADC values are in decimal

Set PCR Parameters **PP(step, time, temperature);**

- *step* = defines the step of the PCR cycle
 - 1 – Reverse Transcription
 - 2 – Pre-Denaturation
 - 3 – Denaturation
 - 4 – Annealing
 - 5 – Extension
 - 6 – Post-Extention
- *time* = length of time of each step [seconds]
- *temperature* = temperature of each step [°C]

Do PCR **DP(cycles, T_{Room});**

- **All PCR parameters and chip characteristics must be set prior to executing this command**
- *cycles* = number of PCR cycles to perform
- *T_{Room}* = current heat-sink temperature (must be entered with the format of [°C] x 10; i.e. 22.5[°C] x 10 = 225
- returns at 10 [Hz]:
'Cycle # <TAB> Transition # <TAB> Clockcount <TAB> DAC <TAB> ADC <TAB> T_{Heater} <TAB> T_{Room} <TAB> T_{TC1} <TAB> T_{TC2} <TAB> T_{ave} \r\n'

- *Cycle #* - the current PCR cycle
- *Transition #* - the descriptor for the temperature ramps between PCR steps
- *Clockcount* – effectively time in ms
- *DAC* – SMU board channel 1 setting (decimal)
- *ADC* – SMU board channel 1 reading (decimal)
- T_{Heater} – Calculated heater temperature based on entered chip parameters
- T_{Room} – Measured room temperature from the Temperature board
- T_{TC1} – Measured value from thermocouple 1 (attached to copper heat-sink)
- T_{TC2} – Measured value from thermocouple 2 (attached to exterior of TTK)
- T_{ave} – Average value from the two thermocouples

Melting Curve Analysis **TM(start_temp, end_temp, ramp_rate);**

- *start_temp* = the starting temperature of the transition
- *end_temp* = the ending temperature of the transition
- *ramp_rate* = rate in [°C/sec] of the temperature transition

Read Temperature **TE(time);**

- *time* – length of time in [ms] to read from the Temperature board
- measures three temperatures from the Temperature board inside the TTK at a rate of 10[Hz]
- returns: $'T_{Room} <TAB> T_{TC1} <TAB> T_{TC2} <TAB> T_{ave} \backslashr\n'$

Set LED (MCA) **TL(on/off);**

- *on/off* = toggles the LED for MCA-equipped systems; 1 = On, 0 = Off

PUMPING AND VALVE COMMANDS

Set Valves **VL(board_address, value);**

- sets the status of valves for up to two Valve boards; it is up to the user to keep track of the values on each boards

- *board_address* = the address of the board with valves to be set
- *value* = the byte value corresponding to the valves to be set

Perform Pumping **PM(cycles);**

- *cycles* = number of pump cycles to perform

Setup Pumping **SP(board_address, v1, v2, v3, period);**

- *board_address* = the address of the valve board to be controlled
- *v1,v2,v3* = the respective valve numbers to actuate (1-6)
- *period* = the frequency with which to actuate the valves

SAMPLE PREPARATION COMMANDS

Direct XY Movement **XY(x_pos, y_pos);**

- *x_pos* = position on the x-axis of the stage to move to
- *y_pos* = position on the y-axis of the stage to move to
- values are from 0-1000; each being 25 [μm]

Circle XY Movement **CM(x_center, y_center, radius, cycles, CW/CCW);**

- *x_center* = x-axis coordinate of the circle
- *y_center* = y-axis coordinate of the circle
- values are from 0 to 1000, each being 25 [μm]
- *radius* = radius of the stage movement (must be smaller than the x and y coordinate values)
- *cycles* = number of times to repeat the circle movement
- *CW/CCW* = move in a clock-wise (0) or counter clock-wise (1) fashion

Wiggle XY Movement **WM(x_center, y_center, radius, cycles, CW/CCW);**

- *x_center* = x-axis coordinate of the wiggle

- *y_center* = y-axis coordinate of the wiggle
- values are from 0 to 1000, each being 25 [μm]
- *radius* = radius of the stage movement (must be smaller than the x and y coordinate values)
- *cycles* = number of times to repeat the wiggle movement
- *CW/CCW* = move in clockwise (0); or counter clock-wise (1) fashion

Set XY Stage Velocity SV(frequency);

- *frequency* = sets velocity of stage motions

B.4 Firmware Messages

Num	Message	Occurrence
#000	Task Completed!	Successful completion of requested task
#001	Program Downloaded!	Program downloaded onto EEPROM successfully
#002	End of Program!	EEPROM script finished running
#003	System Reset!	System was successfully reset
#004	Program Successfully Aborted!	Program was successfully aborted
#005	Operating Mode Changed!	Operating mode changed
#006	Task Aborted!	Current task aborted successfully
#007	Ready To Load Program!	EEPROM program will load begin loading on next loop
#008	Optical Detection Mode Changed!	Indicates the user has switch between PD to/from CCD
#009	Sample Prep Mode Changed!	Indicates the user has switched to/from XY or Micro-Servo sample preparation modes
#300	Working....	Status message sent during sys operation
#500	Error: Program Exceeds Memory!	The EEPROM is full, but the firmware has not yet received the '!' character
#501	Error: Syntax Error!	First two letters of sent command does not match any known commands
#502	Error: Current Exceeded Limit!	High voltage current exceeds 45 uA during a CE run, or during setting/reading of the HV board
#503	Error: Invalid Relay Number!	Number entered into Relay command is invalid (> 4)
#504	Error: Unknown Board is Selected!	Invalid board chosen when reading/writing to ADC/DAC
#505	Danger: Unsafe Operation!	Temperature of heater chamber exceeded 200°C
#506	Error: Not Implemented!	Required board is not present for entered command
#507	Error: Sample Prep Mode Not Set!	The sample preparation mode must match the hardware in the system

FIRMWARE MESSAGE NOTES

Messages are written in the following format:

- First character: #
 - this is so that the software and user can differentiate the number before the message between data and a message number

- Message Number
 - these numbers are included to make it easier for any software built on top of the firmware to parse the messages
 - $x = 000$ – corresponds specifically to 'Task Completed!'
 - $000 < x < 500$ – status (i.e. non-error) messages
 - $x > 500$ – reserved for error messages

- User Message
 - this message notifies the user of the message number's meaning
 - the number of characters contained in the message is not an issue, as messages are not sent during time critical operations; after all messages are sent, firmware waits for the users next response

C. SOFTWARE USER GUIDE

C.1 Installing the GUI

The installer for the GUI (version 3.47) can be found on the supplementary CD. This installer can be run on any Windows XP or Vista computer just like any other regular installer.

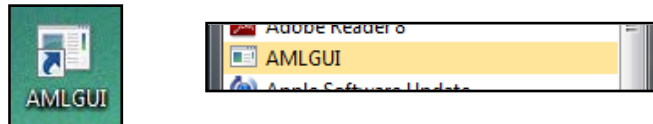
After the installation is done, there will be an AMLGUI.exe file located in the Start Menu. If you would prefer a shortcut on the desktop, then you can right-click on this file and go to “Create Shortcut” or “Move to Desktop”.

You are now ready to start the GUI.

Please note: The GUI does not contain the driver necessary to connect the TTK to the computer. This is also provided on the supplementary CD, and it should be installed when prompted by Windows.

C.2 Starting the GUI

Click on the AML-GUI icon found on the desktop or in the Start Menu.

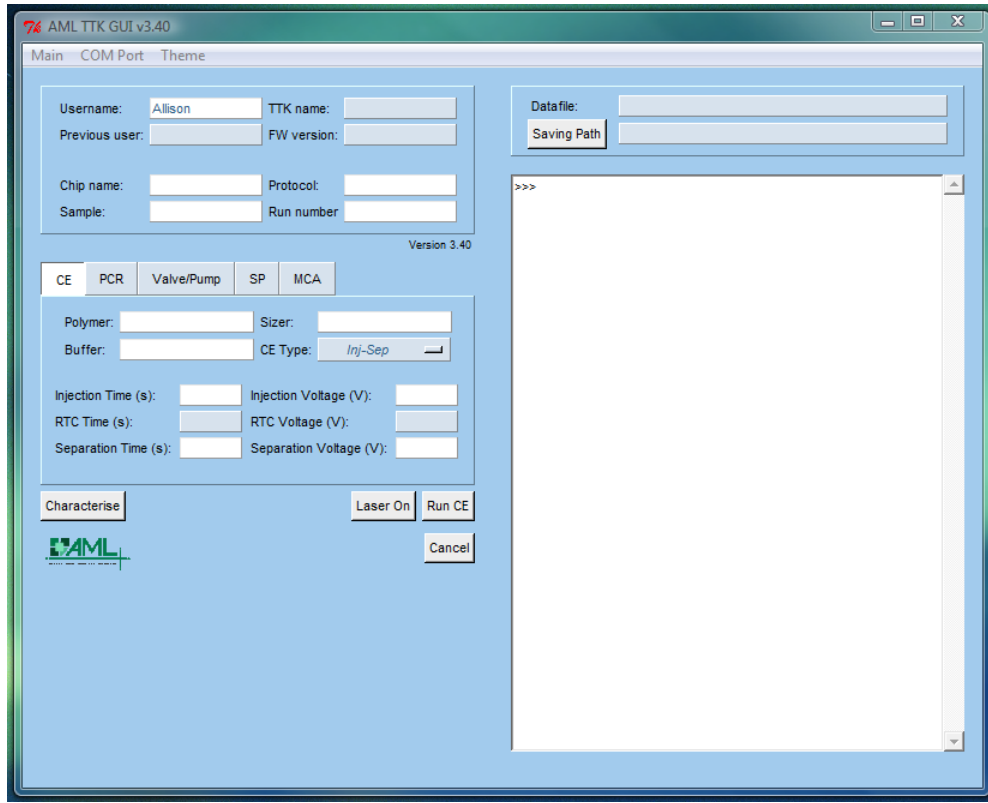


The User Interface should then open, as seen below.

If it does not open and there was an error, Windows will tell you that an error has occurred and it can be found in AMLGUI.exe.log . This file can be found in

C:/Program Files/AML/TTKGUI/

and should be brought to the AML so that the problem can be diagnosed and solved.



C.3 User Interface

The user interface can be seen above. A general trend to note is that blue entry bars cannot be altered by the user; they are merely there for information.

MENU BAR



The Menu Bar runs along the top of the GUI and takes care of Windows related issues.

Main

- Update → updates the TTK specific information without performing any functions on the TTK(this info will be automatically updated prior to any runs, so its use is not a necessary)
- Load → loads a previously saved parameter *.txt file
- Save → saves the current info, CE and PCR run parameters into a *.txt file

- Exit → self-explanatory

COM Port

This drop-down menu contains eight COM ports to choose from. You will need to know which COM port you have connected the TTK to, and choose that number so that a check appears beside it. Once this is done, as long as you plug the USB cable into the same port, the GUI will always remember which COM port to choose (even if it has been closed and re-started).

Theme

This is the colour scheme of the GUI. There are currently three themes to choose from. Once you have chosen your preference, the GUI will also always remember this preference.

THE INFORMATION PANEL

The **information panel** is located in the top right corner of the GUI. All entry bars are referred to as *information parameters*. Parameters are as follows:

- Username → name of the operator
- Chip name → ID of the bottom plate
- Protocol → name of your protocol
- Sample → DNA sample being run
- TTK name → TTK currently connected
- Previous user → previous user of the TTK
- FW version → FW version on the TTK
- Run number * → # of the experiment

Username:	<input type="text" value="Allison"/>	TTK name:	<input type="text"/>
Previous user:	<input type="text"/>	FW version:	<input type="text"/>
Chip name:	<input type="text"/>	Protocol:	<input type="text"/>
Sample:	<input type="text"/>	Run number:	<input type="text"/>

Version 3.40

The *run number* is a system run number assigned by the TTK you are using.

* Run numbers have not been implemented at the time of writing as it would require changing the numbers of previous experiments. You should have your own numbering system.

Writable parameters must be entered before executing any commands. If they are not, the software will send a message to the **terminal window**, asking for them to be entered.

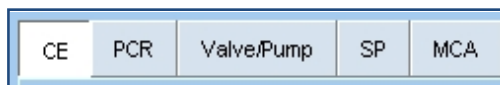
The version number of the software is also located at the bottom of the information panel.

C.4 Notebook Buttons

The **notebook buttons** alternate between different parameters and command buttons, depending on what kind of experiment or action you would like to perform.

The buttons are as follows:

- Capillary Electrophoresis (CE)
- Polymerase Chain Reaction (PCR)
- Valving/Pumping
- Sample Preparation (SP)
- Melt Curve Analysis (MCA)



The rest of the **user interface** remains the same, no matter which notebook button is depressed.

CAPILLARY ELECTROPHORESIS (CE)

The **CE** notebook button makes all the capillary electrophoresis entry bars available; the software refers to them as *CE parameters*. Parameters are as follows:

Writable parameters are as follows:

- Polymer → separation matrix
- sizer → DNA ladder
- Buffer → CE buffer
- Injection Time/Voltage
- RTC Time/Voltage
- Separation Time/Voltage
- CE Type → regular injection or RTC

Writable parameters must be entered before executing CE. If they are not, or are entered improperly, the software will send a message to the **terminal window**.

The CE type can be changed between Inj-Sep and RTC Inj-Sep with the dropdown menu. This makes the RTC Time and Voltage fields alternate between read-only and writable, respectively.

There are also three buttons in the CE sheet.

Characterise This button is used to characterise a new laser upon installation. Please refer to section 3.2.

Laser On This button is used to turn on/off the laser. Once the button is pressed, the text changes to *Laser Off*, allowing the same button to toggle the laser on and off.

Run CE Runs capillary electrophoresis based on the entered CE parameters.

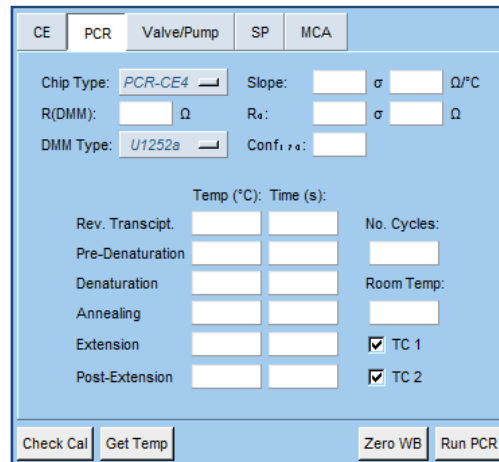
Run CE cannot be run with a separation time of 0s or the GUI will fail!

POLYMERASE CHAIN REACTION (PCR)

The **PCR** notebook button makes all the polymerase chain reaction entry bars available; the software refers to them as *PCR parameters*. Parameters are as follows:

- R (DMM)
- Slope value/sigma
- R₀ value/sigma
- Confidence interval at 170°C
- Room temp
- No. cycles
- PCR step temperatures and times

Writable parameters must be entered before executing PCR. If they are not, or are entered improperly, the software will send a message to the **terminal window**.



In addition to these entry bars, there are two drop down menus:

- Chip type → [chip design model](#)

- DMM type → DMM model ID

There are also four buttons and two checkboxes in the PCR sheet.

- Check Cal** This button takes the values entered in for the chip heater parameters and compares the calibration data to the physically measured DMM data to determine if the calibration is still valid. This check will automatically be completed every time before beginning PCR, but this button is here to allow the user the ability to check chip values without needing to begin PCR. Please refer to section 2.2 for more information.
- Get Temp** This button sends a read temperature comment for 2 seconds, reads in the temperature data from TC1 (which must be connected to the heatsink), averages it, and puts the value into the Room Temp entry.
- Zero WB** Prints the wheatstone bridge value until the *Cancel* button is pressed.
- Run PCR** Runs polymerase chain reaction based on the entered PCR parameters.
- TC1 & TC2** These boxes should be checked if there are any thermocouples connected on the system. The GUI will remember which thermocouples are connected for the last device you connected to it. You must change it if the system changes. Please note TC1 & TC2 must be connected from the temperature board to the heatsink beside the microfluidic chip for optimal operation.

VALVING AND PUMPING

The **Valve/Pump** notebook button makes all the valving and pumping entry bars available; the software refers to them as *VP parameters*.

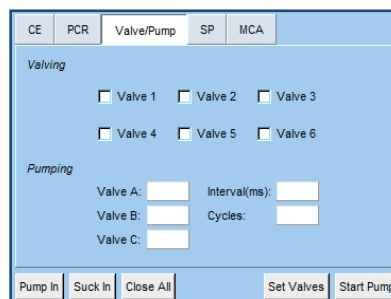
Valving

Six checkboxes are listed, one represented for each valve. If there is no check, the valve is “closed”, or has positive pressure applied. If there is a check, the valve is “open” or has vacuum applied.

Pumping

Writable parameters are as follows:

- Valve A,B,C → the first, second, third valve numbers used for pumping, respectively
- Pump Interval (ms) → the time between each subsequent valve being open and closed
- Cycles → the number of times to cycle through the three valves



Writable parameters must be entered before pumping begins. If they are not, or are entered improperly, the software will send a message to the **terminal window**.

There are also five buttons in the Valve/Pump sheet.

Pump In/Suck In Loads preset valve number for Valves A, B, C to reflect pump/suck and checks off the respective valves so that the user may just enter the interval/cycles and press Set Valve and then Start Pump.

Close All Removes all the checks from the valve boxes so the user may then press Set Valves.

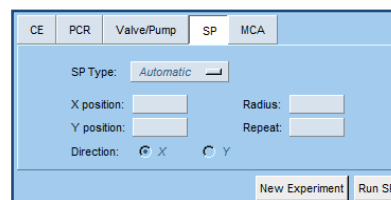
Set Valves Sets the valves on the TTK system to reflect the state represented by the check buttons.

Start Pump Begins the pumping sequence as specified by the pumping parameters.

SAMPLE PREPARATION (SP)

The **SP** notebook button makes all the valving and pumping entry bars available; the software refers to them as *SP parameters*.

Before performing any SP, the SP Type must be chosen. Depending on which type of SP is chosen, the appropriate entry bars will become writable or read-only.



Automatic

This is the coded SP program to move the magnet along the SP channel on a PCRCE4 chip.

- All entry bars are read-only

Direct

This moves the magnet from its current position directly to the position specified (X,Y).

- X position, Y position are writable
- Radius, Repeat, Direction are read-only

Circle

This moves the magnet in a circle of a specified radius around a position (X,Y) a set number of times.

- X position, Y position, Radius, Repeat, Direction are all writable

Wiggle

This moves the magnet back and forth across a specified width around a position (X,Y) a set number of times.

- X position, Y position, Radius, Repeat, Direction are all writable

There are also two buttons in the SP sheet.

New Experiment This button closes the report for the current html file and resets the SP counter so that your next “Run SP” experiment will begin a new report and text file. It is to be used to differentiate between SP runs.

Run SP This runs the SP command currently specified in the sheet.

MELT CURVE ANALYSIS (MCA)

The **MCA** notebook button makes all the valving and pumping entry bars available; the software refers to them as *VP parameters*.

The chip heater calibration and check area is identical to the PCR sheet and acts in precisely the same manner. Unique to the MCA sheet is:

- Start temperature
- End temperature
- Ramp

There are also two unique buttons:

LED On This button is used to turn on/off the LED. Once the button is pressed, the text changes to *LED Off*, allowing the same button to toggle the LED on and off.

Run MCA Runs melt curve analysis based on the entered MCA parameters.

C.5 Other Components

TERMINAL WINDOW

The purpose of the terminal is two-fold:

1. For the user to be able to enter commands that talk to the firmware directly (i.e. CLI)
2. For the software to be able to display messages and incoming data to the user

The “>>>” symbols also indicate the *state* of the terminal window. If these symbols are not the last text in the window, then the software is not ready to receive more commands or have any command buttons pressed.

OTHER USER INTERFACE COMPONENTS

There are a few additional components to the GUI that need to be addressed, but do not fit into a specific category.

The first is the *Cancel* button. This button appears at the bottom of the window, no matter which **notebook button** is depressed. It can be used to cancel CE, PCR, Zero WB, and any manually entered CLI commands in the **terminal window**.

Datafile is a read-only entry bar that displays the filename of a file the software is currently appending data to. If no file is being appended, then this entry remains blank.

The *Saving Path* button is used to choose a file in which to save data files. If a path is not chosen, the software will tell the user to specify a *data directory* through the **terminal window**.

POP-UP WINDOWS

A few pop-up windows appear over the course of the experiment. These are self-explanatory and should be followed as directed.

D. LIMIT OF DETECTION PROTOCOL

This protocol specifically details how to estimate the limit of detection (LOD) on a PD-based TTK with a PCR-CE4 chip and BKV labeled primer. However, this technique is valid for any existing or new LIF-CE system and any fluorescently tagged primer. Primers are used for the LOD due to their known concentration. This saves time and steps, as compared to using purified sample.

PREPARE YOUR LABELLED PRIMER MIX

Dilute your end-labelled primer down from 10uM into three separate tubes of 3uM, 2uM and 1uM concentrations respectively with PCR-grade water.

Primer Dilutions	Volumes (μL)		
Ingredient	0.3x	0.2x	0.1x
10uM 3' BKV-RevAni-Cy5	3.0	2.0	1.0
Cy5-5'- TCAAACACCCTAACCTCTTCTACCTG-3'			
H2O, PCR grade	7.0	8.0	9.0
Total:	10.0	10.0	10.0

Mix the PCR reagents required to give the same ionic concentration as a typical PCR product with $1\mu\text{L}$ of each dilution, as specified below. This is the same BKV PCR Recipe as used in Appendix E, but with water substituted for unlabelled primer, template and Taq. **Do not thermal cycle.**

Reagents	Vo (μL)	Source
10X PCR buffer	2.5	Invitrogen Cat # 10966-034
10uM 5' BKV-ForAni (25b)	x	IDT Ref # 37822830
0.3x, 0.2x, or 0.1xRevPrimer	0.75	IDT Ref # 39804571
10mM dNTPs	0.5	Invitrogen Cat # 10297-018
50mM MgCl_2 (4mM final conc'n)	2.0	Invitrogen Cat # 10966-034
5 U/uL Pt. Taq	x	Invitrogen Cat # 10966-034
BKV DNA template	x	Dr. Pang, ProvLabs
1% BSA	0.5	Sigma B8667
DMSO (4% @ final conc'n)	1.0	Fisher, 99.7% stock
H ₂ O, PCR grade	17.75	MP Biomedicals Inc. Cat # 821739
Total:	25.0	

Limit of Detection Protocol

In this protocol, BKV Cy5-labelled reverse primer is used, so the final 0.3x, 0.2x, and 0.1xLODmix will have total end-labelled primer concentrations of 0.749ng/ μ L, 0.498ng/ μ L, and 0.249ng/ μ L, respectively.

As a guideline, the LOD for a CCD based system is approximately 0.1ng, and a PD based system: 0.1-10ng.

PERFORM CE ON THE DILUTIONS

Ensure 4% LPA and 1xTTE buffer have been made within the last 30 days; the 1xTTE buffer should have a pH of approximately 8.23 on the Accumet BASIC AB15 pH meter.

Fill a previously DC coated PCRCE4 chip with 4% LPA , and pipette 4uL of 1xTTE buffer into CB1, CB2 & CB3. Pipette 3uL of 0.1xTTE and 1uL of sample (your diluted mix) into CB0.

Run on the TTK:

- first run: Inject for 80s @ 200 V; Separate for 250s @ 600 V
- subsequent runs: Inject for 20s @ 200 V; Separate for 250s @ 600 V

Repeat each concentration at least twice

EXTRAPOLATION

Once all runs are completed, determine the average standard deviation of the noise from the first 50 seconds of separation data. Multiply this number by three. This is the value for your limit of detection (V).

Graph peak height vs. DNA concentration, and do a linear regression on the points. Determine when this line will intersect your limit of detection peak determined in the previous step. This is your limit of detection (ng).

E. TTK PCRCE4 ON-CHIP PCR & CE PROTOCOL

Revision 1.41 Written by Allison C.E. Bidulock

E.1 General Considerations

This protocol is written for the use with β 2M DNA extracted from a cheek swab from a healthy volunteer as this is our standard protocol. This protocol may be modified with approval for use with other samples.

BKV AS A BIO-HAZARD

The sample used in this protocol is a purified BKV DNA which has been extracted from 200 μ L of urine using a QIAGEN DNA mini-kit according to the manufacturer's protocol (QIAGEN Inc., Ontario, Canada) and was eluted from the column with 200 μ L of elution buffer for urine. Precision was analyzed based on the noise band crossing point values of 60 replicated plasmid DNAs (3.3 and 6.3 log₁₀ copies).

Please see Pang, X.L. et al¹²⁷ (2007) and Pang, X.L. et al¹²⁸ (2008).

“DNA ONLY GAINS A BIOLOGICAL FUNCTION BY BEING INSERTED INTO A LIVING CELL. HENCE WORK WITH DNA ITSELF ('NAKED' DNA) IS NOT GENERALLY THOUGHT TO CONSTITUTE A SAFETY HAZARD EVEN IF NEW NUCLEIC ACID MOLECULES ARE FORMED. RISKS ASSOCIATED WITH MOST ACTIVITIES THAT MIGHT FORESEEABLY BE UNDERTAKEN WITH NAKED DNA, SUCH AS GEL ELECTROPHORESIS, CUTTING WITH RESTRICTION ENZYMES, LIGATION AND THE POLYMERASE CHAIN REACTION (PCR) CAN THEREFORE BE CONTROLLED BY NORMAL GOOD LABORATORY PRACTICE.

THE ONE EXCEPTION TO THIS IS FULL LENGTH COPIES OF VIRAL DNA THAT ARE INFECTIOUS IN THEIR OWN RIGHT. THESE ARE LEGALLY REGARDED AS MICROORGANISMS EVEN WHEN THEY ARE NOT ENCAPSULATED OR ENVELOPED. THIS MEANS THAT IF FULL-LENGTH VIRAL DNA (SUCH AS DNA FROM PHAGE LAMBDA) WERE TO BE COMBINED WITH DNA FROM OTHER SOURCES, A GENETICALLY-MODIFIED ORGANISM WOULD HAVE BEEN CREATED.” (TAKEN FROM THE NATIONAL CENTRE FOR BIOTECHNOLOGY EDUCATION IN THE UNITED KINGDOM)

Therefore, while purified, naked DNA can generally be regarded as safe, DNA from patient sources may not have been screened to ensure that it is free from

contaminating viruses. This means we must still treat our purified BKV DNA as a bio-hazardous sample.

Thus, gloves and lab coats must be worn at ALL TIMES when handling any chips, reagents, or utensils that may have come into contact with bio-hazardous material.

WHAT IS BIO-HAZARDOUS?

On-Chip PCR Product

This is bio-hazardous. All on-chip products contain portions of the PCR mix that was not temperature cycled, and thus are bio-hazardous. These products must be kept in PCR tube boxes in the fridge and labelled as bio-hazardous.

PCR-CE-4 chips

Prior to the PCR-CE Runs: PCR-CE4 chips are fabricated in the NanoFab and stored in clean containers for transport; they must be transported in covered, clean containers to avoid contamination of chips.

Post PCR-CE Runs: the SP channel, PCR chamber, CE channels and all wells should be soaked with 0.1N NaOH for 10 minutes. The PCR chamber is filled using the TTK system. 5uL of NaOH is pipetted into the SP and PCR Sample wells, opening the valves 4,5,6 and sucking the NaOH through the PCR chamber and surrounding channels by cycling valves 1,2,3 in the same manner as you would load your sample. The chip is then removed from the TTK and taken to the bio-hazardous fume-hood, where the CE channels are filled with NaOH by pipetting 5uL into CB0, CB1, and CB2 and sucking with vacuum from CB3. The vacuum should be attached to a filtered bubbler flask filled with 10% bleach. The PCR chamber and CE channels should then be flushed out with 10uL of water with the same procedure as above. The outside of the chip should then be wiped with 70% ethanol.

TTK

If the TTK is to be removed from the biosafety area, the entire outside casing, gantry and all platinum electrodes must be cleaned with 70% ethanol.

Transportation of On-Chip PCR Products and Unsafe PCRCE4 chips

If PCR product or used PCRCE4 chips are to be transported outside the biosafety area, they must be placed in a sealed, bio-safe container. The outside of this container must then be wiped down with 70% ethanol and labelled: "Bio-hazardous: Used with BKV Sample".

IN THE EVENT OF A SPILL

- ❖ Don protective apparel if necessary
- ❖ Place absorbent material over the spill
- ❖ Pour sufficient amount of an appropriate disinfectant (10% Bleach, 70% Ethanol) just beyond the periphery of the spill and allow the disinfectant to diffuse towards the centre of the bio-hazard spill
- ❖ Do not pour solutions directly over the spilled material since this may cause splashes and generate aerosols
- ❖ Leave the room, lock the door and post a sign to prohibit entry
- ❖ Allow sufficient time for the disinfectant to inactivate the spilled hazard before returning to the room for clean-up and thorough rinsing (15 to 30 minutes)
- ❖ Heave rubber gloves are advisable when sharp objects are involved
- ❖ All materials from the clean-up should be bagged in a bio-hazard bag and sent for autoclaving or incineration

E.2 System Requirements

System

To perform PCR in a TTK, the system should contain the following:

- Power Board (*Rev00*)
- MCU Board (*Rev02*)
- SMU Board (*Rev03*)
- Valve Board (*Rev02*)
- Temperature Board (*Rev01*)
- Wheatstone Bridge Board (*Rev00*)

To perform CE in a TTK, the following boards should be in the system:

- Power Board (*Rev00*)
- MCU Board (*Rev02*)
- High Voltage Board (*Rev03*)
- Optics Board (*Rev03*)

Furthermore, the appropriate, chip-specific gantry is needed to run the microchip.

Positive pressure

1/8" tubing should be connected to a regulator on a positive pressure line. The regulator should be set to allow 20 psi of pressure. Less than this and your valves may not stay sealed during PCR. More than this and you become close to the valve threshold (30 psi).

Negative Pressure

1/8" tubing should be connected to a filtered bubble flask filled with 10% bleach, which is in turn connected to the vacuum source; shut off at the wall. Standard vacuum sources have sufficient negative pressure to allow for smooth fluid pumping on a PCRCE4 chip; however, all other connections to this source must be sealed.

Microfluidic Chip

This microfluidic chip should be capable of performing PCR and CE on the system (i.e. be of the appropriate type).

Furthermore:

- the heater element should have undergone annealing after fabrication and be properly characterised
- the heater ring should have no pinholes or defects
- no delamination should be present around the PCR path (chamber, channels, valves)
- the valves should be inspected to ensure they are neither stuck open nor closed
- there should be no delamination anywhere along the CE portion of the chip
- the channels should be etched cleanly, without jagged corners
- the top plate must be diced cleanly, without significant scratches along its surface
- if using a glass-PDMS-glass chip, the PDMS should be trimmed back as far as possible

Other

Fluke 179 or U1252a DMM for heater resistance measurements

E.3 On-Chip PCR Procedure

- **Before beginning anything, the TTK should be powered on with the lid closed for at least 15 minutes to allow time for the system to thermally equilibrate**
- **Gloves and lab coats must be worn at ALL TIMES when handling any chips, reagents, or utensils**
- **The pogo pins must never come into contact with the heatsink or components will be damaged**

PREPARE THE PCRCE4 CHIP

1. Place the PCRCE4 chip under the microscope, and ensure all valve ports are neither stuck open nor closed by visual inspection (punch out PDMS if needed) and no holes or defects are present on the heater ring. If valves appear closed, you may attempt to open them by blowing through the PCR input or output wells with the nitrogen gun. Chips that have sat longer than 2-3 weeks should always be inspected carefully, and any chips that have stuck valves cannot be used. Heater rings with defects must also not be used.

2. Open the AML GUI; enter in the general run details into the Information Panel (top left panel), and enter the PCR thermal-cycler parameters into the PCR Panel to match the conventional system.
3. Ensure air and vacuum are on, and connected to the TTK; ensure all other branches that are not connected to the TTK are closed so optimal pressure is maintained. It is also recommended to not pump at the same time as another TTK on the same pressure lines.
4. Place the chip on the stage, with the heater ring and chamber in the centre of the carved-out circle; adjust the chip holder as necessary. If the chamber is centered on the heater, you can do this by placing the CE channel in the centre of the GRIN lens and the heater pads in the middle of the hallowed out region on the gantry. If the chamber is off center, it is more important for the heater ring to be centered.
5. Clip the top into place, ensuring the pogo pins are in good contact without being fully depressed, and that the valve ports completely seal (no air is heard hissing from the stage). By rule of thumb, if the gantry merely rests over the chip without depressing the clips and no sound can be heard, the chip is in good alignment for the valves.
 - ▶ The pogo-pins are not designed to be fully depressed onto the heater and should not be fully screwed down onto the heater. The best method to ensure the pogo pins are in good contact is to screw them down until resistance is felt and then screw them half a turn up.
6. Close the lid and go to make your PCR mix while the system thermally equilibrates.
7. Open the lid on the system, and disconnect the banana clips from their jacks. Plug these banana clips into a well-charged, battery operated DMM (Fluke 179 or U1252a only, preferably U1252a). Measure the chip heater resistance, and enter this value and the DMM model being used into the GUI. Disconnect the banana clips from the DMM and re-connect them to the operating wires.

8. Select which thermocouples are connected to the system. (A thermocouple must be connected from TC1 to the heat sink). Click the “Get Temp” button. This will retrieve the heatsink temperature and add 0.5°C to it to account for the increased temperature in the system between idle and operation states.
9. Zero the Wheatstone Bridge using the “Zero WB” button on the PCR Panel; adjust knob until the number is greater than 0 but less than 20; let it run for a bit to ensure the value is not drifting beyond ± 5 . Press “Cancel” once this has been achieved.
10. Once these three things are done, enter in all the calibration data for the chip in the appropriate entry bars and press “Check Cal/DMM”. This verifies the calibration data to the DMM data, and will determine if the resistances match within error.
11. If the chip does not match within error, you can:
 - ▶ begin again with a different chip (safest)
 - ▶ continue with the PCR (worst)

To begin again, return to step 4. To continue, move on to loading the sample.

PREPARE YOUR MASTER MIX

1. Fill a PCR box with ice, and retrieve your PCR reagents; dNTPs and Platinum Taq should be kept in the -30°C freezer, while all other reagents can be kept in the fridge.
2. When you are seated with your box, wipe the PCR bench with ethanol; it is also a good idea to put some on your gloves and rub them together to remove any contaminants you may have picked up along the way.
3. Take a 1.5mL autoclaved tube from the 'PCR ONLY' container and label 'MM' for master mix. Pop open the lid, and place in your icebox.

4. **To ensure no contamination, from this point on, you must not talk and must ensure your arms do not pass over the open tube.** If you need to talk to someone, close the lid, move back from the bench, and begin your discussion.
5. Add your PCR reagents to the MM tube according to one of the above recipes – except for the template! –and close the lid. Once this is completed, take your template and MM tube to the bio-hazardous fume-hood. Wipe down all surfaces with 70% ethanol and re-clean your gloves before beginning. You may then pipette your template into your MM tube. Re-wipe all the surfaces and clean your gloves. Return the template to your icebox. Next, you must centrifuge the mix to ensure all reagents are in the bottom of the tube, and then vortex briefly once centrifuged.
6. Take a PCR tube from the ‘PCR ONLY’ package, and label it for your conventional thermal-cycler mix (TC). Return to the bio-hazardous fume-hood, pipette 10 μ L into the thermal-cycler tube and close the lid tight. Re-wipe all the surfaces and clean your gloves. Place your TC into the thermal-cycler; start.
7. Return your reagents to the fridge/freezer (as specified in point 1), and put the lid on your ice container to keep your master mix in the dark and on ice. Place by the TTK for upcoming use. Mix can be stored in the box for the remainder of the working day, on the order of 5-6 hours, with minimal concern.

BE CONCERNED ABOUT CONTAMINATION OF YOUR PCR BY UNWANTED DNA THAT COULD BE AMPLIFIED BY MISTAKE. POSSIBLE SOURCES OF SUCH CONTAMINANTS INCLUDE: TRACES OF PREVIOUSLY-AMPLIFIED PCR PRODUCTS, TRACES OF PREVIOUSLY-USED GENOMIC TEMPLATE STOCKS AND YOUR OWN CELLS. CONTAMINATING DNA CAN BE TRANSFERRED FROM GLOVES, TIPS, TUBES AND PIPETTES THAT HAVE HAD CONTACT WITH THE SUSPECT SOURCES. TO REDUCE THE RISK OF CONTAMINATION, USE ONLY PCR-DEDICATED PIPETTES (AND KEEP THEM IN THE PCR SET-UP AREA), WEAR NEW GLOVES, USE STERILE FILTER TIPS AND TUBES AND DO NOT OPEN THE “PCR COMPONENTS” FREEZER BOX (NOR THE TUBES WITHIN) OUTSIDE OF THE PCR SET-UP AREA. (TAKEN FROM “PCR – ASSEMBLING A REACTION”, BY TIM FOOTZ)

LOAD THE CHIP WITH SAMPLE

1. Keeping the tube and pipette a safe distance from your person or behind a shield, carefully open the tube and pipette 5 μ L of master mix into the PCR sample well of the chip. Do **not** fully depress all liquid out of the pipette tip as this both unsafe (aerosol generation) and can also leave a bubble of air on top of the well. Some of the mix may bleed into the SP portion of the PCRCE4 chip, but this will not affect your loading.
2. Go to the Valve/Pump tab on the GUI and click the “Suck In” button. This will check off three valves, and give three valve numbers into the pumping area. Click “Set Valves” to open the three checked valves. You must listen to ensure you hear the click of the relays. If you do not, you will need to power off and power on your system.
3. Pump for 3 cycles at 500ms intervals, using the “Pump” button. Watch while pumping to ensure the chamber fills and the mix just reaches the PCR output well. If the mix does not reach, pump for an extra cycle or two as necessary for the mix to reach this well, and make sure to note it on the PCR run notes.
4. Choose the “Close All” button, and press “Set Valves”. Remove any excess master mix from the PCR sample well, and discard along with the pipette tip into a bio-safety bag.
5. Pipette 5 μ L of autoclaved water into the sample well and depress and release the stopper without fully depressing the liquid into the well. This will wash the well of the PCR mix. Dispose of that tip and using a new tip, remove any excess liquid from the well. This is to prevent the PCR buffer ions sticking to the walls of the well and changing the concentration of ions in your flush-out buffer.
6. Check to ensure all valves are closed and all parameters are entered into the GUI; click “Run PCR” on the PCR tab.

7. If your calibration data did not pass the verification step, you will now be prompted to continue with the entered calibration data or to modify the slope assuming the TCR of the chip has not changed. Choose the option you would prefer, and click OK.
8. Wait for the TTK to stabilize at its pre-denaturation temperature, and then open the viewing flap on the lid to look at the PCR chamber; note any bubbles or evaporation you may see in your run notes.

REMOVING THE TTK PRODUCT

1. Once the PCR run has completed, pipette 5 μ L of your flush-out buffer into the PCR sample well.
2. Go to the Valve/Pump tab on the GUI and click the "Suck In" button. This will check off three valves, and give three valve numbers in the pumping area. Click "Set Valves" to open the three checked valves.
3. Pump for 8 cycles at 500ms intervals, using the "Pump" button. Watch while pumping to ensure the PCR sample well is emptied of buffer, and product creates a little dome in the PCR output well.
4. Shut off the air pressure and vacuum, and disconnect the pressure tubes from the TTK. This will remove any residual pressures in the line, making it safe to lift the gantry; otherwise, your product is likely to be scattered.
5. Lift off the gantry, and transfer the product from the PCR output well into a PCR tube. Label it with your product number and place with your conventionally cycled product in the fridge.
6. Lower the gantry back onto the chip, choose "Get Temp" and then "Check Cal/DMM". The values should still agree within error. If not, note this in your lab book and in your report as this means the resistance of the chip may have changed during the run. This chip should then be given to Abraham for forensic testing.

ANY DEVIATIONS FROM THIS PROTOCOL, COMPLICATIONS OR COMMENTS SHOULD BE INCLUDED IN THE RUN NOTES. BE OBSERVANT AND NOTEFUL.

PCR CONDITIONS

BKV Recipes

Recipe A1 Ingredient	Reagent Volumes (µL)		9 January 2009 Source
	1 rxn	-ve ctrl	
10X PCR buffer	2.5	2.5	Invitrogen Cat # 10966-034
10uM 5' BKV-ForAni (25b)	0.5	0.5	IDT Ref # 37822830
10uM 3' BKV-RevAni-Cy5 (26b)	0.75	0.75	IDT Ref # 39804571
10mM dNTPs	0.5	0.5	Invitrogen Cat # 10297-018
50mM MgCl ₂ (4mM final conc'n)	2.0	2.0	Invitrogen Cat # 10966-034
5 U/uL Pt. Taq (x2)	1.0	1.0	Invitrogen Cat # 10966-034
Purified BKV DNA template, 10 ⁷ copies/mL	0.5	X	Dr. Pang, ProVLabs
1% BSA	0.5	0.5	Sigma B8667
DMSO (4% @ final conc'n)	1.0	1.0	Fisher, 99.7% stock
H ₂ O, PCR grade	15.75	16.25	MP Biomedicals Inc. Cat # 821739
Total:	25.0	25.0	

Recipe A2 Ingredient	Reagent Volumes (µL)		9 January 2009 Source
	1 rxn	-ve ctrl	
10X PCR buffer	2.5	2.5	Invitrogen Cat # 10966-034
10uM 5' BKV-ForAni-Alexa647N	0.5	1.0	IDT Ref # 45215441
10uM 3' BKV-RevAni-Alexa647N	0.5	1.0	IDT Ref # 43870805
10mM dNTPs	0.5	0.5	Invitrogen Cat # 10297-018
50mM MgCl ₂ (4mM final conc'n)	2.0	2.0	Invitrogen Cat # 10966-034
5 U/uL Pt. Taq (x2)	1.0	1.0	Invitrogen Cat # 10966-034
Purified BKV DNA template, 10 ⁷ copies/mL	0.5	X	Dr. Pang, ProVLabs
1% BSA	0.5	0.5	Sigma B8667
DMSO (4% @ final conc'n)	1.0	1.0	Fisher, 99.7% stock
H ₂ O, PCR grade	16.0	16.5	MP Biomedicals Inc. Cat # 821739

Total:	25.0	25.0
---------------	------	------

BKV-FORANI: 5'- GTGACCAACACAGCTACCACAGTGT-3'
 BKV-REVANI-CY5: Cy5-5'- TCAAACACCCTAACCTCTTCTACCTG-3'
 BKV-FORANI-ALEXA647N: ALEXA647N-5'- GTGACCAACACAGCTACCACAGTGT-3'
 BKV-REVANI-ALEXA647N: ALEXA647N-5'- TCAAACACCCTAACCTCTTCTACCTG-3'

STOCK AND INITIAL ALIQUOTED PCR REAGENTS ARE STORED IN A -30OC NON-FROST-FREE FREEZER IN A BOX DEDICATED FOR PCR REAGENTS (I.E. NO PCR PRODUCTS ARE CONTAINED WITHIN). A SEPARATE BOX ALSO IN THE FREEZER IS RESERVED FOR STOCKS OF PRIMERS. ONLY EPPENDORF 1.5ML TUBES (PCR CLEAN) ARE USED FOR MAKING ALIQUOTS AND DILUTIONS. 10XPCR BUFFER, 50MM MgCl2 AND 5U/μLPT TAQ ARE ALIQUOTED FROM INVITROGEN PT TAQ DNA POLYMERASE KITS TO MAKE THAWING QUICKER AND TO PRESERVE STOCKS. 500μLALIQUOTS OF PCR GRADE A WATER (DNASE- AND RNASE-FREE) ARE KEPT REFRIGERATED AND ARE TO BE USED AS DILUENT WHEN NEEDED. 10MM DNTPS ARE ALSO ALIQUOTED OUT FOR PURPOSES AS MENTIONED ABOVE. THE STOCK IS OBTAINED FROM SIGMA D7295-0.2ML. PRIMERS ARE DILUTED AS INDICATED FOR SPECIFIC PCR RECIPES. (WRITTEN WITH THE HELP OF JANA)

Thermal-Cycling Profile

PCR Step	Temperature (°C)	Time (s)
Pre-Denaturation	94	120
Denaturation	94	10
Annealing	56	20
Extension	70	20
Post-Extension	70	120
Cycles: 35		

UNREPRESENTATIVE DATA

Multiple PCR chamber loadings with SigmaCote chips

If PCR mix is flushed into the PCR chamber or surrounding input/output channels and then dried (in preparation to re-load the sample) and re-loaded, the on-chip PCR will result in several strong unspecific peaks. This has been observed with chips passivated with SigmaCote and is likely due to poor passivation leading to a concentration of some PCR reagents. Chips with other passivation coatings have not been tested for this at the time of writing this document.

As per protocol, it generally takes about 3 pump cycles to lead the sample from the input well into the chamber. However, if this procedure is not strictly adhered to, and the chamber is filled with excessive pumping (the mixture slides back and forth down the channel while loading) then we again see non-specific peaks with SigmaCote chips. It should take no more than 4 cycles to load the PCR chamber of a SigmaCote chip.

Air bubbles/evaporation in the PCR chamber

If there are significant bubbles present (or generated) in the PCR chamber during pre-denaturation (the highest temperature of the PCR run will lead to the bubble being the largest), even less volume will be present and thus the process will be less effective. Although not thoroughly tested, it is suggested that if 10-20% of the chamber is filled with bubbles, this is sufficient enough to foul up the PCR, as there is some pushing out of the PCR mix from the chamber during cycling.

Consistent air bubble/evaporation problems must be investigated as this suggests chip protocol errors (bonding, passivation) or a leak on the vacuum/pressure line between the o-rings and the line. As air leaks are generally very apparent due to the sound of leaking, the vacuum would be the primary suspect.

Less than 4L recovered from the PCR chamber

If less than 4 μ L of sample is recovered after the buffer flush through via the PCR chamber, it suggests that a valving or chip bonding problem occurred during the course of the run. Visual inspection of the chip and investigation of the vacuum/positive pressure lines should be able to answer why. This product is not longer representative as there is the possibility that sufficient mix may not have been present within the chamber during thermal-cycling to be effective.

TROUBLESHOOTING

Wheatstone Bridge reads 65535 and won't zero

The pogo pins are most likely not in good contact with the heater. Screw both pogo pins down until you feel slight resistance, and then half turn then up.

If the problem still isn't solved, the pogo pins likely came in contact with the heatsink and the 10 Ω precision resistor has blown. As this can sometimes have detrimental effects on the power board as well, the system should be cleaned according to a biohazard protocol and brought to the AML for fixing.

Reading room temperature gives abnormal values

Either the room temperature board is not installed or there is an error with it. This will need to be investigated in the AML.

Danger: Unsafe Operation!

There are two methods that can incur this error:

DAC set to 3500, heater temperature not rising

This is most often due to an error with the power board. Setting the DAC manually to 3000 and measuring the voltage coming off the power board with a DMM is the easiest way to check this.

If the 24 V line is giving 24 V, the power board is fine and the chip should be checked.

If the 24 V line isn't reaching 24 V, the system should be cleaned according to a biohazard protocol and brought to the AML for fixing. This must be checked when the SMU DAC is set, not when idling the system.

DAC is not set to 3500, seemingly random time-out

This means the ADC must have reported that the heater temperature was at 200°C for two reporting periods, the temperature at which PDMS melts.

Sometimes this will happen if the pogo pins are not in good contact, as the controller sees an open circuit and thinks it's exceeded 200°C. In this case, screw both pogo pins down until you feel slight resistance, and then half turn then up.

This may also occur if a poor power adaptor is being used with the system or there is electrical noise on the power line, creating unreal temperature spikes in the PCR data. Each system should only be using the power adaptor that is assigned to them.

Random Temperature Spikes

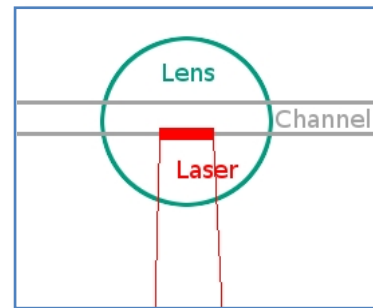
Temperature “spikes” are often isolated, unreal changes in temperature during PCR. These are most often caused by a power supply either from the adaptor or the wall. A few isolated occurrences will not harm your PCR and are likely due to wall power. However, if many are seen close together, it is most likely a poor adaptor. Check to ensure you are using the correct adaptor for the system, and if so, bring the system and the adaptor to the AML for further testing.

ALL DIFFICULTIES SHOULD BE NOTED IN THE RUN NOTES

E.4 On-Chip CE Procedure

FOCUSING THE CHIP

1. Focus the microscope over the photodiode with the CE channel of your empty chip in the center of the lens. The chip is easiest to focus when it is empty (ratio of refraction indices is higher).
2. Adjust the z-axis until you see bright illumination on the wall of the CE channel (pictured on the right) with the laser at approximately the height of the channel.
3. The laser in the system should be characterised upon its installation and a warm up time should have been deduced from this characterisation (approx. 15-20 min). **The laser must be warmed up for this length of time prior to any CE experiments.** After this initial warm up, the laser should remain on until all of your CE experiments are completed. If it is accidentally shut off (e.g. current max-out), it should be re-warmed for 1-2 minutes or variations in baseline should be expected for this amount of time.



CHIP LOADING

1. Ensure all reagents were made within the last 30 days (4% LPA, 1xTTE).
2. Take 4% LPA into a fitted 1mL pipette tip attached to a 1mL syringe. Insert the tip to the CB3 well and make sure you have a good seal. Gently apply pressure and let the mix fill the channels. Loading may take 30s, but do not apply too much pressure so as to crack the chip or destroy the polymer. Wait until the polymer fully fills all channels.

SAFETY NOTE: the polymer should just exit the channels into CB0, CB1 & CB2; no bubbling should occur as this can create aerosols. The syringe and chip must be secure in your grasp; do not allow the syringe to slip and splatter polymer at you.

3. Carefully remove the syringe, and pipette out the excess polymer from CB3. Pipette 4uL of 1xTTE buffer into CB1, CB2, & CB3. If you are testing your TC product, pipette 0.5uL of sample into CB0 and 3.5uL of your flush-out buffer (0.1 or 0.01xTTE). If you are testing TTK product, pipette 4uL of sample into CB0 behind an aerosol shield.

CE CONDITIONS

- ❖ **First Injection:** 80 seconds; **Subsequent Injections:** 20 seconds @ 200V
- ❖ **Separation:** 250 seconds @ 600 V

According to a static buffer depletion equation given in Brask *et al*⁷⁴, our current running conditions deplete the buffer in the sample well after approximately 8 seconds of injecting. A careful eye should be kept on running currents and run-to-run reproducibility to ensure no adverse effects appear due to buffer depletion.

ANY DEVIATIONS FROM THIS PROTOCOL, COMPLICATIONS OR COMMENTS SHOULD BE INCLUDED IN THE RUN NOTES. BE OBSERVANT AND NOTEFUL.

CHIP CLEANING AFTER CE

1. To remove polymer, suck the CE wells dry and pull out the polymer with the vacuum. Cap CB0, CB1, CB2 with water, and rinse the chip using the vacuum from CB3. Remove any excess water and inspect for debris. **OR:**
1. Cover the entire chip with a Technicloth wipe and soak the wipe with 70% ethanol. Pull the wipe down the chip to expose only CB3. Take autoclaved or milli-Q water into a fitted 1mL pipette tip attached to a 1mL syringe. The water must fill the entire tip of the syringe. Insert the tip to the CB3 well using a layer of Parafilm as a gasket to promote the seal between the syringe and glass well. Gently apply pressure, pushing to remove the polymer. Once you can see the water flowing out of the other 3 wells (including the sample well) underneath the ethanol soaked wipe, remove the plunger from the syringe prior to removing the syringe from the chip. At this point any biohazardous material from the micro-channel and sample well will have been sufficiently diluted, washed out and contained within the 70% ethanol soaked Technicloth wipe. Dispose of the wipe in the appropriate biohazardous waste container.

SAFETY NOTE: the polymer should just exit the channels into CB0, CB1 & CB2 and then the water should move through with constant flow; no bubbling should occur as this can create aerosols! The syringe and chip must be secure in your grasp; do not allow the syringe to slip and splatter polymer at you.

Wrap a dry Technicloth wipe around the chip exposing the same well that never came into contact with a sample, apply positive pressure using the filtered nitrogen gun to dry the chip channel and inspect for debris. Finally use the air gun to dry out the remaining wells. Any water spray at this point is deemed safe and clean, and will mostly be absorbed by the dry cloth wrapped around the chip.

CE REAGENTS

- Polymer: 10% LPA (Polysciences, Inc, Warrington, PA (cat #19901; MW 600,000-1,000,000; 10% in water)
- Dynamic Coating: (The Gel Co., San Francisco, CA (Dynamic coating, cat #DEH-100)) – store at 4C
- Buffer: Tris (Fisher Scientific, #BP152-500), TAPS (Sigma #T5120) and Na₂EDTA (Sigma #ED2SS) – store at RT

10xTTE (500 mM Tris-base, 500 mM TAPS, 10 mM Na₂EDTA) preparation

1. Combine the following reagents into a conical tube:
2. 3.027g of Tris for a final concentration of 0.5mM
3. 6.082g of TAPS acid for a final concentration of 0.5mM
4. 0.186g of Na₂EDTA for a final concentration of 0.01mM
5. Mix well, and then check the pH of the 10xTTE. The pH should be 8.3 ± 0.3 . If the pH is not in this range, then discard the buffer.
6. The pH should subsequently be measured every month before mixing new aliquots of 4% LPA and 1xTTE.

This formulation of buffer is based on the recipe published in Applied Biosystem's "ABIPrism377 DNA Sequencer". This can be stored at room temperature for up to 4 weeks.

4% LPA preparation

1. Add 500uL of autoclaved water and 100uL of 10xTTE into a 1mL Eppendorf tube. Add 400 mg of 10% LPA to this tube.
2. Vortex very well. LPA is very viscous and takes time to dissolve. Once dissolved, centrifuge for 30s at 400 rpm. Vortex for 5s again.

This can be stored at room temperature for up to 30 days.

Coating Method

Fill the channels with dynamic coating. Leave for 10 min. Wash the channels with water and dry.

OTHER CONSIDERATIONS

Warm Up

The lasers need to be warmed up for 10-20 minutes, depending on the laser itself. Rough warm up times can be determined from the laser calibration that is done after installation.

Baselines

Baselines are extremely important! They indicate how much light is being coupled to the CE channel or how much scatter is being directed at the photodiode. When used with the same chip, they can be a first indicator of the laser output power decreasing. For version 1/2 chips, baselines should be between 1-2 V.

Unrepresentative Data

- If the laser is accidentally turned off before the run or in between consecutive runs, the user has to make a choice: leave the chip for at least a minute while the laser warms up again (with a consequence that the chip dries out), or attempt the run with the likelihood of a varying baseline. As such, these runs are questionable.
- If the TTK is bumped, there can be large sudden variations in the baseline that appear to be peaks or disguise real peaks.
- High or low baselines (e.g. <1V or >3V) because of chip fabrication (which may be caused by dicing, alignment, bonding) indicate that not enough light or too much light is being coupled.
- Laser power less than 4.2 mW using the LaserCheck handheld optical power meter (if this is so, the laser needs to be replaced) decreases the intensity of peaks.

- Surface coating (e.g. Dynamic Coating) degradation on the CE channels results in lower product peak intensities, and may disguise a product peak. This can be tested by running the chip on the μ TK with 1 μ L of AlfaExpress.
- Misalignment of the chip resulting in insufficient light coupling.

TROUBLESHOOTING

Current Exceeded the Limit!

The current on the given step has exceeded 45 μ A. Reduce the voltage by 50 V and continue running for the remaining time. This most often happens on the first long injection of a CE run.

ALL DIFFICULTIES SHOULD BE NOTED IN THE RUN NOTES

F. AML TTK SP-PCR-CE PROTOCOL FOR PCR-CE-4 CHIPS

Revision 1.05 Written by Allison C.E. Bidulock

F.1 General Considerations

This protocol is written for the use with β 2M DNA extracted from a cheek swab from a healthy volunteer as this is our standard protocol. This protocol may be modified with approval for use with other samples.

β 2M AS A BIO-HAZARD

The sample used in this protocol is β 2M DNA extracted from a cheek swab from a healthy volunteer as per ethics approval in place with the MDG. However, because the complete medical history of the volunteer is unknown, the cheek swab should be handled as a biohazard. When performing PCR positive control runs, purified β 2M DNA is used. This purified DNA was extracted from red blood cells collected and cleaned up from a healthy volunteer with informed consent. The DNA purification process was a multi-step process primarily involving chloroform. For more details, see DNA extraction from pellets, MDG protocol, Jennifer, 23 May 2000.

“DNA ONLY GAINS A BIOLOGICAL FUNCTION BY BEING INSERTED INTO A LIVING CELL. HENCE WORK WITH DNA ITSELF ('NAKED' DNA) IS NOT GENERALLY THOUGHT TO CONSTITUTE A SAFETY HAZARD EVEN IF NEW NUCLEIC ACID MOLECULES ARE FORMED. RISKS ASSOCIATED WITH MOST ACTIVITIES THAT MIGHT FORESEEABLY BE UNDERTAKEN WITH NAKED DNA, SUCH AS GEL ELECTROPHORESIS, CUTTING WITH RESTRICTION ENZYMES, LIGATION AND THE POLYMERASE CHAIN REACTION (PCR) CAN THEREFORE BE CONTROLLED BY NORMAL GOOD LABORATORY PRACTICE.

THE ONE EXCEPTION TO THIS IS FULL LENGTH COPIES OF VIRAL DNA THAT ARE INFECTIOUS IN THEIR OWN RIGHT. THESE ARE LEGALLY REGARDED AS MICROORGANISMS EVEN WHEN THEY ARE NOT ENCAPSULATED OR ENVELOPED. THIS MEANS THAT IF FULL-LENGTH VIRAL DNA (SUCH AS DNA FROM PHAGE LAMBDA) WERE TO BE COMBINED WITH DNA FROM OTHER SOURCES, A GENETICALLY-MODIFIED ORGANISM WOULD HAVE BEEN CREATED.” (TAKEN FROM THE NATIONAL CENTRE FOR BIOTECHNOLOGY EDUCATION IN THE UNITED KINGDOM)

Therefore, while purified, naked DNA can generally be regarded as safe, DNA from patient sources may not have been screened to ensure that it is free from contaminating viruses. This means we must treat our cheek swab sample and purified β 2M sample as bio-hazardous.

Thus, gloves and lab coats must be worn at ALL TIMES when handling any chips, reagents, or utensils that may have come into contact with bio-hazardous material.

WHAT IS BIO-HAZARDOUS?

On-Chip PCR Product

This is bio-hazardous. All on-chip products contain portions of the PCR mix that was not temperature cycled, and thus are bio-hazardous. These products must be kept in PCR tube boxes in the fridge and labeled as bio-hazardous.

PCR-CE-4 chips

Prior to the PCR-CE Runs: PCR-CE4 chips are fabricated in the Nano-Fab and stored in clean containers for transport; they must be transported in covered, clean containers to avoid contamination of chips.

Post PCR-CE Runs: the SP channel, PCR chamber, CE channels and all wells should be soaked with 0.1N NaOH for 10 minutes. The PCR chamber is filled using the TTK system. 5uL of NaOH is pipetted into the SP and PCR Sample wells, opening the valves 4,5,6 and sucking the NaOH through the PCR chamber and surrounding channels by cycling valves 1,2,3 in the same manner as you would load your sample. The chip is then removed from the TTK and taken to the bio-hazardous fume-hood, where the CE channels are filled with NaOH by pipetting 5uL into CB0, CB1, and CB2 and sucking with vacuum from CB3. The vacuum should be attached to a filtered bubbler flask filled with 10% bleach. The PCR chamber and CE channels should then be flushed out with 10uL of water with

the same procedure as above. The outside of the chip should then be wiped with 70% ethanol.

TTK

If the TTK is to be removed from the MDG, the entire outside casing, gantry and all platinum electrodes must be cleaned with 70% ethanol.

Transportation of On-Chip PCR Products and Unsafe PCRCE4 chips

If PCR product or used PCRCE4 chips are to be transported outside the MDG, they must be placed in a sealed, bio-safe container. The outside of this container must then be wiped down with 70% ethanol and labelled: "Bio-hazardous: Used with Buccal Sample".

IN THE EVENT OF A SPILL

- ❖ Don protective apparel if necessary
- ❖ Place absorbent material over the spill
- ❖ Pour sufficient amount of an appropriate disinfectant (10% Bleach, 70% Ethanol) just beyond the periphery of the spill and allow the disinfectant to diffuse towards the centre of the bio-hazard spill
- ❖ Do not pour solutions directly over the spilled material since this may cause splashes and generate aerosols
- ❖ Leave the room, lock the door and post a sign to prohibit entry
- ❖ Allow sufficient time for the disinfectant to inactivate the spilled hazard before returning to the room for clean-up and thorough rinsing (15 to 30 minutes)
- ❖ Heave rubber gloves are advisable when sharp objects are involved
- ❖ All materials from the clean-up should be bagged in a bio-hazard bag and sent for autoclaving or incineration

F.2 On-chip SP-PCR Procedure

Gloves and lab coats must be worn at ALL TIMES when handling any chips, reagents, or utensils that may have come into contact with bio-hazardous material.

PREPARE THE SAMPLE AND BIND THE DNA (ONCE MONTHLY)

1. Lysis buffer, Proteinase K, Chargeswitch™ magnetic beads and purification buffer used are all from an Invitrogen Chargeswitch™ direct gDNA kit. 10% Tween20 used is from Sigma Aldrich.
2. Add 500µL of lysis buffer into a labelled 1.5mL tube (Tube 1). Rub a clean swab against the inside of the cheeks 5-6 times to collect buccal cells. Place the swab in the lysis buffer. Let the tube sit for 15 minutes, swirling the swab frequently.
3. Put the swab into a cut pipette tip, and insert the pipette tip into a fresh 1.5mL tube (Tube 2). Break off the wooden portion of the swab so that it fits into the tube. Centrifuge Tube 2 (containing the swab within a pipette tip) for 1 minute. Transfer the resulting liquid into Tube 1 (the original lysis buffer mix). Discard the swab, pipette tip and Tube 2 into biohazard waste container.
4. Add 5µL Proteinase K. Proteinase K does not tolerate multiple freeze thaw cycles. It is best to use small disposable aliquots of the enzyme that can be changed each week. Mix the solution vigorously with a pipette. Let tube sit for 10 minutes.
5. Add 5µL of Chargeswitch™ magnetic beads to the mixture. Mix thoroughly by pipetting solution repeatedly. Repeat with 25µL of purification buffer. Repeat with 12µL of 10% Tween20 (Sigma Aldrich). Let tube sit for 1 minute.
6. Store lysate mixture on ice if purifications will be done immediately. Otherwise, store lysate mixture at 4°C. This mixture should be made fresh once a month for optimal results.

PREPARE YOUR MASTER MIX

BE CONCERNED ABOUT CONTAMINATION OF YOUR PCR BY UNWANTED DNA THAT COULD BE AMPLIFIED BY MISTAKE. POSSIBLE SOURCES OF SUCH CONTAMINANTS INCLUDE: TRACES OF PREVIOUSLY-AMPLIFIED PCR PRODUCTS, TRACES OF PREVIOUSLY-USED GENOMIC TEMPLATE STOCKS AND YOUR OWN CELLS. CONTAMINATING DNA CAN BE TRANSFERRED FROM GLOVES, TIPS, TUBES AND PIPETTES THAT HAVE HAD CONTACT WITH THE SUSPECT SOURCES. TO REDUCE THE RISK OF CONTAMINATION, USE ONLY PCR-DEDICATED PIPETTES (AND KEEP THEM IN THE PCR SET-UP AREA), WEAR NEW GLOVES, USE STERILE FILTER TIPS AND TUBES AND DO NOT OPEN THE "PCR COMPONENTS" FREEZER BOX (NOR THE TUBES WITHIN) OUTSIDE OF THE PCR SET-UP AREA. (TAKEN FROM "PCR – ASSEMBLING A REACTION", BY TIM FOOTZ)

1. Fill a PCR box with ice, and retrieve your PCR reagents; dNTPs and Platinum Taq should be kept in the -30°C freezer, while all other reagents can be kept in the fridge.
2. When you are seated with your box, wipe the PCR bench with 70% ethanol; it is also a good idea to clean your gloves at this point to remove any contaminants you may have picked up along the way.
3. Take a 1.5mL autoclaved tube from the 'PCR ONLY' container and label 'MM' for master mix. Pop open the lid, and place in your icebox. To ensure no contamination, from this point on, you must not talk and must ensure your arms do not pass over the open tube. If you need to talk to someone, close the lid, move back from the bench, and begin your discussion.
4. Add your PCR reagents to the MM tube according to your recipe and close the lid. Take enough PCR tubes from the 'PCR ONLY' package for two conventionally thermo-cycler mixes (TC+, TC-) and as many SP runs you will perform that day (SP#). Label appropriately. Pipette $9.6\mu\text{L}$ of the mix into the TC and SP tubes, close the lid tight, and briefly centrifuge. Pipette $0.4\mu\text{L}$ of PCR-grade water into TC-. Re-wipe all surfaces.
5. Take your template and TC+ tube to the class II A bio-safety cabinet or the Biohazard DNA Containment (designated sealed aerosol-proof cabinet). Wipe down all surfaces and tubes with 70% ethanol and re-clean your gloves before

beginning. Pipette your template (0.4 μ L) into the TC+ tube, close the lid tight and briefly centrifuge. Re-wipe all the surfaces and tubes and clean your gloves. Return the template to your icebox. Place your TC+ and TC- into the thermal-cycler; start.

6. Return your reagents to the fridge/freezer (as specified in point 1), and put the lid on your ice container to keep your master mix in the dark and on ice. Place by the TTK for upcoming use. Mix can be stored in the box for the remainder of the working day, on the order of 5-6 hours, with minimal concern.

PREPARE THE PCRCE4 CHIP

1. Place the PCRCE4 chip under the microscope and ensure all valve ports are open by visual inspection only (punch out if needed). If valves appear closed, you may attempt to open them by blowing through the PCR section with a filtered nitrogen gun.
2. Open the AML GUI; enter in the general run details into the Information Panel, and enter the PCR thermal-cycler parameters into the PCR Panel to match the conventional system.
3. Measure the chip heater resistance using probes from the Fluke 179 DMM and look up the slope on a calibration chart; enter these values into the GUI under the PCR tab as well. Select which thermocouples are connected to the system, if any. (It is recommended that a thermocouple be connected from TC1 to the heat sink).
4. Place the chip on the TTK gantry directly above the X-Y stage. On Belle, this means placing the chip all the way to the right. It is recommended to use a dissecting microscope to observe magnetic bead movement and to aid in chip manipulations, however it is not necessary.

PURIFY THE DNA

1. Fill the SP output well (PCR sample input well) with 5 μ L separation buffer (25% sucrose, 1% Tween20 in Invitrogen wash buffer). It should just form a dome over the well without over-spilling. Wait for the fluid to flow up the channel to the SP

input well by capillary action. If the liquid does not fill the channel by capillary action, use a 1mL syringe (a fitted pipette tip attached) to suck the liquid from the SP input well. The channel must be filled completely with minimal separation buffer entering the SP input well.

2. Open the SP Panel on the GUI. Click "New SP Experiment". Choosing "Direct" motion, enter (510, 800) into the X,Y co-ordinate fields respectively. Click "Run SP". The stage should move so the right edge of the magnet is just at the entrance to the SP channel at the SP input well without being under the well itself. Adjust the X,Y co-ordinates if necessary.
3. Fill the input well with 4 μ L of well-mixed bead lysate solution (Tube 2). The beads should move towards the magnet and form a short column (about 1mm wide) in the separation channel.
4. Choose "Automatic" motion and click "Run SP". The magnet should gradually move towards the SP output well followed by the bead column. When the magnet motion stops (under the PCR input well), remove excess lysate solution from the SP input well. The beads should form a pellet inside the SP output well. If this is not the case, "Direct" motion commands may be required.
5. Remove any remaining separation buffer from the PCR input well with a 1 μ L pipette. Repeat 3-4 times to empty most, if not all, the separation buffer completely from the PCR input well. This must be done gently to ensure the beads (immobilized by the SP magnet) remain in the well. To minimize the chance of contamination, discard the pipette tip in a bio-waste container frequently.
6. Rinse the PCR input well and the beads three times (using a new tip each time) with 4 μ L PCR-grade water by depressing the pipette plunger to the first stop and releasing multiple times. This should be done gently to keep the beads inside the well. Move the magnet to (0,0) using the direct command.

7. Pipette 5 μ L of the PCR master mix into the PCR input well, and pump depress and release the plunger to mix.

CLEAN AND RE-PREP PCRCE4 CHIP

1. Ensure air and vacuum are on, and connected to the TTK, with the positive pressure gauge at an effective psi of 20; ensure all other branches not connected to the TTK are closed so optimal pressure is maintained (at present, there are two branches off the positive pressure line and two off of the vacuum in the MDG). It is also recommended to not pump at the same time as another TTK on the same pressure lines.
2. Move the chip down the stage, so the chamber is in the centre of the carved circle; adjust the chip holder as necessary. You can do this by placing the CE channel in the centre of the GRIN lens and the heater pads in the middle of the hallowed out region on the gantry.
3. Clip the top into place, ensuring the pogo pins are in good contact without being fully depressed, and that the valve ports completely seal (no air is heard hissing from the stage). By rule of thumb, if the gantry merely rests over the chip without depressing the clips and no sound can be heard, the chip is in good alignment for the valves.
4. Zero the Wheatstone Bridge using the "Zero WB" button on the PCR Panel; adjust knob until the number is greater than 0 but less than 20; let it run for a bit to ensure the value is not drifting significantly. Press "Cancel" once this has been achieved.
5. Type TE(2000); into the command box; three columns of numbers will appear on the screen. If TC1 is connected, the middle column should be monitored; if no thermocouples are connected, the first column should be monitored. Choose the highest temperature seen in the monitored column, and add 0.5 C to it. This is the room temperature to be entered into the PCR Panel on the GUI.

6. Load the chip with sample:
7. Go to the Valve/Pump tab on the GUI and click the “Suck In” button. This will check off three valves, and give three valve numbers into the pumping area. Click “Set Valves” to open the three checked valves. You must listen to ensure you hear the click of the valves. If you do not, you will need to power off and power on your system.
8. Pump for 3 cycles at 500ms intervals, using the “Pump” button. Watch while pumping to ensure the chamber fills and the mix just reaches the PCR output well. If the mix does not reach, pump for an extra cycle or two as necessary for the mix to reach this well, and make sure to note it on the PCR run notes.

SAFETY NOTE: The PCR mix must not be pumped any faster than this for risk of splatter! At 500ms the bio-hazardous mix fills the output well at a rate of about 0.3 μ L/s with constant flow and no aerosols.

9. Close valves one at a time, starting with the valve closest to the chamber and working outwards (first 4, 5, then 6). Remove any excess master mix from the PCR sample well, and discard along with the pipette tip into a bio-safety bag.
10. Pipette 5 μ L of autoclaved water into the sample well and depress and release the stopped without fully depressing the liquid into the well. This will wash the well of the PCR mix. Dispose of that tip and using a new tip, remove any excess liquid from the well. This is to prevent the PCR buffer ions sticking to the walls of the well and changing the concentration of ions in your flush-out buffer.
11. Check to ensure all valves are closed and all parameters are entered into the GUI; click “Run PCR” on the PCR tab.
12. Wait for the TTK to stabilize at its pre-denaturation temperature, and then open the viewing flap on the lid to look at the PCR chamber; note any bubbles or evaporation you may see in your run notes.

REMOVING THE TTK PRODUCT:

1. Once the PCR run has completed, pipette 5 μ L of your flush-out buffer into the PCR sample well.
2. Go to the Valve/Pump tab on the GUI and click the “Suck In” button. This will check off three valves, and give three valve numbers into the pumping area. Click “Set Valves” to open the three checked valves.
3. Pump for 8 cycles at 500ms intervals, using the “Pump” button. Watch while pumping to ensure the PCR sample well is emptied of buffer, and product creates a little dome in the PCR output well.
4. Shut off the air pressure and vacuum, and disconnect the pressure tubes from the TTK. This will remove any residual pressures in the line, making it safe to lift the gantry; otherwise, your product is likely to be scattered.
5. Lift off the gantry, and transfer the product from the PCR output well into a PCR tube. Label it with your product number, as a bio-hazard, and place with your conventionally cycled product in the fridge.
6. PCRCE4 chips and the TTK must be decontaminated before leaving the lab. Please see Section F.1 for more information.

F.3 On-Chip CE Procedure**FOCUSING THE CHIP**

1. Focus the microscope over the photodiode with the CE channel of your empty chip in the center of the lens. The chip is easiest to focus when it is empty (ratio of refraction indices is higher).
2. Adjust the z-axis until you see bright illumination on the wall of the CE channel with the laser at approximately the height of the channel.
3. The laser in the system should be characterised upon its installation and a warm up time should have been deduced from this characterisation (approx. 15-20 min).

The laser must be warmed up for this length of time prior to any CE experiments.

After this initial warm up, the laser should remain on until all of your CE experiments are completed. If it is accidentally shut off (e.g. current max-out), it should be re-warmed for 1-2 minutes or variations in baseline should be expected for this amount of time.

CHIP LOADING

3. Ensure all reagents were made within the last 30 days (4% LPA, 1xTTE).
4. Take 4% LPA into a fitted 1mL pipette tip attached to a 1mL syringe. Insert the tip to the CB3 well and make sure you have a good seal. Gently apply pressure and let the mix fill the channels. Loading may take 30s, but do not apply too much pressure so as to crack the chip or destroy the polymer. Wait until the polymer fully fills all channels.

SAFETY NOTE: the polymer should just exit the channels into CB0, CB1 & CB2; no bubbling should occur as this can create aerosols. The syringe and chip must be secure in your grasp; do not allow the syringe to slip and splatter polymer at you.

4. Carefully remove the syringe, and pipette out the excess polymer from CB3. Pipette 4 μ L of 1xTTE buffer into CB1, CB2, & CB3. If you are testing your TC product, pipette 0.5 μ L of sample into CB0 and 3.5 μ L of your flush-out buffer (0.1 or 0.01xTTE). If you are testing TTK product, pipette 4 μ L of sample into CB0 behind an aerosol shield.

CE CONDITIONS

- ❖ **First Injection:** 80 seconds; **Subsequent Injections:** 20 seconds @ 200V
- ❖ **Separation:** 250 seconds @ 600 V

According to a static buffer depletion equation given in Brask *et al*⁷⁴, our current running conditions deplete the buffer in the sample well after approximately 8 seconds of

injecting. A careful eye should be kept on running currents and run-to-run reproducibility to ensure no adverse effects appear due to buffer depletion.

CHIP CLEANING AFTER CE

2. To remove polymer, suck the CE wells dry and pull out the polymer with the vacuum. Cap CB0, CB1, CB2 with water, and rinse the chip using the vacuum from CB3. Remove any excess water and inspect for debris. **OR:**
2. Cover the entire chip with a Technicloth wipe and soak the wipe with 70% ethanol. Pull the wipe down the chip to expose only CB3. Take autoclaved or milli-Q water into a fitted 1mL pipette tip attached to a 1mL syringe. The water must fill the entire tip of the syringe. Insert the tip to the CB3 well using a layer of Parafilm as a gasket to promote the seal between the syringe and glass well. Gently apply pressure, pushing to remove the polymer. Once you can see the water flowing out of the other 3 wells (including the sample well) underneath the ethanol soaked wipe, remove the plunger from the syringe prior to removing the syringe from the chip. At this point any biohazardous material from the micro-channel and sample well will have been sufficiently diluted, washed out and contained within the 70% ethanol soaked Technicloth wipe. Dispose of the wipe in the appropriate biohazardous waste container.

SAFETY NOTE: the polymer should just exit the channels into CB0, CB1 & CB2 and then the water should move through with constant flow; no bubbling should occur as this can create aerosols! The syringe and chip must be secure in your grasp; do not allow the syringe to slip and splatter polymer at you.

2. Wrap a dry Technicloth wipe around the chip exposing the same well that never came into contact with a sample, apply positive pressure using the filtered nitrogen gun to dry the chip channel and inspect for debris. Finally use the air gun to dry out the remaining wells. Any water spray at this point is deemed safe and clean, and will mostly be absorbed by the dry cloth wrapped around the chip.

ANY DEVIATIONS FROM THIS PROTOCOL, COMPLICATIONS OR COMMENTS SHOULD BE INCLUDED IN THE RUN NOTES. BE OBSERVANT AND NOTEFUL.

F.4 PCR Conditions

β2M RECIPE

β2M Recipe Ingredient	Reagent Volumes (μL)			
	SP Mix	+ve ctrl	-ve ctrl	-ve ctrl
10X PCR buffer	2.5	2.5	2.5	2.5
10uM 5' β2M-ForAni 5'-CCAGCAGAGAATGGAAAGTC-3'	0.5	0.5	0.5	0.5
10uM 3' β2M-RevAni-Alexa647N Alexa647-5'- ACTTAACTATCTGGGCTGTGAC-3'	0.5	0.5	0.5	0.5
10mM dNTPs	0.5	0.5	0.5	0.5
50mM MgCl ₂ (4mM final conc'n)	2.0	2.0	2.0	2.0
5 U/uL Pt. Taq (x2)	0.5	0.5	0.5	0.5
50 ng/nL β2M DNA	x	1.0	x	x
1% BSA	0.5	0.5	0.5	0.5
DMSO (4% @ final conc'n)	1.0	1.0	1.0	1.0
Magnetic Chargeswitch™ Beads	x	x	x	1.0
H ₂ O, PCR grade	17.0	16.0	17.0	16.0
Total:	25.0	25.0	25.0	25.0

STOCK AND INITIAL ALIQUOTED PCR REAGENTS ARE STORED IN A -30oC NON-FROST-FREE FREEZER IN A BOX DEDICATED FOR PCR REAGENTS (I.E. NO PCR PRODUCTS ARE CONTAINED WITHIN). A SEPARATE BOX ALSO IN THE FREEZER IS RESERVED FOR STOCKS OF PRIMERS. ONLY EPPENDORF 1.5ML TUBES (PCR CLEAN) ARE USED FOR MAKING ALIQUOTS AND DILUTIONS. 10XPCR BUFFER, 50MM MgCl₂ AND 5U/μL PT TAQ ARE ALIQUOTED FROM INVITROGEN PT TAQ DNA POLYMERASE KITS TO MAKE THAWING QUICKER AND TO PRESERVE STOCKS. 500μL ALIQUOTS OF PCR GRADE A WATER (DNASE- AND RNASE-FREE) ARE KEPT REFRIGERATED AND ARE TO BE USED AS DILUENT WHEN NEEDED. 10MM DNTPS ARE ALSO ALIQUOTED OUT FOR PURPOSES AS MENTIONED ABOVE. THE STOCK IS OBTAINED FROM SIGMA D7295-0.2ML. PRIMERS ARE DILUTED AS INDICATED FOR SPECIFIC PCR RECIPES. (WRITTEN WITH THE HELP OF JANA)

THERMAL-CYCLING PROFILE

PCR Step	Temperature (°C)	Time (s)
Pre-Denaturation	94	120
Denaturation	94	30
Annealing	60	30
Extension	72	30
Post-Extension	72	120
Cycles: 35		

F.5 CE Reagents

- ❖ Polymer: 10% LPA (Polysciences, Inc, Warrington, PA (cat #19901; MW 600,000-1,000,000; 10% in water)
- ❖ Dynamic Coating: (The Gel Co., San Francisco, CA (Dynamic coating, cat #DEH-100)) – store at 4C
- ❖ Buffer: Tris (Fisher Scientific, #BP152-500), TAPS (Sigma #T5120) and Na₂EDTA (Sigma #ED2SS) – store at RT

10XTTE (500 MM TRIS-BASE, 500 MM TAPS, 10 MM NA₂EDTA) PREPARATION

7. Combine the following reagents into a conical tube:
8. 3.027g of Tris for a final concentration of 0.5mM
9. 6.082g of TAPS acid for a final concentration of 0.5mM
10. 0.186g of Na₂EDTA for a final concentration of 0.01mM
11. Mix well, and then check the pH of the 10xTTE. The pH should be 8.3 ± 0.3. If the pH is not in this range, then discard the buffer.

This formulation of buffer is based on the recipe published in Applied Biosystem's "ABIPrism377 DNA Sequencer". This can be stored at room temperature for up to 4 weeks.

4% LPA PREPARATION

3. Add 500uL of water and 100uL of 10xTTE into a 1mL Eppendorf tube. Add 400 mg of 10% LPA to this tube.

4. Vortex very well. LPA is very viscous and takes time to dissolve. Once dissolved, centrifuge for 30s at 400 rpm. Vortex for 5s again.

This can be stored at room temperature for up to 30 days.

COATING METHOD

Fill the channels with dynamic coating. Leave for 10 min. Wash the channels with water and dry.

F.6 Unrepresentative Data

MULTIPLE PCR CHAMBER LOADINGS

If PCR mix is flushed into the PCR chamber or surrounding input/output channels, and then dried (in preparation to re-load the sample) and re-loaded, the on-chip PCR will result in several strong (unspecific) peaks. This will also occur if the sample is loaded and then re-loaded with no intermediate drying, or it takes more than 5-6 cycles to load the chip and the mixture slides back and forth along the channel walls. Presently soaking the chip in water prior to re-filling has been attempted with no observable difference. No other cleaning methods have been attempted.

AIR BUBBLES/EVAPORATION IN THE PCR CHAMBER

If there are significant bubbles present (or generated) in the PCR chamber during pre-denaturation (the highest temperature of the PCR run; when the bubble should be the largest), even less volume will be present, and thus, the process will be less effective.

Although not thoroughly tested, it is suggested that if 10-20% of the chamber is filled with bubbles, this is sufficient enough to foul up the PCR, as there is some pushing out of the PCR mix from the chamber during cycling.

LESS THAN 4UL RECOVERED FROM THE PCR CHAMBER

If less than 4uL volume of sample is recovered after the buffer flush through via the PCR chamber, there is a chance that a bubble developed during the run, the chip was

partially delaminated during thermal-cycling, or the valving was inadequate (however, the latter should be noted when loading the chip). Less recovery of the PCR product suggests that not enough mix may have been present within the chamber during thermal-cycling to be effective.

ERRORS OCCURRING DURING CE

If the laser is turned off before the run or in between consecutive runs, the user has to make a choice: leave the chip for at least a minute while the laser warms up again (with a consequence that the chip dries out), or attempt the run with the likelihood of a varying baseline. As such, these runs are questionable.

Subsequently, if the TTK is bumped, there can be large sudden variations in the baseline that appear to be peaks, or disguise real peaks.

High or low baseline (e.g. <1V or >3V) because of chip fabrication, which may be caused by dicing, alignment, or bonding. These baselines could mean that not enough light, or conversely, too much light is being coupled.

Laser power is less than 4.2mW using the LaserCheck handheld optical power meter, the laser needs to be replaced (ensure 645 nm is set as the wavelength).

If surface coating (e.g. Dynamic Coating) has degraded on the chip surface, this may cause a lower product peak resolution. This can be tested by running the chip on the uTK with 1uL of AlfaExpress.

Misalignment of the chip, resulting in not enough light coupled into the channel.

ALL DIFFICULTIES SHOULD BE NOTED IN THE RUN NOTES